INVESTIGATION INTO THE FIRING AND SYNAPTIC PROPERTIES OF MOTONEURONS IN DEVELOPING ZEBRAFISH

Stephanie Gaudreau

Thesis submitted to the University of Ottawa
in partial Fulfillment of the requirements for the
Doctorate in Philosophy Degree in Biology

Department of Biology
Faculty of Science
University of Ottawa

Acknowledgements

It is difficult to put into words just how grateful I am to my supervisor Dr. Tuan Bui for his support. Tuan, over the years, you have provided me with invaluable mentorship, guidance, and knowledge. It has been a privilege to work with you and experience the research environment you create for your trainees. Thank you for challenging me and pushing me beyond my comfort zone. Beyond your academic guidance, I am greatly appreciative of your patience, kindness, and sense of humour. Thank you for helping me fill the last several years with great memories and laughter. As I near the end of my doctorate and consequently my time here in the Bui Lab, I am filled with gratitude for your unwavering belief in me, the opportunities you've provided, and the support you've consistently offered. I am even grateful for your constant overpromising of my patching skills to others. I hope I'm fortunate enough to continue working with you in the future.

To all current and former Bui Lab members I've worked with throughout the years, thank you all for being helpful, kind, and supportive. I extend a special thanks to Dr. Alex Laliberté whose knowledge over a broad range of topics never ceases to amaze me. Thank you, Alex, for your unwavering willingness to help everyone and anyone you cross paths with. Thank you, Dr. Sara Goltash, Lauren Couvrette, Sarah Chiasson, Emam Khan, and Shahriar Nasiri for helpful discussions and most importantly, fun times. To former Bui Lab members Dr. Yann Roussel and Dr. Benjamin Lindsey, thank you for the time you dedicated to training me during my undergrad and for the invaluable knowledge you've shared.

To my thesis advisory committee, Dr. John Lewis and Dr. Michael Jonz, thank you for your invaluable insights and guidance. Your expertise, perspectives, and helpful discussions have played an important role in shaping this work.

To Dr. Emily Standen, thank you for your support over the years. Your cheerful nature and helpful conversations have been a constant source of encouragement.

To Maddy Reed and Mary Upshall, I could not have done this without you. One of the greatest things to have come from completing this doctorate was meeting both of you. I am forever grateful for our coffee breaks that always seemed to get longer and longer, and for all the great memories we've shared over the years. Thank you for believing in me, for supporting me, for laughing with me.

To my parents, thank you for your unwavering support – it has truly meant the world to me. To my twin sister Kirsten, thank you for always being there for me and for cheering me on.

To my brother Justin, thank you for your constant support and for giving me the coolest niece and nephew on the planet – they were the best distraction of all time. Even though I'm certain no one quite knew what I was doing this whole time, thank you for thinking (or pretending) it was cool.

To my partner, Zacc Corradini-Carrière, thank you for being my greatest supporter. Whether or not you were always truly listening, I appreciate you sitting through my daily recounts of experiments – through both the successes and the setbacks. Thank you for celebrating the small wins with me and for supporting long lab days. I am beyond grateful for your patience, your understanding, and, most of all, your unwavering belief in me from the very start.

Finally, thank you to the Natural Sciences and Engineering Research Council of Canada and the Éric Poulin Centre for Neuromuscular Disease affiliated with the University of Ottawa for their financial support.

Abstract

Movement is the driving force of survival for many animals yet the full repertoire of movements an animal can produce is not present at birth. The study of motor maturation – how simple movements are turned into complex ones – is invaluable to our understanding of motor control by the nervous system. Uncovering how the neuromuscular system changes throughout development can reveal insights into fundamental principles and mechanisms underlying how movement is produced. This thesis leverages the accessibility of the neuromuscular system in developing zebrafish to 1) validate a screening method that makes use of optogenetics for the assessment of neuromuscular junction function in the context of disease, and 2) uncover the role of an ion current in network-wide and motoneuron-specific behaviour during motor maturation. We then identify for the first time the presence of a subthreshold non-inactivating potassium current known as the M-current (I_M) in zebrafish spinal circuits for locomotion, revealing its role in regulating swimming episode and motor burst duration during fictive locomotion in spinalized animals. We further our investigation into the role of I_M in the context of locomotion by revealing its role in the control of primary motoneuron excitability and regulation of repetitive firing. Moreover, we show that the magnitude of I_M and the role it plays in primary motoneurons changes during early development. We also characterize developmental changes to the persistent sodium current (I_{NaP}), the L-type channel mediated calcium current (I_{CaL}), and P/Q-type mediated calcium current ($I_{CaP/Q}$) in primary motoneurons, emphasizing the contributions of I_{NaP} with I_M to the control of repetitive firing. Finally, we investigate I_M as a target of spinal neuromodulation during development and identify muscarine as an enhancer and serotonin via 5-HT_{1A} receptors as an inhibitor of I_M in primary motoneurons. Interestingly, we reveal that enhancement by muscarine and inhibition by 5-HT_{1A} receptor signaling is not consistent across larval development but could be tied to

developmental changes in I_M. Our findings detail how several ion currents interact to shape motoneuron firing during development as motor maturation progresses. Our findings also reveal mechanisms by which ion currents in zebrafish motoneurons are differentially modulated during development, perhaps to facilitate motor maturation. This work highlights the intricacies of the expression, function, and modulation of the diverse ion currents expressed in motoneurons during development.

Résumé

Le mouvement est la force motrice de la survie de nombreux animaux, mais le répertoire complet des mouvements qu'un animal peut produire n'est pas présent à la naissance. L'étude de la maturation motrice - comment des mouvements simples se transforment en mouvements complexes - est inestimable pour notre compréhension du contrôle moteur par le système nerveux. Découvrir comment le système neuromusculaire change tout au long du développement peut révéler des informations sur les principes et mécanismes fondamentaux sous-jacents à la production du mouvement. Cette thèse exploite l'accessibilité du système neuromusculaire chez le poisson zèbre en développement pour 1) valider une méthode de dépistage qui utilise l'optogénétique pour l'évaluation de la fonction de jonction neuromusculaire dans le contexte de la maladie, et 2) découvrir le rôle d'un courant ionique dans le comportement à l'échelle du réseau et spécifique aux motoneurones pendant la maturation motrice. Nous identifions ensuite pour la première fois la présence d'un courant potassique non-inactivant sous-seuil connu sous le nom de courant M (I_M) dans les circuits spinaux du poisson zèbre pour la locomotion, révélant son rôle dans la régulation de l'épisode de nage et de la durée des rafales motrices pendant la locomotion fictive chez les animaux spinalisés. Nous approfondissons notre étude du rôle de l'I_M dans le contexte de la locomotion en révélant son rôle dans le contrôle de l'excitabilité des motoneurones primaires et la régulation des décharges répétitives. De plus, nous montrons que l'amplitude de l'I_M et le rôle qu'il joue dans les motoneurones primaires changent au cours du développement précoce. Nous caractérisons également les changements développementaux du courant sodique persistant (I_{NaP}), du courant calcique médié par le canal de type L (I_{CaL}) et du courant calcique médié par le canal de type P/Q ($I_{CaP/Q}$) dans les motoneurones primaires, en soulignant les contributions de l'I_{NaP} avec l'I_M au contrôle des décharges répétitives. Enfin, nous étudions l'I_M comme cible de la

neuromodulation spinale au cours du développement et identifions la muscarine comme un activateur et la sérotonine via les récepteurs 5-HT1A comme un inhibiteur de l'I_M dans les motoneurones primaires. Il est intéressant de noter que nous révélons que l'amélioration par la muscarine et l'inhibition par la signalisation des récepteurs 5-HT1A ne sont pas cohérentes tout au long du développement larvaire, mais pourraient être liées à des changements développementaux de l'I_M. Nos résultats détaillent la manière dont plusieurs courants ioniques interagissent pour façonner la décharge des motoneurones au cours du développement à mesure que la maturation motrice progresse. Nos résultats révèlent également des mécanismes par lesquels les courants ioniques des motoneurones du poisson zèbre sont modulés différemment au cours du développement, peut-être pour faciliter la maturation motrice. Ce travail met en évidence les complexités de l'expression, de la fonction et de la modulation des divers courants ioniques exprimés dans les motoneurones au cours du développement.

Co-Authorship

The studies described in Chapter 2 are part of an ongoing collaboration with the lab of Dr. Hanns Lochmüller. Jarred Lau generated the morpholino knockdown animals and provided all the animals used for electrophysiology experiments described in Chapter 2.

Table of Contents

List of Figures

List of Abbreviations

ACh: acetylcholine

aCSF: artificial cerebrospinal fluid

AIS: axon initial segment

ALS: amyotrophic lateral sclerosis

AUC: area under the curve

CaP: caudal primary motoneuron

ChAT: choline acetyltransferase

ChR2: channelrhodopsin

cKO: conditional knockout

CMS: congenital myasthenic syndrome

CRN: cranial relay neurons

DA: dopamine

dpf: days post-fertilization

dRoP: dorsal rostral primary motoneuron

EPC: endplate current

EPP: endplate potential

fps: frames per second

GAN: giant axonal neuropathy

hpf: hours post-fertilization

HVA: high-voltage activated

IBI: inter-burst interval

IC: ipsilateral caudal

I_{CaL}: L-type calcium current

$I_{CaP/Q}$: P/Q-type calcium current

I_h: hyperpolarization-activated inward current

$I_{K(Ca)}$: calcium-dependent potassium current

I_M: M-current

I_{NaP}: persistent sodium current

KD: knockdown

LVA: low-voltage activated

mAChR: muscarinic acetylcholine receptor

M-cell: Mauthner cell

mEPC: miniature endplate current

MiP: middle primary motoneuron

MO: morpholino

M_1R: muscarinic acetylcholine receptor 1

mV: millivolt

NE: norepinephrine

nM: nanomolar

NMD: neuromuscular disease

NMJ: neuromuscular junction

nAChR: nicotinic acetylcholine receptor

nMLF: nucleus of the medial longitudinal fasciculus

pA: picoampere

PIC: persistent inward current

PIP_2: phosphatidylinositol 4,5-biphosphate

pMN: primary motoneuron

SMA: spinal muscular atrophy

sMN: secondary motoneuron

syt2: synaptotagmin-2

syt11b: synaptotagmin-11b

TB: tail beat

vRoP: ventral rostral primary motoneuron

5-HT: serotonin

$5\text{-}HT_{1A}$: serotonin 1A

μM: micromolar

μm: micrometer

Chapter 1

General Introduction

1.1 Introduction

The driving force of survival for most animals is the ability to move from one place to another. Locomotion is a fundamental form of movement endowing animals with the skills necessary to survive and to navigate their environment effectively. All locomotor behaviours – whether walking, swimming, or flying – rely on underlying networks of neurons whose activity guides coordinated muscle contraction to propel the animal. These neural networks are found all along the rostrocaudal axis of the nervous system, from the telencephalon to the brainstem all the way to the spinal cord. Ultimately, these locomotor circuits control the neuromuscular system to coordinate muscle activity to generate locomotion.

The full repertoire of locomotor movements available to an animal is not in place instantaneously after birth. Instead, there is a gradual maturation of locomotor circuits during development. For example, developing mammals display early rhythmic leg movements in the womb and shortly after birth without the weight bearing necessary to fully locomote. Gradually, the pattern of limb movements matures to support different rhythms and patterns of limb movements and weight bearing such that more coordinated forms of walking, running, and swimming are present (Dominici et al. 2011).

How do motor circuits across the nervous system change, if at all, to enable the emergence of new locomotor maneuvers during development? Possible loci of developmental changes to mature

locomotor control include but are not limited to the addition of new neurons (Pujala and Koyama 2019), changes in synaptic connectivity between distant regions and within local locomotor circuits (Roussel et al. 2021), alterations to the active and passive properties of neurons (Gao and Ziskind-Conhaim 1998; Sharples and Miles 2021), and changes to the neuromuscular system through alterations of neuromuscular function or the composition and maturation of body musculature. Any changes within these regions could affect neural dynamics and neuromuscular control in such a way as to lead to new patterns of muscle activity generating new forms of locomotion.

Identifying mechanisms driving the emergence of new locomotor movements can be challenging. In some species, the maturation of locomotor movements is gradual and relatively long without well-identified milestones. The generation of embryonic or postnatal animals can be relatively long. Access to components of the locomotor circuits can also be limited.

Zebrafish have become a sought-out animal model for the study of developmental processes, their increasing popularity owing to a myriad of advantageous features. Across fields, zebrafish are attractive for use because of the relatively low costs associated with their housing and maintenance. The high fecundity of zebrafish is also advantageous across research disciplines. A single female zebrafish can produce hundreds of embryos per clutch every few days. Not only does this render large scale analyses and high throughput experiments feasible but aids with the generation of effective transgenic strains. Importantly, zebrafish are a genetically amenable system within which numerous successful genetic manipulations and transgenic lines have been effectively generated, such as, but not limited to, the use of the Tol2 transposon, CRISPR-Cas9, Gal4/UAS, and

morpholino systems for gene knock-outs, knock-ins, or knock-downs (Albadri, Del Bene, and Revenu 2017; Asakawa et al. 2008; Chang et al. 2013; Hwang et al. 2013; Jao, Wente, and Chen 2013; Kroll et al. 2021; Nasevicius and Ekker 2000; Scheer and Campos-Ortega 1999; Suster et al. 2009). Moreover, zebrafish develop rapidly. Zebrafish embryos reach larval stages in 3 days, reaching juvenile and adult stages by four and twelve weeks, respectively (Kimmel et al. 1995; Parichy et al. 2009). This reduces the waiting period required between experiments as new generations of zebrafish are generated. It also permits efficient transgenic line generation as zebrafish reach adulthood rapidly. Lastly, approximately 70% of the human genome is shared with zebrafish, with around 80% of human disease genes found in zebrafish (Howe et al. 2013), rendering them a useful vertebrate model for both understanding basic mechanisms of animal function as well as disease development.

One notable advantage of the zebrafish is the rapid and stereotyped development of locomotor control such that changes within locomotor circuits can be associated with the emergence of well-described locomotor maneuvers (Knogler et al. 2014; Lambert, Bonkowsky, and Masino 2012; Roussel et al. 2020, 2021). My thesis aims to identify specific mechanisms within locomotor circuits and the neuromuscular system that propel the maturation of locomotor movements in developing zebrafish. Since many of the components of neural locomotor circuits and the neuromuscular system are well-conserved across vertebrates, sharing fundamental principles underlying structure and function, the findings described herein may apply to locomotor circuits of many species.

1.2 Zebrafish musculature

Understanding zebrafish musculature is an essential preface to describing the development of locomotion in zebrafish. Axial musculature powers swimming movements in zebrafish. It is divided into epaxial and hypaxial zones referring to dorsal and ventral muscles relative to the horizontal septum, respectively (van Meer et al. 2024). Within both of these zones, individual muscle fibers known as myomeres are connected to one another by myosepts (van Meer et al. 2024).

In developing zebrafish, muscle fibers are organized into about 30 muscle somites (W van Raamsdonk et al. 1982). These are transient structures that eventually give rise to mature musculature and vertebrae (Henry et al. 2005). Within the first day of development, zebrafish embryos possess basic muscle structures, including fast muscle fibers (Keenan and Currie 2019). At this stage, a single layer of slow muscle fibers has migrated superficially just beneath the skin of the embryo (Keenan and Currie 2019; W van Raamsdonk et al. 1982). During embryonic and larval stages, the bulk of the musculature is comprised of fast muscles. This organization of medially-located fast muscle fibers with slow muscle fibers located superficially persists into adulthood as the muscle fibers continue to mature and grow, though in adult stages there exists a middle layer of intermediate muscle fibers (Keenan and Currie 2019). Rapid development of functional musculature permits production of movement very early on during zebrafish development.

1.3 Early development of zebrafish locomotor control

On the backdrop of a developing body musculature, the earliest movements recorded in developing zebrafish occur at 17 hours post-fertilization (hpf) when embryos perform large amplitude body bends (Saint-Amant and Drapeau 1998). This behaviour is termed 'coiling' and consists of one-sided bends of the tail reaching the head of the embryo and coming back down to its resting position. Next, a few hours later, by 24 hpf, embryos begin to produce two successive coils to either side of the head (Knogler et al. 2014). This is known as double coiling and is thought to be an intermediate left-right alternating movement that precedes and paves the way for the apparition of swimming by 2 days post-fertilization (dpf) (Drapeau et al. 2002a). At this age, uncoordinated swimming made up of large amplitude tail bends is produced in response to touch or other aversive stimuli. By 3 dpf, larval zebrafish begin to swim spontaneously. Swimming at this age is relatively infrequent and consists of long (typically 1 s in duration) periods of left-right alternating tail beats (Drapeau et al. 2002a). This swimming behaviour is an immature form of larval swimming known as 'burst swimming' (Buss and Drapeau 2001). By 4 dpf, larval zebrafish exhibit their most mature form of swimming known as 'beat-and-glide' swimming. It is characterized by increasingly frequent shorter (averaging around 200 ms in duration) periods of low amplitude left-right alternating tail beats interspersed with periods of gliding (Drapeau et al. 2002a).

The rapid and stereotyped emergence of new locomotor behaviours during zebrafish development (**Fig. 1.1**) offers a tantalizing opportunity to identify mechanisms by which locomotor control matures. Linking structural or physiological changes within neural circuits, neurons or the neuromuscular system with the emergence of new behaviours is a powerful approach for the delineation of function of the components of locomotor circuits and neuromusculature.

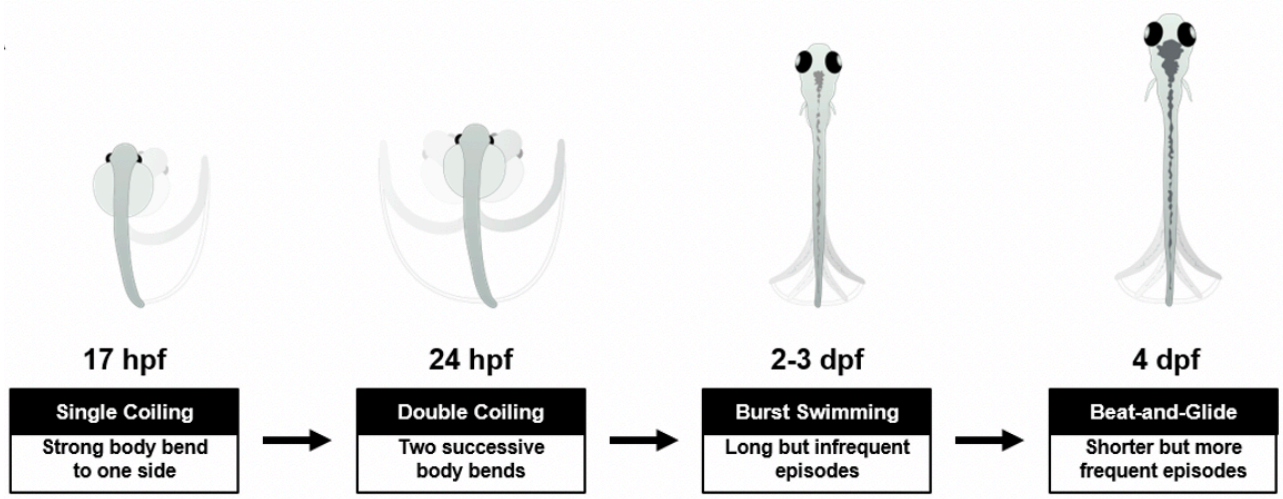

Figure 1.1. Development of zebrafish locomotor movements during early development. Coilings are eventually replaced by swimming consisting of rhythmic left-right alternating tail beats appears around 2-3 dpf, with further refinements by 4 dpf. Adapted from Roussel et al., (2021).

1.4 Maturation of spinal locomotor circuits guides maturation of locomotor control

Underlying the development of progressively more complex locomotor behaviours is the maturation of spinal circuits that guide locomotion. These spinal locomotor circuits are found in most if not all vertebrates and were first described over a century ago when it was observed that the isolated (i.e., in the absence of descending commands from the brain and brainstem) cat spinal cord could generate rhythmic locomotor-like movements (Brown 1914). Once active, spinal locomotor circuits produce the sustained rhythm and pattern of muscle activity needed for the repetitive rhythmic movements that make up locomotion (Orlovsky et al. 1999). These circuits are highly organized, contained within specific regions of the spinal cord, and are associated with well-established stereotyped motor outputs (Drapeau et al. 2002a; Goulding 2009; Mackay-Lyons 2002; Wiggin, Peck, and Masino 2014).

Appreciable headway has been made in the identification and characterization of the spinal neurons that make up spinal locomotor circuits in larval zebrafish, thereby elucidating possible functional roles of neurons critical to the execution of swimming. There are several classification schemes for spinal neurons, with some being based upon the morphology and axonal trajectories of the neurons (Robert R Bernhardt et al. 1990). A more recent molecular classification scheme is based upon the development of spinal neurons and the transcriptional code that defines each neuron. During embryonic development, progenitor domains arise that each express a particular set of transcription factors. Populations of postmitotic neurons, each with distinctive sets of morphological, neurotransmitter, axonal, and firing properties arise. These cardinal populations include the dI1 to dI6, and V0 to V3 neurons, and motoneurons (Lu, Niu, and Alaynick 2015). Spinal neurons amongst these cardinal populations emerge in a distinct spatiotemporal order (Robert R Bernhardt et al. 1990). The first ones to arise are primary motoneurons (pMNs) at around 9 hpf (P. Z. Myers, Eisen, and Westerfield 1986). pMNs are mainly involved in large amplitude movements during early development (L Saint-Amant and Drapeau 2000). Within the next few hours, other spinal neurons also important to larger amplitude early movements are generated (Robert R Bernhardt et al. 1990). A second wave of spinal neuron generation occurs around 24 hpf, giving rise to secondary MNs (sMNs) – the motoneurons involved in slower swimming movements – as well as more spinal interneuron populations important to the execution of swimming (Robert R Bernhardt et al. 1990).

The very early coiling movements are shown to be driven by rostrally located spinal pacemaker neurons known as ipsilateral caudal (IC) neurons (Tong and Jonathan Robert McDearmid 2012).

Electrical coupling between these intrinsically rhythmic clusters of pacemaker cells, located within either side of the spinal cord, and with more caudally located spinal interneurons and pMNs is the basic architecture of the network guiding single coiling movements from 17 to 24 hpf (Saint-Amant and Drapeau 1998). It is a network composed entirely of the spinal neurons emerging from the first wave of spinal neurogenesis. After this, the neurons from the second-wave of neurogenesis begin their progressive incorporation such that by 24 hpf, additional neurons now exist within the pre-established single coiling circuit to permit double coiling (Knogler et al. 2014; Roussel et al. 2021; Saint-Amant and Drapeau 1998). In addition to the incorporation of new neurons, the purely electrical transmission scaffold (Saint-Amant and Drapeau 2001) becomes one that is hybrid, containing both electric and chemical synapses (Knogler et al., 2014). The exact changes that occur next to pave the way for burst swimming at 2-3 dpf are not as well described. It is hypothesized that IC pacemaker neurons may still provide rhythmic excitation to spinal circuits during burst swimming (Roussel et al. 2020). At this stage, additional neurons are added into the network, in addition to novel connections and refinement of existing ones (Roussel et al. 2021). While the electrical scaffold is still present, chemical neurotransmission becomes more and more involved in the production of movement (Buss and Drapeau 2001; Roussel et al. 2020, 2021). The maturation that proceeds next gives rise to beat-and-glide swimming (Drapeau et al. 2002a). A recent modelling study suggests that the transition to beat-and-glide swimming involves an even greater reliance of spinal locomotor circuits on chemical synapses as well as reconfiguration of the existing network, meaning that no additional neurons are being generated at this stage (Roussel et al. 2021). Rather, connectivity between existing neurons is being reorganized. The idea is that by this stage of swimming, spinal locomotor circuits do not rely anymore on pacemaker neurons like IC neurons to guide their behaviour but rather operate as network oscillators (Roussel et al. 2020,

2021). In this framework, rostrocaudally propagating activity alternates between the left and right side of the body via rhythmicity generated through well-curated connectivity patterns and a refinement of specific neuronal firing behaviours set up via intrinsic membrane dynamics. While we are starting to piece together how individual components organize themselves to form functional spinal locomotor circuits, much remains to be understood about how intrinsic firing behaviours of spinal neurons might mature throughout development to shape behavioural motor maturation.

1.5 Developing zebrafish motoneurons

Motoneuron development could be crucial to the emergence of new locomotor movements during development due to their critical role in controlling muscles. As mentioned already, the first born motoneurons are pMNs and there exist four types of pMNs that are present in every segment throughout the spinal cord: the dorsal rostral primary (dRoP), the ventral rostral primary (vRoP), the middle primary (MiP), and the caudal primary (CaP). Each of the four pMNs innervate distinct quadrants of fast musculature. The dRoP sends axonal projections to the ventral half of the dorsal muscle while the vRoP innervates the dorsal part of ventral musculature. MiP motoneurons innervate the dorsal-most quadrant of muscles while CaP motoneurons innervate the ventral-most quadrant of muscles. sMNs on the other hand have much less specific patterns of innervation to muscles. First, some sMNs innervate fast muscle fibers in addition to slow muscle fibers. Indeed, synapses formed by pMNs onto fast muscles are shared with a subset of secondary motoneurons (Wen et al. 2020). These are known as m-type sMNs comprising the largest sMNs innervating deep fast muscles (Bello-Rojas et al. 2019). Next, ms-type sMNs innervate both superficial fast

muscle as well as slow muscle with s-type sMNs innervating only superficial slow muscle (Bello-Rojas et al. 2019).

pMNs are involved with coiling during the first few days of development. Although coiling disappears as development progresses, primitive reflexive movements like the escape response can still be executed (Drapeau et al. 2002a; Jiao et al. 2023; Nair, Nguyen, and McHenry 2017; Park et al. 2018; Roberts et al. 2016; Temizer et al. 2015). Escape responses to tactile or auditory stimuli are characterized by an initial large body bend (often termed C-bend) and can be followed by several swimming episodes which are often swimming bursts with their characteristic large amplitude body oscillations (Budick and O'Malley 2000). pMNs play a more prominent role in the execution of escape response than sMNs (Fetcho and Faber 1988; Fetcho and O'Malley 1995; Liu and Westerfield 1988; Wen et al. 2020). The latter will come to dominate locomotor behaviour later in development with the emergence of free-swimming behaviour, characterized by lower frequency and amplitude tail movements (Liu and Westerfield 1988). sMNs are functionally divided into subtypes related to the speed of swimming at hand such that slow sMNs, intermediate sMNs and fast sMNs are activated primarily during these respective swimming speeds. In fact, as swim speed increases, slow to fast sMN recruitment is done in an additive fashion such that more and more motoneurons are added to the active pool (Fetcho and McLean 2010; McLean et al. 2007; Menelaou and McLean 2012).

Though currently limited, there is evidence that the intrinsic and firing properties of motoneurons might be changing during the stereotyped changes in movements that arise as zebrafish develop from embryonic to larval stages. Changes to the action potential waveform have been observed in

MiP and CaP MNs as they develop from 24 hpf to 48 hpf (Moreno and Ribera 2009). These same pMNs are unable to fire repetitively at 24 hpf but do so reliably by 48 hpf (Moreno and Ribera 2009). Moreover, Buss and Drapeau detail a decrease in input resistance accompanied by an increase in rheobase in motoneurons from 2 dpf to 3-4 dpf, while membrane capacitance remains similar across ages (Buss, Bourque, and Drapeau 2003). These observed changes to membrane and firing properties of motoneurons could be caused by changes in protein expression, ion currents or changes in neuromodulation to name a few. In addition to these changes in motoneuron properties, neuromuscular function has also been shown to change during zebrafish development (Walogorsky et al. 2012). There is, therefore, mounting evidence that motoneurons are developing at several different levels but how each level of motoneuron development is responsible for the emergence of novel and refined locomotor behaviours in developing zebrafish remains unknown.

1.6 The neuromuscular junction

Neural control of movements is made possible by the neuromuscular system, linking neuronal networks within the central nervous system to muscles of the peripheral nervous system. All vertebrate neuromuscular systems contain three major components: motoneurons, peripheral nerves, and muscle. The final relay between the nervous system and body musculature is the motoneuron. Motoneurons along the length of the vertebrate spinal cord send axonal projections to specific muscle targets that vary depending on the location of the motoneurons within the spinal column. This synapse between the motoneuron and the muscle is known as the neuromuscular junction (NMJ). If the motoneuron is the "final common path" that links the nervous system with the neuromuscular system, the NMJ is the lynchpin of that connection (Sherrington, C. S. 1904).

The first anatomical observations of NMJs date back to the 19th century (Rudolf, Khan, and Witzemann 2019). The postsynaptic muscle membrane of the NMJ has a distinctive structure composed of junctional folds. These increase the surface area over which NMJs can be formed. While a few studies during 19th century suggested chemical interaction between motoneurons and muscle, it was not until the mid-20th century that this suspicion was confirmed (Rudolf et al. 2019). Motoneurons release acetylcholine (ACh) at their synaptic terminals in the vicinity of their targeted muscle fibers (Eccles, John C, Bernhard Katz, and Stephen W Kuffler 1941; Eccles, Katz, and Kuffler 1942). The latter express ligand binding nicotinic ACh receptors (nAChRs) that recognize ACh release by motoneuron terminals. Upon ACh binding, nAChRs enter their open conformational state, allowing flow of positive ions known as cations through the channel pore. Resulting net flow of inward current depolarizes the membrane causing release of calcium from intracellular stores. This spike in intracellular calcium is what leads to the activation of contractile proteins causing muscle contraction.

The neuromuscular junction has proven invaluable to uncovering fundamental properties of signal transmission owing to its accessibility and conserved structure. Importantly, electrophysiological studies in the frog NMJ confirmed the principle of quantal release of neurotransmitter at a synapse (del Castillo and Katz 1954; Fatt and Katz 1952). While the structure and function of the NMJ is well-characterized today, there remain insights to be uncovered on the properties of the neuromuscular system in developing and mature nervous systems.

1.7 Zebrafish to study the developing neuromuscular system

The use of larval zebrafish during early development to study the neuromuscular system takes advantage not only of their rapid development but also their optical transparency. The latter allows for ease of visualization of the components of the neuromuscular system such as spinal neurons, peripheral nerves, and muscle fibers. Because of their rapid development, researchers can follow developmental changes to each of these components of the neuromuscular system. The rapid development of zebrafish within the first few days following fertilization also endows researchers with the unique opportunity to follow them as they transition through well-timed and stereotyped progressions in the locomotor movements they can produce. As embryonic zebrafish progress to larval stages, anatomical changes to neuromuscular system components can readily be linked to observable changes in behaviour, shedding light onto underlying changes to physiology. When studied in zebrafish models of gene disruption, for example through transgenesis or morpholinos, these optical and developmental features of zebrafish have proven beneficial to the study of NMJ function. Morpholino knockdowns of synaptotagmin proteins (*syt2* and syt7) and choline acetyltransferase (ChAT) in developing zebrafish have revealed their contributions to synaptic transmission at the motoneuron axon terminal and have shed light onto developmental repercussions to NMJ structure and function (Wang, Wen, and Brehm 2008; Wen et al. 2010). Furthermore, studies in mutant rapsyn-deficient zebrafish have highlighted this protein's involvement in preventing synaptic fatigue (Wen, Hubbard, et al. 2016). Beyond gene disruption models, the use of distinct calcium channels for neurotransmitter release at pMN and sMN axon terminals were also revealed in developing zebrafish (Wen et al. 2020).

The advent of optogenetic approaches to study neural function and the transparency of developing zebrafish has the potential to accelerate our understanding of NMJ function with additional benefits related to the discovery of pathophysiological and molecular mechanisms underlying diseases of the neuromuscular system. Examples of neuromuscular diseases whose research has benefitted from the study of the neuromuscular junction in zebrafish include giant axonal neuropathy (GAN), muscular dystrophies, spinal muscular atrophy (SMA), amyotrophic lateral sclerosis (ALS), and congenital myasthenic syndromes (CMS), (Berger and Currie 2012; Chia et al. 2022; Lescouzères et al. 2023; Singh and Patten 2022; Walogorsky et al. 2012; Wen et al. 2010; Wen, Hubbard, et al. 2016). Developing a new approach to study NMJ function for studies into the development of locomotor control and the pathophysiology of neuromuscular diseases is the focus of Chapter 2.

1.8 Intrinsic properties of neurons

Signal transmission at the NMJ ultimately occurs as a direct result of motoneuron firing which is determined both by intrinsic and extrinsic properties. Intrinsic properties of neurons refer to the features specific to an individual neuron without taking into consideration its place within a network. These features include a neuron's size and shape which often dictate its membrane properties such as capacitance and input resistance. Input resistance is a measure of how a neuron will respond to synaptic input. Higher input resistance means that a neuron requires less synaptic input than a neuron possessing lower input resistance for a given change in membrane potential, such as reaching the threshold for action potential generation. Smaller neurons tend to have higher input resistances compared to larger ones. Capacitance is how much charge a neuron's membrane can store and is inversely proportional to input resistance. Both capacitance and input resistance

influence how quickly a neuron's membrane potential will change in response to current, which is often reported as the membrane time constant or tau (Rall 1957, 1960).

1.9 Intrinsic properties of vertebrate motoneurons

A longstanding principle governing motoneuron recruitment is that of the size principle, brought forth by Henneman in the mid-20th century. This principle dictates that motoneuron size determines recruitment wherein smaller motoneurons are more excitable than larger motoneurons and thus smaller motoneurons get recruited first and larger motoneurons get recruited later as the size of the motoneuron pool required increases. This framework is based on the principle that larger neurons require stronger drive to fire compared to small neurons. While evidence exists of this theory holding true across invertebrate and vertebrate species, from fruit flies (Azevedo et al. 2020) to humans (Jabre and Spellman 1996), there may be more to the recruitment of motoneurons apart from their size. Gabriel et al. reveal that orderly recruitment of different motoneuron pools during varying swim speeds does not crucially rely on neuron size in adult zebrafish (Gabriel et al. 2011). Instead, recruitment is guided both extrinsically by the amplitude of synaptic inputs as well as intrinsically by motoneuron subtype-specific intrinsic properties unrelated to size (Gabriel et al. 2011). While recruitment of motoneurons progresses from small to large motoneurons as swimming frequency increases in the larval zebrafish, Kishore et al. reveal that motoneurons with lowest input resistances (i.e. putatively the largest motoneurons) receive a favoured increase in synaptic drive during faster swim frequencies (Kishore, Bagnall, and McLean 2014), challenging the size principle as the sole causal factor of recruitment order. How exactly biophysical properties of zebrafish motoneurons, other than their size, may influence their means of recruitment, remains

largely unknown. New findings related to this would shed light onto the nuanced principles that may underlie motoneuron recruitment.

1.10 Ion currents

A major contributor to the biophysics of neurons are ion channels, which are essential to the function of all neurons. They mediate the inflow and outflow of a variety of ionic currents necessary to the control of neuronal excitation and inhibition. There exist many groups of ion channels that are selective to certain ions, notably those of sodium, potassium, calcium, and chloride (Hille, Bertil 2001).

1.10.1 Sodium channels

Ionic conductances involved in the generation of the action potential are well-characterized. Voltage-gated sodium, calcium, and potassium channels exhibiting fast kinetics mediate these currents. Voltage-gated sodium channels from the Nav family (Nav1.1-1.9) are responsible for the rapid depolarization of membrane potential during the upshoot phase of the action potential, allowing inward flow of sodium ions when resting membrane potential reaches threshold.

While the fast, inactivating sodium currents associated with action potentials are expressed in most neurons, some sodium currents are more limited in their expression. I_{NaP} represents the small portion of sodium current that does not vanish quickly with fast inactivation of voltage-gated sodium channels. This persistent sodium current either shows no inactivation or a slow inactivation and arises from mechanisms that are not fully known (Müller, Draguhn, and Egorov 2024). I_{NaP} promotes either sustained repetitive firing (Lee and Heckman 2001) or burst firing and is

demonstrated to be involved in the rhythmogenesis of mammalian inspiration (Del Negro et al. 2002; Pace et al. 2007), mastication (Brocard et al. 2006), and locomotion (Tazerart, Vinay, and Brocard 2008a), with some evidence suggesting I_{NaP} could be involved in zebrafish locomotor rhythm generation as well (Song et al. 2020b; Tong and Jonathan Robert McDearmid 2012). I_{NaP} has been identified as a major component of the persistent inward currents (PICs) observed in motoneurons across species (Kuo et al. 2006; Lee and Heckman 2001; Li, Gorassini, and Bennett 2004; Schwindt and Crill 1980; Tazerart, Vinay, and Brocard 2008b; Tong and Jonathan Robert McDearmid 2012).

1.10.2 Potassium channels

The delayed activation of voltage-sensitive potassium channels after the initial opening of Nav channels, generates the necessary outflow of potassium ions to repolarize membrane potential. This, in conjunction with inactivation of Nav channels, results in the falling phase of the action potential. Identified groups of voltage-gated potassium channels involved in action potential termination include rapid delayed rectifier channels such as those from the *Shaker* potassium channels (Kv1 family), *Shal* potassium channels (Kv4 family), *Shab* potassium channels (Kv2 family), and *Shaw* potassium channels (Kv3 family). Together, delayed rectifier potassium channels and the fast-inactivating voltage-gated sodium channels are effective at generating action potentials necessary for signal transmission. The varying expression profiles of these complex classes of voltage-gated channel families endows neurons with unique firing capabilities, alongside the presence of other ion currents.

In addition to the delayed rectifier channels, there are a diverse set of other potassium channels with variations in voltage-dependencies, kinetics, and other properties. Contributing to burst termination in neurons, the calcium-dependent potassium current ($I_{K(Ca)}$) is known to be involved in rhythm generation. This current is an outward potassium current activated by a surge in intracellular calcium that arises from increased neuronal activity during bursting. $I_{K(Ca)}$ can promote burst termination by hyperpolarizing the neuron following periods of activity when intracellular calcium is increased. $I_{K(Ca)}$ is evidenced to be involved in the generation of rhythm for locomotion (el Manira, Tegnér, and Grillner 1994; McKiernan 2013) and respiration (Zavala-Tecuapetla et al. 2008).

While the involvement of $I_{K(Ca)}$ in rhythmogenesis has been acknowledged for decades, the subthreshold non-inactivating potassium current known as the M-current (I_M) has more recently been implicated in inspiratory burst termination (Revill et al. 2021) as well as an important regulator of the mouse locomotor rhythm (Verneuil et al. 2020a). I_M is a voltage-gated non-inactivating potassium current with slow activation beginning near resting membrane potentials and peaking around -10 to -20 mV (Brown and Adams 1980). The Kv7 channel family mediates I_M, with channels formed by Kv7.2/7.3 subunits specifically associated with neuronal expression of I_M (Brown and Passmore 2009). I_M can shape neuron firing behaviour by decreasing excitability, for example through increased rheobase for action potentials (Sharples et al. 2023; Verneuil et al. 2020a), or through spike frequency adaptation (Benda, Longtin, and Maler 2005). These possible influences of I_M on firing behaviour explains why this current has been involved in burst firing termination, regulating the precision of firing in motoneurons (Bothe et al. 2024; Dewell and

Gabbiani 2018) as well as dampening spinal locomotor neuron excitability (Buskila et al. 2019; Jia et al. 2008; Sharples et al. 2023; Verneuil et al. 2020a; Ye et al. 2022).

1.10.3 Calcium channels

Voltage-gated calcium channels are divided into two major categories: low-voltage-activated (LVA) and high-voltage-activated (HVA) calcium channels. The LVA group is made up of T-type channels (formed by $Ca_V3.1$-$Ca_V3.3$ channel subunits) (Harding and Zamponi 2022) that mediate transient calcium currents activated at relatively hyperpolarized membrane potentials nearing resting membrane potential (Huguenard 1996). T-type calcium currents have been implicated in burst firing (Huguenard 1996; Lauzadis et al. 2020; Vickstrom et al. 2020). HVA channels include L-type, N-type, P/Q-type, and R-type calcium channels. Characteristic of the L-type current mediated by $Ca_V1.2$ and $Ca_V1.3$ channel subunits (Roca-Lapirot et al. 2018) is its long-lasting activity caused by its prolonged open state once active. In addition to I_{NaP}, L-type calcium currents (I_{CaL}) have been identified as the calcium component of PICs (Carlin et al. 2000; Li and Bennett 2003; Li et al. 2004). N-type and P/Q type calcium channels are mediated by $Ca_V2.2$ and $Ca_V2.1$ subunits, respectively. These two groups of calcium channels are active over similar voltage ranges and are commonly implicated in neurotransmitter release at synaptic terminals (Luebke, Dunlap, and Turner 1993; Takahashi and Momiyama 1993; Wheeler, Randall, and Tsien 1994). The last member of the HVA calcium currents is the R-type current (mediated by $Ca_V2.3$ channel subunits (Catterall 2000) with known implications in mediating dendritic calcium entry (Kavalali et al. 1997; Sabatini and Svoboda 2000) as well as transmitter release (Gasparini et al. 2001; Wu, Borst, and Sakmann 1998).

The interplay of different ion currents and their respective conductance densities give rise to distinct firing behaviours that can be observed in specialized groups of neurons, such as those that comprise motoneuron populations.

1.10.4 Ion currents in motoneurons and known developmental changes

Important findings regarding the identification of ion currents expressed in motoneurons stem largely from work conducted in mammalian and reptile models. Motoneurons, of course, possess voltage-gated sodium and potassium currents necessary to the production and termination of action potentials. Expression of additional ion channels enhance motoneuron membrane dynamics endowing them with particular firing properties suited to their function. Work in the cat and mouse spinal cords have revealed an important role for I_{NaP} in endowing mouse motoneurons with bursting properties (Lee and Heckman 2001; Tazerart et al. 2008b). I_{NaP} has been revealed in primary motoneurons of zebrafish at 1-day post-fertilization (Tong and McDearmid 2012) yet no further characterization of this current in zebrafish motoneurons has been done. Recent work in mice preparations has also revealed an important role for I_M in controlling motoneuron recruitment (Sharples et al. 2023). I_M has also been shown to underlie precise timing profiles of rattling motoneurons of the rattlesnake (Bothe et al. 2024). This study showed that differential involvement of I_M tuned to specific types of motoneurons promotes firing activity necessary for their distinct functions. Other than rodents and rattlesnakes, I_M is also found in the motoneurons of turtles (Alaburda, Aidas, Perrier, Jean-François, and Hounsgaard, Jørn 2002) and even invertebrate motoneurons (Trimmer 1994). There is currently no knowledge on the presence of I_M in motoneurons of zebrafish.

Studies in motoneurons conclude that they express certain combinations of HVA calcium channels listed above. Interestingly, primary and secondary motoneurons in larval zebrafish use distinct types of HVA calcium channels for neurotransmitter release. While neurotransmitter release in secondary motoneurons involves N-type calcium currents, primary motoneurons importantly rely on P/Q type calcium currents (Wen et al. 2020).

Important changes to the involvement of specific ion currents in motoneurons during development have been made in rodent models, which have shorter developmental times than other mammalian models. These include increases to overall outward potassium conductance and sodium influx during embryonic to neonatal development to shorten the duration and increase the amplitude of the motoneuron action potential, respectively, in rats (Gao and Ziskind-Conhaim 1998). $I_{K(Ca)}$ in rat motoneurons also increases after birth with a role in regulating repetitive firing (Gao and Ziskind-Conhaim 1998). Sharples et al. demonstrate that the hyperpolarization-activated inward current (I_h) increases during postnatal development in only fast motoneurons and not slow motoneurons (Sharples and Miles 2021). Zebrafish develop even faster than mice and the emergence of locomotor movements is rapid and stereotyped during stages where the nervous system is more readily accessible. These features make this species an incredibly attractive model to developmental studies. While certain currents have been identified in motoneurons at precise ages (Buss et al. 2003; Tong and Jonathan Robert McDearmid 2012), the expression of a wider range of ion currents remains to be explored. More importantly, how these motoneuron ion currents change during the various transitions in locomotor behaviours remains to be investigated.

Intriguingly, there are strong reasons to suspect that developmental changes to ion currents in motoneurons could be brought on by the action of neuromodulators, as they are known mediators of voltage-gated ion channel activity. Indeed, serotonin (5-HT) and norepinephrine (NE) have been shown to influence the activity of both sodium and calcium PICs in motoneurons of the turtle (Hounsgaard and Kiehn 1985, 1989; Perrier and Delgado-Lezama 2005; Perrier and Hounsgaard 2003), rat (Berger and Takahashi 1990; Elliott and Wallis 1992; Harvey et al. 2006; Li et al. 2007; Takahashi and Berger 1990), and cat (Lee and Heckman 1996, 2000). These studies speak to the diverse ways by which ion currents can be influenced by neuromodulation. Multifaceted endogenous modulation of ion channel activity renders neuronal behaviour flexible, and in the context of motoneurons, can ensure fine-tuning of their activity in a motor context-specific manner. It would be reasonable to think that changes in ion channel activity observed during development could be spurred by the actions of neuromodulators.

Indeed, neuromodulators have been shown to have prominent influence on the development of zebrafish motor circuits. Serotonin is shown to reduce periods of inactivity in zebrafish larvae as of 4 dpf but not earlier (Brustein et al. 2003). Blocking dopamine (DA) reuptake at 3 dpf reduces overall swimming activity but has no effect to swimming at 5 dpf, suggesting a transient role for dopamine in modulating spinal circuit activity during development (Thirumalai and Cline 2008). Lambert et al. reveal that dopamine signaling via D_4 receptors is important for the developmental transition from burst swimming to beat-and-glide swimming to occur from 3 to 4 dpf (Lambert et al. 2012). The precise target neurons of these neuromodulatory influences within the spinal cord, however, remain largely unknown.

Chapter 2

Electrophysiological validation of an optogenetic approach for the screening of novel gene candidates underlying congenital myasthenic syndromes

Gaudreau, SF, Lau, J, Lochmüller, H, & Bui, TV

2.1 ABSTRACT

Congenital myasthenic syndromes (CMS) are rare inherited diseases of the neuromuscular junction. Many genes have been identified in association with CMS but many more likely remain to be identified. We have developed a novel optogenetic approach to study the function of the neuromuscular junction in larval zebrafish. This approach allows us to use blue-light illumination to activate spinal motoneurons expressing channelrhodopsin-2 (ChR2) and to electrophysiologically record the elicited response in innervated muscle fibers. We employ this optogenetic approach in identified CMS gene synaptotagmin-2 (*syt2*) morpholino knock-down (KD) fish. To validate our approach, we compare our recordings of endplate currents (EPC) to a previous study of *syt2* knockdown where neuromuscular function was investigated using paired electrical stimulation of primary motoneurons with electrophysiological recording of innervated muscle fibers. Our results show similarities in EPC properties but also differences that may be due to limitations in stimulation frequency as well as concurrent activation of multiple motoneurons innervating a single muscle fiber. However, our approach could be useful in determining the activation of single muscle fibers during physiological activity of spinal circuits.

2.2 INTRODUCTION

Congenital myasthenic syndromes (CMS) are a diverse group of rare inherited neuromuscular disorders, present at birth, appearing in early childhood or even later in adult life, which can lead to severe and fatigable muscle weakness (Ohno et al. 2023). At the root of CMS are protein defects leading to abnormal signal transmission at the motor endplate. These genetic defects can theoretically affect any protein involved in signal transmission from the motoneuron to the muscle cell. At the presynaptic level, genetic mutations lead to disruption of acetylcholine (ACh) release. At the synaptic level, these mutations can affect receptor anchorage, and neuromuscular junction (NMJ) structure while at the post-synaptic level, these could affect ACh binding as well as acetylcholine receptor (AChR) densities. Indeed, the most common forms of CMS affect the nicotinic acetylcholine receptor (nAChR), leading to reduced numbers of nAChRs at the motor endplate, slow dissociation rate of ACh from nAChRs, or abnormally brief binding of ACh to nAChRs, for example (Abicht, Müller, and Lochmüller 1993; Engel et al. 2015; Ohno et al. 2023; Ramdas, Beeson, and Dong 2024). Currently, there are 35 identified CMS genes (Abicht et al. 1993; Ohno et al. 2023; Ramdas et al. 2024).

CMS diagnosis is usually established in two waves, the first being a generic diagnosis based on family history, fatigable weakness observed in skeletal muscles, and electromyography testing (Abicht et al. 1993). The second consists of a genetic diagnosis wherein patients must undergo extensive genetic sequencing to pinpoint either previously identified CMS mutations or to uncover novel ones (Abicht et al. 1993; Engel et al. 2015). Genetic diagnosis of CMS permits appropriate individualized therapies to be set in place. The accessibility of the NMJ to pharmacological

intervention has led to the development of affordable and effective treatments for some CMS subtypes such as those underlying receptor deficiency (Lee, Beeson, and Palace 2018).

An accurate genetic CMS diagnosis along with an understanding of how the molecular defects disturb NMJ structure and function are central to developing effective therapies. Unfortunately, many individuals remain without a genetic CMS diagnosis. Establishing suitable treatment plans for these patients is challenging and often ineffective due to lack of identified mechanisms underlying the fatigable weakness. DNA sequencing studies of patients diagnosed with CMS along with their family members are the primary method of identifying novel gene candidates whose dysfunction may lead to CMS. Confirming that these gene candidates are the underlying genetic cause of CMS in patients without genetic diagnosis requires testing whether loss of function of gene candidates perturbs motor function.

Larval zebrafish are incredibly attractive to the screening of novel gene candidates to which mutations may lead to NMJ dysfunction. First, their high fecundity and rapid development render them favourable to screening studies. Next, their genetic amenability permits efficient generation of CRISPR-Cas9 or morpholino (MO) mediated gene knock-outs and knock-downs (Chang et al. 2013; Hwang et al. 2013; Jao et al. 2013; Kroll et al. 2021; Nasevicius and Ekker 2000). The rapid development of zebrafish is evidenced by motor systems that are functional as early as 17 hours post-fertilization (hpf) (Saint-Amant and Drapeau 1998). As development progresses, they transition through well-defined and stereotyped motor movements, ultimately reaching mature larval swimming by 4 days post-fertilization (dpf) (Saint-Amant and Drapeau 1998). These stereotyped movement patterns facilitate the assessment of compromised motor behaviours.

Additionally, orthologous genes associated with the NMJ appear to share common functions across vertebrates (Berger and Currie 2012) highlighting that the key functional architecture of the zebrafish NMJ is similar to humans. Altogether, these advantageous features of larval zebrafish facilitate high throughput testing of how loss of function of NMJ proteins perturbs motor function. Indeed, larval zebrafish have been used to generate numerous models of neuromuscular diseases (NMD). These include but are not limited to muscular dystrophies (Berger and Currie 2012), amyotrophic lateral sclerosis (ALS) (Chia et al. 2022), spinal muscular atrophy (SMA) (Singh and Patten 2022), as well as CMS (Walogorsky et al. 2012; Wen et al. 2010; Wen, Hubbard, et al. 2016).

Accurate validation of novel CMS gene candidates using zebrafish includes assessment of locomotor behaviour as well as NMJ function (McMacken et al. 2017). Typical motor assays include observing chorion movement in embryos as well swimming activity observed in free-swimming larvae (O'Connor et al. 2018; Park et al. 2014). A well-established method for assessing neural activity across the NMJ in larval zebrafish involves a paired patch-clamping method targeting a primary motoneuron and corresponding fast muscle cell simultaneously (Wen and Brehm 2010a). Endplate currents (EPCs) at the level of the skeletal muscle are recorded in voltage-clamp configuration during electrical stimulation of the motoneuron (Wen and Brehm 2010a). Using this technique, effects to NMJ signal transmission in numerous loss of function experiments have revealed the roles of numerous NMJ proteins, shedding light onto fundamental physiological properties of signal transmission at the NMJ of larval zebrafish (Wen et al. 2010, 2020; Wen, Hubbard, et al. 2013; Wen, Linhoff, et al. 2013; Wen, McGinley, et al. 2016).

In this study, we propose a technically less challenging and potentially faster approach to screen for novel CMS gene candidates. We aim to test motor function at the whole-animal level down to the NMJ. Our alternative approach utilizes a transgenic zebrafish line, 1020:UAS;Gal4:ChR2(H134)-mCherry line (Antinucci et al. 2020; Wyart, Bene, et al. 2009), wherein blue light activated channelrhodopsin-2 (ChR2) is expressed in spinal interneurons as well as both primary and secondary motoneurons. Optogenetic excitation of these neurons by blue light illumination of the spinal cord elicits swimming in larval zebrafish (Wyart, Del Bene, et al. 2009). By circumventing the need to attach individual electrodes to both a motoneuron and a muscle fiber that is innervated by the stimulated motoneuron, optogenetic stimulation in this transgenic zebrafish line can be used to easily excite motoneurons for investigations into both locomotor and NMJ function.

Using the previously identified CMS gene synaptotagmin-2 (*syt2*) (Whittaker et al. 2015) to generate knockdowns in 1020:UAS;Gal4:ChR2(H134)-mCherry embryos, we demonstrate that this optogenetic approach permits assessment of movement and NMJ function that are both activated optogenetically. Not only is this screening procedure technically more approachable, but it also provides a behaviourally relevant assessment of NMJ function. We highlight the benefits of using this approach as a tool for screening CMS genes all the while underscoring its limitations.

s

2.3 MATERIALS AND METHODS

2.3.1 Animal care

All experiments were performed in accordance with the protocol approved by the University of Ottawa's Animal Care Committee (BL-4416). Adult zebrafish are maintained at 28.5°C with a 14 hour on/10 hour off light cycle, with lights off at 11PM and on at 9AM. Embryos are fertilized between 9AM-10AM and stored in embryo medium (system water with 0.1% methylene blue) at 28.5°C until used for experimentation at 2-5 days post-fertilization (dpf).

2.3.2 Morpholino knockdowns

All microinjections were performed by Jarred Lau from the Lochmüller lab. Zebrafish from three groups were used for experimentation: uninjected animals (uninjected), animals having received an injection lacking the morpholino construct (control MO), and those having received the injection containing the morpholino construct (*syt2* KD).

2.3.3 Preparation for electrophysiology

Larval *1020:Gal4;UAS:ChR2(H134)-mCherry* (Antinucci et al. 2020; Wyart, Bene, et al. 2009) zebrafish aged 2-3 dpf were prepared for electrophysiology similarly to as is described previously (Wen and Brehm 2010b). Larvae were anesthetized in 0.02% tricaine (MS-222, Aqualife TMS; Syndel Laboratories) before being pinned down through the notochord onto a Sylgard (Dow Corning) coated dish. Pins were made using tungsten wire (diameter of 0.025 mm); one was placed caudally near the tip of the tail, and the other was placed rostrally near the center of the yolk sac. Spinalization was performed using fine surgical scissors at the level of somites 2-3. The skin was then peeled back between the two pins using fine forceps. Next, larvae were bathed in a 2M formamide solution (Millipore Sigma, F9037; 2-5 minute incubation time). The formamide

solution was rinsed out 4-5 times with extracellular recording solution (see below in 2.3.4 *Electrophysiology*). Superficial slow muscle fiber removal was performed using suction through a wide-bored glass capillary (typically, the tips are gently broken to get a sufficiently large tip for muscle removal). Muscles overlaying the spinal cord were not removed.

2.3.4 Electrophysiology

Extracellular recording solution consisted of artificial cerebrospinal fluid (aCSF) containing: 134 mM NaCl, 2.9 mM KCl, 1.2 mM $MgCl_2$, 2.1 mM $CaCl_2$, 10 mM dextrose, and 10 mM HEPES, (pH of 7.8 adjusted with NaOH and osmolarity between 280-290 adjusted with sucrose). Borosilicate glass capillaries (outer diameter: 1.5 mm; inner diameter: 1.1 mm, Sutter Instruments, catalog #BF150-110-10) were used to form pipette tips having a resistance between 2-3 MΩ. These microelectrodes were backfilled with intracellular recording solution consisting of: 116 mM potassium gluconate, 16 mM KCl, 2 mM $MgCl_2$, 10 mM HEPES, 10 mM EGTA, and 4 mM Na_2ATP, osmolarity adjusted to 290 mOsm, pH 7.2 adjusted with KOH (Buss, Robert R. and Drapeau, Pierre 2000). Ventral fast muscle fibers innervated by caudal primary (CaP) motoneurons were targeted for patch-clamp electrophysiology. Once a giga-ohm seal was formed, light suction was applied to break into the membrane of the muscle fiber. As described in Wen and Brehm (2010a), membrane potential was held at -50 mV for the duration of the recording. To stimulate motoneurons optogenetically, blue light (480 nm) illumination was applied over an area of the spinal cord corresponding to approximately one spinal segment that contains the CaP motoneuron innervating ventral fast muscle fibers. Individual light pulses were delivered at a duration of 5 ms. The signal was recorded in voltage-clamp mode, amplified and filtered at 10 kHz with a Multiclamp 700B from Axon Instruments (Molecular Devices) and finally digitized with a

Digidata 1550 (Molecular Devices). Recordings were made from mid-body somites located within 4 somites rostral and 4 somites caudal to the anal pore.

2.3.5 Electrophysiology data and statistical analysis

All electrophysiological data was saved as .abf files. We used the open-source pyABF python package to import and read .abf files in Spyder (version 5.1.5). Analysis of recordings was semi-automated using Python (version 3.9.12) to detect spontaneous miniature end-plate currents (mEPCs) as well as evoked end-plate currents (EPCs). Quantal content, number of release sites, and release probability and levels of steady-state depression were estimated as described by (Wen, Hubbard, et al. 2016). Assessment of the contributions of synchronous and asynchronous release at the neuromuscular junction was done in a manner similar to that described in Wen et al. (2010). Time windows for synchronous events were, however, individually calibrated (between 10 – 15 ms from the start of the blue-light pulse) to each muscle cell, as some trains of pulses resulted in a progressive increase in the delay to trigger an action potential, (likely due to kinetic properties of channelrhodopsin proteins (Lin et al. 2009)), observed as a delay in EPC onset. Data are reported as mean ± SD. Kruskal-Wallis test with Dunn's multiple comparisons test and one-way ANOVA with Tukey's multiple comparisons test were used to compare non-parametric and parametric data sets, respectively. Two-way repeated measures ANOVA with Tukey's test for multiple comparisons was used to compare EPC amplitude across stimulus time and between treatment groups (**Fig. 2.3 & Fig. 2.5**).

2.4 RESULTS

2.4.1 Frequency of miniature end-plate currents increased in syt2 KD fish

We chose to generate *syt2* morpholino knock-down (KD) fish using the *1020:Gal4;UAS:ChR2(H134)-mCherry* line (**Fig. 2.1**) specifically due to the fact that NMJ function in *syt2* KD fish has already been described (Wen et al. 2010). This has facilitated direct comparisons with Wen et al. (2010)'s data to validate our proposed optogenetic approach to assess NMJ function. A key characteristic of neuromuscular junction function in *syt2* KD fish is the increase in the occurrence of spontaneous miniature end-plate currents (mEPCs) recorded in fast muscle fibers innervated by CaP motoneurons, as described previously by Wen & Brehm (Wen et al. 2010). We first assessed the frequency of mEPCs (**Fig. 2.2*A*-C**) and found that the number of spontaneous mEPCs generated in ventral fast muscle fibers in our *syt2* KD fish was significantly increased compared to controls (**Fig. 2.2*E***; uninjected control: 0.08271 ± 0.09527 events/s; control MO: 0.1621 ± 0.2377 events/s; *syt2* KD : 1.822 ± 1.719 events/s), confirming successful knock-down of *syt2*. We also assessed whether there were any differences in the mean normalized amplitude (normalized to the maximum amplitude found in each individual muscle cell) of these spontaneous end-plate currents and found only a significant decrease in *syt2* KD fish compared to uninjected control fish but not control MO fish (**Fig. 2.2*D***; uninjected control: 0.3934 ± 0.1375; control MO: 0.3476 ± 0.1515; *syt2* KD : 0.3047 ± 0.1060).

2.4.2 Short blue light pulses effectively stimulate motoneurons to evoke EPCs recorded from muscle fibers

We next sought to determine whether short pulses of blue light were successful in exciting CaP motoneurons. We delivered 5 ms blue light pulses (480 nm) over approximately one spinal segment and found this to be sufficient to evoke an EPC in recorded ventral fast muscle fibers (**Fig. 2.3**). To quantify the amplitude of evoked EPCs, we delivered five 5 ms blue-light pulses with a 52-second inter-pulse delay and took the average amplitude of the EPCs evoked (**Fig. 2.3*A-D***). When assessing the amplitude of the EPCs across blue-light pulses, we found no significant effect of the pulse number ($P = 0.5383$), nor did we find a significant effect of the treatment groups ($P = 0.6538$) (**Fig. 2.3*E*)**. We next utilized the mean EPC amplitude to estimate release properties at the NMJ. We found a significant decrease in the estimate of quantal content in *syt2* KD fish compared to both uninjected control and control MO groups (uninjected: 6.00 ± 4.56; control MO: 9.08 ± 11.03; *syt2* KD: 3.27 ± 2.88). On the other hand, we observed no effects to estimates of number of release sites (uninjected: 12.33 ± 10.11; control MO: 12.38 ± 13.25; *syt2* KD: 5.62 ± 4.08) or release probability (uninjected: 0.6421 ± 0.2536; control MO: 0.7451 ± 0.1970; *syt2* KD: 0.6615 ± 0.2713).

2.4.3 Using optogenetic stimulation to assess steady-state depression at the neuromuscular junction

We next wanted to determine whether optogenetic motoneuron stimulation could provide us insight into assessment of steady-state depression at the NMJ, as is done with electrical motoneuron stimulation (Wen, Hubbard, et al. 2016). While Wen et al. did not assess steady-state depression in *syt2* KD fish in their work (Wen et al. 2010), we deemed it useful to assess the feasibility of assessing steady-state depression with this optogenetic approach. Similarly to Wen et al. (2016), to assess steady-state depression, we introduced thirty 5-ms blue light pulses

delivered at a frequency of 20 Hz (**Fig. 2.4**). We find no significant difference in the level of steady-state depression between groups (**Fig. 2.4*D***; uninjected: 0.5230 ± 0.3168; control MO: 0.7184 ± 0.2687; *syt2* KD: 0.5918 ± 0.3170). We did however notice that *syt2* KD fish had more instances where optogenetic stimulation during the 20 Hz stimulation failed to evoke an EPC in the fast muscle fiber. We find only a significant increase in the percentage of failures to elicit an EPC in *syt2* KD fish when compared to the control MO fish but not the uninjected fish (**Fig. 2.4*E***; uninjected: 9.33 ± 10.56 %; control MO: 3.75 ± 8.25 %; *syt2* KD: 16.47 ± 17.18 %). Additionally, we tested higher frequencies of optogenetic stimulation including 50 Hz and 100 Hz (data not shown) but found that these are both too high to reliably excite motoneurons given the temporal properties of channelrhodopsin proteins (Lin et al. 2009). These data demonstrate that optogenetic stimulation at 20 Hz is successful and may be used to assess steady-state depression in other zebrafish models of CMS.

2.4.4 Using optogenetic stimulation to assess contributions of synchronous and asynchronous release at the neuromuscular junction

We next assessed contributions of synchronous and asynchronous release using our optogenetic approach to motoneuron stimulation (**Fig. 2.5**). Synchronous neurotransmitter release induced by the membrane depolarization from action potentials invading the NMJ release gives way to asynchronous release, which is not synchronous with incoming action potentials, during periods of high frequency activity. This asynchronous release is caused by leftover increased levels of calcium in between high frequency action potentials and is thought to help sustain transmitter release during high frequency firing (Kaeser and Regehr 2014). Synchronous release at the neuromuscular junction in *syt2* KD fish has already been assessed using electrical stimulation of

CaP motoneurons during whole-cell patch-clamping experiments (Wen et al. 2010). We can therefore compare our optogenetic motoneuron stimulation approach to their electrical stimulation. Wen et al. (2010) evaluated the effect of *syt2* KD on synchronous versus asynchronous release at the NMJ by electrically stimulating the CaP motoneuron at a frequency of 100 Hz for 10 seconds. Given the temporal constraints of our ChR2 line, we had to modify the stimulation protocol described in Wen et al. (2010) and deliver 5-ms blue-light pulses at a frequency of 20 Hz instead of 100 Hz for 10 seconds (**Fig. 2.5*A*)**. As expected, we found a significantly lower contribution of normalized asynchronous release compared to normalized synchronous release in uninjected, control MO, and *syt2* KD groups (**Fig. 2.5*B*)** while finding no significant differences in both total synchronous and asynchronous release across groups (**Fig. 2.5*C&G*;** uninjected synchronous release: 5.995 ± 2.954; control MO synchronous release: 5.963 ± 2.143; *syt2* KD synchronous release: 5.866 ± 1.613; uninjected asynchronous release: 1.317 ± 1.847; control MO asynchronous release: 1.208 ± 1.455; *syt2* KD asynchronous release: 2.393 ± 1.787). Next, when comparing the fraction of synchronous release over total release, we found no significant difference between groups (**Fig. 2.5*D***; uninjected: 0.793 ± 0.199; control MO: 0.829 ± 0.191; *syt2* KD: 0.733 ± 0.135). We also found no significant differences in total asynchronous fractional release between groups (**Fig. 2.5*G***; uninjected: 0.207 ± 0.199; control MO: 0.171 ± 0.191; *syt2* KD: 0.267 ± 0.135). When comparing synchronous fractional release in the first second of stimulation, no significant differences were found between groups (**Fig. 2.5*E***; uninjected: 0.113 ± 0.052; control MO: 0.130 ± 0.046; *syt2* KD: 0.127 ± 0.080). This was also the case when comparing asynchronous release during the first second of stimulation (**Fig. 2.5*I***; uninjected: 0.019 ± 0.020; control MO: 0.025 ± 0.036; *syt2* KD: 0.014 ± 0.014). As the contributions of asynchronous release typically increase with prolonged high-frequency stimulation, we next compared fractional release during the last

second of stimulation. We found no significant effects to synchronous fractional release during the last second of stimulation between groups (**Fig. 2.5*F***; uninjected: 0.066 ± 0.045; control MO: 0.066 ± 0.037; *syt2* KD: 0.063 ± 0.023); however, we did find a significant overall effect of the treatment groups while post-hoc multiple comparison tests failed to reveal significant differences between groups when comparing fractional asynchronous release in the last second (**Fig. 2.5*J***; uninjected: 0.024 ± 0.022; control MO: 0.020 ± 0.021; *syt2* KD: 0.051 ± 0.027). Finally, while stimulation time had a significant decreasing effect overall on mean area under the curve (AUC) corresponding to synchronous release, no significant differences in synchronous release were revealed during any other stimulation bins (i.e. seconds 2-9) both within and across treatment groups (**Fig. 2.5*K***). For asynchronous release, we found a significant increase in mean AUC corresponding to asynchronous release between seconds 5 and 6 compared to second 10 in *syt2* KD animals (*syt2* KD 5-second bin: 0.023 ± 0.012; *syt2* KD 6-second bin: 0.020 ± 0.005; *syt2* KD 10-second bin: 0.045 ± 0.028) (**Fig. 2.5*L***).

2.5 DISCUSSION

In this study, we generated *syt2* morpholino knock downs in 1020:Gal4;UAS:ChR2(H134)-mCherry (Antinucci et al., 2020; Wyart et al., 2009) fish to investigate an optogenetic approach to motoneuron activation for the assessment of locomotor and NMJ function in the screening of novel CMS gene candidates. We chose *syt2* as is it a known CMS gene and deficits to the NMJ when *syt2* is knocked down have been previously described (Wen et al. 2010), facilitating validation of our optogenetic approach. We found that while optogenetic motoneuron activation has its limitations, it may prove to be a useful tool for the rapid screening of novel CMS genes, a process that typically requires impressive yet challenging electrophysiology techniques (Wen and Brehm 2010b).

2.5.1 The use of 1020:Gal4;UAS:ChR2(H134)-mCherry fish to optogenetically stimulate motoneurons

In this zebrafish line, ChR2 proteins have been shown to be expressed in spinal interneurons as well as motoneurons (Antinucci et al. 2020; Wyart, Bene, et al. 2009). Additionally, upon blue light stimulation, 1020:Gal4;UAS:ChR2(H134)-mCherry fish can produce locomotion (Wyart, Bene, et al. 2009). The ability to use blue light to trigger locomotion for the assessment of locomotor function as well as to trigger motoneuron excitation for the assessment of NMJ function rendered the use of this line extremely favorable to our goal. Indeed, this line has been used previously to excite motoneurons while performing patch-clamp electrophysiology in skeletal muscle to investigate calcium channel contributions (Wen et al. 2020). While 1020:Gal4;UAS:ChR2(H134)-mCherry embryos were heterogeneous in both the neurons expressing ChR2 as well as in the levels of ChR2 expressed (**Fig 2.1**), we focused our data

collection to fish expressing the highest levels of ChR2. Nevertheless, EPCs recorded from muscle fibers were variable from fish to fish, likely a result of the endogenous variability in ChR2 expression locations and levels.

2.5.2 Interpretation of endplate dynamics with our optogenetic approach

Defects to NMJ function in *syt2* knockdown fish described previously by Wen et al. (2010) were done by investigating the NMJ of caudal primary (CaP) motoneurons to fast ventral muscle fibers. In contrast, our optogenetic stimulation is not limited to the CaP motoneuron. It is important to note that while restriction of optogenetic excitation to individual motoneurons can be performed with advanced microscopy techniques such as two-photon microscopy, we illuminated entire spinal segments within which were located the motoneurons innervating the targeted muscle fiber. It is therefore likely that recorded endplate currents in the ventral fast muscle fibers include signal transmission from the CaP motoneuron as well as secondary motoneurons that innervate this ventral-most quadrant of musculature due to the polyneuronal innervation of individual muscle fibers found in zebrafish (Bello-Rojas et al. 2019; Wen et al. 2020; Westerfield, McMurray, and Eisen 1986). In fact, according to Wen and colleagues (2020), the 1020:Gal4;UAS:ChR2(H134)-mCherry line may express ChR2 mostly in secondary motoneurons (Wen et al. 2020), though we have observed frequent expression in primary motoneurons. Our data may therefore more accurately represent population level EPCs rather than purely CaP-associated EPCs investigated by Wen et al., 2010.

Furthermore, our full-segment blue light excitation approach inevitably excites any spinal interneurons expressing ChR2 as well. Indeed, we notice instances of doublet and triplet EPCs

generated in response to our optogenetic stimulation. These are likely a result of polysynaptic motoneuron activation while the first EPC generated with short latency could be a summation of multiple EPCs from more than one motoneuron. Regardless of the nature of the EPCs (whether single motoneuron driven or population driven), this approach effectively stimulates motoneurons for assessment of NMJ function, though it is imperative that interpretations of the results take into consideration these factors.

While our measures of estimated number of release sites fell within the normal range for controls, our estimates of quantal content and release probability fell below their respective averages as it relates to the CaP motoneuron (Wen, Hubbard, et al. 2016). Motoneuron population driven EPCs likely lead to increased variability in the amplitude of recorded EPCs. There is also the possibility that our optogenetic approach mainly activated secondary motoneurons at the exclusion of CaP motoneurons. As mentioned above, 1020:Gal4;UAS:ChR2(H134)-mCherry fish may exhibit ChR2 expression predominantly in sMNs. The lower release probability and quantal content released from sMNs when compared to pMNs (Wen et al. 2020) could explain our own lower estimates of these measures of neurotransmission. While we found visual evidence of that CaP motoneuron express ChR2 through mCherry expression, it is possible that optogenetic stimulation proves less effective in depolarizing the larger primary motoneuron to threshold (Srinivasan et al. 2018). Whichever the level of optogenetic CaP motoneuron activation, this level may be consistent enough across treatment groups that comparisons to controls are still able to reveal differences in properties of population-level signal transmission.

The observed decreased in quantal content in *syt2* KD fish is in line with *syt2* knock down studies in mice that demonstrate a reduction in endplate potential (EPP) amplitude as well as quantal content (Pang et al. 2006). Concurrently, *syt2* KD in zebrafish demonstrate a reduction in the magnitude of synchronous compared to controls (Wen et al. 2010). This supports that while population EPCs or EPCs lacking contribution from the CaP motoneuron are likely to make up the dataset using our approach, important differences between *syt2* KD and control fish can indeed be identified.

2.5.3 Temporal constraints linked to channelrhodopsin kinetics

Channelrhodopsin proteins are associated with known temporal constraints given the kinetic properties of opsins (Zamani et al. 2017). The reliability of optogenetics to excite motoneurons (measured as a resultant EPC in skeletal muscle) when using a 5-ms blue light pulse was increased compared to a 1-ms pulse during 20 Hz stimulation trains (see **Supplemental Figure 2.1**). This is likely caused by a combined effect of insufficient cation influx during a period of 1-ms channel opening as well as variable expression levels of ChR2. If expression levels of ChR2 in motoneurons are relatively low, a 1-ms blue light pulse may not allow sufficient cation influx to reach spike threshold while a 5-ms permits greater activation of ChR2.

High frequency stimulation protocols are important to the study of signal transmission, shedding light onto features of synaptic release, facilitation, and depression using common protocols that include the paired-pulse ratio as well as high frequency stimulation trains. While the Brehm lab did not assess the effects of *syt2* knockdown on steady-state depression, we chose to do so to elucidate the use of optogenetic stimulation at high frequencies for NMJ function assessment.

Previous work by the Brehm lab successfully stimulated the CaP motoneuron at 20, 50, and 100 Hz using electrical stimulation to assess steady-state depression occurring at the NMJ (Wen, Hubbard, et al. 2016). We were unable to stimulate motoneurons optogenetically at 50 Hz nor 100 Hz (data not shown) but had success with 20 Hz. This is in line with known temporal constraints of ChR2 proteins permitting reliable high frequency stimulation up to 30 Hz (Boyden et al. 2005). Interestingly, levels of steady-state depression observed in controls in response to optogenetic motoneuron stimulation are lower compared to electrical stimulation delivered at 20 Hz to CaP motoneurons (Wen, Hubbard, et al. 2016). This confounding result speaks to the likelihood of secondary motoneuron activation alone or in conjunction with CaP motoneuron within a spinal segment. Neurotransmitter release from sMNs shows facilitation in response to repetitive stimulation as opposed to synaptic fatigue exhibited by pMNs (Wen et al. 2020).

Wen et al. (2010) investigated the role of *syt2* to synchronous versus asynchronous release at the NMJ (Wen et al. 2010). Their stimulation protocol consisted of a 100 Hz train lasting 10 seconds. Direct comparisons between our optogenetic approach to excite motoneurons with their data was not possible as optogenetic stimulation at 100 Hz cannot be achieved. We chose instead to deliver a 20 Hz train of 5-ms blue light pulses over the course of 10 seconds. While we did indeed see the apparition of asynchronous events towards the end of the 10 second stimulation protocol, it is unclear whether 20 Hz for this length of time is sufficient to fully capture asynchronous versus synchronous contributions. Previous work reveals that during 10-s 100 Hz stimulation, synchronous release rapidly declines as asynchronous release rapidly increases within the first few seconds of stimulation (Wen et al. 2010). Contributions from synchronous release continue to decline and those from asynchronous release begin declining mid-way through the stimulation

protocol (Wen et al. 2010). With our 10-s 20 Hz optogenetic stimulation protocol, we observe a steady yet modest decrease in contributions from synchronous release with a similarly steady yet modest increase in asynchronous events throughout the stimulation protocol. Lower frequency stimulation is likely to be less effective at depleting vesicle stores, making it harder to investigate effects to synchronous release. The lower frequency of our stimulation protocol is also likely to be behind the failure to notice a sharp increase in asynchronous events early within the stimulation window – 20 Hz stimulation may be ineffective in prolonging the inter-spike raises in intracellular calcium levels that trigger asynchronous release. It is possible that lower train rates may require longer stimulation durations that have not been tested in this study. Furthermore, while the CaP motoneuron exhibits a high probability of release, that of sMNs is significantly lower (Wen et al. 2020) meaning their synchronous versus asynchronous release profiles over the same time course of stimulation would not resemble the profile observed for the primary CaP motoneuron.

2.5.4 Advantages associated with optogenetically assessing NMJ function

Traditional studies of NMJ function by electrical stimulation of individual motoneurons and recording evoked EPCs in innervated muscle fibers provide important insights into individual neuromuscular connections. While single synapse studies are imperative to the understanding of individual protein contributions to signal transmission across the NMJ, our population level approach for NMJ function assessment is more representative of the neuromuscular system in action during movement production, especially considering that motoneurons are polyneuronally innervated in zebrafish (Bello-Rojas et al. 2019; Wen et al. 2020; Westerfield et al. 1986), the optogenetic approach employed here serves as a valuable complement to traditional NMJ studies by investigating a physiologically relevant link between behaviour and NMJ function through

population-evoked EPCs. The findings in this study will be crucial to interpreting ongoing work from the Lochmüller lab utilizing optogenetic stimulation to assess deficits to locomotor movement in *syt2* KD fish (data not shown).

The necessity of patch-clamping a single cell rather than concurrent patch-clamping of two cells make our optogenetic approach less technically challenging, thereby facilitating higher throughput for screening CMS gene candidates. Indeed, we started testing the function of the NMJ in synaptotagmin-11b (*syt11b*) knockdown fish (**Supplemental Figure 2.2**). *syt11b* is involved in vesicle trafficking (Shimojo et al. 2019; Trovò et al. 2024) and was identified as a possible gene candidate for a patient portraying CMS symptoms that remained without a molecular CMS diagnosis by the Lochmüller lab (data unavailable). However, further parental genetic testing revealed that it was impossible for *syt11b* to have been the genetic cause. We therefore terminated experiments looking into *syt11b* at this point. Nonetheless, these experiments serve as a steppingstone for the implementation of optogenetics to rapidly yet effectively assess NMJ function in future CMS gene candidate knockdown experiments.

This approach also offers flexibility to the assessment of NMJ function. While we chose to stimulate motoneurons within one segment of the spinal cord, one could choose to stimulate over more spinal segments or restrict excitation to individual motoneurons. Furthermore, the generation of fast genetically encoded calcium indicators restricted to muscle fibers could be utilized in conjunction with optogenetic activation of motoneurons like that described in this study for an increasingly less technically challenging method for NMJ function assessment, albeit bearing its own set of limitations.

2.5.5 Concluding remarks

The optogenetic approach described in this study to excite motoneurons using the 1020:Gal4;UAS:ChR2(H134)-mCherry line effectively reveals important differences in *syt2* KD fish described previously, though with some discrepancies due to both the nature of optogenetics as well as our method of stimulation. Keeping these limitations in mind, our results support our approach as a potentially useful, relatively facile, and high throughput means to screen for gene candidates underlying genetically undiagnosed cases of CMS.

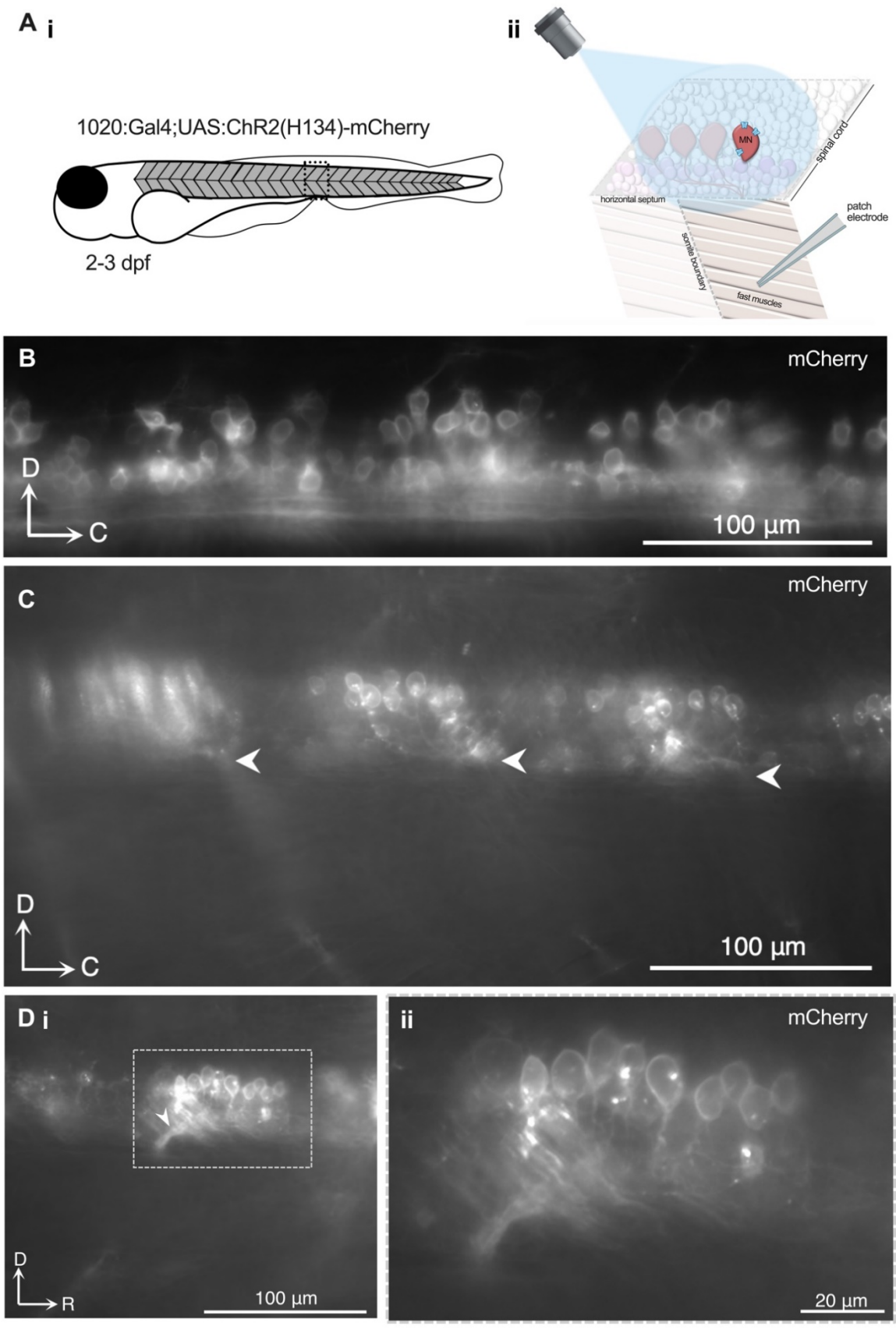
A i
1020:Gal4;UAS:ChR2(H134)-mCherry
2-3 dpf
ii
MN
spinal cord
horizontal septum
patch electrode
somite boundary
fast muscles
B
mCherry
D
C
100 µm
C
mCherry
D
C
100 µm
D i
D
R
100 µm
ii
mCherry
20 µm

Figure 2.1. Channelrhodopsin expression restricted to spinal interneurons and motoneurons in 1020:Gal4;UAS:ChR2(H134)-mCherry fish. ***A***, Schematic oversimplification of experimental setup wherein 480 nm optogenetic excitation is delivered to an entire spinal segment within which reside the motoneurons innervating the patch-clamped fast muscle fiber. ***B***-***D***, Example images taken from 3 individual transgenic zebrafish to show variability of channelrhodopsin (mCherry) expression. ***B***, Image of the spinal cord containing mCherry-positive spinal neurons in a 2 dpf zebrafish. ***C***, Image of the spinal cord containing mCherry-positive spinal neurons and dorsal-most section of the ventral musculature where motoneuron axons are present in a 4 dpf zebrafish. ***D,*** Image of the spinal cord containing mCherry-positive spinal neurons and dorsal-most section of the ventral musculature in a different 4 dpf zebrafish from ***C***. Boxed area (*i*) is enlarged in (*ii*). Arrow heads are pointing to ventral roots containing motoneuron axons that exit the spinal cord to innervate muscles. MN: motoneuron.

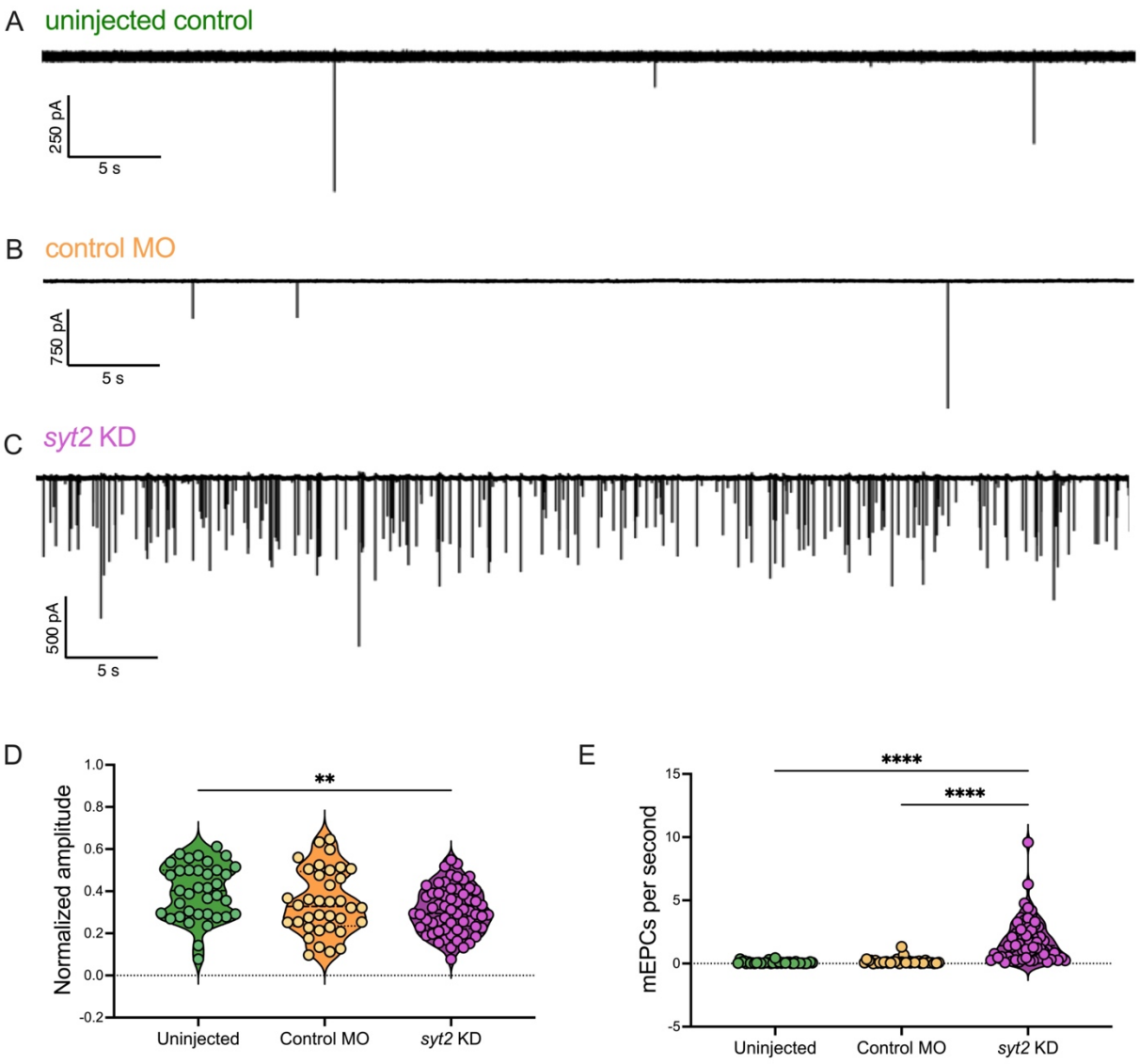
A uninjected control
250 pA
5 s
B control MO
750 pA
5 s
C syt2 KD
500 pA
5 s
D
Normalized amplitude
1.0
0.8
0.6
0.4
0.2
0.0
-0.2
**
Uninjected
Control MO
syt2 KD
E
mEPCs per second
15
10
5
0
-5
****
****
Uninjected
Control MO
syt2 KD

Figure 2.2. Spontaneous miniature end-plate currents affected in *syt2* KD fish. ***A,*** Representative trace of spontaneous mEPCs recorded from a ventral fast muscle fiber of an uninjected control fish ($n = 37$; $N = 21$). ***B,*** Representative trace of spontaneous mEPCs recorded from a ventral fast muscle fiber of a control MO fish ($n = 36$; $N = 17$). ***C,*** Representative trace of spontaneous mEPCs recorded from a ventral fast muscle fiber of a *syt2* KD fish ($n = 61$; $N = 28$). ***D,*** Mean normalized amplitude of spontaneous mEPCs (uninjected versus control MO: $P = 0.2014$; uninjected versus *syt2* KD: $P = 0.0035$; control MO versus *syt2* KD: $P = 0.7174$). ***E,*** Number of spontaneous mEPCs recorded per second (uninjected versus control MO: $P = 0.3829$; uninjected versus *syt2* KD: $P < 0.0001$; control MO versus *syt2* KD: $P < 0.0001$). *Statistical analysis,* Kruskal-Wallis test with Dunn's multiple comparisons test. ** $P < 0.005$; **** $P < 0.0001$; otherwise not statistically significant.

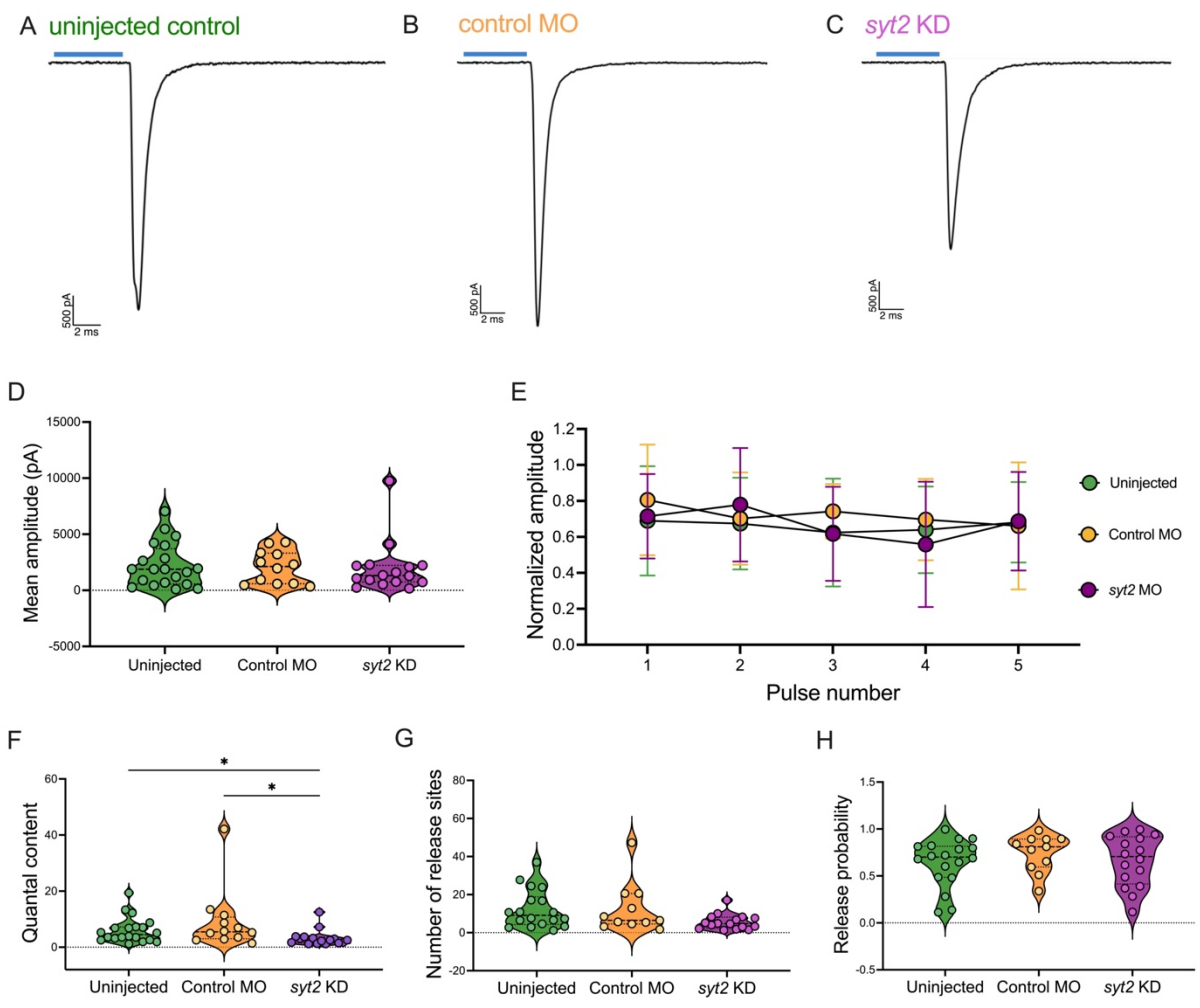
A uninjected control
B control MO
C syt2 KD
500 pA
2 ms
D
Mean amplitude (pA)
15000
10000
5000
0
-5000
Uninjected
Control MO
syt2 KD
E
Normalized amplitude
1.2
1.0
0.8
0.6
0.4
0.2
0.0
1
2
3
4
5
Pulse number
Uninjected
Control MO
syt2 MO
F
Quantal content
60
40
20
0
*
*
Uninjected
Control MO
syt2 KD
G
Number of release sites
80
60
40
20
0
-20
Uninjected
Control MO
syt2 KD
H
Release probability
1.5
1.0
0.5
0.0
-0.5
Uninjected
Control MO
syt2 KD

Figure 2.3. Optogenetic activation of motoneurons evokes EPCs in fast muscle fibers. ***A-C*** Representative traces of evoked end-plate currents recorded from ventral fast muscle fibers in response to a 5-ms blue light pulse in uninjected (***A***; $n = 20$; $N = 11$), control MO (***B***; $n = 12$; $N = 7$), and *syt2* KD (***C***; $n = 16$; $N = 10$) fish. ***D***, Mean amplitude of evoked EPCs (uninjected versus control MO: $P > 0.9999$; uninjected versus *syt2* KD: $P > 0.9999$; control MO versus *syt2* KD: $P > 0.9999$). ***E***, Normalized amplitude of the evoked EPCs across the five successive blue light pulses delivered (pulse number effect: $P = 0.5385$; group effect: $P = 0.6538$). ***F***, Estimated quantal content (uninjected versus control MO: $P > 0.9999$; uninjected versus *syt2* KD: $P = 0.0459$; control MO versus *syt2* KD: $P = 0.0300$). ***G***, Estimated number of release sites (uninjected versus control MO: $P > 0.9999$; uninjected versus *syt2* KD: $P = 0.1042$; control MO versus *syt2* KD: $P = 0.3693$). ***H***, Estimated release probability (uninjected versus control MO: $P > 0.9999$; uninjected versus *syt2* KD: $P > 0.9999$; control MO versus *syt2* KD: $P > 0.9999$). *Statistical analysis,* Kruskal-Wallis test with Dunn's test for multiple comparisons (***D, F-H***); Two-way repeated measures ANOVA with Tukey's test for multiple comparisons (***E***); * $P < 0.05$; otherwise, not statistically significant.

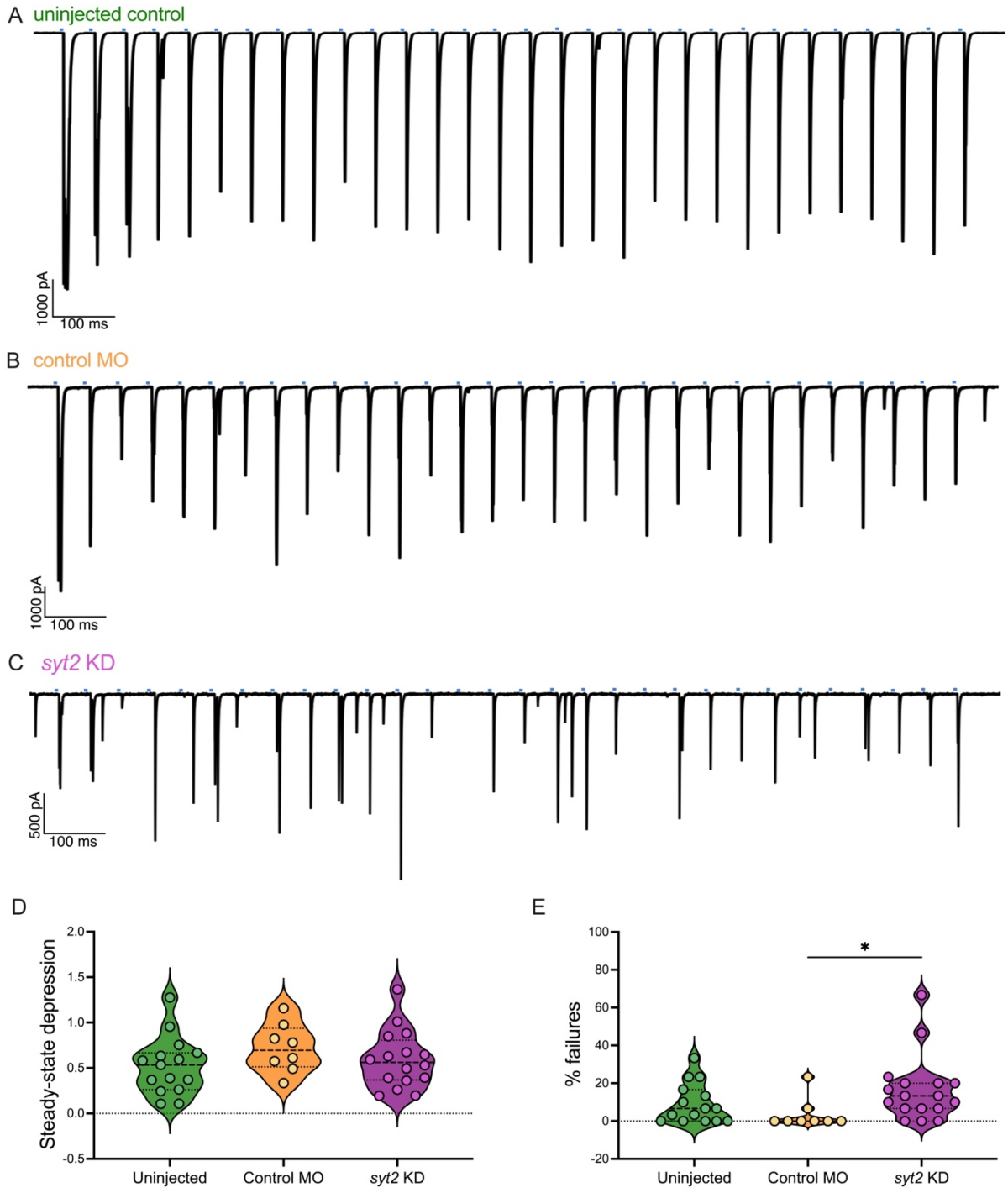
A uninjected control
1000 pA
100 ms
B control MO
1000 pA
100 ms
C syt2 KD
500 pA
100 ms
D
Steady-state depression
2.0
1.5
1.0
0.5
0.0
-0.5
Uninjected
Control MO
syt2 KD
E
% failures
100
80
60
40
20
0
-20
*
Uninjected
Control MO
syt2 KD

Figure 2.4. Assessment of high frequency optogenetic motoneuron activation to estimate steady-state depression. ***A-C***, Representative traces of EPCs recorded from ventral fast muscle fibers elicited in response to thirty 5-ms pulses delivered at 20 Hz in uninjected (***A***; $n = 15$; $N = 10$), control MO (***B***; $n = 8$; $N = 5$), and *syt2* KD fish (***C***; $n = 17$; $N = 10$). ***D***, Measure of steady-state depression (uninjected versus control MO: $P = 0.3274$; uninjected versus *syt2* KD: $P = 0.8092$; control MO versus *syt2* KD: $P = 0.6136$). ***E***, Percentage of failures to evoke an EPC during the 20 Hz thirty pulse stimulus (uninjected versus control MO: $P = 0.4312$; uninjected versus *syt2* KD: $P = 0.6252$; control MO versus *syt2* KD: $P = 0.0340$). *Statistical analysis,* One-way ANOVA with Tukey's multiple comparisons test (***D***) and Kruskal-Wallis test with Dunn's test for multiple comparisons (***E***). * $P < 0.05$; otherwise, not statistically significant.

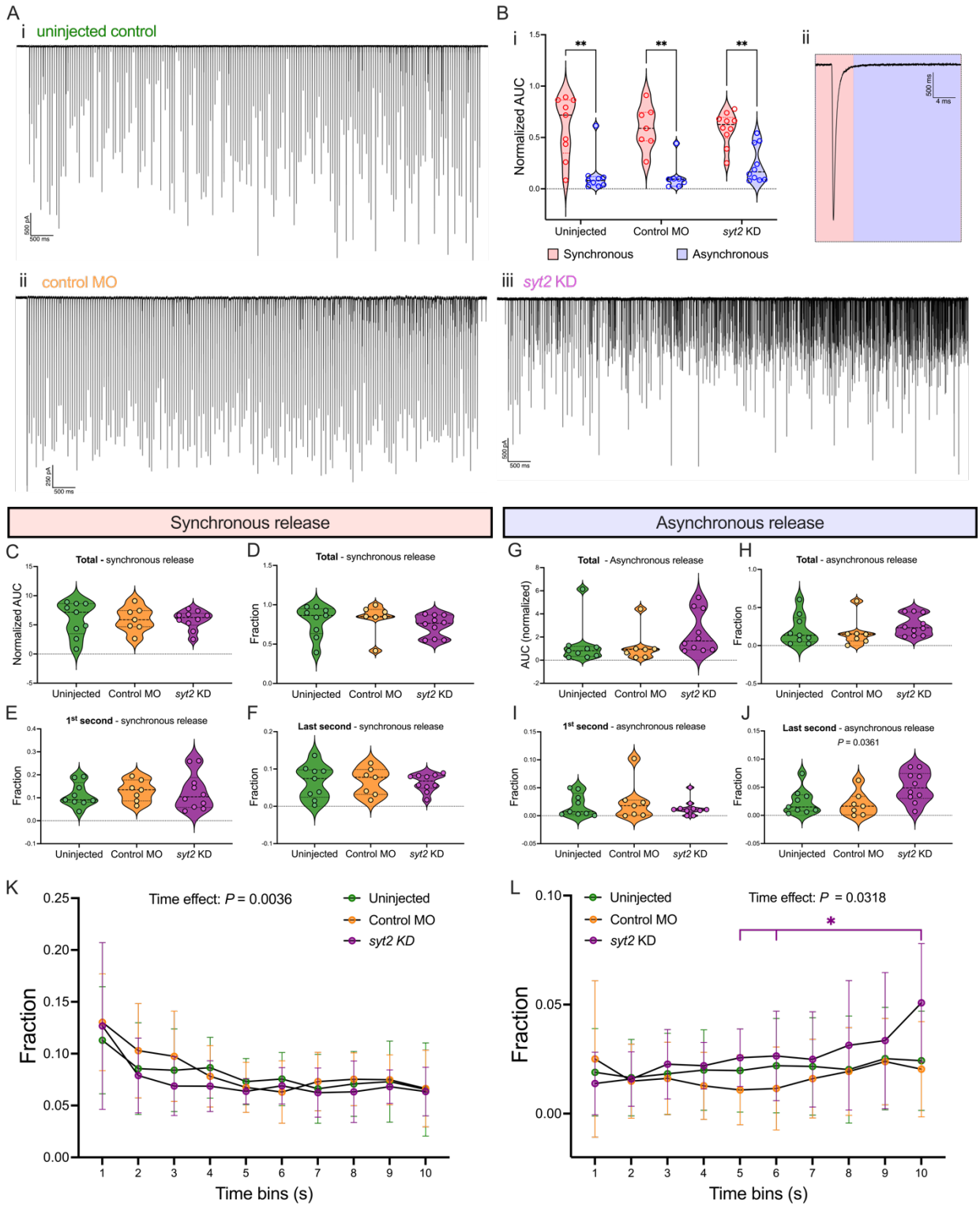
A
i uninjected control
ii control MO
iii syt2 KD
B
i
Normalized AUC
Uninjected
Control MO
syt2 KD
Synchronous
Asynchronous
ii
Synchronous release
Asynchronous release
C
Total - synchronous release
Normalized AUC
D
Total - synchronous release
Fraction
E
1st second - synchronous release
Fraction
F
Last second - synchronous release
Fraction
G
Total - Asynchronous release
AUC (normalized)
H
Total - asynchronous release
Fraction
I
1st second - asynchronous release
Fraction
J
Last second - asynchronous release
P = 0.0361
Fraction
K
Time effect: P = 0.0036
Uninjected
Control MO
syt2 KD
Fraction
Time bins (s)
L
Time effect: P = 0.0318
Uninjected
Control MO
syt2 KD
Fraction
Time bins (s)

Figure 2.5. Using optogenetic stimulation to assess contributions of synchronous and asynchronous release. ***A***, Representative traces of EPCs recorded from ventral fast muscle fibers during 10-s, 20 Hz stimulation of 5 ms blue light pulses in uninjected (***i***; $n = 9$; $N = 8$), control MO (**ii**; $n = 7$; $N = 5$), and *syt2* KD (**iii**; $n = 10$; $N = 8$). ***B***, Comparison of normalized area under the curve (AUC) of synchronous and asynchronous release within uninjected, control MO, and *syt2* KD groups (***i***) with synchronous versus asynchronous time distinctions in the right panel (***ii***). ***C***, Total normalized synchronous release (AUC) over the 10-s stimulation (uninjected versus control MO: $P > 0.9999$; uninjected versus *syt2* KD: $P > 0.9999$; control MO versus *syt2* KD: $P > 0.9999$). ***D***, Fraction of total release corresponding to synchronous release during the 10-second stimulation (uninjected versus control MO: $P > 0.9999$; uninjected versus *syt2* KD: $P > 0.9999$; control MO versus *syt2* KD: $P > 0.9999$). ***E***, Fraction of release corresponding to synchronous release during the 1st second of stimulation (uninjected versus control MO: $P > 0.9999$; uninjected versus *syt2* KD: $P > 0.9999$; control MO versus *syt2* KD; $P > 0.9999$). ***F***, Fraction of release corresponding to synchronous release during the last second of stimulation (uninjected versus control MO: $P > 0.9999$; uninjected versus *syt2* KD: $P > 0.9999$; control MO versus *syt2* KD: $P > 0.9999$). ***G***, Total normalized asynchronous release (AUC) over the 10-s stimulation (uninjected versus control MO: $P > 0.9999$; uninjected versus *syt2* KD: $P = 0.1271$; control MO versus *syt2* KD: $P = 0.2137$). ***H***, Fraction of total release corresponding to asynchronous release during the 10-s stimulation (uninjected versus control MO: $P > 0.9999$; uninjected versus *syt2* KD: $P = 0.8837$; control MO versus *syt2* KD: $P > 0.9999$). ***I***, Fraction of release corresponding to asynchronous release during the 1st second of stimulation (uninjected versus control MO: $P > 0.9999$; uninjected versus *syt2* KD: $P > 0.9999$; control MO versus *syt2* KD: $P > 0.9999$). ***J***, Fraction of release corresponding to asynchronous release during the last second of stimulation (uninjected versus control MO: $P >$

0.9999; uninjected versus *syt2* KD: $P = 0.1423$; control MO versus *syt2* KD: $P = 0.0558$). ***K***, Fractional synchronous release across 1-second time bins during the 10-s stimulation (treatment group effect: $P = 0.5686$). ***L***, Fractional asynchronous release across 1-second time bins during the 10-second stimulation (treatment group effect: $P = 0.5686$). *Statistical analysis,* Mann-Whitney tests (***B***), Kruskal-Wallis test with Dunn's test for multiple comparisons (***C-J***), and two-way ANOVA with Tukey's multiple comparisons test (***K-L***). * $P < 0.05$, ** $P < 0.01$; otherwise, not statistically significant.

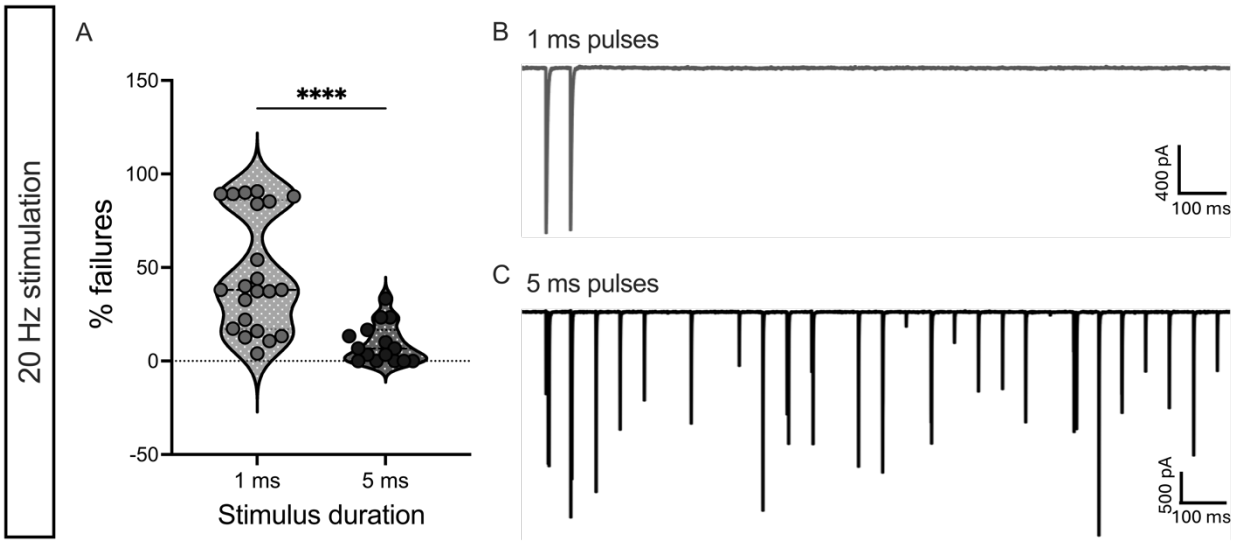
20 Hz stimulation
A
150
100
50
0
-50
% failures
****
1 ms
5 ms
Stimulus duration
B
1 ms pulses
400 pA
100 ms
C
5 ms pulses
500 pA
100 ms

Supplemental Figure 2.1. 1-ms optogenetic excitation proves unreliable to evoke end-plate currents in muscle fibers. ***A***, Percentage of failures observed during a stimulation train consisting of 30 pulses delivered at 20 Hz recorded from a control fast muscle fiber. ***B***, Example trace of EPCs recorded from a muscle fiber during corresponding spinal segment stimulation using 1 ms pulses. ***C***, Example trace of EPCs recorded from a muscle fiber during corresponding spinal segment stimulation using 5 ms pulses. *Statistical analysis,* two-tailed Mann-Whitney test. **** $P < 0.0001$.

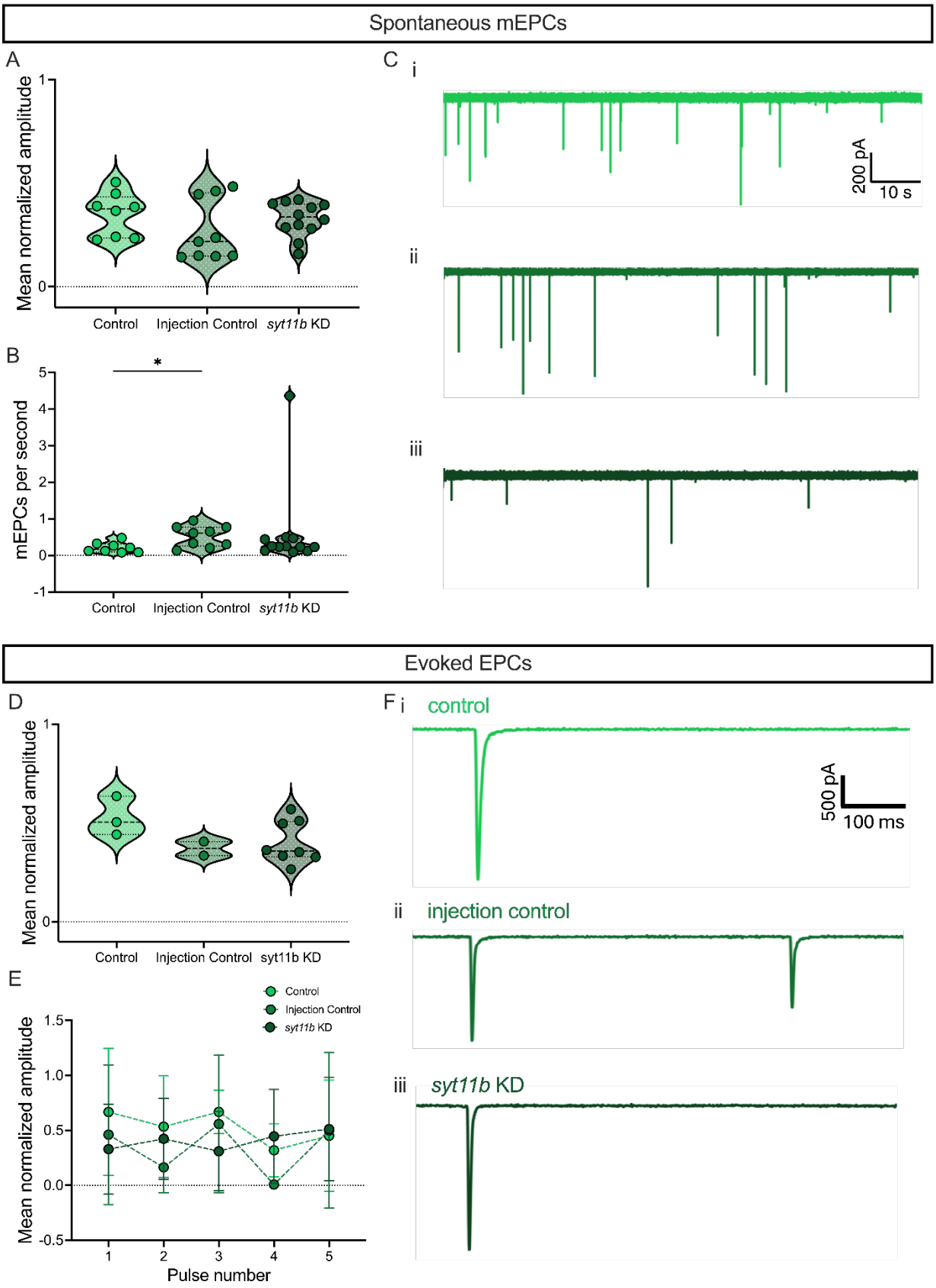
Spontaneous mEPCs
A
Mean normalized amplitude
1
0
Control
Injection Control
syt11b KD
B
*
mEPCs per second
5
4
3
2
1
0
-1
Control
Injection Control
syt11b KD
C
i
200 pA
10 s
ii
iii
Evoked EPCs
D
Mean normalized amplitude
1
0
Control
Injection Control
syt11b KD
E
Control
Injection Control
syt11b KD
Mean normalized amplitude
1.5
1.0
0.5
0.0
-0.5
1
2
3
4
5
Pulse number
F i
control
500 pA
100 ms
ii
injection control
iii
syt11b KD

Supplemental Figure 2.2. Preliminary neuromuscular junction function assessment in *syt11b* knockdown fish. ***A***, Mean normalized amplitude of spontaneous miniature end-plate currents (mEPCs) recorded from uninjected controls (n = 8; N = 2), injection controls (n = 9; N = 3), and *syt11b* KD fish (n = 12; N = 3). ***B***, Frequency of mEPCs. ***Ci-iii***, Examples traces of recordings from fast muscle fibers held at –50 mV in (***i***) uninjected control, (***ii***) injection control, and (***iii***) *syt11b* KD fish. ***D***, Mean normalized amplitude of EPCs evoked by five 5 ms blue light pulses separated by a 52 second inter-pulse interval. ***E***, Mean normalized amplitude of evoked EPCs across pulse number. ***F***, Examples of EPCs evoked by a 5 ms blue light pulse in (***i***) uninjected control, (***ii***) injection control, and (***iii***) *syt11b* KD fish. *Statistical analysis,* Kruskal-Wallis test with Dunn's test for multiple comparisons (***A***, ***B***, ***D***) and mixed-effects analysis (***E***). * $P < 0.05$; otherwise not statistically significant.

Chapter 3

Pharmacological modulation of the M-current shapes locomotor function in developing zebrafish

Gaudreau, SF & Bui, TV

Some of the data presented in this chapter appears in Gaudreau and Bui 2025 (*Journal of Neurophysiology)*, https://doi.org/10.1152/jn.00003.2025.

3.1 ABSTRACT

The M-current (I_M) is a non-inactivating potassium current that has been implicated in the control of locomotion in mammals, where it was shown to shape the rhythm governing locomotor movements. We tested whether I_M might also be involved in the control of locomotor movements in developing zebrafish. Specifically, we investigated the involvement of I_M in the execution of escape responses and swimming movement of zebrafish aged 4-5 days post-fertilization (dpf) using XE-991and ICA-069673, a pharmacological blocker and enhancer of I_M, respectively. We found that I_M may influence the number of swim bouts in an escape response but not the duration of the first bout nor its tail beat frequency. Enhancing I_M reduced the distance swam with slow or fast swimming maneuvers by freely behaving larval zebrafish. We then studied whether the I_M is involved in locomotor output by spinal circuits using various approaches to induce motor activity in spinalized 4-5 dpf zebrafish. We found that while modulating I_M during NMDA-evoked swimming activity had negligible effects, modulating I_M during swimming activity evoked by a generalized depolarization of the spinal cord affected specific swimming parameters. In particular,

XE-991 and ICA-069673 had opposite effects on overall spiking activity, swimming episode frequency and duration, and the number of bursts within each episode. In summary, I_M was found to be involved in certain facets of escape response and swimming in larval zebrafish, and some of this influence resides within the expression of this current in spinal circuits.

3.2 INTRODUCTION

The driving force of survival for most animals is the ability to move from one place to another. All locomotor behaviours – whether walking, swimming, or flying – rely on networks of neurons that translate motor commands or sensory input into locomotor maneuvers that propel the animal. In vertebrates, locomotion is mainly controlled by spinal locomotor circuits that produce intrinsically generated rhythmic activity to guide muscle contraction (Orlovsky, Grigori, Deliagina, T. G., and Grillner, Sten 2012). This ability of spinal locomotor circuits to be rhythmic is thought to be determined by 1) neuron firing behaviours, which are contingent on the different ionic currents flowing in and out of the neurons, as well as 2) the connectivity patterns between neurons (Friesen and Stent 1978). Ion currents contributing to rhythm generation are those involved in ramping up (inward depolarizing currents) or dampening (outward hyperpolarizing currents) excitability of the neuron for relatively prolonged periods thanks to their slower kinetics (i.e., activation, inactivation, and deactivation processes of the currents) (Harris-Warrick 2010). Currents contributing to rhythmogenesis of networks in a wide range of species have been identified.

Some currents, such as a persistent sodium current, have been identified in spinal locomotor circuits across many vertebrates. This persistent sodium current is important for rhythm generation and sustained neuron firing (Ramirez et al. 2011; Tazerart et al. 2008b; Zhong, Masino, and Harris-Warrick 2007). As locomotion is often characterized by bursts of neural activity of varying

durations based upon the demands of the locomotor maneuver, a potassium current, namely the slowly-activating, non-inactivating M-current (I_M), has been identified as a counterpoint to the persistent sodium current in the mammalian spinal cord (Verneuil et al. 2020b). I_M is a widely expressed potassium current (Marrion 1997) mediated by Kv7.2/7.3 channels (Wang et al. 1998). Spinal expression of I_M has been identified in spinal motoneurons of many vertebrates, including mice (Sharples et al. 2023; Verneuil et al. 2020b) , rattlesnakes (Bothe, Maximilian S. et al. 2024), turtles (Alaburda, Aidas et al. 2002) and in invertebrate motoneurons (Trimmer 1994). Together with the persistent current, I_M can precisely control rhythm and burst duration underlying rhythmic locomotor movements through expression in spinal neurons that control locomotion (Verneuil et al. 2020b).

In this study, we determine for the first time whether I_M plays a role in modulating locomotor behaviour in the developing larval zebrafish. Within less than a week of development, larval zebrafish can generate escape responses and spontaneous exploratory swimming behaviours (Saint-Amant and Drapeau 1998). We study whether pharmacological modulators of I_M modulate the escape response and swimming. We then use spinalized larval zebrafish preparations to determine whether pharmacological modulation of I_M exclusively in the spinal cord can modulate locomotor activity.

3.3 MATERIAL AND METHODS

3.3.1 Animal Care

All experiments were performed in accordance with the protocol approved by the University of Ottawa's Animal Care Committee (BL-4416). Adult zebrafish are maintained at 28.5°C with a 14 hour on/10 hour off light cycle, with lights off at 11PM and on at 9AM. Embryos are fertilized between 9AM-10AM and stored in embryo medium (system water with 0.1% methylene blue) at 28.5°C until used for experimentation at 4-5 days post-fertilization (dpf). Larvae with gross morphological defects were excluded. Assignment of animals to various experiments and treatment groups was done randomly.

3.3.2 Escape response

4-5 dpf fish were placed in wells of a 24-well plate (well diameter of 15.5 mm) in water. The sex of zebrafish at these early developmental stages could not be identified. The escape response was evoked using tactile stimuli applied by a tungsten wire touch of the head or the tail and recorded with an iPhone 14 at a 240 frames per second (fps) recording rate. Escape responses were analyzed using manual inspection of the video recordings.

3.3.3 Swimming behaviour

Swimming in freely behaving zebrafish was tested using the Zebrabox (Viewpoint Life Sciences). 4-5 dpf zebrafish were arrayed in a 24-well plate containing water and motor activity was recorded with a monochrome camera in 20-minute sessions. Video recordings were analyzed using Zebralab software (Tracking205-95W. Version 3,52,3,59). Parameters for detecting zebrafish movement were empirically defined to optimize detection of swimming movement with minimal false

positives. We categorized activity as inactive if swimming speed was lesser than 2mm/s, slow swimming if speed was between 2 and 10 mm/s, and fast if speed was above 10 mm/s.

3.3.4 Pharmacology

XE-991 (Millipore Sigma, X2254) and ICA-069673 (Millipore Sigma, SML1616) were dissolved in dimethyl sulfoxide (DMSO; final concentrations of DMSO did not exceed 0.06%) before dissolution to their final concentration of 10 μM in either water or artificial cerebrospinal fluid (aCSF). *N*-Methyl-*D*-aspartic acid (NMDA; Millipore Sigma, M3262) was dissolved in aCSF to its final concentration of 200 μM.

3.3.5 Preparation for electrophysiology

Larval zebrafish were anesthetized in 0.02% tricaine (MS-222, Aqualife TMS; Syndel Laboratories) before being pinned down through the notochord onto a Sylgard (Dow Corning) coated dish. Pins were made using tungsten wire (0.025 mm); one was placed caudally near the tip of the tail, and the other was placed rostrally near the center of the yolk sac. Spinalization was performed using fine surgical scissors at the level of segments 2-3. The skin was then peeled back between the two pins using fine forceps. Next, larvae were bathed in 1 mg/mL collagenase (Millipore Sigma, C7657; 15-minute incubation time). The collagenase solution was rinsed out 4-5 times with extracellular recording solution (see below). Muscle removal was performed using suction through a wide-bored glass capillary (typically, the tips are gently broken to get a sufficiently large tip for muscle removal). Only a few muscle fibers were removed at the level of the horizontal septum to expose the peripheral motor nerve for extracellular electrophysiology.

3.3.6 Electrophysiology recordings

Extracellular recording solution consisted of artificial cerebrospinal fluid (aCSF) containing: 134 mM NaCl, 2.9 mM KCl, 1.2 mM $MgCl_2$, 2.1 mM $CaCl_2$, 10 mM dextrose, and 10 mM HEPES, (pH of 7.8 adjusted with NaOH and osmolarity between 280-290 adjusted with sucrose). d-tubocurarine (10 µM; Millipore Sigma, catalog # 93750) was added to the aCSF to block muscle contractions. Borosilicate glass microelectrodes (outer diameter: 1.5 mm; inner diameter: 1.1 mm, Sutter Instruments, catalog #BF150-110-10) were backfilled with extracellular recording solution for extracellular nerve recordings. The peripheral motor nerve was targeted at the horizontal septum separating dorsal and ventral muscle somites. Light suction was applied. The signal was recorded in current clamp mode, amplified and filtered at 10 kHz with a Multiclamp 700B from Axon Instruments (Molecular Devices) and finally digitized with a Digidata 1550 (Molecular Devices). Recordings were made from mid-body somites located within 4 somites rostral and 4 somites caudal to the anal pore.

3.3.7 Analysis

All electrophysiological data was saved as .abf files. We used the open-source pyABF python package to import and read .abf files in Spyder (version 5.1.5). Analysis of recordings was semi-automated using Python (version 3.9.12, RRID:SCR_008394) scripts tailored to each recording to detect spikes, swimming episodes and bursts. We identified swimming episodes and bursts in our recordings by first smoothing the recordings using a moving average smoothing. Subsequently, episodes and bursts were identified as large deviations from baseline, lasting 80-2000 ms and 3-35 ms in duration, respectively. Statistical analysis was performed using Prism by GraphPad (Version 10.4.0 (527), RRID:SCR_002798). Data are reported as mean ± SD. We performed a power analysis using GraphPad with the following parameters for paired t-tests: Significance level

(alpha) = 0.05 (two-tailed); Target Power = 0.8; Standardized effect size = 1. The recommended group size from this analysis was 10 per group. Our sample sizes for most experiments were close to that recommendation.

The non-parametric two-tailed Wilcoxon matched-pairs signed rank test was used when comparing the means of two non-normally distributed matched paired data sets. Paired t-tests were used to compare the means of normally distributed data sets. Mann-Whitney tests and unpaired t-tests were used for non-normally distributed and normally distributed data sets, respectively. For all tests, significance is denoted by asterisks in figures.

3.4 RESULTS

3.4.1 Effect of I_M on escape responses in 4-5 dpf zebrafish

We first tested the role of I_M in the escape responses of 4-5 dpf larval zebrafish. Escape responses (**Fig. 3.1**) were evoked either by tactile stimuli applied to the head (n = 5 taps; N = 10 animals) or tail (n = 5 taps; N = 9-10 animals). Escape responses are characterized by an initial large-amplitude C-bend immediately followed by a swimming episode. In some escape responses, this first response can be followed by a rapid succession of swimming episodes separated by brief pauses. Pharmacological blockade of I_M by XE-991 had no effects on the number of swimming episodes per escape response, the duration of the first episode, nor the tail beat frequency within the first episode of escape responses evoked by either head or tail stimuli (**Fig. 3.1*B-D***). On the other hand, enhancing I_M by application of ICA-069673 reduced the number of escape responses evoked by tail but not head stimuli (**Fig. 3.1*E***). The duration and tail beat frequency of escape responses evoked by either form of stimuli were unaffected by ICA-069673 (**Fig. 3.1*F***). These data suggest that I_M plays a minimal role in the escape response though enhancement of the current could limit the overall length of escape responses to tail stimuli by limiting the number of swimming episodes.

3.4.2 Effect of I_M on swimming in 4-5 dpf zebrafish

We tested the swimming of freely behaving 4-5 dpf zebrafish when XE-991 or ICA-069673 was applied (**Fig. 3.2*A-B***). The activity was partitioned into inactive (locomotor movements with speeds below 2 mm/s including stationary epochs), slow (locomotor movements with speeds between 2-10 mm/s), and fast (locomotor movements with speeds above 10 mm/s) swimming. XE-991 did not affect the amount of swimming (**Fig. 3.2*C-E***) nor the distance travelled during slow, fast, or total swimming (**Fig. 3.2*F-H***). On the other hand, ICA-069673 decreased the amount

(quantified as ratio of time spent swimming over the 20-minute recording period) of fast swimming (control: 0.1736 ± 0.1474; ICA-069673: 0.0373 ± 0.0434) and total swimming (control: 0.4883 ± 0.2904; ICA-069673: 0.2586 ± 0.2146) while not affecting the amount of slow swimming (**Fig. 3.2*I-K***). The distance travelled via slow (control: 41.22 ± 25.27 cm/min; ICA-069673: 25.80 ± 22.69 cm/min) and fast swimming (control: 77.42 ± 73.60 cm/min; ICA-069673: 6.74 ± 7.92 cm/min), as well as the total distance (control: 118.60 ± 90.02 cm/min; ICA-069673: 32.53 ± 28.89 cm/min), were reduced by ICA-069673 with noticeably greater effect on distance travelled via fast swimming (**Fig. 3.2*L-N***). These results suggest that at a basal state, I_M does not affect swimming, but enhancement of this current can affect the amount of fast swimming and the overall distance of slow and fast swimming movements.

3.4.3 Pharmacological modulation of I_M results in modest changes to locomotion in intact larvae

Changes in overall swimming observed by pharmacological modulation of I_M in larval zebrafish could result from changes to specific features of locomotor behaviour such as frequency, duration of swimming episodes or the duration of the bursts that compose each episode. To determine how pharmacological modulation of I_M affected swimming through modulation of these features, locomotor activity from the motor nerves of larval zebrafish aged 4 or 5 dpf (n = 10) was first recorded before and after bath application of 10 μM XE-991 using motor nerve recordings (**Fig. 3.3*A***). The features of every detectable episode within a recording were analyzed to compare the locomotor activity of control episodes to that of swim episodes during inhibition of I_M by XE-991 (**Fig. 3.3*C-K***). Blocking I_M with XE-991 results in an increase in burst duration (**Fig. 3.3*F***) as well as a decrease in the inter-burst interval (**Fig. 3.3*I***) and increase in the variability of burst durations

within an episode (**Fig. 3.3*K***). Episode frequency and duration, the number of burst episodes and the frequency of bursts, inter-burst interval variability, and peak signal amplitude were unaltered by XE-991. On the other hand, enhancement of I_M by 10 μM ICA-069673 did not alter any of the analyzed features of locomotor activity significantly, other than resulting in an increase in the variability of the durations of bursts within an episode (**Fig. 3.3*K***). Considering the modest effects of pharmacological modulation of I_M to locomotor features, we posited that long recordings from motor nerves could be accompanied by time-related changes, time either directly influencing locomotor activity or it is influencing the quality of the recording and/or preparation. To this end, we analyzed the features of locomotion recorded from motor nerves of intact larval zebrafish for a 90-minute period. When we compared the features of the first, second, and third 30-minute time bins, we find no significant differences (**Supplemental Figure 3.1**). Therefore, we do not suspect there to be any confounding effects to the data caused by the length of recording time. The concentrations chosen were based on prior concentration testing during nerve recordings in intact larvae where 1 μM, 2.5 μM, 5 μM, and 10 μM were tested for both XE-991 (**Supplemental Figure 3.2**) and ICA-069673 (**Supplemental Figure 3.3**). In this intact preparation, pharmacological modulation of I_M can occur across all levels of the nervous system. We therefore wondered whether supraspinal effects to I_M may be masking effects to locomotor features brought on by changes to I_M occurring within the spinal cord itself.

3.4.4 Fictive locomotion is altered by pharmacological modulation of I_M

Given the central role of spinal locomotor circuits in locomotion, we next asked whether modulation of I_M in spinal circuits could affect motor output by performing electrophysiological recordings of swimming activity from motor nerves in larval zebrafish having undergone a

complete spinal cord transection just below the brainstem (Timothy D Wiggin et al. 2012). Swimming activity in the isolated spinal cord of larval zebrafish can be induced by adding NMDA to promote the excitability of spinal networks (McDearmid and Drapeau 2006). We first performed recordings of motor nerve activity in 4-5 dpf larval zebrafish following spinalization exposed to 200 μM NMDA (n = 26). Fictive locomotion that persisted long enough to subsequently introduce a modulator of I_M was seen only in five preparations. In these five preparations, 10 μM XE-991 was applied to the preparation after a few minutes of NMDA-evoked fictive locomotion and activity was recorded for several minutes following XE-991 application. There were no significant differences in any of the features of locomotion analyzed (**Fig. 3.4*A*-*H***).

In those spinal preparations where NMDA did not evoke fictive locomotion (**Fig. 3.4*I***), the addition of XE-991 seemed to increase overall activity recorded from the nerve (**Fig. 3.4*J***), quantified as an increase in peak amplitude, time-integral of the signal, number of spiking events, and standard deviation of the signal 30 seconds before and 30 seconds after drug application (**Fig. 3.4*K*-*N***). Thus, decreasing I_M in spinal circuits can increase motor output in certain conditions.

3.4.5 Pharmacological modulation of IM affects fictive locomotion evoked by an increase in extracellular K^+

The Mg^{2+} block of NMDA receptors endows the receptor current with a non-linear conductance that facilitates rhythmogenesis in spinal networks (Cowley et al. 2005). In the preceding experiments, exposure of the spinalized zebrafish spinal cord to 200 μM NMDA could create an environment for spinal circuits overwhelming other endogenous ion currents such that any changes to I_M were rendered imperceptible when recording network-wide activity from the motor nerve.

Therefore, we performed motor nerve recordings in spinalized larval zebrafish bathed in aCSF containing a higher concentration of potassium ions. With extracellular K^+ elevated to 11.6 mM, rhythmic activity was evoked. While the rhythmic activity was more variable than NMDA application, episodes of swimming consisting of multiple locomotor bursts were observable (**Fig. 3.5*A-B***). We proceeded to either block or enhance I_M while recording activity from motor nerves and analyzed effects on fictive locomotion (**Fig. 3.5*A-B***). There was no change in the peak signal amplitude (**Fig. 3.5*H***). However, XE-991 increased the spiking activity, whereas ICA-069673 greatly decreased it (**Fig. 3.5*C***). When examining the locomotor features of the motor output from elevated extracellular K^+ (**Fig. 3.5*D*, *E***), XE-991 increased the frequency and duration of locomotor episodes whereas ICA-069673 had a dampening effect on frequency and duration of locomotor episodes (**Fig. 3.5*F, G*).** Within episodes, XE-991 did not affect the frequency of bursts or the burst duration. However, it increased the number of bursts per episode, whereas ICA-069673 decreased the duration but did not affect the number of bursts per episode or the frequency of bursts (**Fig. 3.5*I-K***). To summarize, in spinalized preparations where rhythmic activity was evoked by a generalized depolarization of the membrane potential, reducing I_M increased spiking activity as well as the frequency and duration of locomotor episodes, and the number of bursts per episode, while enhancing I_M had opposite effects on the same locomotor parameters in addition to a decrease in the duration of motor bursts.

3.5 DISCUSSION

The M-current (I_M) is a slowly activating, non-inactivating potassium current mediated by Kv7 channels. I_M can be activated at subthreshold membrane potentials and is known to dampen neuron excitability (Marrion 1997) and limit sustained firing through spike frequency adaptation (Benda and Herz 2003; Madison and Nicoll 1984) in neurons in which it is expressed. I_M expression has been found in spinal circuits of several vertebrates (Alaburda, Aidas et al. 2002; Bothe, Maximilian S. et al. 2024; Sharples et al. 2023; Verneuil et al. 2020b). Only recently has I_M been revealed for the first time as a major player in limiting bursting activity in spinal neurons involved in rodent locomotion (Verneuil et al. 2020b). Until now, the involvement of I_M in shaping the locomotor function of zebrafish remained uninvestigated.

3.5.1 The M-current and escape responses

We first assessed a possible role for I_M in shaping locomotion using behavioural assays, starting with its role in the execution of the escape response, a primitive reflexive movement. We found that pharmacological modulation of I_M does not alter the duration, nor the tail beat frequency produced during the first episode of the escape response. The lack of effect on duration and tail beat frequency is in line with the notion that the escape response is a robust behaviour. In fact, it has been shown that modulating the kinematics of the escape response does not impact the survival of larval zebrafish (Nair et al. 2017). It is therefore possible that the influence of I_M on neuronal excitability is too subtle to influence such a robust primitive reflex when the descending activation of spinal circuits is strong.

While pharmacological modulation of I_M had no noticeable effects on the initial phase of the escape responses, effects were observed on the swimming episodes that followed the initial phase. Indeed, enhancement of I_M by ICA-069673 resulted in a reduction in the average number of episodes produced during tail but not head touch-evoked escape responses. The swimming episodes that succeed the initial C-bend triggered by the Mauthner cell (M-cell) in response to startling auditive stimuli have been shown to involve a feedforward excitation of the midbrain nucleus of the Medial Longitudinal Fasciculus (nMLF) by brainstem Cranial Relay Neurons (CRN) (Xu, Lulu et al. 2021). The nMLF is composed of spinally-projecting neurons that have been implicated with the control of swim posture and swimming in zebrafish (Berg et al. 2023; Thiele, Donovan, and Baier 2014). The reduced number of swimming episodes during tail touch-evoked escape responses following ICA-069673 administration speaks to the possible expression of I_M at the level of the CRN, the nMLF or in downstream spinal neurons.

The lack of effect of ICA-069673 in response to head touch-evoked responses may be linked to the cells that trigger tail versus head touch-evoked responses. Escape responses can be classified based on the reticulospinal neurons activated by the aversive sensory stimulus: those initiated by the Mauthner cell (M-cell) and those initiated by M-cell homologs (Kohashi, Tsunehiko and Oda, Yoichi 2008). It has been demonstrated that whereas tail stimulation requires the M-cells, the activity of M-cells is not critical to responses evoked by head stimuli and non-M-cell homologs can mediate head-evoked escape responses (Kohashi, Tsunehiko and Oda, Yoichi 2008; Liu and Fetcho 1999; Liu and Hale 2017; O'Malley, Kao, and Fetcho 1996). In both cases, the M-cell or M-cell homologs will activate, putatively in the case of the M-cell homologs (Gahtan and O'Malley 2003), contralateral spinal motoneurons to initiate a large amplitude C-bend (Fetcho and

Faber 1988), followed by successive left-right alternating tail beats and possible multiple swimming episodes. A notable difference between the M-cell and M-cell homologs is that the former responds to stimuli with a single spike whereas the latter respond with tonic firing (Nakayama and Oda 2004). While the swimming episodes of escape responses mediated by the M-cell have been shown to involve the feedforward excitation of nMLF by CRN neurons (Xu, Lulu et al. 2021), the involvement of this circuit in non-M-cell escape responses by M-cell homologs remains to be confirmed. However, assuming that both M-cells and M-cell homologs employ the same circuitry, the lack of effects of ICA-069673 on the head-touch evoked escape responses, putatively mediated by M-cell homologs, may be linked to their longer-lasting firing responses as compared to the single spiking evoked in M-cells during tail-touch evoked escape responses.

Inhibition of I_M by XE-991 did not alter the number of episodes produced during escape responses evoked by head or touch stimuli. We propose that the drive to spinal circuits during escape responses may be so strong that any increase in excitability of spinal neurons caused by inhibition of I_M by XE-991 fails to result in noticeable effects. Alternatively, the baseline of I_M may be relatively low such that inhibiting it further by application of XE-991 does not significantly alter the excitability of the neurons in which I_M is expressed.

3.5.2 I_M and free swimming in larval zebrafish

Similar to the escape responses, we found that inhibition of I_M did not affect slow, fast, or total spontaneous swimming produced by larval zebrafish (**Fig. 3.2**). Enhancing I_M, on the other hand, resulted in a reduction in both distance swam and amount of time spent swimming, notably at fast

speeds. Effects observed with ICA-069673 but not XE-991 on spontaneous swimming in freely behaving larval zebrafish are in line with a possible low baseline expression of I_M. Furthermore, larger effects observed with ICA-069673 on fast swimming than on slow swimming suggest that the magnitude of I_M expressed in neurons of faster swim circuits is higher than that of slower swim circuits.

3.5.3 Nerve recordings in intact larval zebrafish preparations

Our extracellular motor nerve recordings in intact larval zebrafish showed few effects to locomotor features during pharmacological modulation of I_M. XE-991 increased the duration of motor bursts and decreased the inter-burst interval. Both XE-991 and ICA-069673 increased the variability of motor burst durations with no other effects from ICA-069673. These results are peculiar for two main reasons: 1) bath application of XE-991 in both the context of assessing escape responses and free-swimming had no effects to measured features of each locomotor behaviour and 2) bath application of ICA-069673 significantly reduced the amount swam during escapes and overall free-swimming. Based on these results, we had expected to see more prominent effects of enhancing I_M by ICA-069673 with subtle effects of inhibiting I_M by XE-991, especially considering the possibility of low baseline expression of I_M. The cause of these discrepancies is likely to stem from the way in which swimming was triggered in these preparations. Zebrafish larvae at ages 4-5 dpf used in this study can swim spontaneously or in response to changes in light intensity (Buss and Drapeau 2001). Both of these swims were present in the swimming activity we recorded from motor nerves, as has been done in previous studies (Buss and Drapeau 2001; McLean and Fetcho 2009; Roussel et al. 2020; Timothy D. Wiggin et al. 2012). However, changes in illumination may in fact trigger an escape response (Colwill and Creton 2011; Emran, Rihel,

and Dowling 2008), rather than low frequency swims similar to those that occur spontaneously. It is likely that unequal proportions of spontaneous and light-evoked swimming were included both within individual zebrafish before and after drug administration as well as across individuals, as the light-induced swimming was evoked most frequently in fish with less spontaneous swimming activity. Uneven contributions of spontaneous and light-evoked swimming, which are inherently different locomotor movements, to the data set would confound our generalized interpretation of the effects of our pharmacological agents to locomotion.

3.5.4 NMDA-evoked fictive locomotion

NMDA successfully evoked consistent fictive locomotion in only five spinalized preparations out of a total of thirty-one (**Fig. 3.4**). A final concentration of 200 μM of NMDA was chosen on the basis that increasingly high concentrations of NMDA leads to increasingly episodic swimming activity more closely resembling spontaneous beat-and-glide locomotion compared to lower concentrations (Timothy D Wiggin et al. 2012). Why exactly NMDA evoked fictive locomotion in only a small number of preparations remains unclear. Nevertheless, in the few that did display fictive locomotion, we found no effects of inhibiting I_M with XE-991 on any features of fictive locomotion analyzed. On the other hand, in the twenty-six preparations wherein no consistent fictive locomotion was evoked, we found that adding 10 μM XE-991 increased overall activity recorded from the motor nerve, supporting the presence of I_M in spinal circuits. We posited that exogenous application of NMDA (200 μM) might provide such a strong rhythmogenic drive to spinal circuits that any changes to I_M were rendered imperceptible when recording network-wide activity from the motor nerve. Specifically, the inward flow of cations through persistently active NMDA receptors could overpower changes to outward potassium ion flow via Kv7.2/7.3 channels.

Furthermore, activation of NMDA receptors has been implicated in modifying the activity of voltage-gated ion channels (Scott F. Davis and Linn 2003; S. F. Davis and Linn 2003). The lack of effect on NMDA-induced locomotion by XE-991 could, therefore, be caused by NMDA-induced changes to voltage-dependent properties of I_M. Indeed, NMDA has been shown to suppress I_M in rat amygdala neurons (Zhang et al. 2022).

3.5.5 Effects of modulating I_M during swimming evoked by high extracellular K+

Due to possible confounding factors brought on by NMDA-evoked fictive locomotion, we also tested the effects of pharmacologically modulating I_M on fictive locomotion evoked by a generalized depolarization of spinal circuits through elevated extracellular potassium and the resulting depolarization of the potassium equilibrium potential (**Fig. 3.5**). It is important to note that though fictive locomotion was successfully evoked by increasing the extracellular potassium concentration to four times the typical concentration, the activity produced was variable both within preparations and across individuals. Both persistent or sporadic swimming activity could occur in each preparation. We, therefore, mainly focused on within-episode analyses. In these experiments, we found that XE-991 and ICA-069673 had opposing effects on episode frequency and episode duration, while ICA-069673 but not XE-991, affected burst duration. In every one of these locomotor parameters, blocking I_M increased locomotor activity, while ICA-069673 reduced locomotor activity. The more inconsistent swimming activity evoked by elevated extracellular K^+ concentration prevented an assessment of how pharmacological modulation of I_M alters the pattern of locomotion.

3.5.6 Basal levels of I_M in larval zebrafish motor circuits

While XE-991 was effective at shaping locomotor activity in the experiments where we induced a generalized depolarization across spinal neurons (**Fig. 3.5**), we found that XE-991 had little effect on the escape response (**Fig. 3.1**) and spontaneous swimming (**Fig. 3.2**). Thus, blocking I_M seemed to be unmasked only in experiments where we raised the basal activation of I_M through generalized depolarization of spinal neurons. ICA-069673, on the other hand, decreased the overall number of swimming episodes during escape (**Fig. 3.1**)**,** spontaneous swimming (**Fig. 3.2**), and fictive locomotion in spinalized animals (**Fig. 3.5**). These results suggest that I_M is present in larval zebrafish motor circuits but possibly at low basal levels, similarly to what has been concluded for immature murine spinal motoneurons (Lombardo, Joseph and Harrington, Melissa A. 2016). Neuromodulatory increases of I_M could thus act to increase its amplitude to produce hypoactivity (Kurennyi, Chen, and Smith 1997; Madamba, Schweitzer, and Siggins 1999a, 1999b; Moore et al. 1988, 1994; Schweitzer, Madamba, and Siggins 1990; Sims et al. 1990; Sims, Singer, and Walsh 1988; Yu 1995).

3.5.7 Role of I_M in spinal circuits for locomotion across vertebrates

Interestingly, pharmacological modulation of I_M does not alter the locomotor frequency, as is shown to be the case in rodent locomotion (Verneuil et al. 2020b). Instead, we find that the involvement of I_M is restricted to influencing the duration of swimming episodes and the duration of bursts within individual episodes. These results reveal that although I_M's involvement in spinal locomotor circuit activity is conserved in zebrafish and mice, the precise role it plays may not be. Verneuil et al. demonstrate that Kv7.2/7.3 channels are ubiquitously expressed across mouse spinal locomotor circuit neurons (Verneuil et al. 2020b). Therefore, I_M is able to exert a level of control over the speed of rodent locomotion by limiting the duration of time spinal locomotor neurons

spend bursting, ultimately leading to faster muscle contraction (Verneuil et al. 2020b). Considering the differences in how I_M shapes locomotor activity in rodents versus zebrafish, it remains to be seen whether larval zebrafish spinal locomotor neurons similarly display ubiquitous expression of I_M as observed in mice. Our data reveal that burst duration is significantly decreased while locomotor frequency remains unaltered during I_M activation. This suggests that higher-order interneurons most involved in rhythm generation either do not express I_M or express I_M at relatively low magnitudes. In contrast, lower-order spinal neurons, such as motoneurons, involved in fine-tuning motor output may be more greatly influenced by I_M.

3.5.8 Conclusion

Our data reveal a role for I_M in influencing locomotor function within spinal circuits of larval zebrafish. Specifically, we show that pharmacologically modulating I_M alters the amount of locomotor activity produced, both during behavioural assays and fictive locomotor preparations. We demonstrate that modulation of I_M within spinal circuits controls episode and burst durations without affecting locomotor frequency or amplitude. This work highlights the differences in the involvement of I_M in locomotor function between larval zebrafish and rodents (Verneuil et al. 2020b). Studying how I_M could be neuromodulated (Brown and Adams 1980) could provide insights into the physiological states in which this current could induce hypoactivity of spinal circuits. For example, the M-current has been implicated in arousal and sleep stability in hypothalamic circuits (Li et al. 2022). Determining where within spinal locomotor circuits I_M is expressed will further elucidate how exactly I_M controls specific features of locomotion in various physiological states.

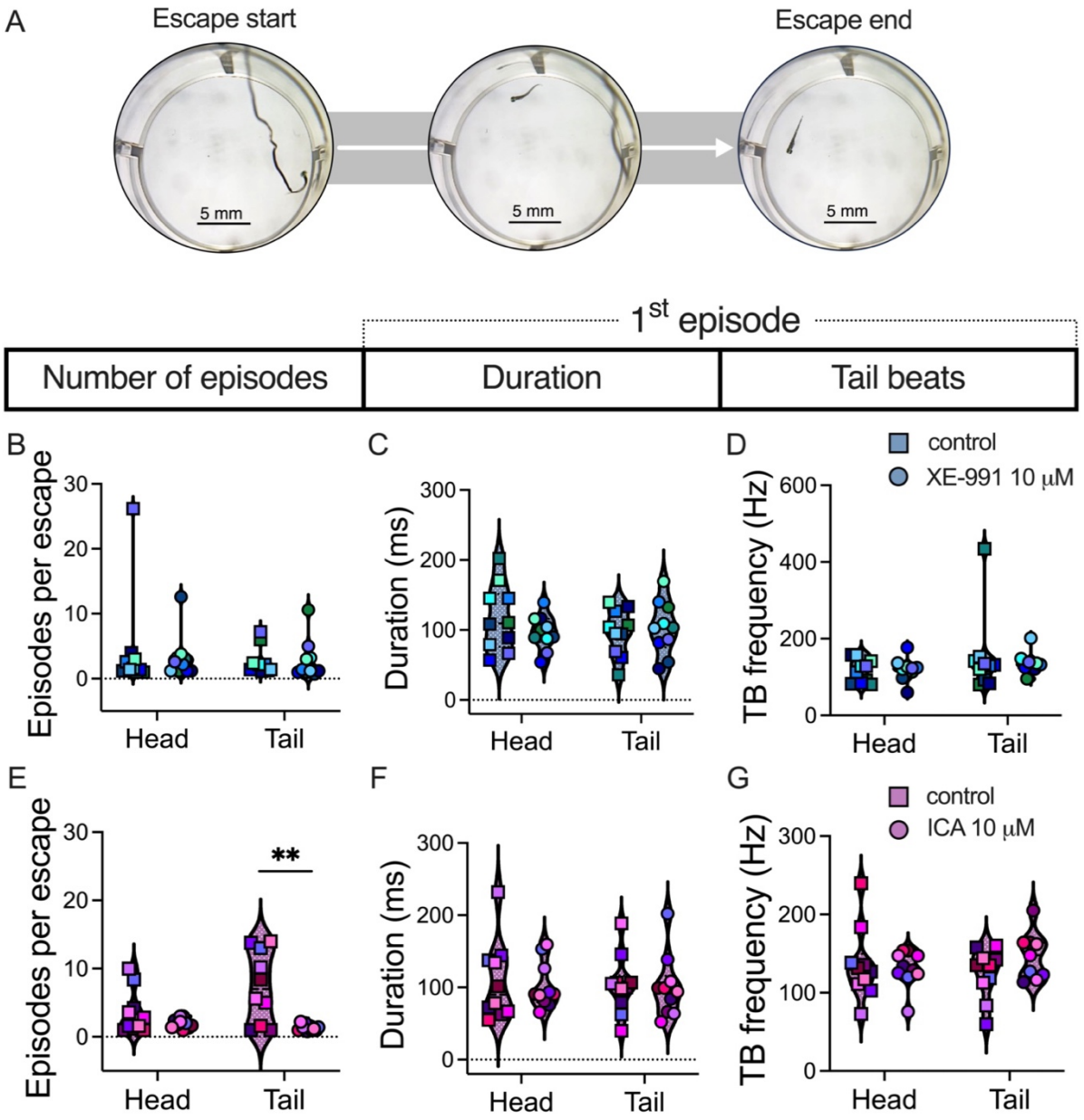
A
Escape start
Escape end
5 mm
5 mm
5 mm
1st episode
Number of episodes
Duration
Tail beats
B
Episodes per escape
Head
Tail
C
Duration (ms)
D
control
XE-991 10 μM
TB frequency (Hz)
E
**
F
G
ICA 10 μM

Figure 3.1. Effects of pharmacological modulation of I_M on the escape response. ***A,*** Overview of touch-evoked escape behaviours of individual 4-5 dpf larvae placed in a well from a 24-well plate. ***B & E,*** Average number of swim episodes produced during a head or tail touch-evoked escape response before and after bath application of 10 μM XE-991 (***B***; n = 10 per group; head: P = 0.9219; tail: P = 0.7480) or 10 μM ICA-069673 (ICA) (***E***; n = 10 per group; head: P = 0.2617). ***C & F,*** Average duration of the first episode produced during a head or tail touch-evoked escape response before and after bath application of 10 μM XE-991 (***C***; n = 10 per group; head: P = 0.1934; tail: P = 0.3750) or 10 μM ICA-069673 (***F***; n = 10 per group; head: P = 0.6953; tail: P = 0.3652). ***D & G,*** Average tail beat frequency of the first episode produced during a head or tail touch-evoked escape response before and after bath application of 10 μM XE-991 (***D***; n =10 per group; head: P = 0.6953; tail: P = 0.1934) or 10 μM ICA-069673 (***G***; head (n = 10): P > 0.9999; tail (n = 9): P = 0.1562). Individual animals before and after drug application are color-matched. *Statistical analysis,* Wilcoxon matched-pairs test; **P < 0.01, otherwise not statistically significant.

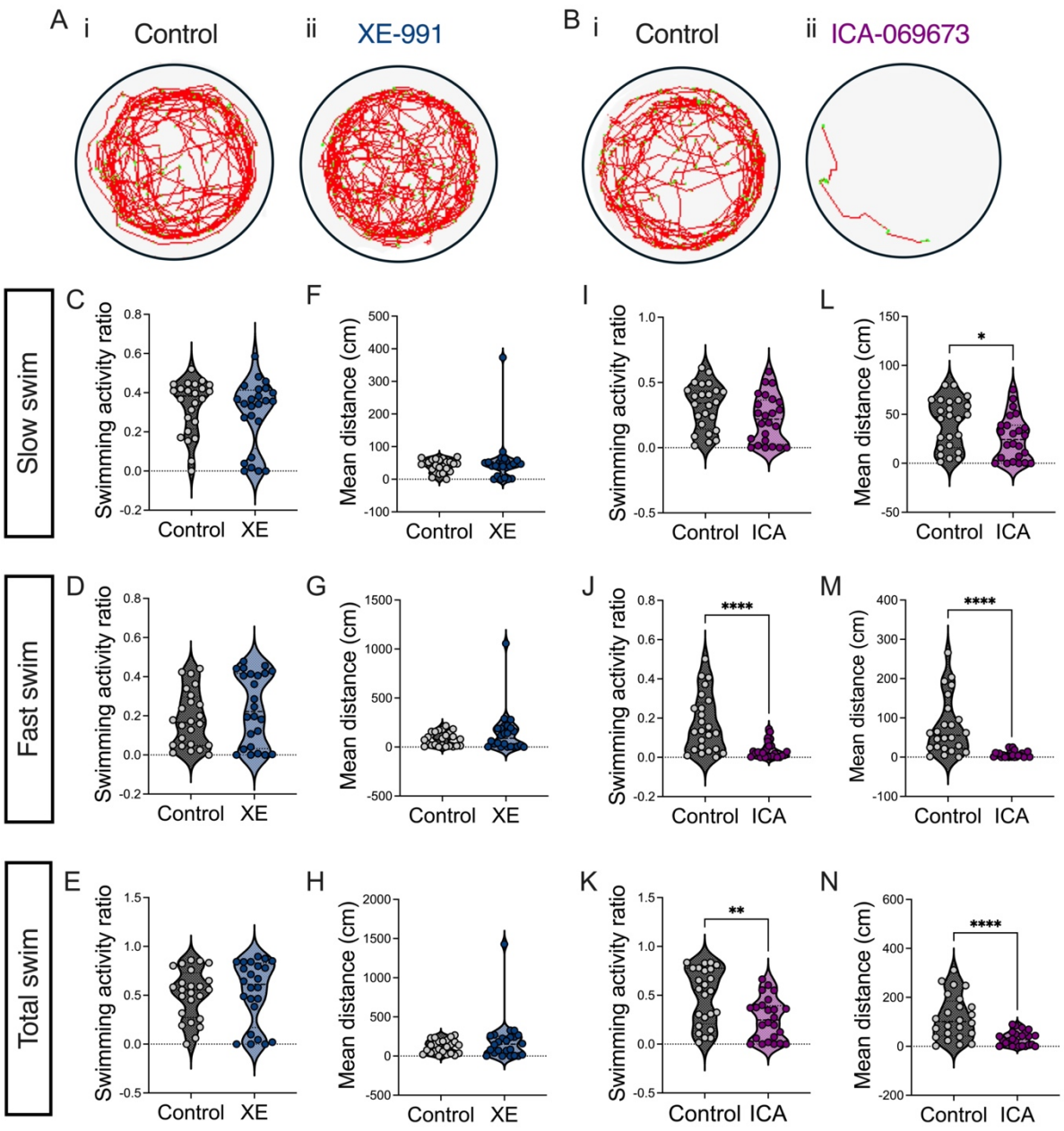
A i Control
ii XE-991
B i Control
ii ICA-069673
Slow swim
Fast swim
Total swim
C
D
E
F
G
H
I
J
K
L
M
N
Swimming activity ratio
Mean distance (cm)
Control
XE
ICA
*
**
****

Figure 3.2. Pharmacological enhancement of I_M reduces spontaneous swimming activity in larval zebrafish. ***A,*** Representative traces of total swimming activity from individual larvae recorded over five minutes from (*i*) control and (*ii*) XE-991 (XE) groups tested concurrently. ***B,*** Representative traces of total swimming activity from individual larvae recorded over five minutes from (*i*) control and (*ii*) ICA-069673 (ICA) groups tested concurrently. ***C-E,*** Effects of pharmacological inhibition of I_M by 10 μM XE-991 on amount of slow (***C***; 2-10 mm/s; $P = 0.3434$), fast (***D***; > 10 mm/s; $P = 0.3983$), and total (***E***; $P = 0.6639$**)** spontaneous swimming activity recorded over 20 minutes. ***F-H***, Effects of pharmacological inhibition of I_M by 10 μM XE-991 on average distance swam per minute during slow (***F***; $P = 0.8340$)**,** fast (***G***; $P = 0.4581$), and total spontaneous swimming (***H***; $P = 0.4707$*).* ***I-K***, Effects of pharmacological enhancement of I_M by 10 μM ICA-069673 on amount of slow (***I***; $P = 0.0794$) fast (***J***), and total (***K*****)** spontaneous swimming activity recorded over 20 minutes. ***L-N***, Effects of pharmacological enhancement of I_M by 10 μM ICA-069673 on average distance swam per minute during slow (***L*****),** fast (***M***), and total spontaneous swimming (***N****). Statistical analysis*, Mann-Whitney test for non-normally distributed data sets and unpaired t-tests for normally distributed data sets. * $P < 0.05$; ** $P < 0.01$; **** $P < 0.0001$; otherwise not statistically significant.

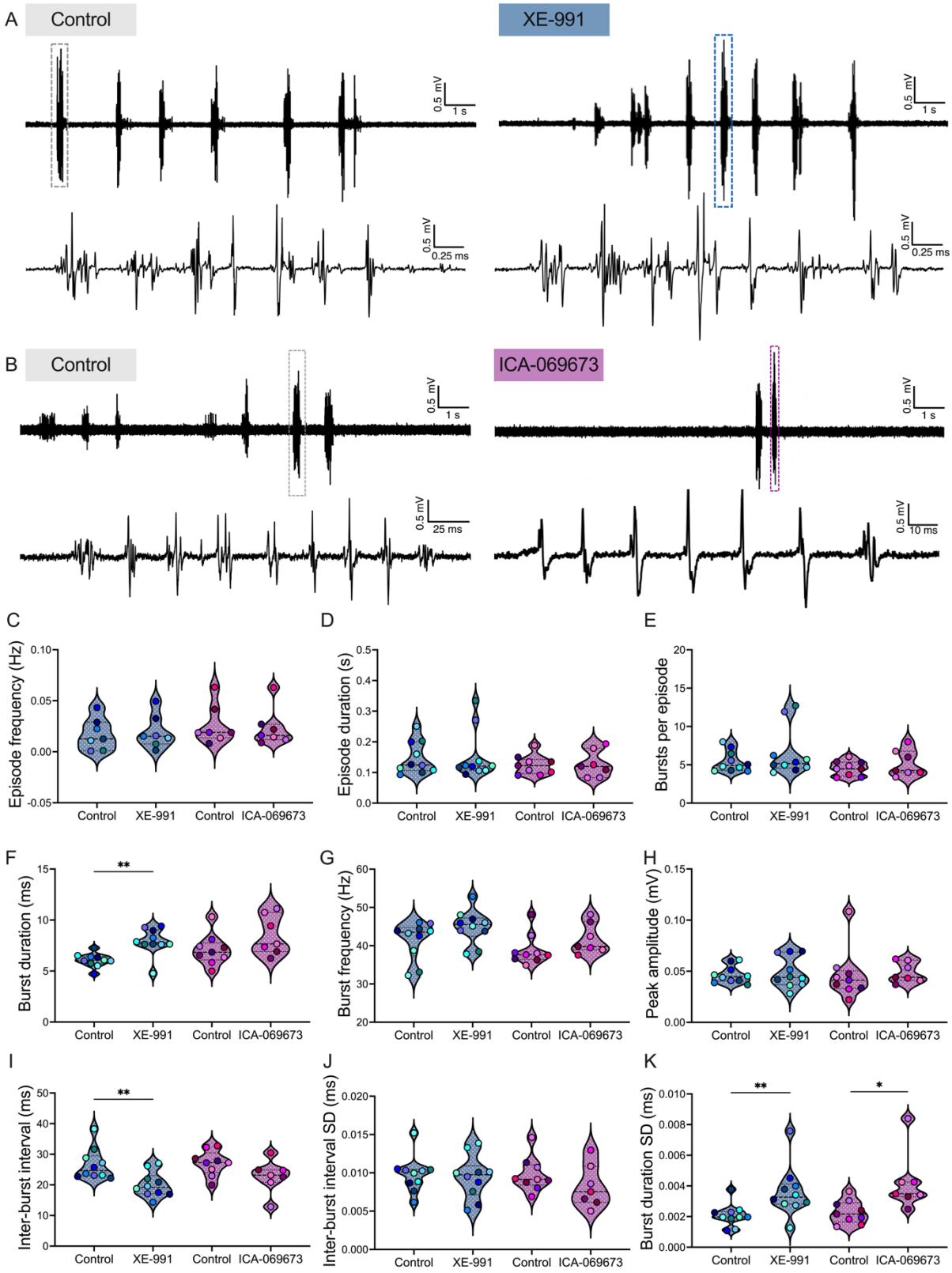
A
Control
XE-991
0.5 mV
1 s
0.25 ms
B
Control
ICA-069673
25 ms
10 ms
C
Episode frequency (Hz)
D
Episode duration (s)
E
Bursts per episode
F
Burst duration (ms)
**
G
Burst frequency (Hz)
H
Peak amplitude (mV)
I
Inter-burst interval (ms)
J
Inter-burst interval SD (ms)
K
Burst duration SD (ms)
*
Control
XE-991
Control
ICA-069673

Figure 3.3. Pharmacological modulation of I_M affects motor bursts during 4-5 dpf larval zebrafish locomotor activity. Activity from peripheral nerves recorded in live paralyzed larval zebrafish aged 4-5 dpf in the presence of I_M inhibitor XE-991 (10 μM) or I_M enhancer ICA-069673 (10 μM). ***A-B***, Representative traces of spontaneous locomotor activity before and after pharmacological modulation of I_M by ICA-069673 (***A,*** n = 7) and XE-991 (***B,*** n = 7); individual locomotor episode traces in bottom panels correspond to episodes present within the dashed boxes in the traces of the upper panels. ***C-K***, Features of locomotor activity before and after I_M inhibition by XE-991 10μM (n =10) or I_M enhancement by ICA-069673 10 μM (control: n = 9, ICA-069673: n = 7). *Statistical analysis,* Wilcoxon matched pairs t-tests. ***D*****,** Episode duration (XE-991: $P >$ 0.9999; ICA-069673: $P = 0.6875$). ***E*****,** Number of motor bursts per swimming episode (XE-991: $P = 0.5566$; ICA-069673: $P = 0.3750$). ***F*****,** Burst duration (XE-991: $P = 0.0059$; ICA-069673: $P = 0.6875$). ***G*****,** Burst frequency (XE-991: $P = 0.0840$; ICA-069673: $P = 0.1562$). ***H*****,** Peak signal amplitude (XE-991: $P = 0.5566$; ICA-069673: $P = 0.5781$). ***I*****,** Inter-burst interval (XE-991: $P = 0.0059$; ICA-069673: $P = 0.1562$). ***J*****,** Variability of motor burst duration (XE-991: $P = 0.0059$; ICA-069673: $P = 0.0156$). ***I*****,** Variability of inter-burst interval duration (XE-991: $P = 0.3750$; ICA-069673: $P = 0.1562$). *Statistical analysis*, Wilcoxon matched-pairs test; $*P < 0.05$; $**P < 0.01$; otherwise not statistically significant.

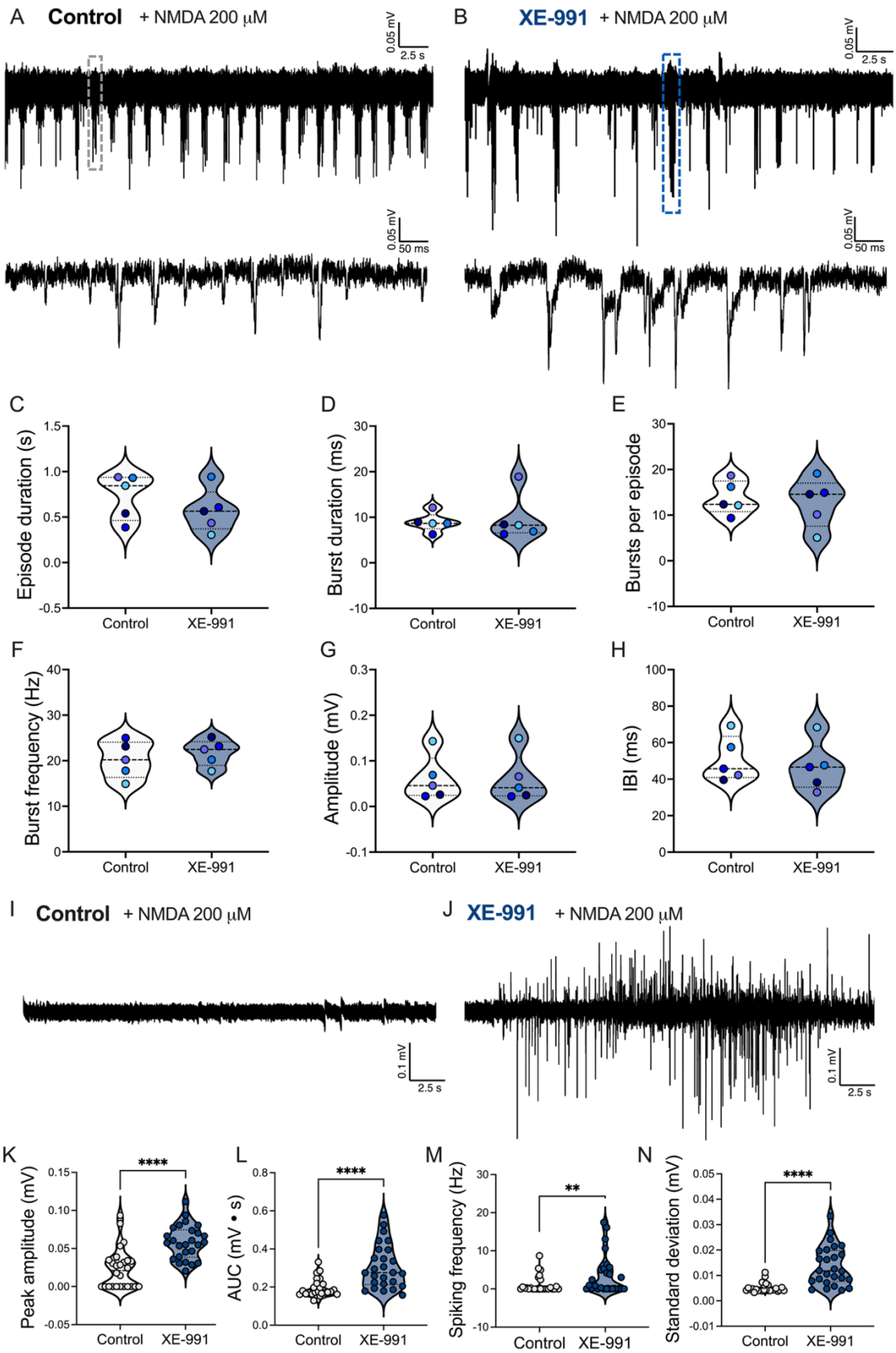
A Control + NMDA 200 μM
B XE-991 + NMDA 200 μM
0.05 mV
2.5 s
0.05 mV
50 ms
C
Episode duration (s)
D
Burst duration (ms)
E
Bursts per episode
F
Burst frequency (Hz)
G
Amplitude (mV)
H
IBI (ms)
Control
XE-991
I Control + NMDA 200 μM
J XE-991 + NMDA 200 μM
0.1 mV
2.5 s
K
Peak amplitude (mV)
L
AUC (mV • s)
M
Spiking frequency (Hz)
N
Standard deviation (mV)
****
**

Figure 3.4. Inhibition of I_M by XE-991 increases nerve activity but does not alter features of NMDA-induced fictive locomotion in spinalized 4-5 dpf larval zebrafish. ***A-H,*** Fictive locomotion induced by 200 μM NMDA recorded from motor nerves of 4-5 dpf spinalized larval zebrafish (n = 5) before and after inhibition of I_M by 10 μM XE-991. ***A-B*****,** Representative traces of locomotor activity induced by 200 μM NMDA (***A***; control) and when 10 μM XE-991 is introduced to the bath (***B***); individual locomotor episode traces in bottom panels correspond to those demarked by the dashed box in the upper traces. ***C,*** Episode duration (P = 0.8125). ***D*****,** Motor burst duration (P = 0.8125). ***E*****,** Locomotor frequency (P = 0.1250). ***F*****,** Amplitude of locomotor activity (P > 0.9999). ***G*****,** Inter-burst interval duration (P = 0.1250*).* ***H,*** Number of motor bursts per episode (P = 0.8125). ***I-J*****,** Representative trace of recording where NMDA application does not generate locomotor activity (***I;*** control), but 10 μM XE-991 enhances motor output (***J***) (n = 26). ***K-N***, Measures of overall activity recorded from motor nerves 30 seconds before and after bath application of 10 μM XE-991 to the recording chamber. ***K,*** Peak amplitude of activity. ***L,*** Area under the curve. ***M,*** Spikes per second. ***N,*** Standard deviation of signal. Individual animals before and after drug application are color-matched. *Statistical analysis,* Wilcoxon matched-pairs test. * = P < 0.05; ** = P < 0.01; **** = P < 0.0001.

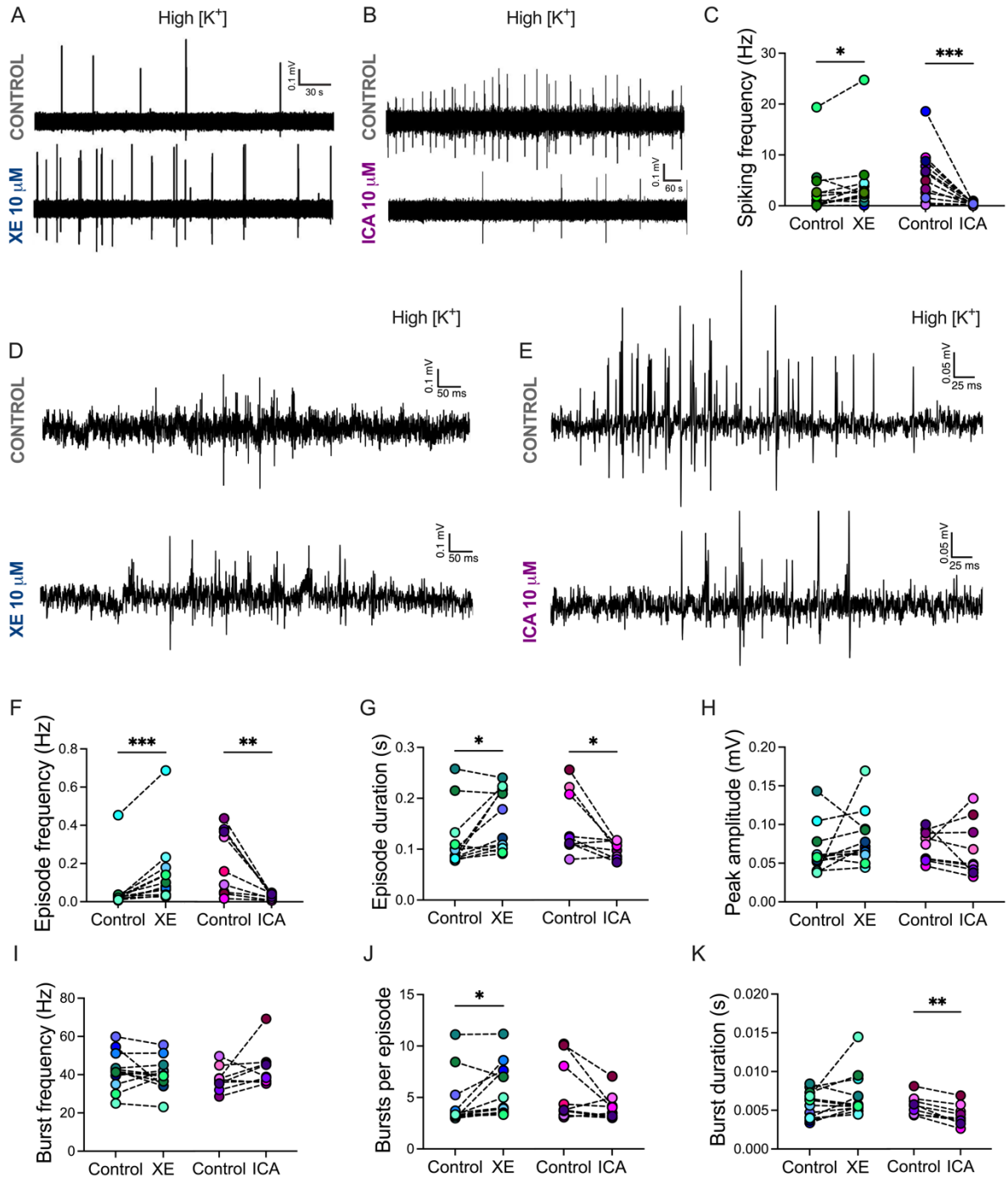
A
High [K+]
CONTROL
XE 10 µM
0.1 mV
30 s
B
High [K+]
CONTROL
ICA 10 µM
0.1 mV
60 s
C
Spiking frequency (Hz)
30
20
10
0
*
***
Control XE
Control ICA
D
High [K+]
CONTROL
XE 10 µM
0.1 mV
50 ms
E
High [K+]
CONTROL
ICA 10 µM
0.05 mV
25 ms
F
Episode frequency (Hz)
0.8
0.6
0.4
0.2
0.0
***
**
Control XE
Control ICA
G
Episode duration (s)
0.3
0.2
0.1
0.0
*
*
Control XE
Control ICA
H
Peak amplitude (mV)
0.20
0.15
0.10
0.05
0.00
Control XE
Control ICA
I
Burst frequency (Hz)
80
60
40
20
0
Control XE
Control ICA
J
Bursts per episode
15
10
5
0
*
Control XE
Control ICA
K
Burst duration (s)
0.020
0.015
0.010
0.005
0.000
**
Control XE
Control ICA

Figure 3.5. Modulating I_M pharmacologically affects fictive locomotion evoked by high extracellular potassium in spinalized larval zebrafish. Fictive locomotion recorded from motor nerves in 4-5 dpf spinalized larval zebrafish bathed in aCSF containing a high concentration of potassium (11.6 mM) to promote excitability of spinal locomotor circuits. ***A,*** Representative traces of fictive locomotion before (control) and after inhibition of I_M by 10 μM XE-991 (XE). ***B,*** Representative traces of fictive locomotion before (control) and after enhancement of I_M by 10 μM ICA-069673 (ICA). ***C,*** Number of spikes generated per second (XE-991: n = 14; ICA-069673: n = 12). ***D,*** Representative traces of fictive locomotor episodes evoked by high extracellular potassium before and after inhibition of I_M by 10 μM XE-991. ***E,*** Representative traces of fictive locomotor episodes evoked by high extracellular potassium before and after enhancement of I_M by 10 μM ICA-069673. ***F-K,*** Measures of locomotor parameters before and after pharmacological modulation of I_M (XE-991: n = 12; ICA-069673: n = 9). ***F,*** Number of episodes generated per second. ***G***, Episode duration. ***H,*** Peak amplitude of activity (XE-991: P = 0.0923; ICA-069673: P = 0.4961). ***I,*** Burst frequency (XE-991: P = 0.3804; ICA-069673: P = 0.1641). ***J,*** Number of bursts generated per episode (ICA-069673: P = 0.1289). ***K,*** Burst duration (XE-991: P = 0.1099). Individual animals before and after drug application are color-matched. *Statistical analysis,* Wilcoxon matched-pairs test. * $P < 0.05$, ** $P < 0.01$, *** $P < 0.001$; otherwise not statistically significant.

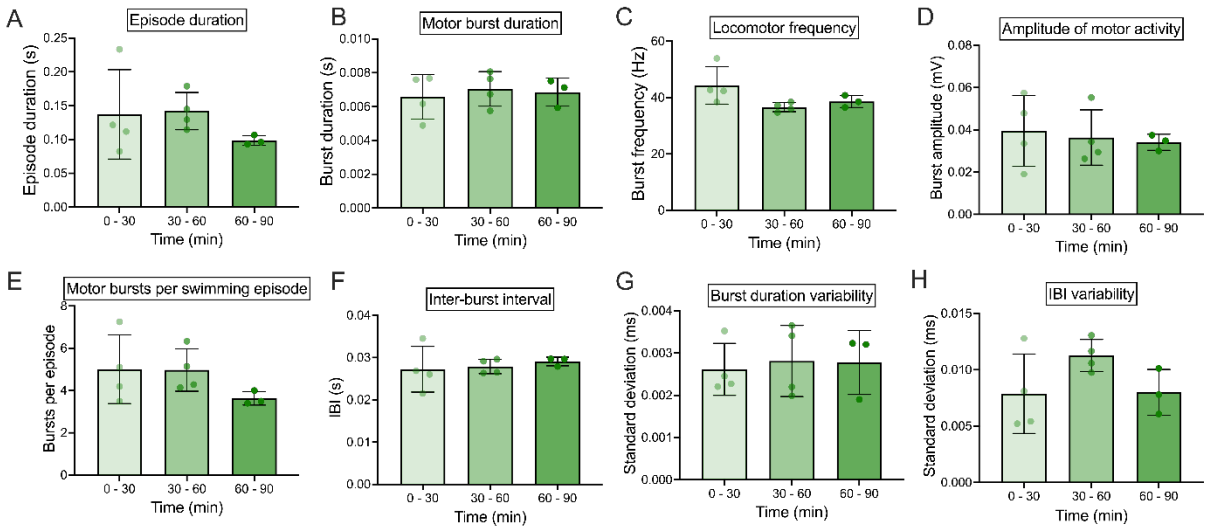
A
Episode duration
Episode duration (s)
0.25
0.20
0.15
0.10
0.05
0.00
0 - 30
30 - 60
60 - 90
Time (min)
B
Motor burst duration
Burst duration (s)
0.010
0.008
0.006
0.004
0.002
0.000
0 - 30
30 - 60
60 - 90
Time (min)
C
Locomotor frequency
Burst frequency (Hz)
60
40
20
0
0 - 30
30 - 60
60 - 90
Time (min)
D
Amplitude of motor activity
Burst amplitude (mV)
0.08
0.06
0.04
0.02
0.00
0 - 30
30 - 60
60 - 90
Time (min)
E
Motor bursts per swimming episode
Bursts per episode
8
6
4
2
0
0 - 30
30 - 60
60 - 90
Time (min)
F
Inter-burst interval
IBI (s)
0.04
0.03
0.02
0.01
0.00
0 - 30
30 - 60
60 - 90
Time (min)
G
Burst duration variability
Standard deviation (ms)
0.004
0.003
0.002
0.001
0.000
0 - 30
30 - 60
60 - 90
Time (min)
H
IBI variability
Standard deviation (ms)
0.015
0.010
0.005
0.000
0 - 30
30 - 60
60 - 90
Time (min)

Supplemental Figure 3.1. Effect of time on features of locomotor activity recorded from motor nerves of 4-5 dpf larval zebrafish. Activity from peripheral nerves recorded in live paralyzed larval zebrafish aged 4-5 dpf over the course of 90 minutes **(*A*-*H*).** Data presented is from gap-free recordings separated into three bins of 30 minutes. ***A***, Episode duration. ***B***, Burst duration. ***C***, Frequency of motor bursts within an episode. ***D***, Motor burst amplitude. ***E***, Number of bursts per episode. ***F,*** Inter-burst interval duration. ***G***, Variability of burst duration measured as standard deviation of average motor burst durations. ***H***, Variability of inter-burst interval (IBI) duration measured as the standard deviation of average inter-burst interval durations. *Statistical analysis,* Kruskal-Wallis test with Dunn's test for multiple comparisons.

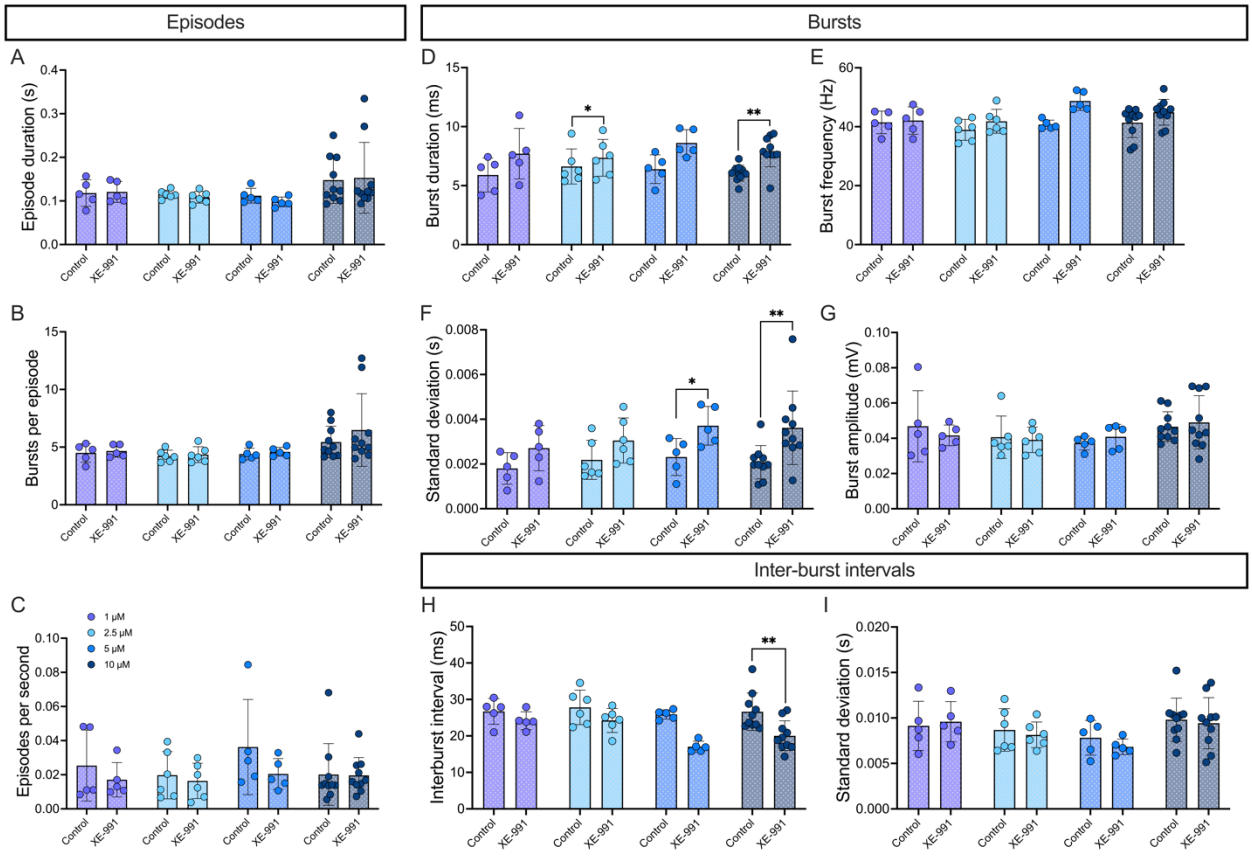
Episodes
Bursts
Inter-burst intervals
A
B
C
D
E
F
G
H
I
Episode duration (s)
Bursts per episode
Episodes per second
Burst duration (ms)
Burst frequency (Hz)
Standard deviation (s)
Burst amplitude (mV)
Interburst interval (ms)
Standard deviation (s)
1 µM
2.5 µM
5 µM
10 µM
Control
XE-991
*
**

Supplemental Figure 3.2. Assessing how various concentrations of XE-991 affect locomotor features of 4-5 dpf larval zebrafish. Activity from peripheral nerves recorded in live paralyzed larval zebrafish aged 4-5 dpf. ***A*-*I***, Features of locomotor activity before and after inhibition of I_M by XE-991: 1 uM (n = 5), 2.5 uM (n = 6), 5 uM (n = 5), and 10 uM (n = 10). ***A***, Average episode duration. ***B***, Average number of bursts per episode. ***C***, Episode frequency. ***D***, Average duration of bursts. ***E***, Burst frequency. ***F***, Standard deviation of burst duration. ***G***, Average burst amplitude. ***H***, Average inter-burst interval duration. ***I***, Standard deviation of inter-burst interval durations. *Statistical analysis*, Wilcoxon matched-pairs t-tests. * $P < 0.05$, ** $P < 0.01$; otherwise, statistically not significant.

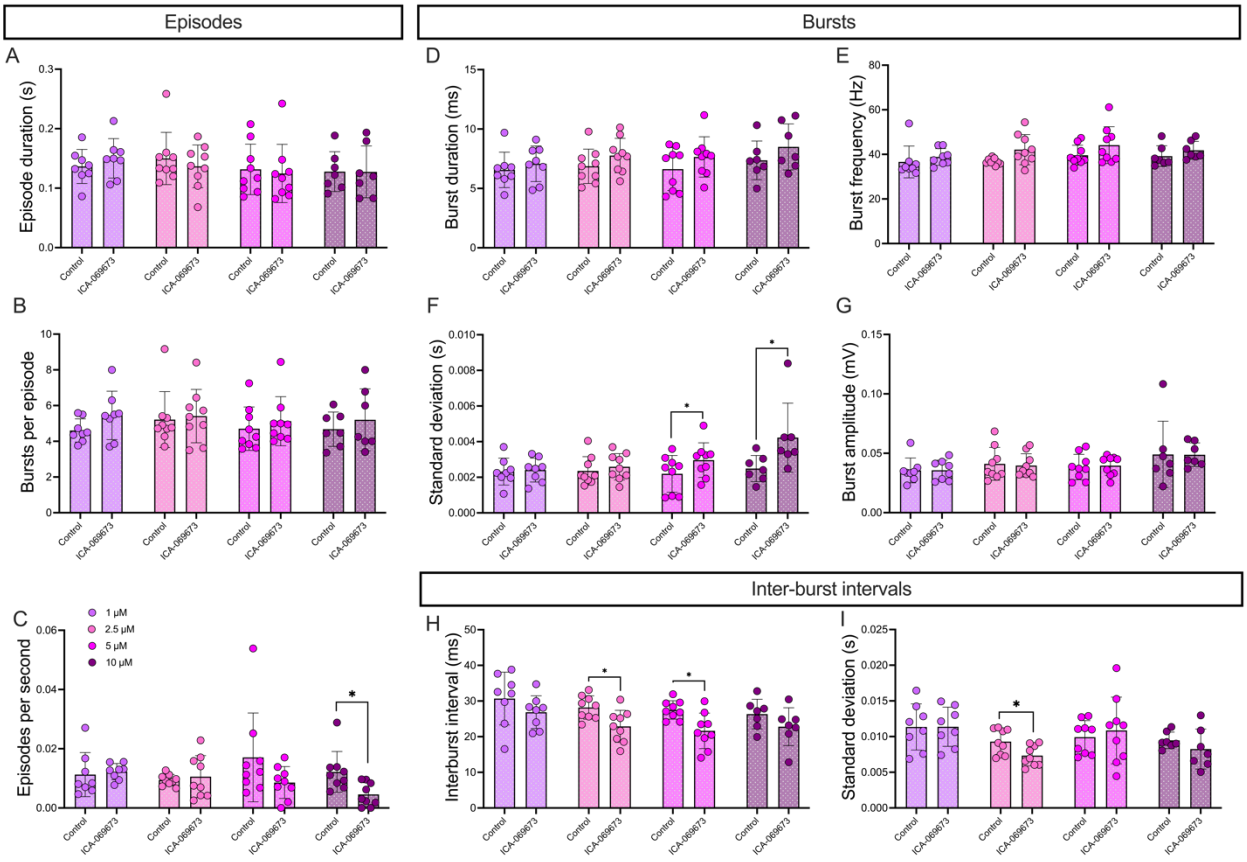
Episodes
Bursts
A
Episode duration (s)
D
Burst duration (ms)
E
Burst frequency (Hz)
B
Bursts per episode
F
Standard deviation (s)
G
Burst amplitude (mV)
C
Episodes per second
1 µM
2.5 µM
5 µM
10 µM
Inter-burst intervals
H
Interburst interval (ms)
I
Standard deviation (s)
Control
ICA-069673

Supplemental Figure 3.3. Assessing how various concentrations of ICA-069673 affect locomotor features of 4-5 dpf larval zebrafish. Activity from peripheral nerves recorded in live paralyzed larval zebrafish aged 4-5 dpf. ***A***-***I***, Features of locomotor activity before and after enhancement of I_M by ICA-069673: 1 uM (n = 8), 2.5 uM (n = 9), 5 uM (n = 9), and 10 uM (n = 7). ***A***, Average episode duration. ***B***, Average number of bursts per episode. ***C***, Episode frequency. ***D***, Average duration of bursts. ***E***, Burst frequency. ***F***, Standard deviation of burst duration. ***G***, Average burst amplitude. ***H***, Average inter-burst interval duration. ***I***, Standard deviation of inter-burst interval durations. *Statistical analysis*, Wilcoxon matched-pairs t-tests. * $P < 0.05$; otherwise, statistically not significant.

Chapter 4

Developmental changes in the control of primary motoneuron firing properties by multiple currents in larval zebrafish

Gaudreau, SF & Bui, TV

4.1 ABSTRACT

Spinal circuits for locomotion undergo maturation during early development. How intrinsic properties of individual spinal neuron populations change throughout motor maturation is not fully understood. Here we determine how several ionic currents underlying neuron excitability change in primary motoneurons during early development (2 – 5 days post-fertilization). We confirm, for the first time, the presence of the persistent outward potassium current known as the M-current, in primary motoneurons. We also reveal the presence of a persistent inward current at 2 to 5 dpf consisting of a riluzole-sensitive persistent inward Na^+ current and a nifedipine-sensitive Ca^{2+} current. An analysis of the amplitude of these currents suggests age-dependent changes at these early developmental timepoints. For instance, we show that the M-current controls excitability of primary motoneurons and its role in excitability control changes during development such that the magnitude of the M-current in primary motoneurons transiently increases at 3 days post-fertilization. We also reveal that contributions of the riluzole-sensitive persistent inward Na+ current and the nifedipine-sensitive Ca^{2+} current to the persistent inward current of primary motoneurons shifts during development. These findings reveal novel mechanisms by which control over excitability of primary motoneurons in larval zebrafish is ensured, underscoring

developmental changes in ion current contributions to intrinsic properties. Broadly, these data support the M-current and persistent inward currents as conserved means to control motoneuron excitability across vertebrates.

4.2 INTRODUCTION

In early development, vertebrates transition through a series of progressively more complex movements. Eventually, underlying spinal locomotor circuits become sufficiently refined to produce locomotion. The precise changes that spinal locomotor circuits undergo during development are still not fully understood. Amongst several possibilities, spinal neurons can undergo changes in synaptic receptors (Laliberte et al. 2022; Wilson, Rempel, and Brownstone 2004) and ion currents (Sharples and Miles 2021) during development.

The developing zebrafish (*Danio rerio*) is an attractive vertebrate model for studying the development of spinal circuits. Larval zebrafish have a relatively simple nervous system such that spinal neurons are easily identifiable and accessible for study (Robert R. Bernhardt et al. 1990; P. Myers, Eisen, and Westerfield 1986). Larval zebrafish are especially well-suited to the study of motor control maturation because of their rapid development and the stereotyped emergence of motor behaviours during this time (Budick and O'Malley 2000; Drapeau et al. 2002b). As of 17 hours post-fertilization (hpf), zebrafish embryos produce large amplitude body bends known as coiling (Kimmel et al. 1995; Saint-Amant and Drapeau 1998). Soon after, around 24 hpf, they can execute consecutive coils to either side of the head, referred to as double coiling (Knogler et al. 2014). At 3 days post-fertilization (dpf), zebrafish larvae exhibit their first instances of spontaneous swimming (Saint-Amant 2010). The swimming is erratic and long-lasting but

infrequent. This swimming rapidly evolves into what is known as the beat-and-glide swim by 4 dpf (Budick and O'Malley 2000; Buss and Drapeau 2001). As the mature form of larval zebrafish locomotion, the beat-and-glide swim consists of more controlled, low-amplitude rhythmic tail beats interspersed by periods of gliding. The described stereotyped transitions in locomotion make it possible to link changes in motor output to changes in spinal circuits, ultimately shedding light onto the mechanisms underlying the spinal control of movement (Knogler et al. 2014; Lambert et al. 2012; Roussel et al. 2020, 2021).

Major changes to spinal locomotor circuits of developing zebrafish have been identified including the addition of new neurons (Myers, Eisen, and Westerfield 1986; Kimmel et al. 1995; Kuwuda et al. 1990; Satou, Kimura, and Higashijima 2012), progressive addition of chemical neurotransmission to a gap-junction-prominent neural scaffold (Knogler et al. 2014; Roussel et al. 2020; Saint-Amant and Drapeau 2001), formation and refinement of synaptic connections (Robert R. Bernhardt et al. 1990; Liu and Westerfield 1988; Roussel et al. 2021) as well as incorporation of neuromodulatory systems (Brustein et al. 2003; Jay, De Faveri, and McDearmid 2015; Lambert et al. 2012; Montgomery et al. 2018; Thirumalai and Cline 2008). Even the firing of spinal neurons changes through development (Buss et al. 2003; Louis Saint-Amant and Drapeau 2000) though the ion currents underlying these changes remain to be fully identified.

Primary motoneurons (pMNs) are the largest and earliest born motoneurons in larval zebrafish (Myers 1985). They control the fastest and largest amplitude movements (Liu and Westerfield 1988). These types of movements make up most of the locomotor repertoire in zebrafish 2 dpf or younger and become less prominent as of the third day of development. By this age, swimming

involves secondary motoneurons (sMNs) with the involvement of pMNs becoming increasingly less prominent (Liu and Westerfield 1988; McLean et al. 2007). Recently, it has been demonstrated that different types of mouse motoneurons express varying magnitudes of the persistent subthreshold potassium current known as the M-current (Sharples et al. 2023). Sharples et al. demonstrate that M-current expression in motoneurons helps control their recruitment (Sharples et al. 2023). Given that the M-current has been shown to work in tandem with the persistent sodium current (I_{NaP}) in mice (Verneuil et al. 2020b), and that zebrafish motoneurons possess a riluzole-sensitive sodium (Na^+) component to persistent inward currents (PICs) at 1 dpf (Tong and Jonathan Robert McDearmid 2012) that is observed across mammalian motoneurons (Drouillas et al. 2023; Li and Bennett 2003; Li et al. 2004), we posited that motoneurons in larval zebrafish may also express the M-current. Furthermore, we hypothesize that the role of the M-current in shaping pMN excitability may change throughout development as the most prominent locomotor movements rely increasingly less on pMNs with the emergence of secondary MNs that are relatively more involved in swimming (Ampatzis et al. 2014; McLean et al. 2007).

Using whole-cell patch-clamp electrophysiology, we reveal for the first time the presence of the M-current in larval zebrafish spinal circuits for locomotion. We demonstrate that the M-current regulates excitability of pMNs and show that the magnitude of the M-current in pMNs changes throughout development. Furthermore, we compliment these findings by characterizing persistent sodium (I_{NaP}) and persistent calcium (I_{CaL}) contributions to the PICs of pMNs during the same developmental window. Together, these data describe for the first time in larval zebrafish the developmental changes to the interplay between ionic conductances that have been well-

characterized in mammalian motoneurons. This work emphasizes shared mechanism over the control of repetitive firing in motoneurons across vertebrates.

4.3 METHODS

4.3.1 Animal Care

All experiments were performed in accordance with the protocol approved by the University of Ottawa's Animal Care Committee (BL-4416). Adult zebrafish are maintained at 28.5°C with a 14 hour on/10 hour off light cycle, with lights off at 11PM and on at 9AM. Embryos are fertilized between 9AM-10AM and stored in embryo medium at 28.5°C until use for experimentation at 2 to 5 dpf.

4.3.2 Preparation for electrophysiology

Larval zebrafish are anesthetized in 0.02% tricaine (MS-222, Aqualife TMS; Syndel Laboratories) before being pinned down through the notochord onto a Sylgard (Dow Corning) coated dish. Pins are made using Tungsten wire (0.25 mm); one is placed caudally near the tip of the tail, and the other is placed rostrally near the center of the yolk sac. Spinalization is performed using fine surgical scissors at the level of segments 2-3. The skin is then peeled back between the two pins using fine forceps. Next, larvae are bathed in 1 mg/mL collagenase (Millipore Sigma; incubation times: 8 minutes at 2 dpf, 10 minutes at 3 dpf, 12 minutes at 4 dpf, and 15 minutes at 5 dpf) to facilitate muscle removal. The collagenase solution is rinsed out 4-5 times with artificial cerebrospinal fluid (aCSF) containing: 134 mM NaCl, 2.9 mM KCl, 1.2 mM $MgCl_2$, 2.1 mM $CaCl_2$, 10 mM dextrose, and 10 mM HEPES (pH of 7.8 adjusted with NaOH and osmolarity between 280-290 adjusted with sucrose). Muscle removal is performed using suction through a

wide-bored glass capillary (typically, the tips are gently broken to get the right sized tip for muscle removal). Muscles overlaying the spinal cord are removed to expose the spinal cord for whole-cell patch-clamp electrophysiology.

4.3.3 Whole-cell patch-clamp electrophysiology

To block muscle contractions during recordings, d-tubocurarine is added to the aCSF (10 μM; Millipore Sigma, catalog # 93750). Electrodes for whole-cell patch-clamp experiments are made using borosilicate glass capillaries (Sutter Instrument; BF150-110-10). Tip resistances ranging from 5 to 7 megaOhms (MΩ) were used. Intracellular recording solution used contained the following: 16 mM KCl, 116 mM K-gluconate, 4 mM $MgCl_2$, 10 mM HEPES, 10 mM EGTA, and 4 mM Na_2-ATP, adjusted to a pH of 7.2-7.3 with KOH. Slight positive pressure was applied during the descent toward the spinal cord to prevent debris from contaminating the tip of the electrode. This positive pressure was used to break the dura thereby exposing the neurons within the spinal cord. Positive pressure was decreased slightly, and targeted neurons were approached with the electrode. When near the neuron (small dent forming in neuron), positive pressure was released and a gigaohm (GΩ) seal (giga-seal) was formed between the tip of the electrode and the cell membrane. Gentle pulses of negative pressure were used to break through the membrane. Membrane holding potential was set to –65 mV and both fast and slow capacitance components were compensated for. Series resistance was routinely compensated for at 80% or higher. The neuron was held at -65 mV until it was time to introduce stimulation protocols. Values reported are not liquid junction potential corrected. pMNs at all ages were targeted based on their characteristically large soma size and dorsoventral positioning restricted to about midway through the spinal column. All pMN subtypes (rostral primary, middle primary, and caudal primary) were

included in the sampling. pMN identity was then confirmed post hoc by assessing axon projection through the ventral root facilitated by the addition of sulforhodamine B to the intracellular recording solution (0.1%; Millipore Sigma). Sampling of pMNs was performed within 4 somites rostral and 4 somites caudal relative to the anal pore. Electrical activity was amplified and filtered at 10 kHz or 20 kHz with a Multiclamp 700B (Axon Instruments, Molecular Devices). The data was then digitized with a Digidata 1550 (Molecular Devices). A HumBug Noise Eliminator (Quest Scientific) was used to attenuate 50/60 Hz electrical noise.

4.3.4 Voltage-clamp protocols and current estimations

To reveal the electrophysiological signature of the M-current, we implemented the standard M-current relaxation protocol (Sharples et al. 2023; Verneuil et al. 2020b). This consisted of holding the neuron at -10 mV and introducing a series of hyperpolarizing voltage steps lasting 1 second each. As the membrane potential becomes hyperpolarized, the M-current deactivates. Current responses show the resulting loss of outward current caused by M-current deactivation. From this, we can estimate the amplitude of the M-current by taking the difference between the peak of the current response and the current at steady-state at the end of the step. The difference between the steady-state current and the peak of this initial current response was used to estimate the amplitude of the M-current.

A 20 mV per second depolarizing voltage ramp was introduced to neurons initially held at -90 mV for 5 seconds. To calculate the amplitude of the persistent inward currents (PICs), the leak current corresponding to the current response from -90 mV to -70 mV was subtracted from the original

trace. The amplitude of the PICs was measured as the difference between the peak in the negative current drop of the PICs and the average current at baseline prior to PICs activation.

4.3.5 Basal membrane properties

To measure membrane properties, 10 repetitions of a 50 ms current step of -5 pA were applied to neurons that were held at -65 mV. The average drop in voltage in response to the current step was used to calculate input resistance, whole-cell capacitance, and the membrane time constant tau.

4.3.6 Firing properties

To measure firing properties, a series of 5 pA current steps from 0 pA to 295 pA were applied to neurons that were held at -65 mV. Rheobase was determined as the first current step to elicit an action potential. Using the action potential generated at rheobase, spike threshold was set as the voltage at which the voltage response reached a slope of 10 mV/ms (Sharples et al., 2023). Instantaneous firing frequency was calculated as the inverse of the time between successive spikes. Steady-state firing frequency was estimated as the average instantaneous firing frequency of the last 5 pairs of spikes during a 500-ms current injection equal to 2x rheobase.

4.3.7 Pharmacology

For pharmacological inhibition and activation of Kv7.2/7.3 channels, 10 μM XE-991 (X2254, Millipore Sigma) and 10 μM ICA-069673 (SML1616, Millipore Sigma) were first dissolved in DMSO (D8418, Millipore Sigma) before final dissolution in aCSF of the recording bath. For pharmacological inhibition of I_{NaP}, L-type calcium channels, and P/Q-type calcium channels, 5 μM riluzole (557324, Millipore Sigma), 20 μM nifedipine (481981, Millipore Sigma), and 300

nM ω-agatoxin (HB1212, Hellobio), respectively, were bath applied. Riluzole and nifedipine were dissolved in DMSO before final dissolution in aCSF.

4.3.8 Data analysis and statistical analysis

All electrophysiological data was saved as .abf files. We used the open-source pyABF python package to import and read .abf files in Spyder (version 5.1.5). Analysis of recordings was semi-automated using Python (version 3.9.12) scripts tailored to each type of recording. Statistical analysis was performed using Prism by GraphPad (Version 10.3.1 (464)). When comparing the means of two non-normally distributed matched paired data sets, the non-parametric Wilcoxon matched-pairs signed rank tests were used. For unmatched pairs, Mann-Whitney tests were used. For comparisons between 3 data sets or more, one-way ANOVA with Tukey's multiple comparisons test was used for normally distributed data and Kruskal-Wallis test with Dunn's multiple comparisons test was used for non-parametric data. Mixed effects model analyses were used to reveal differences in I-V relationships across age groups. For all tests, significance stars are displayed on graphs.

4.4 RESULTS

4.4.1 M-current sensitive to Kv7.2/7.3 channel inhibitor XE-991 revealed in larval zebrafish primary motoneurons

We first sought out to determine whether primary motoneurons (pMNs) in larval zebrafish express the M-current (I_M). To this end, we targeted pMNs for whole-cell patch-clamp electrophysiology in spinalized larval zebrafish aged 3 to 5 dpf. pMNs were located based on their well-described large soma and mid-level positioning within the dorsoventral spinal axis (Bello-Rojas et al. 2019;

P. Myers et al. 1986). Intracellular recording solution containing sulforhodamine-b permitted post-hoc confirmation of pMN identity with axons exiting the ventral root (**Fig. 4.1*A***). To reveal the electrophysiological signature of I_M, we introduced the standard I_M relaxation protocol under voltage-clamp mode. This consists of holding the neuron at -10 mV, a relatively depolarized membrane potential at which I_M should be active and introducing a series of hyperpolarizing voltage steps from -10 mV to -80 mV in increments of 5 mV (**Fig. 4.1*B*-*C***). Current responses to the I_M relaxation protocol in pMNs reveal the presence of the electrophysiological signature of I_M (**Fig. 4.1*D*-*E***). **Figure 4.1*D*** displays the current-voltage relationship of I_M recorded in pMNs (n = 51 neurons; N = 25 fish). In a separate sample group of pMNs (n = 25 neurons; N = 9 fish), we demonstrate that this current is sensitive to bath application of 10 μM XE-991, a selective pharmacological inhibitor of Kv7.2/7.3 channels known to mediate I_M (**Fig. 4.1*D*-*E***). The amplitude of I_M is significantly reduced over voltages ranging from -40 to -20 mV (**Fig. 4*D***). Inhibition of I_M by 10 μM XE-991 is also apparent when comparing the peak amplitude of the measured current (control: 32.90 ± 16.08 pA; XE-991: 22.20 ± 13.26 pA; **Fig. 4.1*F***). The voltage at which I_M is activated (determined for individual neurons as the voltage at which I_M is not zero) is not affected by bath application of XE-991 (control: -49.51 ± 8.38 mV; XE-991: -49.40 ± 10.03 mV; **Fig. 4.1*G***). Similarly, XE-991 does not alter the voltage at which I_M reaches half its maximal amplitude ($V_{1/2}$) when compared to controls (control: -35.07 ± 5.88 mV; XE-991 ± -31.26 ± 9.56 mV; **Fig. 4.1*H***). These findings are in line with the known mechanism of action of XE-991. Overall, these data demonstrate that XE-991-sensitive I_M is present in pMNs of 3-5 dpf zebrafish larvae.

4.4.2 Pharmacological modulation of Kv7.2/7.3 channels alters intrinsic properties of larval zebrafish primary motoneurons

Having confirmed its presence in pMNs of larval zebrafish, we next investigated how I_M influences pMN intrinsic properties by pharmacologically modulating Kv7.2/7.3 channel conductance. Because I_M has been shown to be involved in setting resting membrane potential (Davis, Herring, and Paterson 2020; Sharples et al. 2023; Verneuil et al. 2020b; Wladyka and Kunze 2006), we monitored the effects of pharmacologically activating then subsequently inhibiting Kv7.2/7.3 channels on resting membrane potential of pMNs (**Fig. 4.2**). Whole-cell current-clamp recordings from pMNs of 4-5 dpf larvae reveal a significant hyperpolarization of mean resting membrane potential during Kv7.2/7.3 activation by 10 μM ICA-069673 (control (n = 10): -57.2 ± 2.5 mV; acute ICA-069673 (n = 10): -67.7 ± 3.6 mV; prolonged ICA-069673 (n = 7): -70.6 ± 4.0 mV, **Fig. 4.2*A-B***). While inhibition of Kv7.2/7.3 by XE-991 (n = 7; -66.59 ± 3.8 mV) following activation by ICA-069673 did not depolarize pMN resting membrane potential to voltages near control levels, we did observe an increase in the overall change in membrane potential from start to end of each respective treatment (control: -1.2 ± 0.9 mV; XE 991: 6.4 ± 3.2 mV; **Fig. 4.2*C***) is significantly altered by XE-991 relative to control. When 10 μM ICA-069673 and 10 μM XE-991 were individually bath applied to separate groups of pMNs (**Supplemental Figure 4.1**), ICA-069673 hyperpolarized resting membrane potential relative to controls (control: -61.63 ± 2.70 mV; ICA-069673: -71.46 ± 3.67 mV) but XE-991 did not depolarize it (control: -60.89 ± 3.42 mV; XE-991: -62.60 ± 3.66 mV) when comparing mean resting membrane potential (**Supplemental Figure 4.1*C,F***). We observed a shallow baseline drift during gap-free current-clamp recordings. To account for this, we also quantified and compared the slope as a measure of the rate of change of resting membrane potential over time. As expected, we find an increased negative slope in the

presence of ICA-069673 (control: -0.0044 ± 0.0062 mV/s; ICA-069673: -0.0362 ± 0.0317 mV/s) (**Supplemental Figure 4.1*D***). Conversely, there is a significant increase in the slope of resting membrane potential of pMNs in the presence of XE-991 (control: -0.0086 ± 0.0073 mV/s; XE-991: -0.00057 ± 0.0031 mV/s) (**Supplemental Figure 4.1*G***). We found similar effects when comparing the overall change in membrane potential from start to end of each respective treatment. ICA069673 resulted in an overall greater negative shift from control (control: -1.06 ± 1.67 mV; ICA-069673: -9.81 ± 1.00 mV) while XE-991 resulted in less negative change compared to controls (control: -1.62 ± 1.27 mV; XE-991: -0.54 ± 1.15 mV) (**Supplemental Figure 4.1*E*,*H***). These data suggest that XE-991 does indeed depolarize resting membrane potential, yet the magnitude of depolarization is insufficient to counteract the baseline drift we observe in these recordings. Indeed, it has been shown that XE-991 is a state-dependent inhibitor of Kv7.2/7.3 channels, likely to be more effective when these channels are already in an open conformation (Greene, Kang, and Hoshi 2017). Overall, these data demonstrate that I_M acts to hyperpolarize the resting membrane potential of pMNs.

We also wondered whether pharmacological modulation of I_M might alter the overall state of spinal locomotor circuits. We measured this by quantifying the number of excitatory postsynaptic potentials (EPSPs) received by recorded pMNs over time. We found no difference in the frequency of EPSPs received by pMNs during bath application of 10 μM ICA-069673 or 10 μM XE-991 (control: 3.29 ± 2.76 Hz; ICA-069673 (acute): 3.70 ± 2.10 Hz; ICA-069673 (prolonged): 2.37 ± 1.59 Hz; XE-991: 4.00 ± 4.06 Hz) (**Fig. 4.2*D***).

We next sought out to evaluate how intrinsic firing and membrane properties of pMNs were affected by pharmacological modulation of I_M. When investigating firing properties of pMNs before and after pharmacological modulation of I_M in the same group of pMNs, we suspected that the prolonged recording in whole-cell configuration may be confounding our data (**Supplemental Figure 4.2**). In the same group of pMNs, we held them at -65 mV before introducing 50 ms current steps in increments of 5 pA up to 195 pA, before (control) and after either Kv7.2/7.3 channel inhibition by 10 μM XE-991 or Kv7.2/7.3 channel activation by 10 μM ICA-069673. Rheobase, spike threshold, and maximum number of spikes generated during the current steps were determined from these voltage responses. This data from matched-pairs of pMNs show that inhibiting I_M with 10 μM XE-991 increases their excitability, as measured by a hyperpolarization of the threshold required to elicit an action potential (P = 0.0034; n = 12; control: -29.9 ± 4.3 mV; XE-991: -33.3 ± 5.3 mV) as well as an increase in the number of action potentials produced during the maximal current injection of a series of current steps (P = 0.002; n = 11; control: 2.7 ± 1.0 spikes; XE-991: 5.3 ± 2.2 spikes) though rheobase remained unaltered (P = 0.0557; n = 12; control: 91.3 ± 38.0 pA; XE-991: 85.4 ± 40.9 pA) (**Supplemental Figure 4.2*D*-*E***). On the other hand, we find that enhancing I_M with 10 μM ICA-069673 has no effect on spike threshold (P = 0.4061; n = 24; -30.7 ± 6.2 mV; ICA-069673: -29.0 ± 6.78 mV; **Supplemental Figure 4.2*G***), maximum number of spikes generated (P = 0.1759; n = 23; control: 2.4 ± 1.1 spikes; ICA: 3.0 ± 2.0 spikes; **Supplemental Figure 4.2*H***) nor rheobase (P = 0.1021; n = 24; control: 121.5 ± 43.2 pA; ICA-069673: 111.5 ± 51.0 pA; **Supplemental Figure 4.2*F***). We found this to be peculiar given the strong hyperpolarization of resting membrane potential brought on by pharmacological enhancement of I_M by ICA-069673 (**Fig. 4.2 and Supplemental Figure 4.1**).

To circumvent the possible confounding effect of elapsed recording time, we compared intrinsic properties of pMNs to those of two other entirely separate sample groups of pMNs exposed to either 10 μM ICA-069673 prior to all pMN recordings or exposed to 10 μM XE-991 prior to all pMN recordings (**Fig. 4.3**). We find that spike threshold is significantly depolarized in pMNs when I_M is enhanced by ICA-079673 while it remains unaltered by inhibition of I_M by XE-991 (control: -31.57 ± 5.66 mV; ICA-069673: -25.03 ± 6.22 mV; -29.69 ± 4.03 mV; **Fig. 4.3*D***). Similarly, rheobase is increased by ICA-069673 but unaffected by XE-991 (control: 95.33 ± 40.79 pA; ICA-069673: 128.90 ± 44.64 pA; XE-991: 113.10 ± 36.65 pA; **Fig. 4.3*E***). There was no effect on the maximum number of spikes generated by ICA-069673 nor XE-991 (control: 4.48 ± 1.48 spikes; ICA-069673: 4.03 ± 1.65 spikes; XE-991: 3.96 ± 1.97 spikes; **Fig. 4.3*F***).

Next, we introduced a -5 pA negative current step to pMNs held at -65 mV (**Fig. 4.3*G-I***). From corresponding voltage responses, we calculated input resistance, whole-cell capacitance, and the membrane time constant, τ. We find no effects to input resistance (control: 293.30 ± 172.50 MΩ; ICA-069673: 225.20 ± 96.08 MΩ; XE-991: 217.60 ± 89.23 MΩ; **Fig. 4.3*J***) nor to membrane capacitance (control: 20.39 ± 3.36 pF; ICA-069673: 18.78 ± 3.91 pF; XE-991: 18.74 ± 2.46 pF; **Fig. 4.3*K***) during pharmacological modulation of I_M. We did observe a decrease in the membrane time constant when pMNs are exposed to XE-991 but not when exposed to ICA-069673 (control: 5.91 ± 3.39 ms; ICA-069673: 3.99 ± 1.23 ms; XE-991: 4.06 ± 1.70 ms; **Fig. 4.3*L***).

When comparing these data to the effects of pharmacological modulation of I_M in matched-paired pMNs, we find discrepancies, further supporting our suspicion of confounding time effects to our patch-clamp recordings. Similar to the non-matched data described above, our matched-pairs data

reveal that inhibition of I_M by XE-991 does not alter input resistance (control: 202.4 ± 71.2 MΩ; XE-991: 232.4 ± 101.6 MΩ; **Supplemental Figure 4.2*N***) or whole-cell capacitance (control: 22.1 ± 2.7 pF; XE-991: 22.5 ± 7.4 pF; **Supplemental Figure 4.2*O***). Unlike our non-matched data however, our matched-pairs data reveals that the membrane time constant is unaltered by XE-991 (control: 4.5 ± 1.8 ms; XE-991: 5.2 ± 2.3 ms; **Supplemental Figure 4.2*P***). In our matched-pairs pMN data, ICA-069673 significantly increases input resistance (control: 161.4 ± 40.3 MΩ; ICA-069673: 193.3 ± 58.4 MΩ; **Supplemental Figure 4.2*R***), while it is unaffected in our non-matched data (**Fig. 4.3*J***). Similar to our non-matched pMN data, ICA-069673 does not alter membrane capacitance (control: 22.7 ± 5.4 pF; ICA-069673: 22.8 ± 3.4 pF; **Supplemental Figure 4.2*S***) nor the membrane time constant (control: 3.6 ± 0.9 ms; ICA-069673: 4.4 ± 1.5 ms; **Supplemental Figure 4.2*T***).

We conclude here that long duration patch-clamp recordings may be susceptible to time effects thereby confounding our interpretation of the effects of pharmacological manipulation of I_M (**Supplemental Figure 4.2**). For this reason, we focus our interpretations to our non-matched data (**Fig. 4.3**). Overall, these experiments demonstrate that I_M acts to reduce neuronal excitability in pMNs, as evidenced by effects to firing properties brought on by pharmacological enhancement of I_M conductance by ICA-069673.

4.4.3 Developmental changes to the magnitude of the M-current in primary motoneurons

With evidence to support a role for I_M in regulating excitability of pMNs in larval zebrafish (**Fig. 4.3**), we hypothesized that this role might change throughout development. As slow, low amplitude swimming movements start to dominate, the involvement of pMNs in locomotion diminishes. We

proceeded to characterize properties of I_M in pMNs of larvae aged 2 dpf to 5 dpf (**Fig. 4.4**). At 2 dpf, zebrafish can perform burst swimming in response to touch. By 3 dpf, they start to perform spontaneous burst swimming and by 4 dpf onward, larval zebrafish perform refined swimming known as beat-and-glide swimming. We hypothesized that as zebrafish spinal locomotor circuits mature to generate increasingly refined movements relying less and less on pMNs, increasingly more dampening of intrinsic excitability by I_M may be necessary to ensure pMNs are active only during the fastest movements (e.g. escapes). We investigated the current-voltage relationship of I_M measured in pMNs at 2, 3, 4, and 5 dpf (**Fig. 4.4*A***). Statistical analysis by a two-way ANOVA demonstrates a significant increase in the mean amplitude of I_M across voltages from 2 to 3 dpf and 2 to 5 dpf as well as a significant decrease from 3 to 4 dpf and 3 to 5 dpf (**Fig. 4.4*A***). When comparing the peak amplitude of I_M, we find that the peak amplitude of I_M from 2 dpf to 3 dpf significantly increases (2 dpf: 17.03 ± 11.55 pA; 3 dpf: 42.88 ± 18.44 pA; **Fig. 4.4*C***). Subsequently, the peak amplitude of I_M is reduced by nearly half by 4 dpf (4 dpf: 24.08 ± 10.91 pA; **Fig. 4.4*C***) yet this reduction between 3 and 4 dpf was not statistically significant ($P = 0.0743$). From 4 dpf to 5 dpf, there is no significant change in peak I_M amplitude ($P > 0.9999$; 5 dpf: 28.63 ± 11.56 pA; **Fig. 4.4*C***). When comparing voltage-dependent properties, our data show that the activation voltage of I_M is significantly hyperpolarized at 3 dpf compared to 2 dpf and 4 dpf (2 dpf: -33.89 ± 6.01 mV; 3 dpf: -44.55 ± 5.68 mV; 4 dpf: -35.63 ± 10.63 mV; 5 dpf: -39.09 ± 7.01 mV; **Fig. 4.4*D***). Otherwise, no significant difference in the activation voltage of I_M was found between the age groups. Furthermore, we find that the voltage at which I_M is activated at half its maximal amplitude ($V_{1/2}$) is significantly depolarized at 2 dpf compared to 3 dpf and 5 dpf but not 4 dpf (2 dpf: -27.35 ± 6.58 mV; 3 dpf: -37.64 ± 4.31 mV; 4 dpf: -31.90 ± 6.75 mV; 5 dpf: -37.79 ± 3.37

mV; **Fig. 4.4*E***). These data demonstrate that both amplitude and voltage-dependent properties of I_M change during the 2 dpf to 5 dpf developmental time window.

Intriguingly, the transient increase in the magnitude of I_M between 2 and 3 dpf coincides with the age at which larval zebrafish swim infrequently (Thirumalai and Cline 2008). We analyzed the number of swimming episodes produced in response to touch-evoked escape responses and found a significant reduction in the number of episodes produced at 3 dpf compared to all other ages (2 dpf: 1.96 ± 0.92 episodes; 3 dpf: 1.35 ± 0.35 episodes; 4-5 dpf: 2.73 ± 2.77 episodes; **Supplemental Figure 4.3*B***). Further analyses into the features of these escape responses revealed a reduction in the duration of the first episode produced at 4-5 dpf that is in line with the shortening of episodes that occurs with the transition from burst to beat-and-glide swimming between 3 and 4 dpf (**Supplemental Figure 4.3*C*).** Furthermore, no differences to tail beat frequency of the first episode across age groups were revealed (**Supplemental Figure 4.3*D***). Interestingly, enhancement of I_M by ICA-069673 reduces the number of swimming episodes produced during escape responses at 2 dpf (control: 1.84 ± 0.78 episodes; ICA-069673: 1.21 ± 0.33 episodes; **Supplemental Figure 4.3*F***) and 4-5 dpf (control: 5.45 ± 3.47 episodes; ICA-069673: 1.67 ± 0.47 episodes; **Supplemental Figure 4.3*J***), but not 3 dpf (control: 1.32 ± 0.38 episodes; ICA-069673: 1.13 ± 0.22 episodes; **Supplemental Figure 4.3*H***) which is the age at which the magnitude of I_M was found at its largest (**Fig. 4.4*C***). XE-991 on the other hand failed to result in any changes to the number of episodes produced at all ages (**Supplemental Figure 4.3*E, G, I***). No differences in the episode duration or tail beat frequency were observed with ICA-069673 or XE-991 at any age (**Supplemental Figure 4.3*K-V***). These data demonstrate that the influence of I_M modulation with

respect to the escape response is restricted to how many swimming episodes are produced and that the degree of this influence varies with developmental age.

Next, we sought to determine whether differences in magnitude and voltage-dependency of I_M in pMNs across ages coincided with any differences in intrinsic properties of the pMNs throughout development. We first compared the mean resting membrane potential of pMNs across the four age groups. The membrane potential at rest in 2 dpf pMNs was significantly depolarized compared to the three older age groups (2 dpf: -47.98 ± 5.43 mV; 3 dpf: -58.67 ± 3.61 mV; 4 dpf: -60.73 ± 2.67 mV; 5 dpf: -62.23 ± 3.94 mV; **Fig. 4.4*F***). This relatively depolarized resting membrane potential at 2 dpf coincides with a relative reduction in the magnitude of I_M at 2 dpf (**Fig. 4.2*A*-*C***).

pMNs at 2 dpf displayed a significantly higher input resistance compared to those at 4 dpf and 5 dpf while 3 dpf pMNs had a higher input resistance relative to 4 dpf pMNs only (2 dpf: 550.30 ± 296.20 MΩ; 3 dpf: 340.20 ± 203.60 MΩ; 4 dpf: 227.40 ± 87.46 MΩ; 5 dpf: 292.50 ± 192.10 MΩ; **Fig. 4.4*I***). Similarly, 2 dpf pMNs display higher values of the membrane time constant (τ), compared to 4 and 5 dpf pMNs while 3 dpf pMNs have a larger membrane time constant compared to 4 dpf pMNs (2 dpf: 9.72 ± 3.70 ms; 3 dpf: 6.53 ± 2.04 ms; 4 dpf; 4.69 ± 2.12 ms; 5 dpf: 5.70 ± 3.63 ms; **Fig. 4.4*H***). Membrane capacitance on the other hand shows a significant increase only from 2 dpf to 4 dpf (2 dpf: 19.66 ± 8.20 pF; 3 dpf: 19.35 ± 3.05 pF; 4 dpf: 20.38 ± 3.02 pF; 5 dpf: 19.89 ± 3.27 pF; **Fig. 4.4*J***).

Finally, we investigated changes in firing properties of pMNs from 2 to 5 dpf (**Fig. 4*K*-*N***). There was a significant increase in the number of spikes generated in response to a maximal applied

current (295 pA for 50 ms) from 2 dpf to 3 dpf and 4 dpf with no other significant differences were observed across the ages (2 dpf: 3.44 ± 1.58; 3 dpf: 3.29 ± 1.43; 4 dpf: 4.87 ± 1.71; 5 dpf: 4.14 ± 1.17; **Fig. 4.4*L***). Rheobase was significantly reduced in pMNs at 2 dpf compared to 4 dpf and 5 dpf with no other differences between ages (2 dpf: 54.00 ± 18.54 pA; 3 dpf: 75.00 ± 26.13 pA; 4 dpf: 107.70 ± 50.51 pA; 94.77 ± 31.49 pA; **Fig. 4.4*M***), which is in line with the observed increase in input resistance at 2 dpf (**Fig. 4.4*I***). No significant differences in spike threshold were found across ages (2 dpf: -33.04 ± 5.40 mV; 3 dpf: -32.18 ± 5.63 mV; 4 dpf: -30.76 ± 5.50; 5 dpf: -30.81 ± 3.89 mV; **Fig. 4.4*N***).

Overall, these data reveal a transient but important increase in the magnitude of I_M in 3 dpf pMNs. They also reveal important differences in intrinsic properties notably between 2 dpf and older pMNs.

4.4.4 Inward currents do not mask the magnitude of the M-current in 4 dpf primary motoneurons

Following the finding that the magnitude of I_M increases significantly from 2 dpf to 3 dpf followed by a subsequent reduction by 4 dpf, we wondered whether the true magnitude of I_M at 4 and 5 dpf might be masked by the presence of an inward current either appearing or increasing at 4 dpf. The standard I_M deactivation protocol would not necessarily exclude effects to inward currents. This protocol could lead to deactivation of inward currents active at subthreshold membrane potentials, reducing the observable loss of outward current attributable to I_M deactivation. Previous work has revealed an inward current in zebrafish primary motoneurons that is partially blocked by 5 μM riluzole, a known inhibitor of I_{NaP} (Tong and Jonathan Robert McDearmid 2012). Using this same

concentration of riluzole, we investigated its effects on the current-voltage relationship and properties of I_M in pMNs at 4 dpf compared to a separate group of control pMNs. We also compared these same properties of the latter with a group of pMNs exposed to 20 μM nifedipine, an L-type calcium channel inhibitor. The inward calcium current mediated by the L-type channels (I_{CaL}) has a voltage dependency similar to that of I_{NaP} (Brown, Schwindt, and Crill 1994; Xu and Lipscombe 2001). We find no significant difference in the current-voltage relationship of control pMNs compared to those exposed to riluzole ($P = 0.3541$) as well as those exposed to nifedipine ($P = 0.5880$) (**Fig. 4.5** ***A,B***). The peak amplitude of I_M remained unaltered by both riluzole and nifedipine (control: 28.88 ± 15.66 pA; riluzole: 22.28 ± 5.71 pA; nifedipine: control: 28.61 ± 5.71 pA; **Fig. 4.5*C***). Though nifedipine caused a hyperpolarizing shift in the activation of I_M and riluzole did not (control: -47.05 ± 9.72 mV; riluzole: -53.50 ± 7.47 m; nifedipine: -55.00 ± 4.08 mV; **Fig. 4.5*D***), neither riluzole nor nifedipine altered the voltage at which I_M reaches half its maximal amplitude ($V_{1/2}$) (control: -32.39 ± 6.63 mV; riluzole: -35.27 ± 9.70 mV; nifedipine: -39.69 ± 3.93 mV; **Fig. 4.5E**). These data demonstrate that inward currents attributed to I_{NaP} and I_{CaL} do not mask the magnitude of I_M at 4 dpf and suggest a true reduction of the latter from 3 to 4 dpf.

4.4.5 Characterization of the expression of inward currents in primary motoneurons during early zebrafish development

Given that previous work has revealed that I_M and I_{NaP} work together to regulate burst firing and neuronal excitability (Verneuil et al. 2020b; Yue and Yaari 2004, 2006), we wondered whether the development changes of I_M in pMNs (**Fig. 4.3**) were accompanied by changes to I_{NaP} (**Fig. 4.6**). To this end, we introduced a 20 mV/second depolarizing voltage ramp over the course of 5 seconds in pMNs initially held at -90 mV (**Fig. 4.6*E***). Similar voltage ramps have been used to reveal the

persistent inward currents (PICs) of which I_{NaP} is a main contributor in mammalian MNs as well as 1 dpf zebrafish pMNs (Drouillas et al. 2023; Li and Bennett 2003; Li et al. 2004; Tong and Jonathan Robert McDearmid 2012; Verneuil et al. 2020b). Because I_{CaL} also contributes to the PICs in mammalian MNs (Cheng, Zhang, and Dai 2020; Lee and Heckman 1999; Li and Bennett 2003; Li et al. 2004), we sought to characterize the contribution of the L-type calcium current throughout early zebrafish development as well (**Fig. 4.6**). We compared the electrophysiological signature of the PICs during the slow depolarizing voltage ramps in 4 separate groups of pMNs (control, 5 μM riluzole, 20 μM nifedipine and, 5 μM riluzole + 20 μM nifedipine combined) at 4 different ages (2-5 dpf) (**Fig. 4.6*A*-*D***).

In 2 dpf pMNs, the amplitude of the PICs is significantly reduced by riluzole and nifedipine (control: -59.04 ± 17.17 pA; riluzole: -16.66 ± 6.92 pA; nifedipine: -27.40 ± 8.09 pA; riluzole and nifedipine: -27.68 ± 11.33 pA; **Fig. 4.6*F***). At 3 dpf, the amplitude of the PICs in pMNs is only significantly reduced with riluzole and when both nifedipine and riluzole are applied together (control: -62.18 ± 38.31 pA; riluzole: -34.76 ± 13.11 pA; nifedipine: -41.69 ± 19.82 pA; riluzole and nifedipine combined: -30.39 ± 11.55 pA; **Fig. 4.6*G***). By 4 dpf, the amplitude of the PICs of pMNs is reduced both by individual application of riluzole and nifedipine (control: -61.86 ± 30.18 pA; riluzole: -33.46 ± 29.96 pA; nifedipine: -37.09 ± 14.56 pA: riluzole and nifedipine combined: -40.40 ± 15.58 pA; **Fig. 4.6*H***). At 5 dpf, the amplitude of the PICs in pMNs is significantly reduced only by the joint effect of riluzole and nifedipine (control: -63.89 ± 33.75 pA; riluzole: -66.07 ± 27.18 pA; nifedipine: -41.72 ± 16.30 pA; riluzole and nifedipine combined: -32.43 ± 24.14 pA; **Fig. 4.6*I***). These data show that within each age group, the contributions of I_{NaP} and I_{CaL} to the PICs are different. To further investigate these differences, we next performed direct comparisons

across ages within each treatment group (**Fig. 4.6*J*-*M***). The amplitude of the PICs measured in the control groups of pMNs at 2 to 5 dpf were not significantly different from one another (2 dpf: -59.04 ± 17.17 pA; 3 dpf: -62.18 ± 38.31 pA; 4 dpf: -61.86 ± 30.18 pA; -63.89 ± 33.75 pA; **Fig. 4.6*J***). Because of this, we directly compared the PICs amplitudes of each treatment group across ages. We find that blockade of I_{NaP} by 5 μM riluzole becomes progressively less effective at reducing the peak PICs amplitude from 2 dpf to 5 dpf (2 dpf: -18.26 ± 7.35 p A; 3 dpf: -51.99 ± 13.38 pA; -53.58 ± 29.59 pA; 5 dpf: -82.42 ± 37.36 pA; **Fig. 4.6*K***). Nifedipine, on the other hand, reduces the PICs amplitude similarly across age groups (2 dpf: -32.81 ± 9.31 pA; 3 dpf: -53.44 ± 27.53 pA; 4 dpf: -35.88 ± 16.27 pA; -44.37 ± 28.50 pA; **Fig. 4.6*L***). When both riluzole and nifedipine are bath applied together, we find a larger reduction in the amplitude of the PICs at 2 dpf compared to 4 dpf with no other differences observed across ages (2 dpf: -26.77 ± 12.06 pA; 3 dpf: -36.63 ± 15.87 pA; 4 dpf: -55.54 ± 14.24 pA; -39.53 ± 28.14 pA; **Fig. 4.6*M***). Overall, these data reveal developmental changes to the contribution of I_{NaP} to the PICs measured in pMNs as development progresses from 2 to 5 dpf while the contribution of I_{CaL} appears to remain consistent during this developmental period.

4.4.6 Influence of pharmacological inhibition of I_M on spike-frequency adaptation in primary motoneurons changes during early development

With developmental differences in the magnitude of I_M and I_{NaP} contribution to the PICs in pMNs, we sought to investigate what their respective roles to pMN function might be. Spike-frequency adaptation is the gradual decrease in the rate of action potential generation during sustained depolarization and it is commonly observed in motoneurons (Ampatzis et al. 2013; Brownstone et al. 1992; Granit, Kernell, and Shortess 1963; Kernell and Monster 1982; Lee and Heckman 2001;

Menelaou and McLean 2012; Miles, Dai, and Brownstone 2005; Sawczuk, Powers, and Binder 1995). With I_{NaP} being involved in the maintenance of repetitive firing while I_M has been involved with burst termination, we investigated the effects of pharmacologically blocking each of these currents on spike-frequency adaptation in pMNs during early development (**Figs 4.7-4.9*B***). To this end, after determining the rheobase of individual pMNs, we injected current equal to twice the amplitude of rheobase for a period of 500 ms. **Fig. 4.7** displays examples of the voltage responses to 2x rheobase current injection from individual pMNs from each treatment group (control, 10 μM XE-991, 5 μM riluzole, and both 10 μM XE-991 and 5 μM riluzole combined) across each age groups (2 dpf, 3 dpf, 4 dpf, and 5 dpf) while quantitative analyses of these voltage responses are found in **Figs. 8** and **9**. The rationale behind testing the effects of a combined bath application of XE-991 and riluzole stems from the potential differences in each of their contributions to firing frequency regulation across developmental ages. We calculated the instantaneous firing frequency (f_{inst}) of spikes generated throughout the 500-ms current injection and plotted f_{inst} as a function of spike number for comparison between treatment groups within each age group (**Fig. 4.8*A*, *D*, *G*, *J***). At 2 dpf, while we find no significant effects to the number of spikes generated with XE-991 or riluzole individually, we see a significant decrease when the two pharmacological inhibitors are bath applied in conjunction (control: 5.26 ± 4.31; XE-991: 8.17 ± 8.38; riluzole: 2.82 ± 1.25; XE-991 and riluzole combined: 2.30 ± 1.25; **Fig. 4.8*B***). No differences were found when comparing the maximum instantaneous frequency across treatments at 2 dpf (control: 367.2 ± 112.6 Hz; XE-991: 374.8 ± 140.2 Hz; riluzole: 373.0 ± 103.8 Hz; XE-991 and riluzole combined: 359.9 ± 158.1 Hz; **Fig. 4.8*C***). At 3 dpf, we find that XE-991 increased the number of spikes generated compared to controls with no significant effect of riluzole nor the joint action of XE-991 and riluzole (control: 8.33 ± 6.85; XE-991: 24.00 ± 15.52; riluzole: 4.50 ± 1.38; XE-991 and riluzole combined: 5.36 ±

1.50; **Fig. 4.8*E***). No effects to maximum instantaneous firing frequency were observed at 3 dpf (control: 392.2 ± 185.0 Hz; XE-991: 387.4 ± 70.1 Hz; riluzole: 392.1 ± 96.6 Hz; XE-991 and riluzole combined: 391.6 ± 75.8 Hz; **Fig. 4.8*F***). At 4 dpf, a significant decrease in the number of spikes was observed in the presence of riluzole as well as both XE-991 and riluzole, with no effects brought on by XE-991 in pMNs (control: 32.46 ± 23.85; XE-991: 37.77 ± 28.69; riluzole: 4.18 ± 1.25; XE-991 and riluzole combined: 3.92 ± 0.95; **Fig. 4.8*H***). No differences in the maximum instantaneous firing frequency was observed at 4 dpf across treatments (control: 360.0 ± 95.2 Hz; XE-991: 406.7 ± 75.8 Hz; riluzole: 359.8 ± 83.9 Hz; XE-991 and riluzole combined: 381.8 ± 80.2 Hz; **Fig. 4.8*I***). By 5 dpf, pMNs show no difference in the number of spikes generated in the presence of XE-991 or riluzole alone; however, a significant reduction is observed between control pMNs and those exposed to both XE-991 and riluzole combined while riluzole significantly reduces the number of spikes generated in pMNs compared to those exposed to XE-991 alone (control: 24.38 ± 12.16; XE-991: 43.90 ± 17.35; riluzole: 10.55 ± 5.22; XE-991 and riluzole combined: 6.83 ± 2.41; **Fig. 4.8*K***). Like all other age groups investigated, no effects to maximum instantaneous firing frequency were observed (control: 416.0 ± 138.2 Hz; XE-991: 458.0 ± 114.3 Hz; riluzole: 431.6 ± 102.3 Hz; XE-991 and riluzole combined: 396.3 ± 88.09 Hz; **Fig. 4.8*L***). In summary, we observe effects to features of repetitive firing in pMNs resulting from pharmacological blockade of I_M and I_{NaP} that change during the 2 dpf to 5 dpf developmental window.

To investigate these age-related differences in the contributions of I_M and I_{NaP} to the regulation of repetitive firing further, we first compared features of spike-frequency adaptation measured in control pMNs in 2 dpf, 3 dpf, 4 dpf, and 5 dpf fish. At 4 dpf and 5 dpf, the maximum number of

spikes is significantly increased relative to 2 dpf and 3 dpf (2 dpf: 5.26 ± 4.31 spikes; 3 dpf: 8.33 ± 6.85 spikes; 4 dpf: 32.46 ± 23.85 spikes; 5 dpf: 24.38 ± 24.16 spikes; **Fig. 4.9*B***). We describe above that XE-991 increases the number of spikes at 3 dpf only (**Fig. 4.8**). We calculated the overall change to the number of spikes with XE-991 in pMNs of each age group as the percentage change relative to the median of respective control groups. We find that there is a large increase in the number of spikes generated in the presence of XE-991 relative to controls at 3 dpf compared to 2 dpf and 4 dpf (2 dpf: 104.2 ± 209.4%; 3 dpf: 300.0 ± 258.9%; 4 dpf: 45.3 ± 110.3%; 5 dpf: 75.6 ± 69.4%; **Fig. 4.9*E***). This transient more pronounced influence of I_M blockade of increasing repetitive firing in pMNs at 3 dpf coincides with when the measured magnitude of I_M is at its largest during the 2 dpf to 5 dpf developmental window (**Fig. 4.4*A*, *C***). The same measures of overall change in spike number from control groups was performed in each respective age group of pMNs exposed to 5 μM riluzole. Interestingly, we find a significantly more pronounced decrease from controls at 4 dpf compared to all other ages in the presence of riluzole (2 dpf: -29.55 ± 31.26%; 3 dpf: -25.00 ± 23.03%; 4 dpf: -83.92 ± 4.81%; 5 dpf: -57.82 ± 20.89%; **Fig. 4.9*I***). Finally, we calculated the instantaneous firing frequency of steady-state spiking (f_{SS}). This was done by taking the average of f_{inst} between the last 5 pairs of spikes produced during the 2x rheobase current injection. Because 2 dpf pMNs generated too few spikes, we could not include this age group in our f_{SS} analysis. We find an increase in f_{SS} at 4 dpf relative to 3 dpf in control pMNs (3 dpf: 29.73 ± 3.71 Hz; 4 dpf: 70.73 ± 36.11 Hz; 5 dpf: 47.10 ± 10.97 Hz; **Fig. 4.9*C***). pMNs exposed to XE-991 also display an increase in f_{SS} at 4 dpf relative to 3 dpf (3 dpf: 47.73 ± 18.43 Hz; 4 dpf: 93.49 ± 35.17 Hz; 5 dpf: 68.70 ± 21.36 Hz; **Fig. 4.9*F***) yet when the percentage change from the control median is calculated, no significant differences between ages are found (3 dpf: 55.78 ± 60.16%; 4 dpf: 25.37 ± 66.19%; 5 dpf: 63.77 ± 50.91%; **Fig. 4.9*G***).

In summary, these findings reveal that I_{NaP} is necessary to repetitive firing in pMNs from 2 dpf to 5 dpf. These data demonstrate that I_M is involved in limiting repetitive firing brought on by I_{NaP} most prominently at 3 dpf compared to 2 dpf, 4 dpf, and 5 dpf.

4.4.7 Putative P/Q calcium channels mediate an inward current appearing in primary motoneurons at 4 dpf

During our depolarizing voltage ramp experiments (**Fig. 4.6**), we noticed the appearance of a second inward current at depolarized membrane potentials in pMNs of 4 and 5 dpf larvae (**Fig. 4.10*A***). This second inward current was never present at 2 or 3 dpf and the proportion of pMNs in which it was observed increased from 2 and 3 dpf to 4 and 5 dpf (2 dpf: 0/10 pMNs; 3 dpf: 0/11 pMNs; 4 dpf: 8/22 pMNs; 5 dpf: 10/15 pMNs; **Fig. 4.10*B***). We posited that this second inward current may be a high voltage activated (HVA) calcium current other than the L-type current. It has been shown that pMNs primarily make use of P/Q-type calcium currents for signal transmission at the NMJ compared to N-type calcium channels (Wen et al. 2020). We compared the amplitude of this second inward current in control pMNs compared to that of an entirely separate group of pMNs exposed to 300 nM ω-agatoxin, a potent pharmacological inhibitor of P/Q-type calcium channels (Pringos et al. 2011). We find that that the amplitude of this high-voltage activated inward current is significantly reduced by ω-agatoxin (control: -120.30 ± 46.06 pA; ω-agatoxin: -37.29 ± 6.80 pA; **Fig. 4.10*C***). ω-Agatoxin had no effect on the amplitude of the PICs (control: -100.20 ± 43.02 pA; ω-agatoxin: -106.10 ± 27.77 pA; **Fig. 4.10*D***). These data reveal the appearance of a second inward current at 4 dpf that is made up at least in part by a P/Q-type calcium current ($I_{CaP/Q}$).

DISCUSSION

Since its initial discovery (Brown and Adams 1980), the M-current (I_M) has been shown to limit neuronal excitability and burst firing observed in neurons in many systems (Adams, Brown, and Constanti 1982; Adams, Paul R., Halliwell, James V. 1982; Bordas, Kovacs, and Pal 2015; Davis et al. 2020; Drion et al. 2010; Santini and Porter 2010). The presence of I_M in spinal locomotor circuit neurons was recently demonstrated, where it works in tandem with the persistent sodium current (I_{NaP}) to control burst firing in spinal neurons, ultimately exerting an important control over locomotor speed (Verneuil et al. 2020b). Recently, Sharples et al. showed that varying magnitudes of I_M are expressed in subtypes of mouse motoneurons as a means to control their recruitment (Sharples et al. 2023). Until now, whether I_M was expressed in larval zebrafish motoneurons and involved in controlling their excitability remained uninvestigated.

We used patch-clamp electrophysiology in combination with pharmacology to reveal, for the first time, the presence of a XE-991 sensitive I_M in primary motoneurons. Inhibition by XE-991 or activation by ICA-069673 modified resting membrane potentials, which is consistent with the subthreshold nature of I_M. We observed that pharmacological activation of I_M by ICA-069673 altered firing properties of pMNs, but inhibition by XE-991 did not. Specifically, inhibiting I_M with XE-991 altered none of the features of excitability we measured (rheobase and spike threshold). It is possible therefore that the baseline level of I_M in pMNs is relatively low such that further blockade of its activity does not result in significant changes in measurable excitability. This idea is in line with findings from Chapter 2 where inhibition of I_M by XE-991 alone had no effects to features of the escape response or spontaneous swimming. Alternatively, or perhaps in conjunction, the lack of noticeable effect to excitability measures of pMNs by XE-991 could be

due to incomplete inhibition of the M-current as XE-991 is most effective when Kv7.2/7.3 channels are already in their open conformational state (Greene et al. 2017). In line with this possibility, when XE-991 was bath applied individually, no depolarization of membrane potential was observed, yet a significant depolarization of resting membrane potential by XE-991 occurred following enhancement of I_M by ICA-069673.

4.4.8 Transient increase of I_M in pMNs at 3 dpf

Considering the presence of I_M in larval pMNs, we then set out to understand how membrane dynamics of pMNs might change throughout development as a potential means to foster proper recruitment of motoneurons as locomotor movements that do not rely on pMNs become more prominent. We hypothesized that if I_M were present in zebrafish pMNs, we might observe the magnitude of I_M increasing from 2 dpf to 5 dpf with the need to limit recruitment of pMNs when slow swimming movements emerge. While we do find an increase in the amplitude of I_M at 3 dpf, tripling from its peak amplitude at 2 dpf, this increase is transient. I_M is subsequently reduced to almost half its 3 dpf amplitude by 4 dpf.

One possible explanation for the increase in I_M magnitude from 2 dpf to 3 dpf is an increase in the expression of ion channels that mediate I_M. An increase in the expression of Kv7.2/7.3 channels at 3 dpf could underlie an increase in the magnitude of observed I_M in pMNs at this age. Single cell transcriptional data from developing zebrafish from the open-source database, *Daniocell*, suggest that the *KCNQ3* gene encoding the Kv7.3 subunit may indeed be more highly expressed in motoneurons at 3 dpf compared to 2 dpf, though the differences are subtle (Sur Abhinav et al. 2023). Alternatively, a change in the conductance of I_M could explain the differences in magnitude.

Previous work has identified phosphatidylinositol 4,5-bisphosphate (PIP_2) as an important regulator of Kv7.2/7.3 channel activity whereby opening of Kv7.2/7.3 channels requires membrane PIP_2 (Li et al. 2005; Zhang et al. 2003). It is therefore possible that increases in levels of PIP_2 from 2 dpf to 3 dpf, brought on either by upregulation of PIP_2 synthesis or downregulation of PIP_2 breakdown enzymes, for example, underlie an increase in Kv7.2/7.3 activity. Experiments directly linking Kv7.2/7.3 expressional data to pMNs would be useful to delineate the mechanism underlying the increase of the M-current at 3 dpf from 2 dpf. This would be further complemented by investigation into the expression of PIP_2 in pMNs across development.

Whichever is the underlying mechanism, the observed increase of I_M at 3 dpf was transient, diminishing by nearly half its maximal amplitude by 4 dpf. While changes to Kv7.2/7.3 expression and conductance levels similar but opposite to those described above may also underlie the apparent reduction in I_M by 4 dpf, another possibility is the involvement of other ionic conductances to pMN membrane dynamics. While the standard I_M relaxation protocol used in this study reveals the electrophysiological signature of I_M deactivation, the resulting current responses do not exclude voltage-gated inward currents. Contrary to this possibility, however, we do not observe an increase in measured amplitude of the I_M across voltages when persistent inward currents I_{NaP} and I_{CaL} are inhibited by riluzole and nifedipine, respectively.

Since we observe no masking of I_M by I_{NaP} and I_{CaL} in our recordings at 4 and 5 dpf, and there is a true decrease in I_M after 3 dpf, then our findings demonstrating changes in basal membrane and firing properties of pMNs only from 2 dpf to 3 dpf cannot be explained solely by I_M. The lack of difference in resting membrane potential of 3 dpf pMNs compared to 4 dpf and 5 dpf pMNs despite

a decrease in I_M could instead be due to a parallel increase in some other outward current and/or a decrease in some inward ion current to stabilize resting membrane potential.

Another possibility stems from the limited space-clamping during voltage-clamp experiments at older developmental ages. It is possible that the issue of space-clamp is causing ineffective deactivation of I_M during our voltage steps in our older pMNs as dendritic arborization becomes more extensive during development (Bar-Yehuda and Korngreen 2008; Kishore and Fetcho 2013). In line with this, Nav and Kv7 channels associated with mediating I_{NaP} and I_M, respectively, have been demonstrated to be expressed at high densities at the axon initial segment (AIS) (Verneuil et al. 2020b). Our voltage-clamp protocols could provide effective somatic voltage-clamping but with potential ineffective voltage-clamping of the membrane located near the AIS. With this, developmental differences in measured I_M magnitude may arise from changes to expressional densities of these channels.

Nonetheless, these data suggest that the influence of the I_M on basal excitability of pMNs peaks at 3 dpf, whether because the amplitude of this current is greatest at that stage or other ionic currents start to take on a more prominent role in regulating pMN membrane dynamics together with I_M by 4 dpf.

4.4.9 I_{NaP} and I_M in pMNs across early development

I_{NaP}, whose molecular correlates remain debated, contributes to the persistent inward currents (PICs) that are present in mammalian motoneurons. It has been shown that I_{NaP} and I_M work together as opposing persistent voltage-gated currents to regulate excitability and repetitive firing.

Few studies in zebrafish have investigated the presence of I_{NaP} in spinal circuits for locomotion (Benedetti et al. 2016; Song et al. 2020a) and in only one study has I_{NaP} been revealed in pMNs at 24 hpf (Tong and Jonathan Robert McDearmid 2012). The interplay of I_{NaP} and I_M as a mechanism underlying regulation of repetitive firing might suggest the expectation that complimentary magnitudes of these opposing currents would be observed (i.e. when I_M is large so is I_{NaP}). While we observe a riluzole-mediated reduction to PICs amplitude at 3 dpf when I_M is at its largest, we find that the most significant reduction to PICs amplitude by riluzole occurs at 2 dpf when I_M is smallest in magnitude. With similar magnitudes of I_M at 4 and 5 dpf, riluzole significantly reduces the PICs amplitude at 4 dpf, but not at 5 dpf. We reveal here that contributions to the PICs by I_{NaP} tapers off during early development. While the influence of riluzole in diminishing the amplitude of the PICs appears to decrease 2 to 5 dpf, the number of spikes generated in response to 2x rheobase current injection is significantly reduced at all ages, suggesting an important requirement for I_{NaP} in regulating repetitive firing, regardless of its measured magnitude. Conversely, inhibiting I_M only significantly increased spiking at 3 dpf, suggesting that repetitive firing at 4 dpf and 5 dpf is not as importantly limited by I_M as it is at 3 dpf. These findings emphasize the complex membrane dynamics at play in the control of excitability and repetitive firing in one group of motoneurons during early zebrafish development. The differing interplay between I_M and I_{NaP} at each developmental age could be caused by several factors such as maturation of ion currents and/or pumps not explored in this study, developmental changes to channel voltage-dependency, developmental changes to the identity of channel subunit compositions, and endogenous modulation of channel activity that changes with development.

4.4.10 I_M and behaviour

The consequences of the possible transient peak of I_M in pMNs around 3 dpf for motor control in developing zebrafish remain to be investigated. pMNs are known to be necessary for the execution of the fastest swims, such as the escape response, in larval zebrafish. Our data show that pharmacological enhancement of I_M decreases excitability of pMNs. It is possible that I_M controls the recruitment of pMNs, limiting their involvement to large amplitude and fast movements where constraining the number of action potentials fosters quicker coordination of muscle contraction (Verneuil et al. 2020b). Furthermore, the control of locomotion by spinal circuits in zebrafish is speed-dependent, with speed-specific spinal circuits controlling slow, intermediate, and fast swimming (Ampatzis et al. 2014; McLean et al. 2007). I_M may act to restrict the activation of pMNs during slower locomotion and ensure that pMNs are only active upon sufficient synaptic excitation when necessary, as locomotor speeds increase.

4.4.11 I_M in spinal locomotor circuits

We have focused our initial investigation of I_M in larval zebrafish spinal neurons to pMNs. It is currently unknown whether I_M is expressed in other spinal neurons for locomotion in zebrafish. Verneuil et al. show ubiquitous expression of I_M-mediating Kv7.2/7.3 channels across lumbar locomotor spinal neurons (Verneuil et al. 2020b) and Sharples et al. demonstrate that subtypes of mouse motoneurons express varying magnitudes of I_M to control their recruitment (Sharples et al. 2023). It is possible that sMNs in zebrafish also express I_M yet the role this current plays may vary depending on MN subtype. pMNs display mostly tonic firing in response to current injection while sMNs can exhibit chattering or bursting firing patterns (Menelaou and McLean 2012). While I_M helps to control tonic repetitive firing in pMNs, I_M may exert its influence on the chattering pattern, burst termination or basal excitability levels in sMNs, where spike frequency adaptation is not

frequently observed. These potential differences in the influence of I_M on MN subtypes may arise from differing magnitudes of I_M as well as further subtype-specific differences in other ionic conductances that generate these different firing behaviours. Investigation into the identities of larval zebrafish spinal neurons, other than pMNs, that might express I_M will elucidate further similarities in the role I_M plays in spinal circuits for locomotion across vertebrate species.

4.4.12 Kv7.2/7.3 channels as targets of neuromodulation

Ion channels have been shown to be important targets of neuromodulation because their activity guides neuronal membrane and firing properties. In the case of spinal neurons, neuromodulation of ion channels by neurotransmitters such as serotonin and dopamine is linked to changes in motor activity (Guertin and Hounsgaard 1998; Hounsgaard and Kiehn 1985; Perrier, Alaburda, and Hounsgaard 2003; Picton and Sillar 2016). I_M gets its name from the finding that it is inhibited by acetylcholine via muscarinic receptors in frog sympathetic neurons (Brown and Adams 1980). Whether I_M in pMNs is similarly modulated by acetylcholine in larval zebrafish remains unknown. As spinal locomotor circuits are developing, so is the establishment of supraspinal descending neuromodulatory systems and their influence on these circuits (Brustein et al. 2003; Lambert et al. 2012; Thirumalai and Cline 2008). While the relative contribution of I_M to basal excitability of pMNs seems to taper off after 3 dpf, the continued presence of this current presents a dial for descending systems to shape the excitability of pMNs. Revealing the M-current in pMNs and changes in its amplitude and voltage-dependency in early zebrafish development is an important step to understanding the contributions of this current to motor control. Identifying which neuromodulators and their receptors might modulate the activity of the M-current will further shed

light onto how the activity of spinal locomotor circuits can be fine-tuned supraspinally, either as a result of development or depending on environmental contexts.

4.4.13 Age-dependent appearance of putative P/Q-type calcium channel mediated inward current

Our data seemed to reveal developmental dynamics of another current in pMNs. A high-voltage activated second inward current was found during a voltage ramp in a subset of patched pMNs, which seems to be mediated at least in part by P/Q-type calcium channels that are effectively blocked by ω-agatoxin. Interestingly, we noticed $I_{CaP/Q}$ only in pMNs at 4 and 5 dpf and even at these ages, it was not found in all pMNs. It is possible that there exist P/Q-type calcium channel expressional differences within the pMN population. Indeed, differences in membrane and firing properties have been documented with respect to the caudal primary (CaP) and middle primary (MiP) motoneurons (Moreno and Ribera 2009). Work identifying that P/Q-type calcium channels are crucial to signal transmission across the neuromuscular junction in pMNs compared to sMNs concentrated their investigation on CaP motoneurons (Wen et al. 2020). Perhaps therein lies the reason behind the observed second inward current present in only a subset of the pMNs we recorded from. Confirming whether $I_{CaP/Q}$ is indeed restricted to certain subtypes of pMNs would further delineate within-pMN population differences and how this plays into signal transmission at their respective muscle quadrants (Bello-Rojas et al. 2019).

Although not all pMNs expressed this second inward current at 4 and 5 dpf, it was absent in all pMNs recorded at 2 and 3 dpf, suggesting an age-dependent requirement for $I_{CaP/Q}$. It is possible that P/Q-type channels begin expression in pMNs sometime between the 3 dpf to 4 dpf transition

window. However, the necessity for P/Q-type channels in CaP motoneuron signal transmission at the NMJ was observed as early as 3 dpf (Wen et al. 2020). We therefore should expect to see this putative P/Q-type calcium channel mediated inward current in the 3 dpf pMNs we sampled. Both N-type and P/Q-type calcium channels are implicated in synaptic transmission (Dolphin 2020). Calcium currents mediated by P/Q-type channels have been shown to trigger neurotransmitter release that is more effective compared to N-type channels (Wen et al. 2020; Wu et al. 1999; Zaitsev et al. 2007). It is possible then that as zebrafish develop, P/Q-type calcium channel-mediated neurotransmitter release may be introduced in pMNs as a means to foster higher release probability (Wen et al. 2020). This would favor robust fast muscle activation as more and more slow-muscle-dominant movements are added to the zebrafish locomotor repertoire. Alternatively, it is possible that the P/Q-type calcium current observed in our voltage-clamp experiments is one that is somatic and the calcium current mediated by distant P/Q-type channels expressed at axon terminals, though it may exist, cannot be revealed in our experiments. This may underlie the observed lack of P/Q-type calcium current prior to 4 dpf. Intriguingly, if this is a somatic P/Q-type calcium current we are observing, it could be involved in spike frequency adaptation via its interplay with $I_{K(Ca)}$ (Womack, Chevez, and Khodakhah 2004) rather than neurotransmitter release. This would be in line with it appearing after 3 dpf when repetitive firing in pMNs is more prominent.

4.4.14 Conclusion

Our electrophysiology experiments reveal complex developmental changes in several ion currents of primary motoneurons. We identify the expression of two currents in primary motoneurons: a persistent outward potassium current pharmacologically identified to be the M-current and a

nifedipine sensitive high-threshold calcium current likely mediated by L-type calcium channels. We demonstrate that control of motoneuron excitability by the M-current observed in mice (Sharples et al. 2023) may be conserved in zebrafish. Moreover, we detail the contributions of a persistent sodium current in conjunction with the M-current to the regulation of repetitive firing in motoneurons, further supporting shared features of control over spike frequency across vertebrates. What underlies the developmental changes in the magnitude of the M-current, persistent sodium current, and P/Q-channel mediated calcium current in pMNs as well as how this impacts the emergence and modulation of locomotor behaviour will further reveal how the nervous system controls movements across vertebrates.

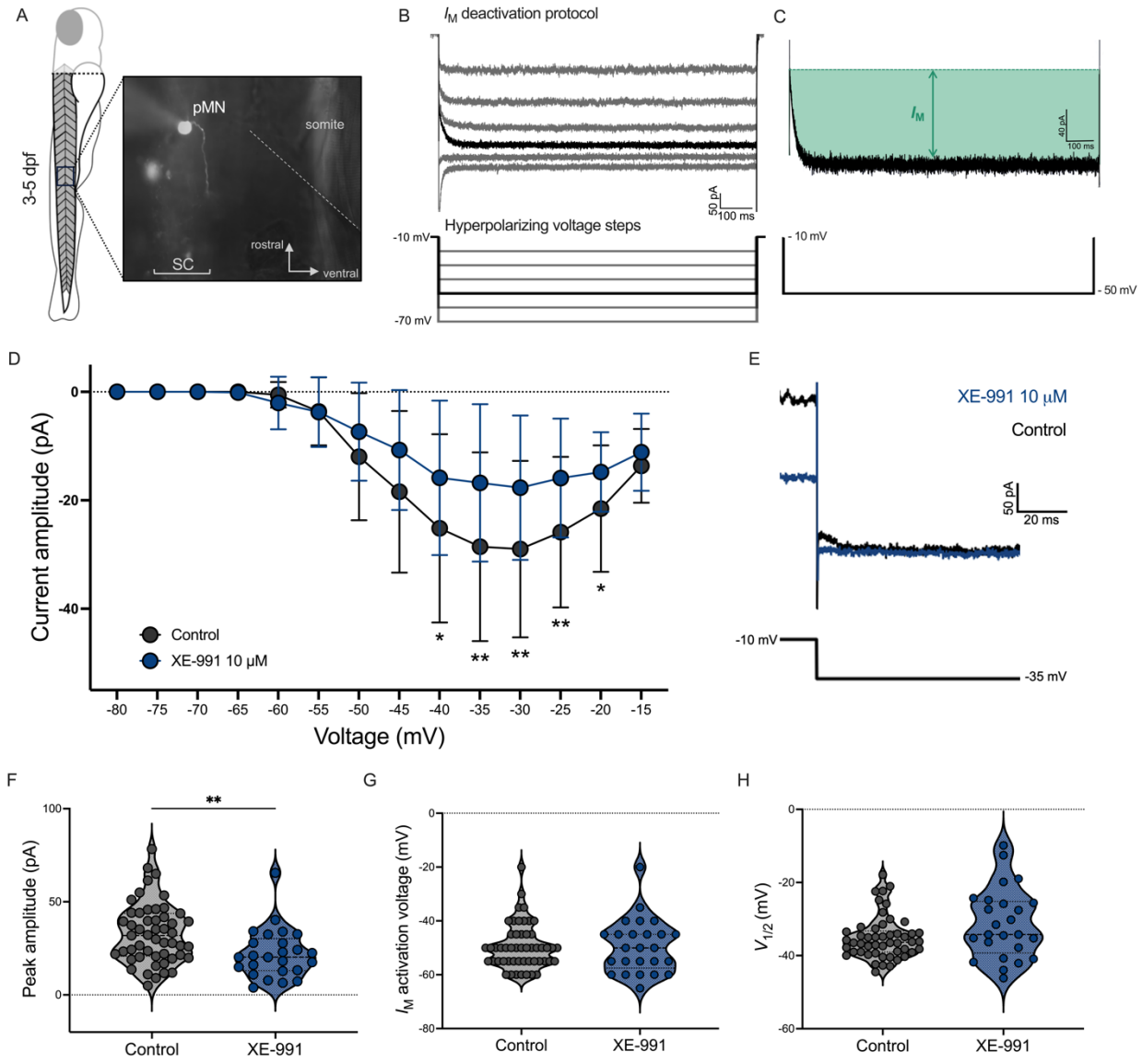
A
3-5 dpf
pMN
somite
SC
rostral
ventral
B
I_M deactivation protocol
50 pA
100 ms
Hyperpolarizing voltage steps
-10 mV
-70 mV
C
I_M
40 pA
100 ms
- 10 mV
- 50 mV
D
Current amplitude (pA)
0
-20
-40
Control
XE-991 10 µM
-80 -75 -70 -65 -60 -55 -50 -45 -40 -35 -30 -25 -20 -15
Voltage (mV)
*
**
**
**
*
E
XE-991 10 µM
Control
50 pA
20 ms
-10 mV
-35 mV
F
Peak amplitude (pA)
100
50
0
**
Control
XE-991
G
I_M activation voltage (mV)
0
-20
-40
-60
-80
Control
XE-991
H
$V_{1/2}$ (mV)
0
-20
-40
-60
Control
XE-991

Figure 4.1. Whole-cell voltage-clamp reveals XE-991-sensitive I_M in primary motoneurons of larval zebrafish. ***A*****,** Schematic depicting larvae aged 3-5 dpf with example of motoneuron filled with sulforhodamine B following patch-clamp recording in a 4 dpf larva. Dashed line demarcates the myotomal border between muscle somites. SC: spinal cord. pMN: primary motoneuron. ***B*****,** *Top:* current traces in response to the standard I_M deactivation protocol during whole-cell recording. *Bottom:* command voltages consisting of stepping down from -10 mV to -70 mV in -5 mV voltage increments. ***C*****,** Current trace response to a -40 mV hyperpolarizing voltage step during the I_M deactivation protocol enlarged from ***B*** (black trace). The amplitude of I_M is estimated as the difference between the initial peak of the current and the steady-state current in response to the voltage step (green shaded area depicts I_M amplitude). ***D*****,** Current-voltage (*I-V*) relationship of I_M measured in control pMNs (n = 51 cells; N = 25 fish; black) and during exposure to Kv7.2/7.3 channel inhibitor XE-991 (10 μM; n = 25 cells; N = 9 fish; blue). ***E*****,** Example current traces from separate pMNs under control (black) and XE-991 treatment (blue) in response to a –25 mV hyperpolarizing voltage step during the I_M deactivation protocol. ***F*****,** Peak I_M amplitude measured from pMNs under control (black) and XE-991 treatment (blue). ***G*****,** Activation voltage of I_M. ***H*****,** Voltage at which I_M reaches half of its maximum amplitude. *Statistical analysis:* Mann-Whitney tests. * $P < 0.05$, ** $P < 0.01$; otherwise, not statistically significant.

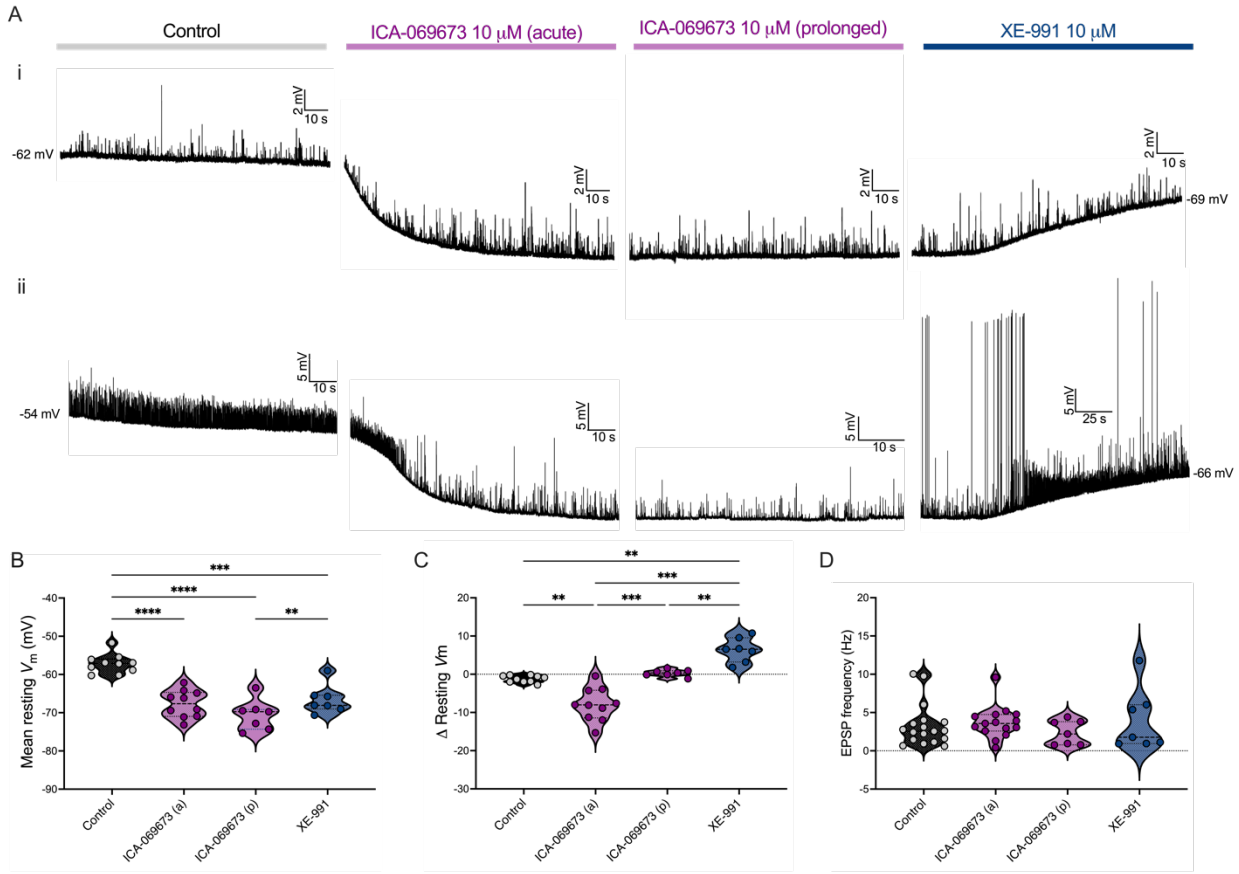
A
Control
ICA-069673 10 μM (acute)
ICA-069673 10 μM (prolonged)
XE-991 10 μM
i
-62 mV
-69 mV
ii
-54 mV
-66 mV
B
Mean resting V_m (mV)
C
Δ Resting Vm
D
EPSP frequency (Hz)
Control
ICA-069673 (a)
ICA-069673 (p)
XE-991

Figure 4.2. Pharmacological manipulation of Kv7.2/7.3 channels mediating I_M alters resting membrane potential of primary motoneurons. ***A*** **(*i-ii*),** Whole-cell current-clamp traces from two pMNs with no holding current before (control; n = 10; N = 10; grey), during acute (n = 10; N = 10; under 3 minutes) and prolonged (n = 7; N = 7; 10-15 minutes) exposure to Kv7.2/7.3 channel enhancer ICA-069673 (10 μM; magenta), and during subsequent exposure to XE-991 (n = 7; N = 7; 10-15 minutes; 10 μM; blue). ***B*****,** Mean resting membrane potential of pMNs during each treatment. ***C*****,** Overall change in resting membrane potential from start to finish of each treatment recording time. ***D*****,** Mean frequency of excitatory postsynaptic potentials (EPSPs). *Statistical analysis,* One-way ANOVA followed by Tukey's multiple comparisons tests. ** $P < 0.01$, *** $P < 0.001$, **** $P < 0.0001$; otherwise, not statistically significant.

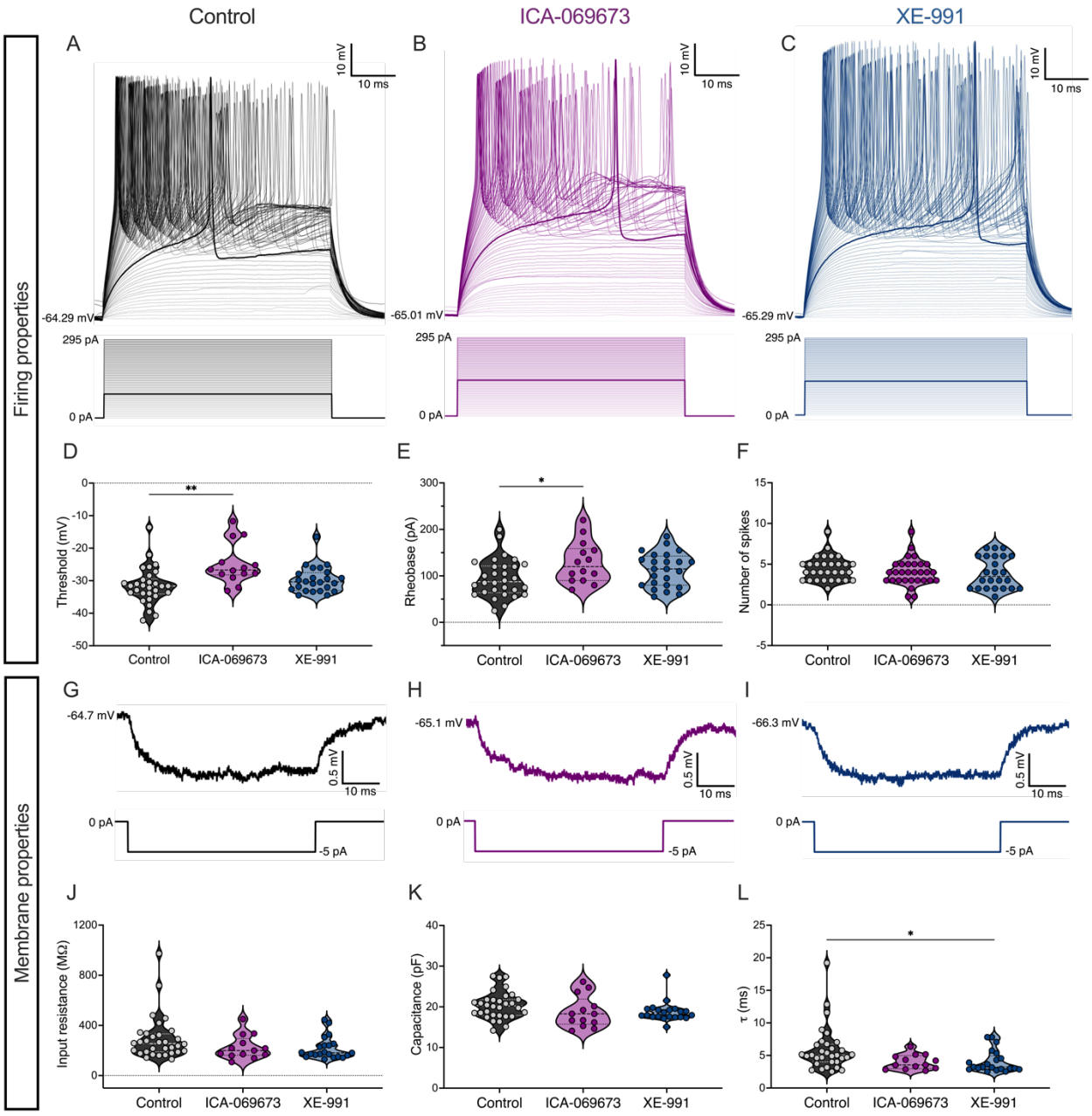
Control
ICA-069673
XE-991
Firing properties
A
B
C
10 mV
10 ms
-64.29 mV
-65.01 mV
-65.29 mV
295 pA
0 pA
D
E
F
Threshold (mV)
Rheobase (pA)
Number of spikes
Control
ICA-069673
XE-991
Membrane properties
G
H
I
-64.7 mV
-65.1 mV
-66.3 mV
0.5 mV
-5 pA
J
K
L
Input resistance (MΩ)
Capacitance (pF)
τ (ms)

Figure 4.3. Pharmacological enhancement of Kv7.2/7.3 channels mediating I_M by ICA-069673 decreases excitability of primary motoneurons in 4-5 dpf larval zebrafish. ***A-C*****,** Example voltage traces (top) from pMNs when injected with 5 pA current increments (bottom) in (***A*****)** control, (***B***) 10 μM ICA-069673 and (***C***) 10 μM XE-991. Current injections corresponding to rheobase and corresponding voltage responses are bolded. ***D-F***, Comparison of firing properties between three separate groups of pMNs: control (n = 30; N = 13; black), 10 μM ICA-069673 (n = 14; N = 4; magenta), and 10 μM XE-991 (n = 24; N = 7; blue). ***D***, Action potential threshold. ***E***, Rheobase. ***F***, Maximum number of spikes generated during a series of 50 ms current steps from 0 pA to 295 pA. ***G-I****,* Example voltage traces from distinct pMNs in response to a –5 pA current step from (***G***) control, (***H***) ICA-069673, and (***I***) XE-991 groups. ***J-L***, Comparison of membrane properties calculated from voltage traces in response to -5 pA current injection between control (n = 32; N = 12), ICA-069673 (n = 13; N = 3), and XE-991 (n = 21; N = 7) pMNs. (***J***) Input resistance, (***K***) Membrane capacitance and (***L***) Membrane time constant, τ. *Statistical analysis,* Kruskal-Wallis test with Dunn's test for multiple comparisons (***D, F, J-L***) and one-way ANOVA with Tukey's test for multiple comparisons (***E***); * $P < 0.05$, ** $P < 0.01$; otherwise, not statistically significant.

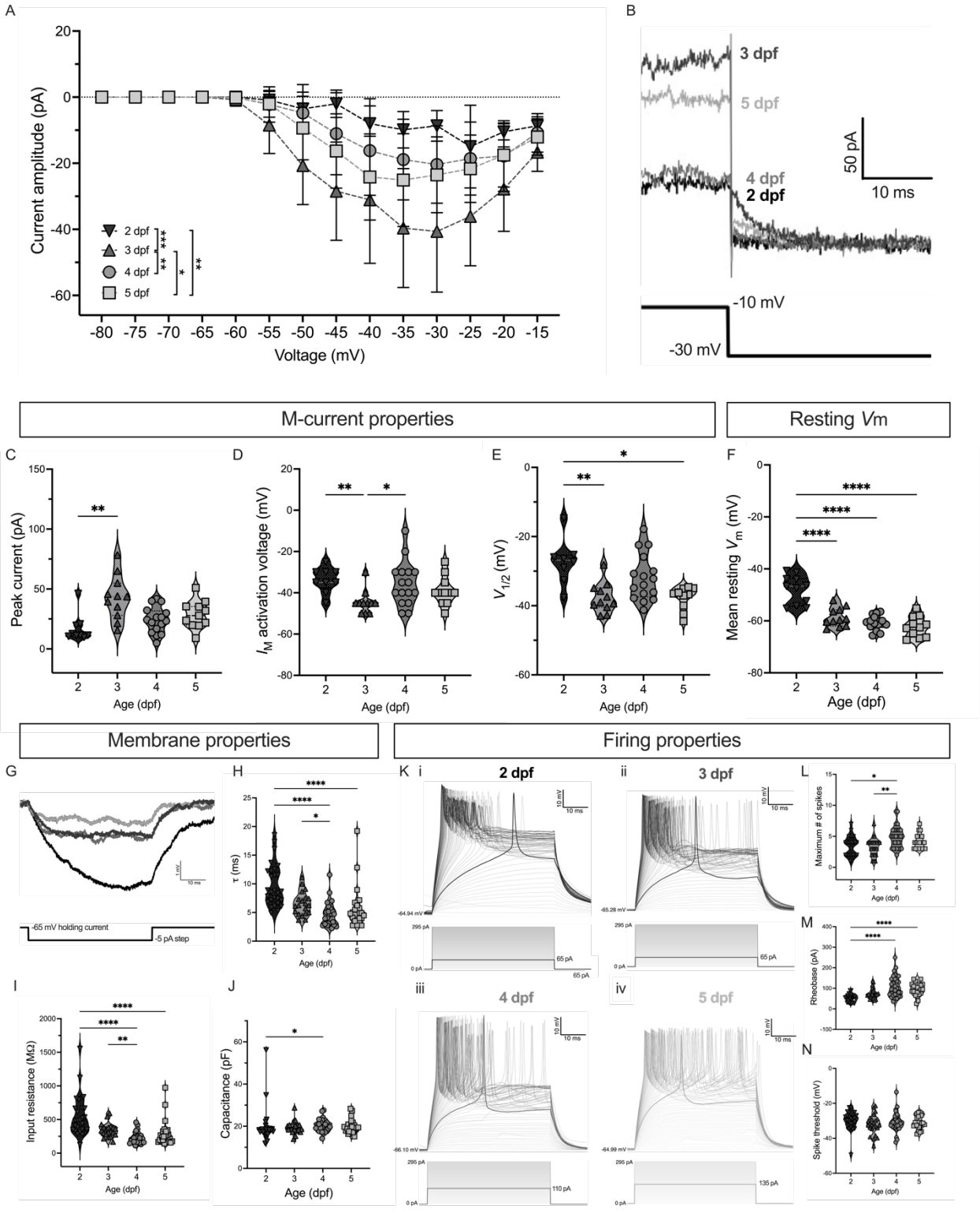
A
Current amplitude (pA)
Voltage (mV)
2 dpf
3 dpf
4 dpf
5 dpf
B
3 dpf
5 dpf
4 dpf
2 dpf
50 pA
10 ms
-10 mV
-30 mV
M-current properties
Resting Vm
C
Peak current (pA)
D
I_M activation voltage (mV)
E
$V_{1/2}$ (mV)
F
Mean resting V_m (mV)
Age (dpf)
Membrane properties
Firing properties
G
-65 mV holding current
-5 pA step
H
τ (ms)
I
Input resistance (MΩ)
J
Capacitance (pF)
K
i 2 dpf
ii 3 dpf
iii 4 dpf
iv 5 dpf
L
Maximum # of spikes
M
Rheobase (pA)
N
Spike threshold (mV)

Figure 4.4. I_M, intrinsic, and firing properties of primary motoneurons during early zebrafish development. ***A***, Current-voltage (I-V) relationship of I_M measured in pMNs from 2 dpf (n = 9; N = 3), 3 dpf (n = 11; N = 7), 4 dpf (n = 16; N = 6), and 5 dpf (n = 11; N = 5) zebrafish. ***B***, Example current traces showing I_M deactivation in 2-5 dpf pMNs in response to a –20 mV voltage step during the standard I_M deactivation protocol. Comparison of ***C*,** peak I_M, ***D*,** activation voltage of I_M, ***E*,** voltage at which I_M reaches half of its maximum amplitude (2 dpf: n = 8; 5 dpf: n = 10; otherwise, sample sizes are the same as in ***A***), and ***F*,** mean resting membrane potential (2 dpf: n = 11, N = 4; 3 dpf: n = 11, N = 7; 4 dpf: n = 16, N = 6; 5 dpf: n = 11, N = 6) of pMNs. ***G*,** Example voltage traces in response to a –5 pA current step from pMNs of zebrafish aged 2 (black), 3 (dark grey), 4 (grey), and 5 dpf (light grey). Comparison of ***H*,** membrane time constant. ***I*,** input resistance. ***J*,** capacitance of 2 dpf (n = 28; N = 10), 3 dpf (n = 20; N = 11), 4 dpf (n = 27; N = 10), and 5 dpf (n = 24; N = 11) pMNs. ***K*,** Example voltage traces in response to a series of positive 5 pA current steps from 0 pA to 295 pA in pMNs from larvae aged 2 (***i***), 3 (***ii***), 4 (***iii***), and 5 (***iv***) dpf. Comparison of ***L*,** maximum number of spikes generated in response to a 295 pA current step; ***M*,** rheobase; ***N*,** spike threshold of 2 dpf (n = 25; N = 11), 3 dpf (n = 24; N = 11), 4 dpf (n = 31; N = 11), and 5 dpf (n = 22; N = 9) pMNs. *Statistical analysis,* Effect of age assessed via mixed-effects model analysis (***A***), Kruskal-Wallis test followed by Dunn's test for multiple comparisons (***C-F, H-J, & L-N***). * $P < 0.05$, ** $P < 0.01$, *** $P < 0.001$, **** $P < 0.0001$; otherwise, not statistically significant.

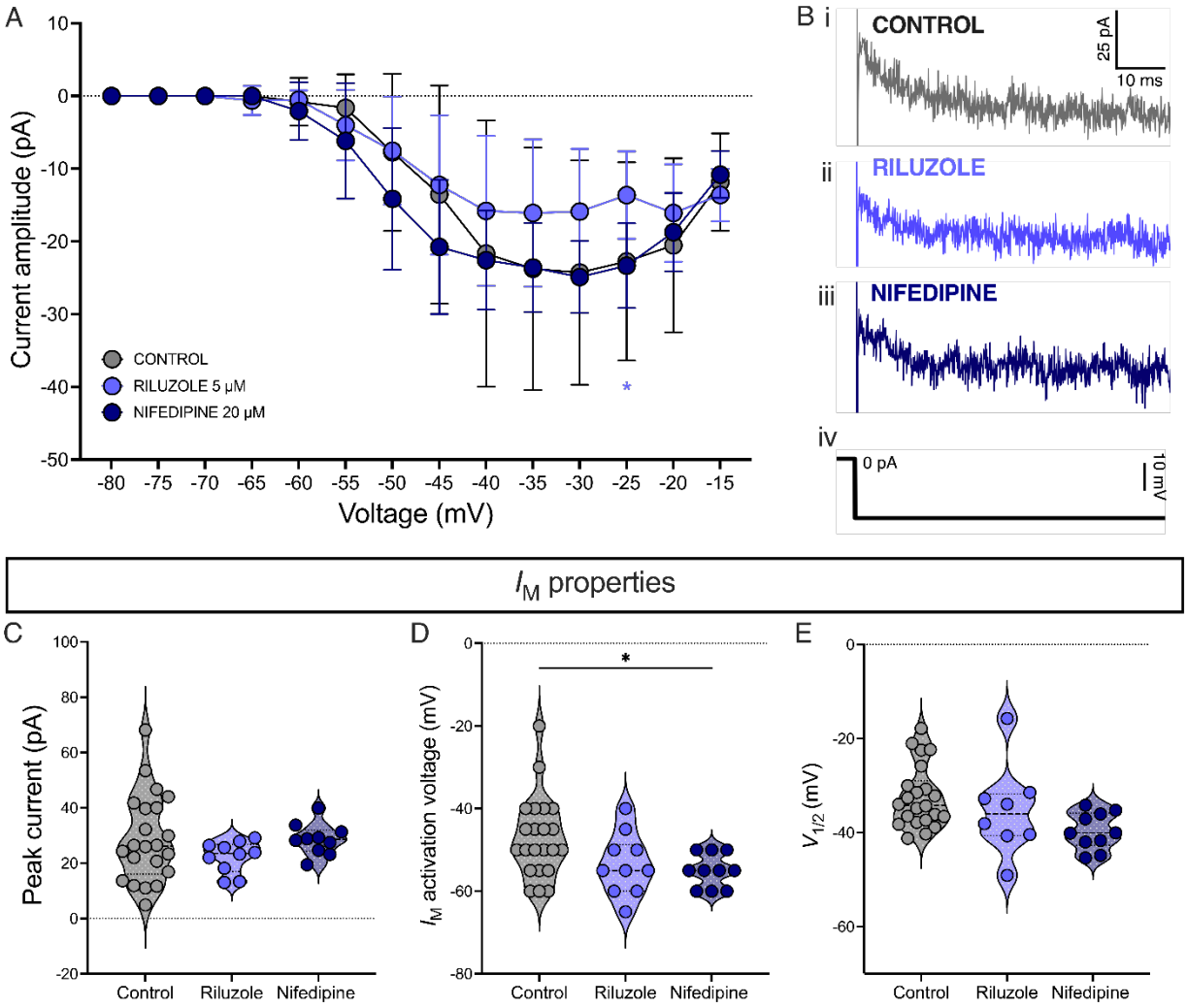
A
Current amplitude (pA)
Voltage (mV)
CONTROL
RILUZOLE 5 µM
NIFEDIPINE 20 µM
B i
CONTROL
25 pA
10 ms
ii
RILUZOLE
iii
NIFEDIPINE
iv
0 pA
10 mV
I_M properties
C
Peak current (pA)
D
I_M activation voltage (mV)
E
$V_{1/2}$ (mV)
Control
Riluzole
Nifedipine

Figure 4.5. I_{NaP} and I_{CaL} do not mask the magnitude of I_M in pMNs at 4 dpf. ***A***, Current-voltage (I-V) relationship of I_M measured in three separate groups of pMNs: control (n = 22; N = 9; grey), 5 μM I_{NaP} inhibitor riluzole (n = 10; N = 3; periwinkle), and 20 μM I_{CaL} inhibitor nifedipine (NIF, n = 10; N = 4; blue). ***B***, (*i-iii*) Example current traces showing I_M deactivation in pMNs from each treatment group in response to (*iv*) a -20 mV hyperpolarizing voltage step from -10 mV holding potential. ***C***, Peak amplitude of I_M. ***D***, Activation voltage of I_M. ***E***, Voltage at which I_M reaches half its maximal amplitude (Riluzole: n = 8; otherwise, sample sizes are the same as in ***A***, ***C***, and ***D***). *Statistical analysis*, two-way ANOVA with Tukey's multiple comparisons test (***A***) and Kruskal-Wallis test with Dunn's test for multiple comparisons (***C***-***E***). * $P < 0.05$; otherwise, not statistically significant.

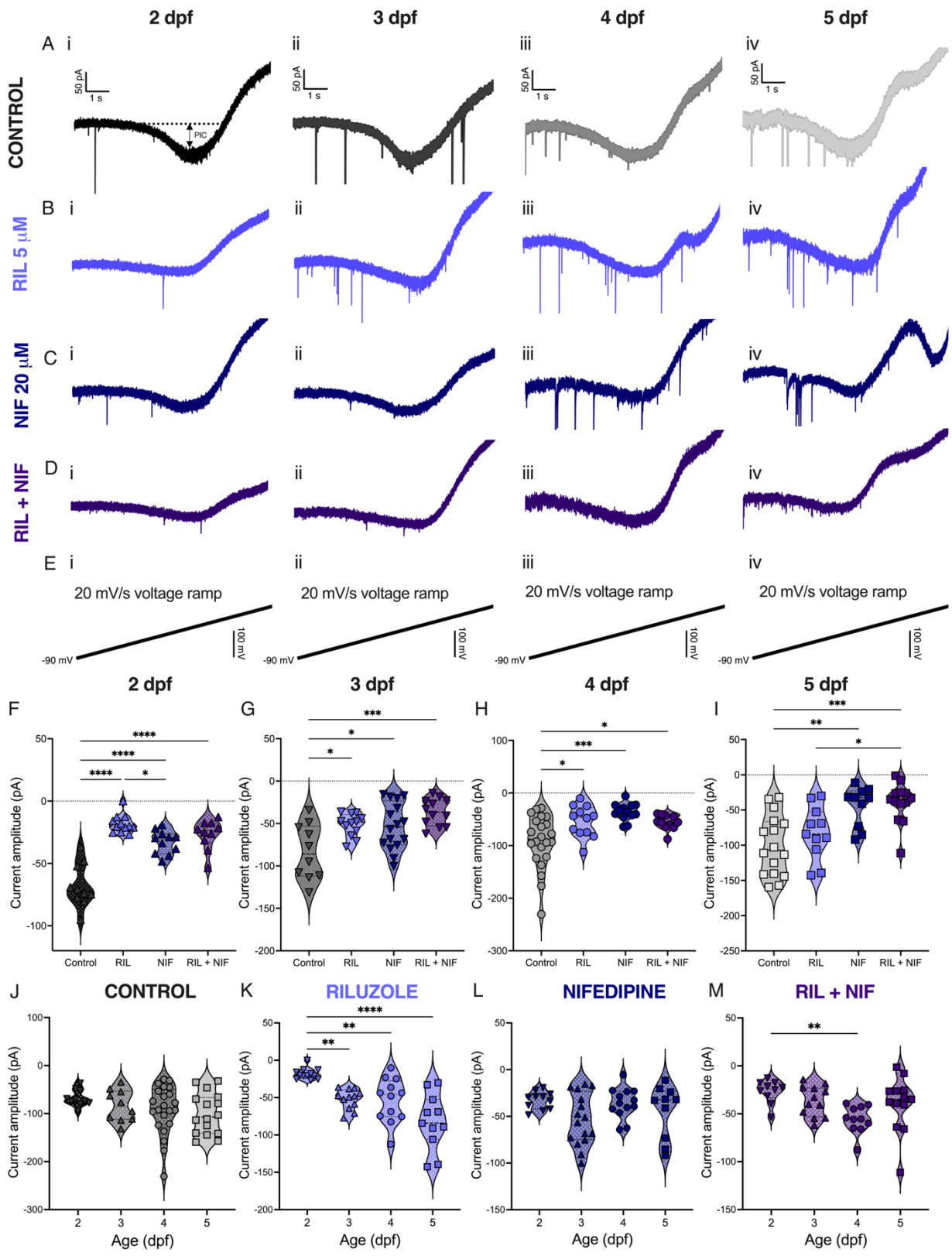
2 dpf
3 dpf
4 dpf
5 dpf
A i
ii
iii
iv
CONTROL
50 pA
1 s
PIC
B i
ii
iii
iv
RIL 5 µM
C i
ii
iii
iv
NIF 20 µM
D i
ii
iii
iv
RIL + NIF
E i
ii
iii
iv
20 mV/s voltage ramp
-90 mV
100 mV
2 dpf
3 dpf
4 dpf
5 dpf
F
G
H
I
Current amplitude (pA)
Control
RIL
NIF
RIL + NIF
J
CONTROL
K
RILUZOLE
L
NIFEDIPINE
M
RIL + NIF
Age (dpf)

Figure 4.6. Persistent inward current in primary motoneurons during early zebrafish development. ***A-E***, Examples of (***A***) control, (***B***) 5 μM riluzole (RIL), (***C***) 20 μM nifedipine (NIF), (***D***) 5 μM riluzole and 20 μM nifedipine (NIF) current traces in response to (***E***) a 20 mV/s voltage ramp from -90 mV to +10 mV revealing a persistent inward current (PIC, see example in ***Ai***) in pMNs from 2 to 5 dpf. Recordings were leak subtracted. Scale bars in ***A*** apply to all recordings within the same age group in ***B***-***D***. ***F-I***, Comparison of the effect of PICs amplitude in pMNs when inhibiting I_{NaP} and I_{CaL} with riluzole and nifedipine, respectively, (***F***) at 2 dpf (control: n = 10, N = 4, black; 5 μM riluzole: n = 12, N = 5, periwinkle; 20 μM nifedipine: n = 11, N = 5, blue; and 5 μM riluzole and 20 μM nifedipine combined: n = 10, N = 4; purple), (***G***) 3 dpf (control: n = 11; N = 3; dark grey; 5 μM riluzole: n = 12, N = 3, periwinkle; 20 μM nifedipine: n = 16, N = 5, blue; and 5 μM riluzole and 20 μM nifedipine combined: n = 12, N = 5, purple), (***H***) at 4 dpf (control: n = 20, N = 4, grey; 5 μM riluzole: n = 12, N = 4, periwinkle; 20 μM nifedipine: n = 13; N = 4; blue; and 5 μM riluzole and 20 μM nifedipine combined: n = 11, N = 3, purple), (***I***) at 5 dpf (control: n = 15, N =8, grey; 5 μM riluzole: n = 11, N = 3, periwinkle; 20 μM nifedipine: n = 9, N = 4, blue; and 5 μM riluzole and 20 μM nifedipine combined: n = 14, N = 8, purple). ***J-M***, Comparison of the effect of PICs amplitude in pMNs when inhibiting I_{NaP} and I_{CaL} with riluzole and nifedipine, respectively, across age groups during development. ***J***, Comparison of control PICs amplitude at 2 to 5 dpf. ***K***, Comparison of the effect of 5 μM riluzole on PICs amplitude at 2 to 5 dpf. ***L***, Comparison of the effect of 20 μM nifedipine on PICs amplitude at 2 to 5 dpf. ***L***, Comparison of the effect of both 5 μM riluzole and 20 μM nifedipine on PICs amplitude at 2 to 5 dpf. *Statistical analysis,* ordinary one-way ANOVA with Tukey's multiple comparison test (***F-M***). * $P < 0.05$, ** $P < 0.01$, *** $P < 0.001$, **** $P < 0.0001$; otherwise, not statistically significant.

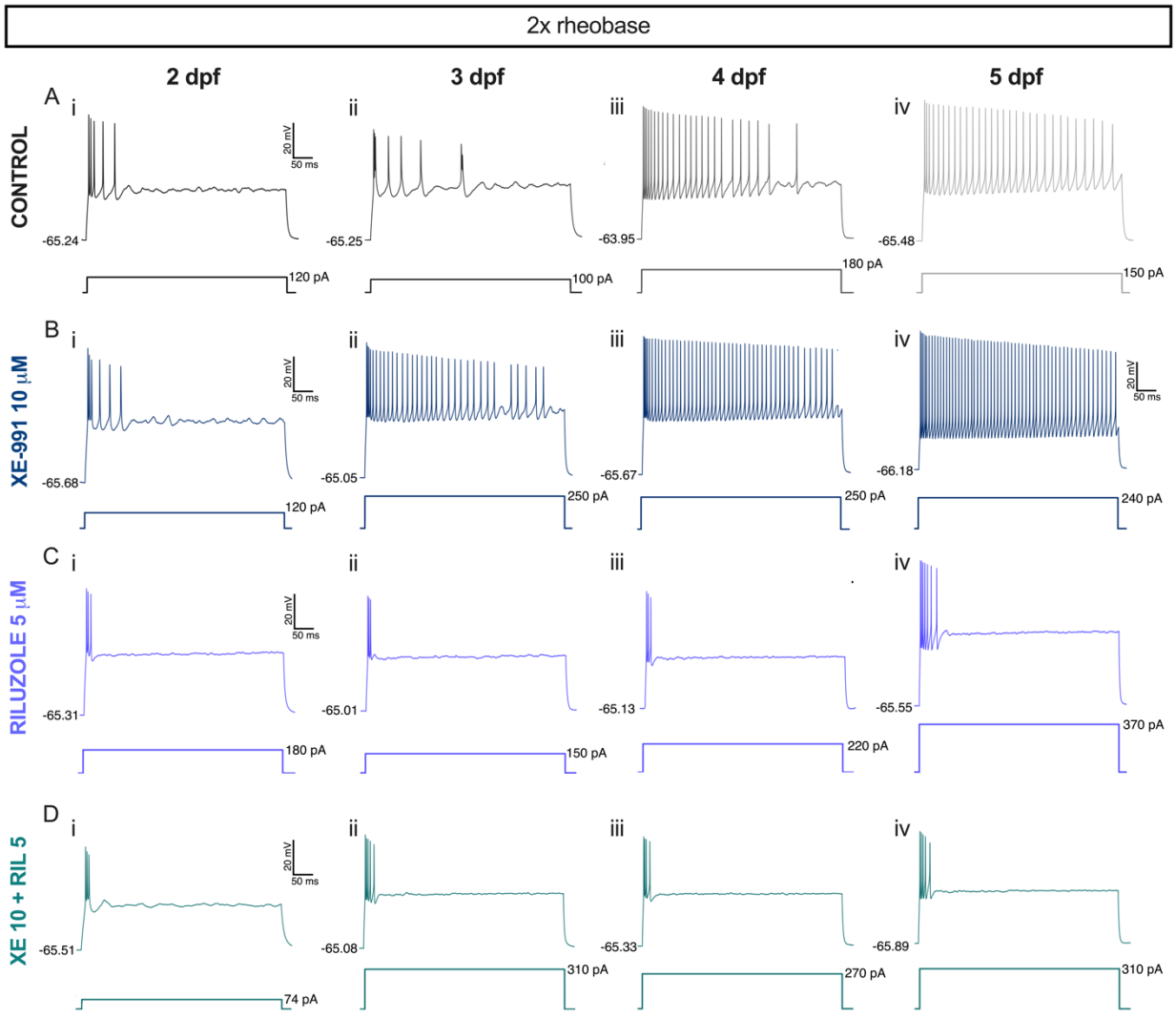
2x rheobase
2 dpf
3 dpf
4 dpf
5 dpf
A
CONTROL
i
ii
iii
iv
20 mV
50 ms
-65.24
120 pA
-65.25
100 pA
-63.95
180 pA
-65.48
150 pA
B
XE-991 10 µM
-65.68
120 pA
-65.05
250 pA
-65.67
250 pA
-66.18
240 pA
C
RILUZOLE 5 µM
-65.31
180 pA
-65.01
150 pA
-65.13
220 pA
-65.55
370 pA
D
XE 10 + RIL 5
-65.51
74 pA
-65.08
310 pA
-65.33
270 pA
-65.89
310 pA

Figure 4.7. Example voltage traces of primary motoneurons in response to current injections during pharmacological inhibition of I_M and I_{NaP} across early zebrafish development. ***A-D***, Examples of voltage responses to 2x rheobase current injection in pMNs from 2 to 5 dpf in (***A***) control, (***B***) when exposed to 10 μM XE-991, (***C***) when exposed to 5 μM riluzole and (***D***) when exposed to both 5 μM riluzole and 10 μM XE-991.

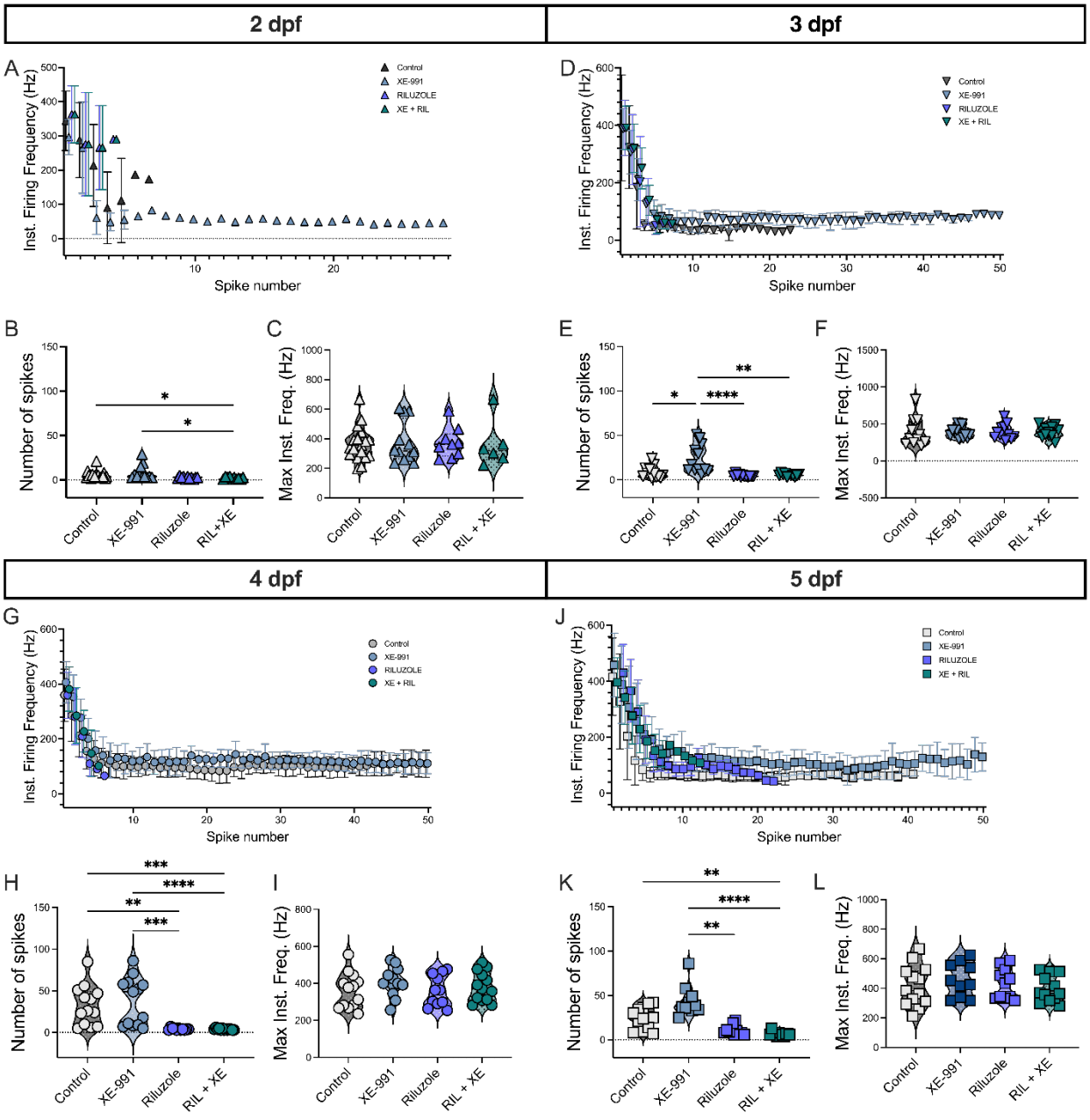
2 dpf
3 dpf
4 dpf
5 dpf
A
B
C
D
E
F
G
H
I
J
K
L
Inst. Firing Frequency (Hz)
Spike number
Control
XE-991
RILUZOLE
XE + RIL
Number of spikes
Max Inst. Freq. (Hz)
Riluzole
RIL + XE
RIL+XE

Figure 4.8. Pharmacological inhibition of I_M and I_{NaP} alters spike frequency adaptation in primary motoneurons. ***A***, Comparison of instantaneous firing frequency calculated from voltage responses to a current injection equal to 2x rheobase (see **Fig. 7**) in four separate groups of 2 dpf pMNs (control: $n = 17$, $N = 7$; XE-991: $n = 10$, $N = 3$; riluzole: $n = 9$, $N = 4$; XE-991 and riluzole: $n = 9$, $N = 3$). ***B,*** Comparison between treatment groups on the number of spikes generated in response to a current injection equal to 2x rheobase at 2 dpf (control: $n = 19$, $N = 7$; XE-991: $n = 12$, $N = 3$; riluzole: $n = 11$, $N = 4$; XE-991 and riluzole: $n = 10$, $N = 3$). ***C***, Comparison between treatment groups on the maximum instantaneous firing frequency generated in response to a current injection equal to 2x rheobase at 2 dpf (control: $n = 19$, $N = 7$; XE-991: $n = 12$, $N = 3$; riluzole: $n = 10$, $N = 4$; XE-991 and riluzole: $n = 6$, $N = 3$). ***D***, Comparison of instantaneous firing frequency calculated from voltage responses to a current injection equal to 2x rheobase in four separate groups of 3 dpf pMNs (control: $n = 12$, $N = 4$; XE-991: $n = 13$, $N = 4$; riluzole: $n = 12$, $N = 3$; XE-991 and riluzole: $n = 12$, $N = 3$). ***E,*** Comparison between treatment groups on the number of spikes generated in response to a current injection equal to 2x rheobase at 3 dpf (control: $n = 12$, $N = 4$; XE-991: $n = 13$, $N = 4$; riluzole: $n = 12$, $N = 3$; XE-991 and riluzole: $n = 11$, $N = 3$). ***F***, Comparison between treatment groups on the maximum instantaneous firing frequency generated in response to a current injection equal to 2x rheobase at 3 dpf (control: $n = 12$, $N = 3$; XE-991: $n = 13$, $N = 4$; riluzole: $n = 12$, $N = 3$; XE-991 and riluzole: $n = 12$, $N = 3$). ***G***, Comparison of instantaneous firing frequency calculated from voltage responses to a current injection equal to 2x rheobase in four separate groups of 4 dpf pMNs (control: $n = 13$, $N = 5$; XE-991: $n = 13$, $N = 5$; riluzole: $n = 11$, $N = 3$; XE-991 and riluzole: $n = 13$, $N = 4$). ***H,*** Comparison between treatment groups on the number of spikes generated in response to a current injection equal to 2x rheobase at 4 dpf. ***I***, Comparison between treatment groups on the maximum instantaneous firing frequency

generated in response to a current injection equal to 2x rheobase at 4 dpf. ***J***, Comparison of instantaneous firing frequency calculated from voltage responses to a current injection equal to 2x rheobase in four separate groups of 5 dpf pMNs (control: $n = 13$, $N = 4$; XE-991: $n = 10$, $N = 4$; riluzole: $n = 11$, $N = 3$; XE-991 and riluzole: $n = 12$, N = 4). ***K,*** Comparison between treatment groups on the number of spikes generated in response to a current injection equal to 2x rheobase at 5 dpf. ***L***, Comparison between treatment groups on the maximum instantaneous firing frequency generated in response to a current injection equal to 2x rheobase at 5 dpf. *Statistical analysis*, Kruskal-Wallis test with Dunn's test for multiple comparisons (***B***-***C***, ***E***, ***H***-***I***, ***K***-***L***) and ordinary one-way ANOVA with Tukey's test for multiple comparisons (***F***). * $P < 0.05$, ** $P < 0.01$, *** $P < 0.001$, **** $P < 0.0001$; otherwise not statistically significant.

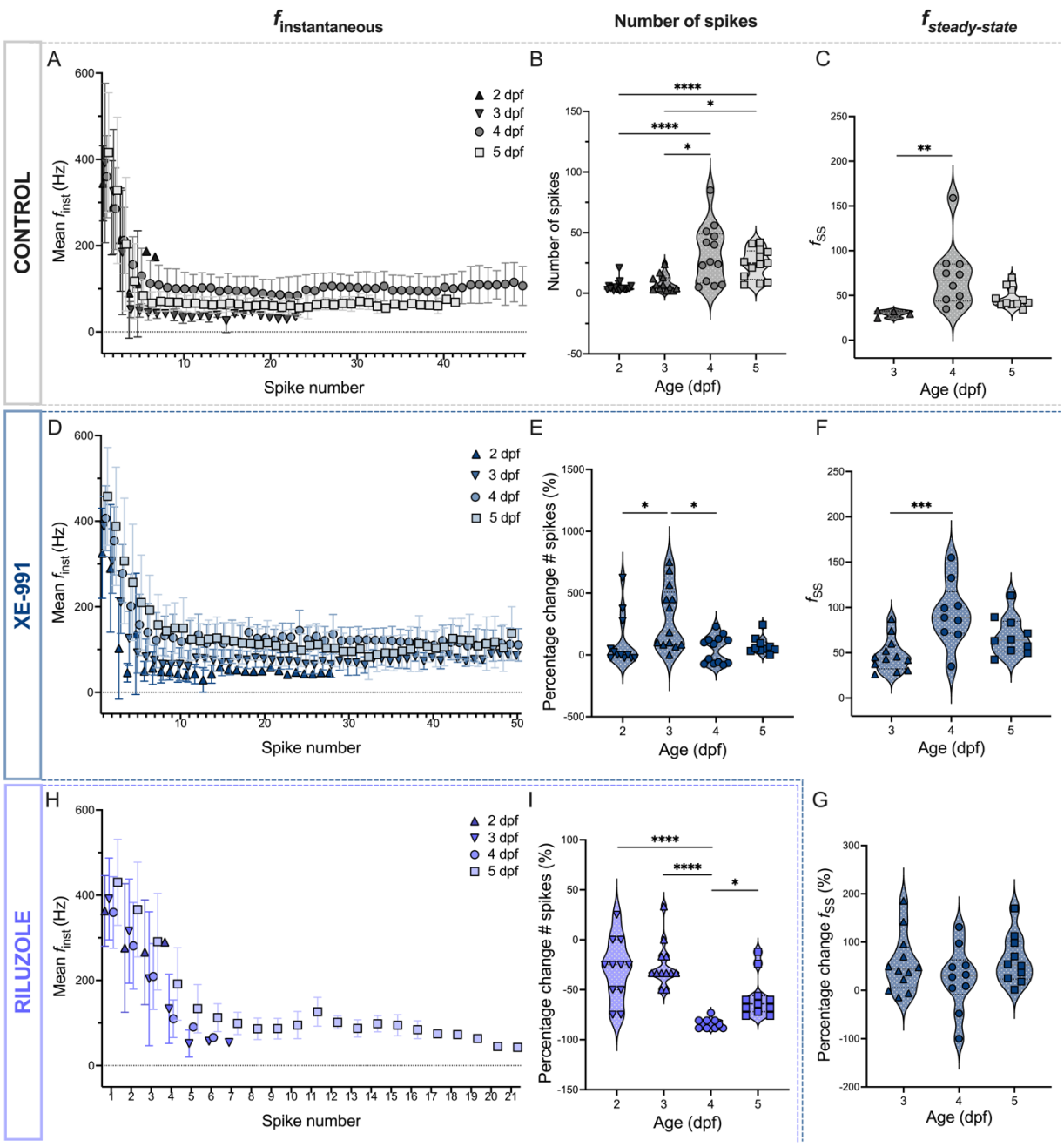
$f_{instantaneous}$
Number of spikes
$f_{steady\text{-}state}$
CONTROL
XE-991
RILUZOLE
A
B
C
D
E
F
G
H
I
2 dpf
3 dpf
4 dpf
5 dpf
Mean f_{inst} (Hz)
Spike number
Number of spikes
Age (dpf)
f_{SS}
Percentage change # spikes (%)
Percentage change f_{SS} (%)

Figure 4.9. Pharmacological inhibition of I_M by XE-991 differentially affects spike frequency adaptation across early development. ***A***, Comparison of instantaneous firing frequency calculated from voltage responses to a current injection equal to 2x rheobase (see **Fig. 4.7**) recorded from pMNs in 2 dpf (n = 17, N = 7), 3 dpf (n = 12, N = 4), 4 dpf (n = 13, N = 5), and 5 dpf (n = 13, N = 4) larvae in control conditions. ***B***, Comparison between developmental ages of the number of spikes generated in response to a current injection equal to 2x rheobase in pMNs (2 dpf: n = 19, N = 7; 3 dpf: n = 12, N = 4; 4 dpf: n = 13, N = 5; 5 dpf: n = 13, N = 4). ***C***, Steady-state instantaneous firing frequency (f_{ss}) in 3 dpf (n = 4; N = 2), 4 dpf (n = 10; N = 5), and 5 dpf (n = 11; N = 4) pMNs. ***D***, Comparison of instantaneous firing frequency calculated from voltage responses to a current injection equal to 2x rheobase recorded from pMNs exposed to 10 μM XE-991 in 2 dpf (n = 12, N = 3), 3 dpf (n = 13, N = 4), 4 dpf (n = 13, N = 5), and 5 dpf (n = 10, N = 4) larvae. ***E***, Comparison between age groups of the number of spikes generated in response to a current injection equal to 2x rheobase in pMNs exposed to 10 μM XE-991 at 2 dpf (n = 12, N = 3), 3 dpf (n = 13, N = 4), 4 dpf (n = 13, N = 5), and 5 dpf (n = 10, N = 4). ***F***, Comparison of steady-state instantaneous firing frequency (f_{ss}) between pMNs of 3 dpf (n = 12; N = 4), 4 dpf (n = 9; N = 4), and 5 dpf (n = 10; N = 4) pMNs exposed to 10 μM XE-991. ***G***, Percentage change of the steady-state firing frequency in 3 dpf, 4 dpf, and 5 dpf pMNs exposed to 10 μM XE-991 compared to the median of their respective controls (sample sizes are the same as in ***F***). ***H***, Comparison of instantaneous firing frequency calculated from voltage responses to a current injection equal to 2x rheobase (see **Fig. 4.7**) recorded from pMNs exposed to 5 μM riluzole in larvae aged 2 dpf (n = 9, N = 4), 3 dpf (n = 12, N = 3), 4 dpf (n = 11, N = 3), and 5 dpf (n = 11, N = 3). ***I***, Comparison of the number of spikes generated in response to a current injection equal to 2x rheobase in pMNs exposed to 5 μM riluzole at 2 dpf (n = 11, N = 4), 3 dpf (n = 12, N = 3),

4 dpf (n = 11, N = 3), and 5 dpf (n = 11, N = 3). *Statistical analysis*, Ordinary one-way ANOVA with Tukey's multiple comparisons test (***F-G***) and Kruskal-Wallis test with Dunn's multiple comparisons test (***B-C, E, I***). * $P < 0.05$, ** $P < 0.01$, *** $P < 0.001$, **** $P < 0.0001$; otherwise, not statistically significant.

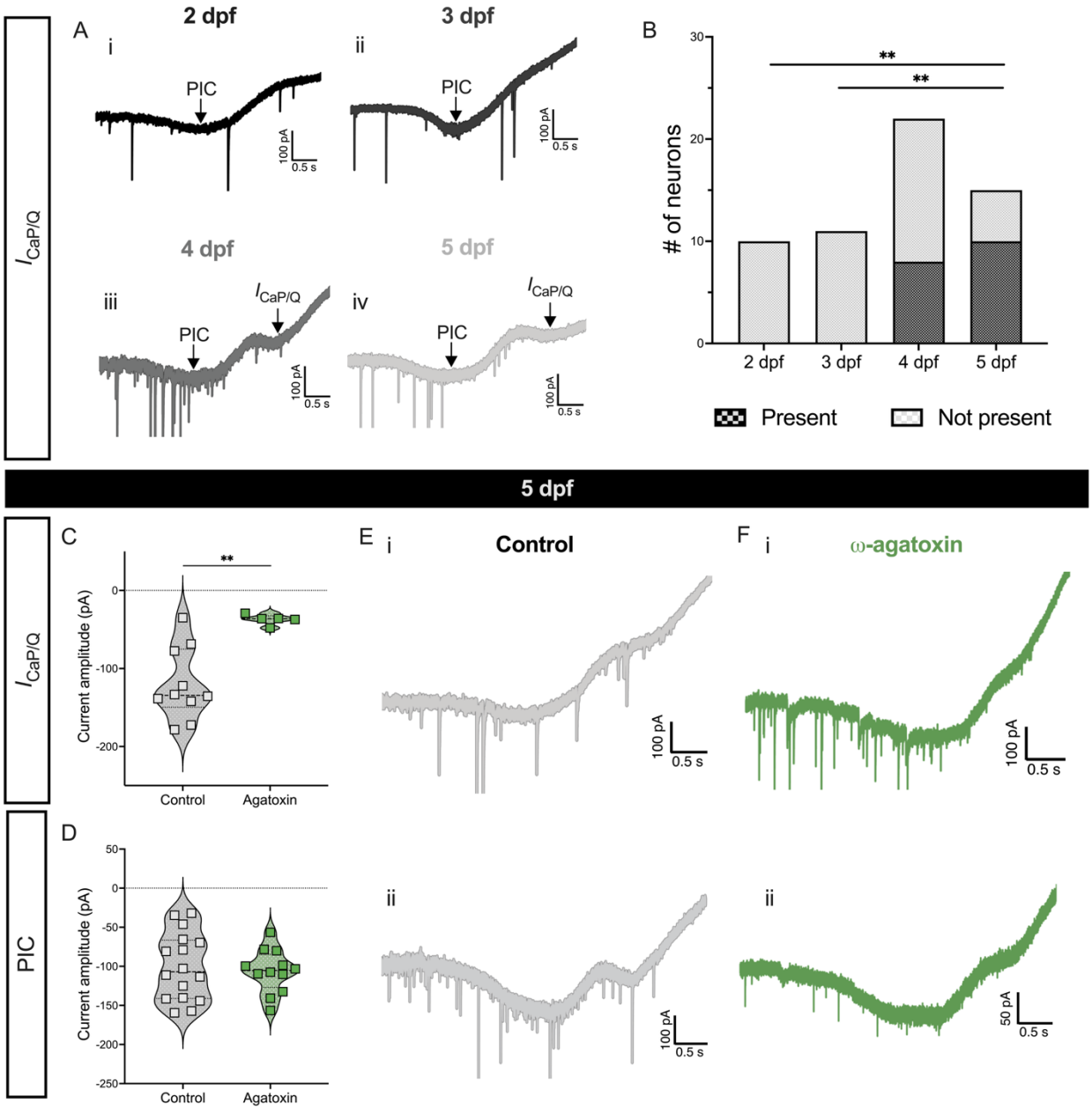
A
2 dpf
i
PIC
100 pA
0.5 s
3 dpf
ii
PIC
100 pA
0.5 s
4 dpf
iii
PIC
$I_{CaP/Q}$
100 pA
0.5 s
5 dpf
iv
PIC
$I_{CaP/Q}$
100 pA
0.5 s
$I_{CaP/Q}$
B
# of neurons
30
20
10
0
**
**
2 dpf
3 dpf
4 dpf
5 dpf
Present
Not present
5 dpf
$I_{CaP/Q}$
C
**
Current amplitude (pA)
0
-100
-200
Control
Agatoxin
PIC
D
Current amplitude (pA)
50
0
-50
-100
-150
-200
-250
Control
Agatoxin
E
i
Control
100 pA
0.5 s
ii
100 pA
0.5 s
F
i
ω-agatoxin
100 pA
0.5 s
ii
50 pA
0.5 s

Figure 4.10. Inward P/Q calcium current emerges at 4 dpf in primary motoneurons during larval development. ***A***, Examples of current traces in response to a 20 mV/s voltage ramp from -90 mV to +10 mV (same as in **Fig. 4.6**) in (*i*) 2 dpf, (*ii*) 3 dpf, (*iii*) 4 dpf, and (*iv*) 5 dpf pMNs. Arrows point to PICs present from 2-5 dpf (*i-iv*) as well as an inward current putatively mediated by P/Q calcium channels that appears at 4 and 5 dpf (*iii* & *iv*). ***B***, Quantification of number of pMNs that express $I_{CaP/Q}$ at 2 dpf, 3 dpf, 4 dpf, and 5 dpf. ***C***, Effect on the amplitude of $I_{CaP/Q}$ in 5 dpf pMNs by the selective inhibitor ω-agatoxin (300 nM; n =5; N = 5) compared to a distinct group of controls (n = 10; N = 6). ***D***, Effect on the amplitude of the PICs in 5 dpf pMNs by the selective inhibitor ω-agatoxin (300 nM; n = 13; N = 3) compared to a distinct group of controls (n = 16, N = 8). ***E***, Examples of control traces from two distinct 5 dpf pMNs containing both a PICs and $I_{CaP/Q}$. ***F***, Examples of traces from two distinct 5 dpf pMNs exposed to 300 nM ω-agatoxin containing both a PICs and $I_{CaP/Q}$. *Statistical analysis,*(***B***) Fisher's exact test with Bonferroni correction (** $P < 0.0017$; otherwise, not statistically significant) and (***C-D***) Mann-Whitney tests (** $P < 0.01$; otherwise, not statistically significant).

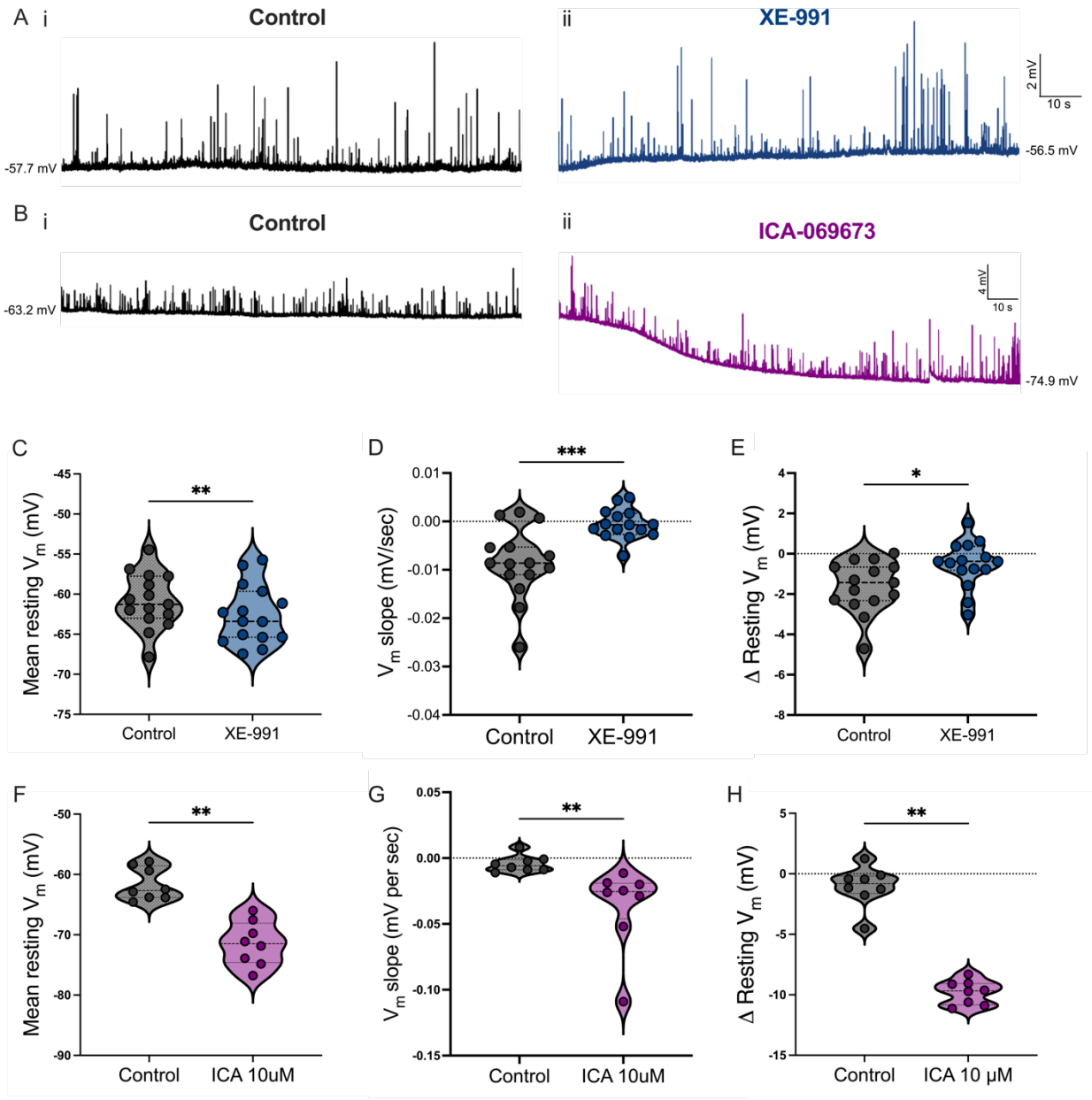
A i
Control
-57.7 mV
ii
XE-991
2 mV
10 s
-56.5 mV
B i
Control
-63.2 mV
ii
ICA-069673
4 mV
10 s
-74.9 mV
C
Mean resting Vm (mV)
**
Control
XE-991
D
Vm slope (mV/sec)
***
Control
XE-991
E
Δ Resting Vm (mV)
*
Control
XE-991
F
Mean resting Vm (mV)
**
Control
ICA 10uM
G
Vm slope (mV per sec)
**
Control
ICA 10uM
H
Δ Resting Vm (mV)
**
Control
ICA 10 μM

Supplemental Figure 4.1. Pharmacological modulation of I_M affects resting membrane potential of spinal neurons. Example trace of resting membrane potential recorded from primary motoneurons of 4-5 dpf larval zebrafish (***A***) in the presence of 10 μM XE-991 (n =15, N = 15) and (***B***) 10 μM ICA-069673 (n = 8; N = 8). ***C*** & ***F***, Mean resting membrane potential. ***D*** & ***G***, Change in mean resting membrane potential from start to end of each condition. ***E*** & ***H***, Slope of resting membrane potential. *Statistical analysis,* Wilcoxon matched-pairs t-tests to compare conditions within same animals. * $P < 0.05$; ** $P < 0.01$; *** $P < 0.001$; otherwise not statistically significant.

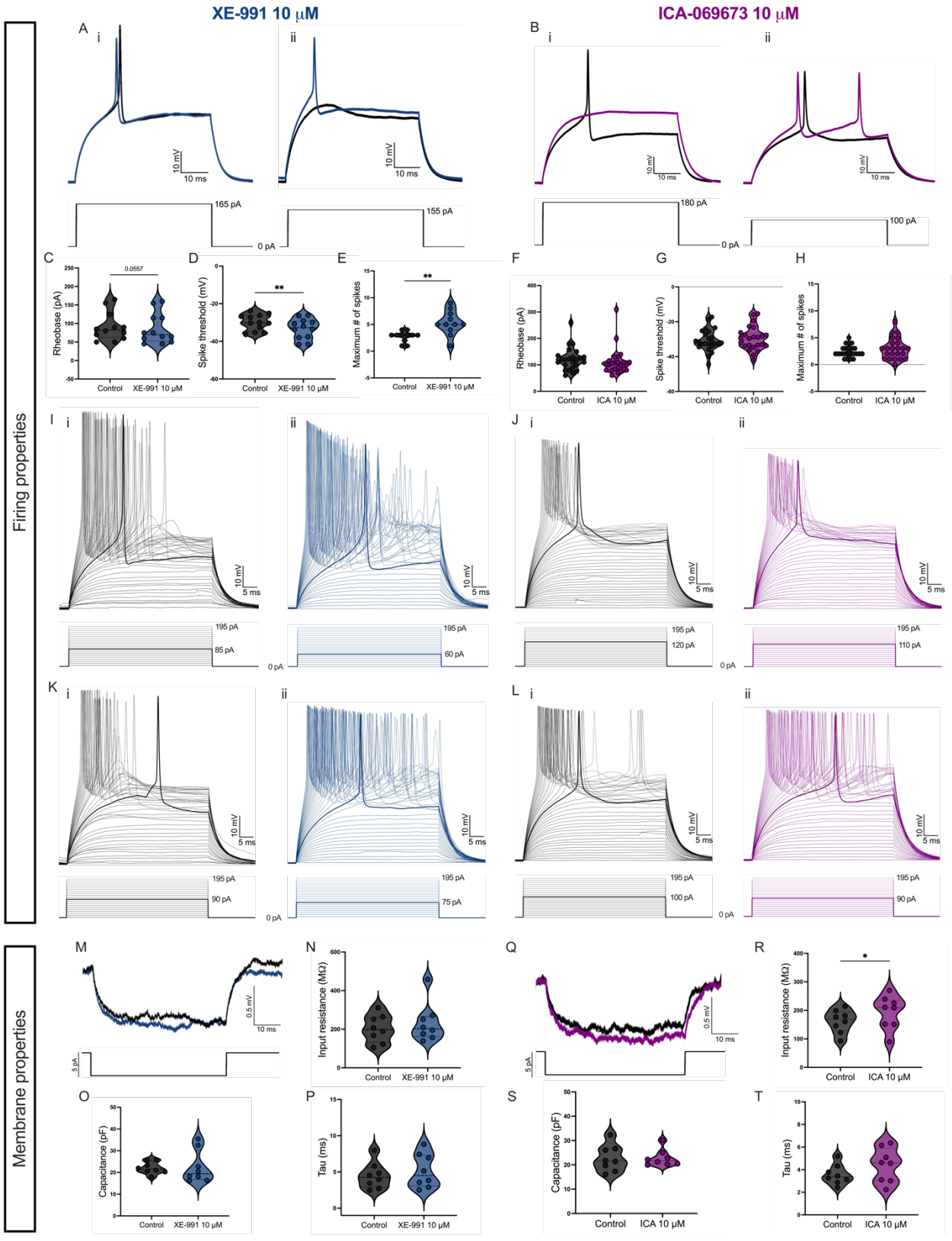
XE-991 10 μM
ICA-069673 10 μM
Firing properties
Membrane properties
A
B
C
D
E
F
G
H
I
J
K
L
M
N
O
P
Q
R
S
T
Rheobase (pA)
Spike threshold (mV)
Maximum # of spikes
Input resistance (MΩ)
Capacitance (pF)
Tau (ms)
Control
XE-991 10 μM
ICA 10 μM
0.0557
**
*
10 mV
10 ms
5 ms
0.5 mV
5 pA
165 pA
155 pA
180 pA
100 pA
0 pA
195 pA
85 pA
60 pA
120 pA
110 pA
90 pA
75 pA
100 pA

Supplemental Figure 4.2. Pharmacological inhibition of Kv7.2/7.3 channels mediating I_M by XE-991 increases excitability of primary motoneurons in 4-5 dpf larval zebrafish. ***A*****,** Examples of action potentials generated by positive current steps in the same pMN before (black) and after 10 μM XE-991 (blue) during whole-cell current-clamp recording in 4 dpf larva. Left and right panels (*i*-*ii*) show traces obtained from two pMNs. ***B*****,** Examples of action potentials generated by positive current steps in the same pMN before (black) and after 10 μM ICA-069673 (magenta). Left and right panels (*i*-*ii*) show traces obtained from two pMNs. ***C*****,** Rheobase before and after 10 μM XE-991. ***D*****,** Spike threshold before and after 10 μM XE-991. ***E*****,** Maximum number of spikes generated during a series of 50 ms current steps from 0 pA to 195 pA before (black) and after 10 μM XE-991 (blue). ***F*****,** Rheobase before and after 10 μM ICA-069673. ***G*****,** Spike threshold before and after 10 μM ICA-069673. ***H*****,** Maximum number of spikes generated during a series of 50 ms current steps from 0 pA to 195 pA before (black) and after 10 μM ICA-069673 (magenta). ***I*****, *K*****,** Example voltage traces from two pMNs in response to a series of 50 ms current steps from 0 pA to 195 pA before (*i*, black) and after 10 μM XE-991 (*ii*, blue). ***J*****, *L*****,** Example voltage traces from two pMNs in response to a series of 50 ms current steps from 0 pA to 195 pA before (*i*, black) and after 10 μM ICA-069673 (*ii*, magenta). ***M*****,** Example voltage trace from the same pMN in response to a –5 pA current step before (black) and after 10 μM XE-991 (blue). ***N*****,** Input resistance before and after XE-991. ***O*****,** Whole-cell capacitance before and after 10 μM XE-991. ***P*****,** Membrane time constant (τ) before and after 10 μM XE-991. ***Q*****,** Example voltage trace from the same pMN in response to a –5 pA current step before (black) and after 10 μM ICA-069673 (blue). ***R*****,** Input resistance before and after 10 μM ICA-069673. ***S*****,** Whole-cell capacitance before and after 10 μM ICA-069673. ***T*****,** Membrane time constant (τ) before and after ICA-069673. *Statistical analysis,*

Wilcoxon matched-pairs signed rank tests: * $P < 0.05$, ** $P < 0.01$; otherwise, not statistically significant.

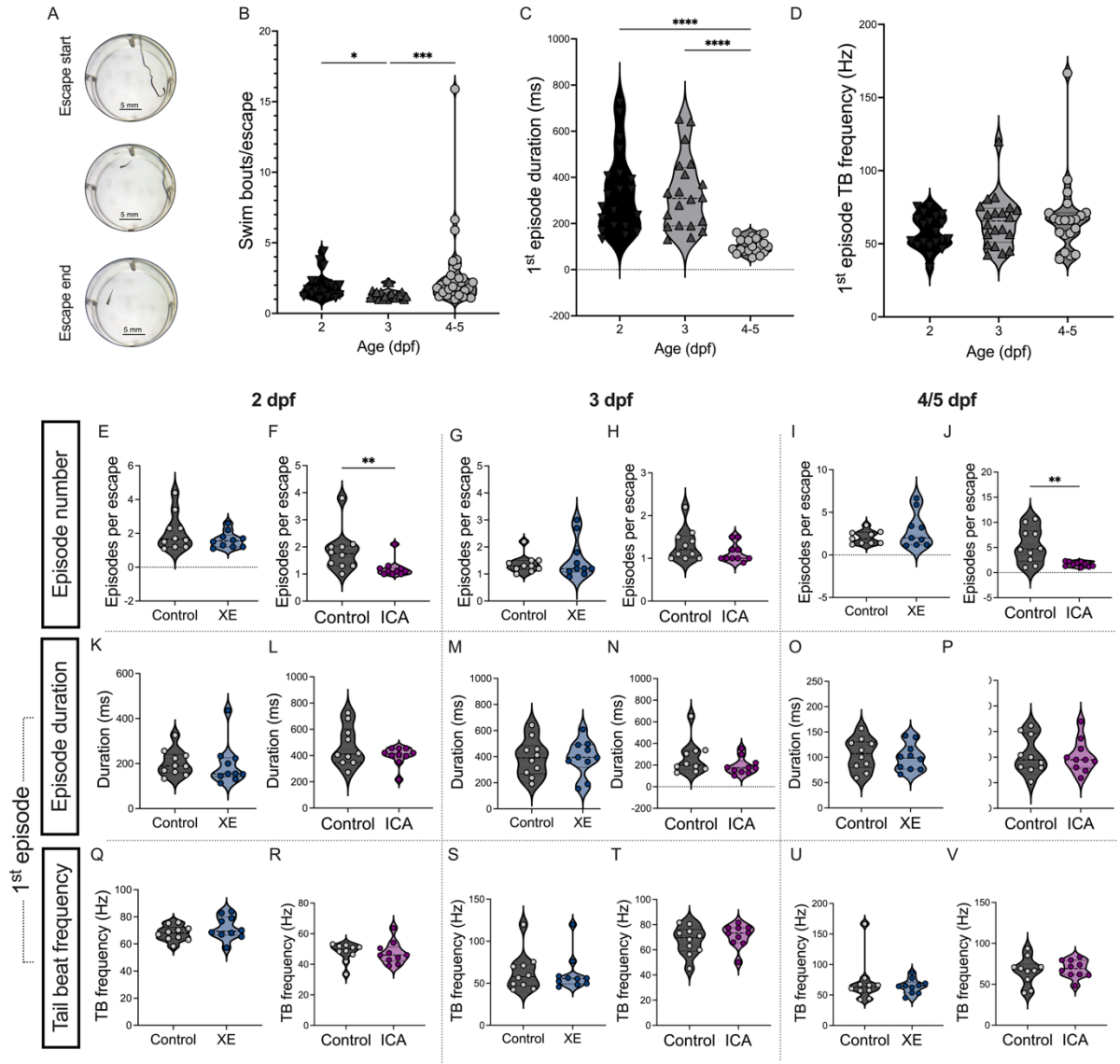
A
Escape start
Escape end
5 mm
B
Swim bouts/escape
Age (dpf)
C
1st episode duration (ms)
Age (dpf)
D
1st episode TB frequency (Hz)
Age (dpf)
2 dpf
3 dpf
4/5 dpf
1st episode
Episode number
Episode duration
Tail beat frequency
Episodes per escape
Duration (ms)
TB frequency (Hz)
Control
XE
ICA

Supplemental Figure 4.3. Developmental differences of pharmacological manipulation of Kv7.2/7.3 channels to features of the escape response. ***A,*** Overview of touch-evoked escape behaviours of individual 2 dpf, 3 dpf, and 4-5 dpf larvae placed in a well from a 24-well plate. Note that 4-5 dpf data is taken from **Chapter 3 - Figure 3.1** to provide comparisons with earlier developmental time points. ***B,*** Average number of swim episodes (swim bouts) produced during touch-evoked escape responses in 2, 3, and 4-5 dpf zebrafish. ***C***, Average duration of the first episode produced in response to the touch stimulus. ***D***, Average tail beat frequency of the first episode produced in response to the touch stimulus. ***E-J***, Mean number of swimming episodes produced per touch-evoked escape response before and after the bath application of (***E***, ***G***, ***I***) 10 µM XE-991 and (***F***, ***H***, ***J***) 10 µM ICA-069673 in (***E-F***) 2 dpf, (***G-H***) 3 dpf, and (***I-J***) 4-5 dpf. ***K-P***, Mean duration of the first swimming episode produced during touch-evoked escape responses before and after the bath application of (***K***, ***M***, ***O***) 10 µM XE-991 and (***L***, ***N***, ***P***) 10 µM ICA-069673 in (***K-L***) 2 dpf, (***M-N***) 3 dpf, and (***O-P***) 4-5 dpf. ***Q-V***, Mean tail beat (TB) frequency of the first swimming episode produced during touch-evoked escape responses before and after the bath application of (***Q***, ***S***, ***U***) 10 µM XE-991 and (***R***, ***T***, ***V***) 10 µM ICA-069673 in (***Q-R***) 2 dpf, (***S-T***) 3 dpf, and (***U-V***) 4-5 dpf. *Statistical analysis,* Kruskal-Wallis test with Dunn's test for multiple comparisons (***B-D***), and Wilcoxon matched-pairs test (***E-V***); * $P < 0.05$, ** $P < 0.01$, *** $P < 0.001$, **** $P < 0.0001$; otherwise not statistically significant.

Chapter 5

Developmental changes in the neuromodulation of the M-current in primary motoneurons of larval zebrafish

Gaudreau, SF & Bui, TV

5.1 ABSTRACT

We recently discovered that the non-inactivating subthreshold potassium current known as the M-current (I_M) is expressed in primary motoneurons of the larval zebrafish. Furthermore, we found that its magnitude and the influence it exerts over the regulation of repetitive firing is most prominent at 3 days post-fertilization. Considering that neuromodulators play a role in the maturation of locomotor control in larval zebrafish, we asked whether neuromodulators might target I_M in primary motoneurons. Our experiments show that enhancement of I_M by muscarine and serotonin is age-dependent, varying from 3 to 5 days post-fertilization. We also show that 5-HT_{1A} signaling inhibits I_M only at 3 days post-fertilization. Furthermore, we demonstrate that DA does not appear to modulate I_M in primary motoneurons. Our findings are consistent with the changes in I_M that we've observed at specific developmental time points and suggest that neuromodulation of I_M could have different effects throughout development of zebrafish locomotion.

5.2 INTRODUCTION

Movement is generated by specialized neuronal networks located within the spinal cord. These spinal locomotor circuits must undergo progressive maturation during development to allow for increasingly refined and complex movements to be made. The exact changes spinal locomotor circuits undergo during maturation are not fully known but there is evidence supporting a role for neuromodulation in motor maturation. For example, both dopamine (DA) and serotonin (5-HT) have been shown to elicit air-stepping in spinally-transected neonatal rats, supporting their contributions to promoting hindlimb stepping (McEwen, Van Hartesveldt, and Stehouwer 1997). While effects to motor output by neuromodulatory systems during development have been described, little is known about the targets of this neuromodulation and the mechanisms by which they shape motor maturation.

The zebrafish is particularly well-suited for the study of motor maturation as their rapid development comprises stereotyped transitions in the movements they produce. Changes in motor behaviour can be readily linked to changes in underlying spinal circuitry. Indeed, DA and 5-HT have both been shown to have important influences on locomotor output during zebrafish development. DA signaling in the spinal cord mediates the important locomotor transition from 3 days post-fertilization (3 dpf) burst swimming to 4 dpf beat and glide swimming (Lambert et al. 2012). It has also been shown to control the excitation of motoneurons (Jha and Thirumalai 2020). 5-HT has been shown to limit the duration of periods of inactivity between successive swimming episodes in developing zebrafish (Brustein et al. 2003). While these findings have proven important to our understanding of how supraspinal regions mediate flexible control over zebrafish

spinal locomotor circuits in the context of development, the mechanisms by which these neuromodulators exert their influence on spinal neurons are unknown.

We have recently identified the presence of the non-inactivating subthreshold potassium current known as the M-current (I_M) in primary motoneurons (pMNs) of larval zebrafish (Chapter 4). We show that I_M's influence on the control of excitability and regulation of repetitive firing changes during early zebrafish development, peaking at 3 dpf. This coincides with the time when larvae are largely inactive and exhibit burst swimming, an immature form of swimming. By 4 dpf, their mature locomotor pattern, known as beat and glide swimming, emerges and they swim much more frequently (Buss and Drapeau 2001; Drapeau et al. 2002b).

Could I_M be a target for neuromodulation during development to facilitate motor maturation? As zebrafish transition from their embryonic stage characterized primarily of large amplitude and reflexive pMN-driven movements to their larval stage encompassing predominantly low amplitude secondary motoneuron (sMN) driven swimming, we posit that I_M in pMNs may be an important target for neuromodulation as pMN recruitment must restricted to specific movements.

In this study, we use electrophysiology to investigate how neuromodulators influence the properties of I_M in pMNs of larval zebrafish from 3 dpf to 5 dpf. Interestingly, we find that muscarine, a known inhibitor of I_M in other systems, does not inhibit I_M in pMNs of larval zebrafish. We find that enhancement of I_M by 5-HT is age-dependent and so is inhibition of I_M by 5-HT via 5-HT_{1A} receptors. Finally, we demonstrate that dopamine does not have an obvious influence over the properties of I_M of pMNs.

5.3 METHODS

5.3.1 Animal Care

All experiments were performed in accordance with the protocol approved by the University of Ottawa's Animal Care Committee (BL-4416). Adult zebrafish are maintained at 28.5°C with a 14 hour on/10 hour off light cycle, with lights off at 11PM and on at 9AM. Embryos are fertilized between 9AM-10AM and stored in embryo medium at 28.5°C until use for experimentation at 2 to 5 dpf.

5.3.2 Preparation for electrophysiology

Larval zebrafish are anesthetized in 0.02% tricaine (MS-222, Aqualife TMS; Syndel Laboratories) before being pinned down through the notochord onto a Sylgard (Dow Corning) coated dish. Pins are made using Tungsten wire (0.25 mm); one is placed caudally near the tip of the tail, and the other is placed rostrally near the center of the yolk sac. Spinalization is performed using fine surgical scissors at the level of segments 2-3. The skin is then peeled back between the two pins using fine forceps. Next, larvae are bathed in 1 mg/mL collagenase (Millipore Sigma; incubation times: 8 minutes at 2 dpf, 10 minutes at 3 dpf, 12 minutes at 4 dpf, and 15 minutes at 5 dpf) to facilitate muscle removal. The collagenase solution is rinsed out 4-5 times with artificial cerebrospinal fluid (aCSF) containing: 134 mM NaCl, 2.9 mM KCl, 1.2 mM $MgCl_2$, 2.1 mM $CaCl_2$, 10 mM dextrose, and 10 mM HEPES (pH of 7.8 adjusted with NaOH and osmolarity between 280-290 adjusted with sucrose). Muscle removal is performed using suction through a wide-bored glass capillary (typically, the tips are gently broken to get the right sized tip for muscle removal). Muscles overlaying the spinal cord are removed to expose the spinal cord for whole-cell patch-clamp electrophysiology.

5.3.3 Whole-cell patch-clamp electrophysiology

To block muscle contractions during recordings, d-tubocurarine is added to the aCSF (10 μM; Millipore Sigma, catalog # 93750). Electrodes for whole-cell patch-clamp experiments are made using borosilicate glass capillaries (Sutter Instrument; BF150-110-10). Tip resistances ranging from 5 to 7 MΩ were used. Intracellular recording solution used contained the following: 16 mM KCl, 116 mM K-gluconate, 4 mM $MgCl_2$, 10 mM HEPES, 10 mM EGTA, and 4 mM Na_2-ATP, adjusted to a pH of 7.2-7.3 with KOH. Slight positive pressure was applied during the descent toward the spinal cord to prevent debris from contaminating the tip of the electrode. This positive pressure was used to break the dura thereby exposing the neurons within the spinal cord. Positive pressure was decreased slightly, and targeted neurons were approached with the electrode. When near the neuron (small dent forming in neuron), positive pressure was released and a gigaohm (GΩ) seal (giga-seal) was formed between the tip of the electrode and the cell membrane. Gentle pulses of negative pressure were used to break through the membrane. Membrane holding potential was set to –65 mV and both fast and slow capacitance components were compensated for. Series resistance was routinely compensated for at 80% or higher. The neuron was held at -65 mV until it was time to introduce stimulation protocols. Values reported are not liquid junction potential corrected. pMNs were targeted as described in Chapter 4 and their identity was confirmed post hoc by assessing axon projection through the ventral root facilitated by the addition of sulforhodamine B to the intracellular recording solution (0.1%; Millipore Sigma). Electrical activity was amplified and filtered at 10 kHz or 20 kHz with a Multiclamp 700B (Axon Instruments, Molecular Devices). The data was then digitized with a Digidata 1550 (Molecular

Devices). A HumBug Noise Eliminator (Quest Scientific) was used to attenuate 50/60 Hz electrical noise.

5.3.4 Voltage-clamp protocols and current estimations

To reveal the electrophysiological signature of the M-current, we implemented the standard M-current relaxation protocol (Sharples et al. 2023; Verneuil et al. 2020b). This consisted of holding the neuron at -10 mV and introducing a series of hyperpolarizing voltage steps lasting 1 second each. As the membrane potential becomes hyperpolarized, the M-current deactivates. Current responses show the resulting loss of outward current caused by M-current deactivation. From this, we can estimate the amplitude of the M-current by taking the difference between the peak of the current response and the current at steady-state at the end of the step. The difference between the steady-state current and the peak of this initial current response was used to estimate the amplitude of the M-current.

5.3.5 Pharmacology

Dopamine hydrochloride (3548, Tocris), serotonin hydrochloride (3547, Tocris), muscarine iodide (3074, Tocris), and 5-HT_{1A} receptor agonist 8-OH-DPAT (1080, Tocris) were dissolved in water before final dissolution in aCSF of the recording bath. All drugs were introduced to the recording bath 5-10 minutes prior to recordings.

5.3.6 Data analysis and statistical analysis

All electrophysiological data was saved as .abf files. We used the open-source pyABF python package to import and read .abf files in Spyder (version 5.1.5). Analysis of recordings was semi-automated using Python (version 3.9.12) scripts tailored to each type of recording. Statistical analysis was performed using Prism by GraphPad (Version 10.3.1 (464)). For comparisons between 2 data sets, Mann-Whitney and unpaired t-tests were used. For comparisons between 3 data sets or more, one-way ANOVA with Tukey's multiple comparisons test was used for normally distributed data and Kruskal-Wallis test with Dunn's multiple comparisons test was used for non-parametric data. For comparisons of current-voltage relationships across 2 or more groups, mixed-effects model analyses with Sidak's multiple comparisons test were used. For all tests, significance stars are displayed on graphs.

5.4 RESULTS

5.4.1 Muscarine enhances I_M in primary motoneurons at 4 and 5 dpf

With the discovery of I_M came the finding that it can be inhibited by muscarine (Brown and Adams 1980). Since our previous work identified I_M in pMNs of larval zebrafish, we sought to investigate the potential for muscarinic inhibition of I_M in these neurons (**Fig. 5.1**). As described in Chapter 4, we utilized the standard I_M voltage-clamp deactivation protocol to reveal its electrophysiological signature in current responses. Comparison of the effects resulting from bath application were made between three entirely distinct sample groups of pMNs: control pMNs and two groups of pMNs having been exposed to either 10 μM muscarine or 100 μM muscarine for several minutes prior to all recordings. Because of differences observed in the magnitude of I_M in pMNs during early zebrafish development, we compared the effects of muscarine at 3 dpf, 4 dpf, and 5 dpf. It is important to note that data obtained from the control groups of pMNs presented throughout has is the same as that presented in Chapter 4. At 3 dpf, exposure to 10 μM muscarine and 100 μM muscarine did not alter the current-voltage relationship of I_M relative to control; however, there was a significant increase in the average amplitude of I_M across voltages when pMNs are exposed to 10 μM muscarine compared to 100 μM muscarine (**Fig. 5.1*A***). No significant differences in peak amplitude of I_M (control: 32.61 ± 14.61 pA; 10 μM muscarine: 42.43 ± 22.11 pA; 100 μM muscarine: 20.01± 16.45 pA; **Fig. 5.1*C***), I_M activation voltage (control: -54.55 ± 5.68 mV; 10 μM muscarine: -49.55 ± 14.74 mV; 100 μM muscarine: -43.50 ± 12.03 mV; **Fig. 5.1*D***), or the voltage at which I_M reaches half its maximal amplitude ($V_{1/2}$) (control: -37.40 ± 3.18 mV; 10 μM muscarine: -35.36 ± 13.93 mV; 100 μM muscarine: -28.28 ± 11.45 mV; **Fig. 5.1*E***) were observed between either 10 μM or 100 μM muscarine and controls. We did however find that peak amplitude of I_M is reduced in pMNs exposed to 100 μM muscarine compared to those exposed to

10 μM muscarine (**Fig. 5.1*C***). Interestingly, at 4 dpf, while 100 μM muscarine did not alter any of the properties of I_M, 10 μM muscarine enhanced I_M. The average amplitude of I_M across voltages is significantly increased in pMNs exposed to 10 μM muscarine compared to controls as well as those exposed to 100 μM muscarine (**Fig. 5.1*F***). The current-voltage relationship of I_M remains unchanged from controls in pMNs exposed to 100 μM muscarine (**Fig. 5.1*F***). The peak amplitude of I_M is also significantly increased in pMNs exposed to 10 μM muscarine compared to control pMNs and those exposed to 100 μM muscarine (control: 17.52 ± 8.46 pA; 10 μM muscarine: 36.05 ± 21.75 pA; 100 μM muscarine: 16.96 ± 11.93 pA; **Fig. 5.1*H***). The activation voltage of I_M (control: -45.62 ± 10.63 mV; 10 μM muscarine: -50.50 ± 6.43 mV; 100 μM muscarine: -52.73 ± 14.72 mV; **Fig. 5.1*I***) and $V_{1/2}$ (control: -32.10 ± 5.91 mV; 10 μM muscarine: -34.70 ± 7.23 mV; 100 μM muscarine: -27.92 ± 13.03 mV; **Fig. 5.1*J***) in pMNs are not significantly altered by either 10 μM muscarine or 100 μM muscarine compared to controls at 4 dpf. By 5 dpf, the average amplitude of I_M across voltages remains increased in pMNs exposed to 10 μM muscarine relative to control pMNs (**Fig. 5.1*K***) yet the peak amplitude is not significantly different between these groups (**Fig. 5.1*M***). While the average amplitude of I_M across voltages in pMNs exposed to 100 μM muscarine is not different from that in control pMNs, it is significantly reduced compared to pMNs exposed to 10 μM muscarine (**Fig. 5.1*K***). Similarly, the peak I_M found in pMNs exposed to 100 μM muscarine is significantly reduced compared to pMNs exposed to 10 μM muscarine but not to control pMNs (control: 21.01 ± 9.04 pA; 10 μM muscarine: 31.88 ± 14.41 pA; 100 μM muscarine: 15.22 ± 9.91 pA; **Fig. 5.1*M***). No differences were observed across any of the groups to the activation voltage of I_M (control: -49.09 ± 7.06 mV; 10 μM muscarine: -50.91 ± 4.91 mV; 100 μM muscarine: -50.00 ± 12.04 mV; **Fig. 5.1*N***). Finally, the $V_{1/2}$ of I_M in pMNs exposed to 100 μM muscarine was significantly depolarized compared to controls, but not to pMNs exposed to 10

μM muscarine (control: -35.95 ± 5.52 mV; 10 μM muscarine: -35.13 ± 5.29 mV; 100 μM muscarine: -28.94 ± 7.89 mV; **Fig. 5.1*O***). Overall, these data suggest that muscarine enhances I_M at a concentration of 10 μM, but not 100 μM, at 4 dpf and 5 dpf, but not 3 dpf.

5.4.2 Effects of dopamine to the properties of I_M in primary motoneurons of larval zebrafish

With the finding that muscarine does not inhibit I_M as has been shown in other species, we sought to determine whether the action of another neurotransmitter had inhibitory influences on I_M. Dopamine has been identified as a neuromodulator with important influence on the function of spinal locomotor circuits in zebrafish during development (Lambert et al. 2012). We aimed to determine whether some of these previously reported effects of dopamine could be occurring via modulation of I_M by dopamine. To this end, we examined possible effects to the properties of I_M in pMNs exposed to either 10 μM or 100 μM DA at 3 dpf, 4 dpf, and 5 dpf. At 3 dpf, the pMNs exposed to 10 μM DA exhibited no changes to the current-voltage relationship of I_M (**Fig. 5.2*A***), the peak amplitude of I_M (control: 32.61 ± 14.61 pA; 10 μM DA: 37.06 ± 23.61 pA; 100 μM DA: 19.34 ± 11.58 pA; **Fig. 5.2*C***), its activation voltage (control: -54.55 ± 5.68 mV**;** 10 μM DA: -47.27 ± 12.72 mV; 100 μM DA: -45.42 ± 12.33 mV; **Fig. 5.2*D***), nor its $V_{1/2}$ (control: -37.40 ± 3.18 mV; 10 μM DA: -31.96 ± 11.54 mV; 100 μM DA: -31.25 ± 10.18 mV; **Fig. 5.2*E***) relative to controls. pMNs exposed to 100 μM DA however showed an overall reduction in the amplitude of I_M across voltages compared to control pMNs (**Fig. 5.2*A***), without affecting peak amplitude (**Fig. 5.2*C***), activation voltage (**Fig. 5.2*D***), or $V_{1/2}$ (**Fig. 5.2*E***). At 4 dpf, no significant effects by either 10 μM DA or 100 μM DA to the current-voltage relationship of I_M (**Fig. 5.2*F***), the peak amplitude of I_M (control: 17.52 ± 8.46 pA; 10 μM DA**:** 33.29 ± 27.16 pA; 100 μM DA: 12.90 ± 6.59 pA; **Fig.**

5.2*H*), the activation voltage of I_M (control: -45.63 ± 10.63 mV; 10 μM DA: -47.00 ± 12.06 mV; 100 μM DA: -39.58 ± 10.76 mV; **Fig. 5.2*I***), or its $V_{1/2}$ (control: -32.10 ± 5.91 mV; 10 μM DA: -33.18 ± 10.77 mV; 100 μM DA: -27.73 ± 8.58 mV; **Fig. 5.2*J***) compared to control pMNs. By 5 dpf, 10 μM DA and 100 μM DA did not alter the current-voltage relationship of I_M (**Fig. 5.2*K***), the activation voltage of I_M (control: -49.09 ± 7.01 mV; 10 μM DA: -50.00 ± 5.59 mV; 100 μM DA: -36.82 ± 14.19 mV; **Fig. 5.2*N***) nor it's $V_{1/2}$ (control: -35.95 ± 5.52 mV; 10 μM DA: -32.57 ± 8.85 mV; 100 μM DA: -26.48 ± 12.43 mV; **Fig. 5.2*O***). The peak amplitude of I_M, however, was increased by 10 μM DA compared to control pMNs and those exposed to 100 μM DA (control: 21.01 ± 9.04 pA; 10 μM DA: 32.55 ± 9.34 pA; 100 μM DA: 15.62 ± 9.06 pA; **Fig. 5.2*M***). Overall, these data reveal no clear effects of dopamine, at both concentrations tested, to the properties of I_M in 3 – 5 dpf pMNs.

5.4.3 The effects of serotonin on the properties of I_M in primary motoneurons of larval zebrafish

Serotonin has been shown to inhibit I_M in pyramidal neurons of the weakly electric fish (Deemyad, Maler, and Chacron 2011) as well as neurons of the hypothalamus in mice (Roepke et al. 2012). We therefore decided to test whether application of exogenous 5-HT at 20 μM and 100 μM altered properties of I_M in pMNs of larval zebrafish (**Fig. 5.3**). At 3 dpf, no differences between the current-voltage relationship of I_M (**Fig. 5.3*A***), the peak amplitude of I_M (control: 32.61 ± 14.61 pA ; 20 μM 5-HT: 40.14 ± 20.47 pA; 100 μM 5-HT: 28.48 ± 12.13 pA; **Fig. 5.3*C***), the activation voltage of I_M (control: -54.55 ± 5.68 mV; 20 μM 5-HT: -55.00 ± 6.67 mV; 100 μM 5-HT: -52.00 ± 7.89 mV; **Fig. 5.3*D***) or its $V_{1/2}$ (control: -37.64 ± 4.31 mV; 20 μM 5-HT: -38.54 ± 7.02 mV; 100 μM 5-HT: -33.77 ± 9.56 mV; **Fig. 5.3*E***) in pMNs across treatment groups were observed. By 4

dpf, the average amplitude of I_M across voltages is increased in pMNs by 20 μM 5-HT, but not 100 μM 5-HT, compared to controls (**Fig. 5.3*F***). Similarly, 20 μM 5-HT, but not 100 μM 5-HT, increases the peak amplitude of I_M measured in pMNs compared to controls (control: 17.52 ± 8.46 pA; 20 μM 5-HT: 32.68 ± 11.16 pA; 100 μM 5-HT: 20.33 ± 13.32 pA; **Fig. 5.3*H***). The activation voltage of I_M is hyperpolarized by 20 μM 5-HT, but not 100 μM 5-HT compared to controls (control: -45.63 ± 10.63 mV; 20 μM 5-HT: -61.25 ± 6.78 mV; 100 μM 5-HT: -53.75 ± 7.72 mV; **Fig. 5.3*I***). Neither 20 μM or 100 μM 5-HT altered $V_{1/2}$ relative to controls (control: -32.10 ± 5.91 mV; 20 μM 5-HT: -36.39 ± 6.76 mV; 100 μM 5-HT: -26.95 ± 9.32 mV; **Fig. 5.3*J***). By 5 dpf, there are no differences across treatment groups to the current-voltage relationship of I_M (**Fig. 5.3*K***), the peak amplitude of I_M (control: 21.01 ± 9.04 pA; 20 μM 5-HT: 26.96 ± 12.26 pA; 100 μM 5-HT: 26.54 ± 15.81 pA; **Fig. 5.3*M***), the activation voltage of I_M (control: -49.09 ± 7.01 mV; 20 μM 5-HT: -50.00 ± 7.07 mV; 100 μM 5-HT: -46.88 ± 3.72 mV; nor I_M's $V_{1/2}$ (control: -35.95 ± 5.52 mV; 20 μM 5-HT: -33.99 ± 6.74 mV; 100 μM 5-HT: -32.30 ± 3.80 mV; **Fig. 5.3*O***). These findings reveal that 5-HT at 20 μM may have an overall enhancing effect on I_M that is most prominent at 4 dpf, while 100 μM 5-HT does not significantly alter properties of I_M in pMNs.

5.4.4 Serotonin signaling via 5HT$_{1A}$ receptors inhibit I_M in primary motoneurons at 3 dpf

We next examined the role of serotonin in the modulation of I_M further by investigating how the selective 5-HT$_{1A}$ receptor agonist 8-OH-DPAT influences the properties of I_M during larval development (**Fig. 5.4**). As with the experiments described above, we compared the properties of I_M between two distinct groups of pMNs, one being control pMNs and the other being pMNs exposed to 10 μM 8-OH-DPAT bath application before recordings began. At 3 dpf, we find that 10 μM 8-OH-DPAT inhibits I_M as is observed by a significant decrease in the average amplitude

of I_M across voltages (**Fig. 5.4*A***), the peak amplitude of I_M (control: 32.61 ± 14.61 pA; 10 μM 8-OH-DPAT: 15.33 ± 11.68 pA; **Fig. 5.4*C***), the depolarization of I_M's activation voltage (control: -54.44 ± 5.68 mV; 10 μM 8-OH-DPAT: -40.45 ± 12.54 mV; **Fig. 5.4*D***) and the depolarization of I_M's $V_{1/2}$ (control: -37.64 ± 4.31 mV**;** 10 μM 8-OH-DPAT: -28.87 ± 9.59 mV; **Fig. 5.4*E***) in pMNs. At 4 dpf, 10 μM 8-OH-DPAT does not alter the current-voltage relationship of I_M (**Fig. 5.3*F***), the peak amplitude of I_M (control: 17.52 ± 8.46 pA; 10 μM 8-OH-DPAT: 25.23 ± 24.00 pA; **Fig. 5.4*H***), the activation voltage of I_M (control: -45.62 ± 10.63 mV; 10 μM 8-OH-DPAT: -38.33 ± 17.36 mV; **Fig. 5.4*I***), nor I_M's $V_{1/2}$ (control: -32.10 ± 5.91 mV**;** 10 μM 8-OH-DPAT: -32.77 ± 9.66 mV; **Fig. 5.4*J***) in pMNs compared to controls. Similarly, at 5 dpf, 10 μM 8-OH-DPAT does not alter the current-voltage relationship of I_M (**Fig. 5.4*K***), the peak amplitude of I_M (control: 21.01 ± 9.04 pA; 10 μM 8-OH-DPAT: 22.18 ± 17.57 pA; **Fig. 5.4*M***), the activation voltage of I_M (control: -49.09 ± 7.01 mV; 10 μM 8-OH-DPAT: -49.44 ± 6.82 mV; **Fig. 5.4*N***), nor I_M's $V_{1/2}$ (control: -35.95 ± 5.52 mV; 10 μM 8-OH-DPAT: -37.36 ± 5.77 mV; **Fig. 5.4*O***) in pMNs compared to controls. These data support an inhibitory influence of serotonin signaling via 5-HT_{1A} receptors on IM at 3 dpf, but not at older larval ages investigated.

5.5 DISCUSSION

Neuromodulators such as DA and 5-HT are known to influence motor maturation, as evidenced by work in the developing zebrafish (Brustein et al. 2003; Lambert et al. 2012). Specific neuronal targets of this modulation however remain largely unknown as do the mechanism by which neuromodulators exert their influence on neurons. In this study, we investigated the subthreshold non-inactivating potassium current, I_M, as a possible target for neuromodulation in spinal locomotor circuits of the developing zebrafish. We characterized the influence of muscarine, DA, and 5-HT on the activity of I_M in primary motoneurons from 3 to 5 dpf as developing zebrafish transition from burst to beat and glide swimming.

5.5.1 Muscarine as an I_M enhancer in pMNs of developing zebrafish

We first investigated how muscarine influences the activity of I_M in pMNs. I_M was named based on the finding that it was inhibited by muscarine at the time of its discovery (Brown and Adams 1980). Because of this, we had expected to see inhibition of I_M in pMNs exposed to muscarine. Intriguingly however, we found that muscarine instead had an enhancing effect on I_M in pMNs at 4 and 5 dpf. Traditional inhibition of I_M by muscarine is mediated by muscarinic acetylcholine receptors (mAChRs) coupled to $G_{q/11}$ proteins whose activation leads to the eventual depletion of phosphatidylinositol 4,5-biphosphate (PIP_2) at the membrane which directly influences the activity of Kv7.2/7.3 channels that mediate I_M (Suh and Hille 2007; Zhang et al. 2003). A study in neurons of the mouse dentate gyrus however reveals that, contrary to most other findings, acetylcholine signaling via M_1 receptors (M_1Rs) actually enhances the activity of I_M by increasing levels of PIP_2 (Carver and Shapiro 2019). Furthermore, it has been demonstrated that muscarinic inhibition of I_M activity, via M_1R signaling can be transient in nature, leading to overcompensation in the form of

increased Kv7.2 subunits to the membrane thereby enhancing I_M (Jiang et al. 2015) . In line with these findings, our data supports the idea that muscarinic influence over levels of PIP_2 and subsequently I_M activity, may be neuron and context specific. Identifying which mAChRs may lead to enhancement of I_M in pMNs would further delineate the mechanisms by which I_M can be modulated. Further studies are necessary to uncover both the source of acetylcholine and contexts in which mAChRs might be activated to enhance I_M in pMNs.

5.5.2 Serotonin as both an enhancer and inhibitor of I_M in pMNs of developing zebrafish

Exogenous application of 5-HT leads to obvious enhancing of I_M in pMNs at 4 dpf. When we specifically target 5-HT_{1A} receptors using the selective agonist 8-OH-DPAT, however, we find that it inhibits I_M at 3 dpf. Several instances of opposing roles of 5-HT have been observed in other systems. For example, 5-HT_2 receptor mediated serotonergic signaling caused membrane depolarization while 5-HT_{1A} receptor mediated serotonergic signaling resulted in hyperpolarization in pyramidal cells of the cortex in rats (Araneda and Andrade 1991). In turtle motoneurons, application of 5-HT to the dendritic tree promoted plateau potentials whereas application to the soma sometimes inhibited spike generation (Perrier and Hounsgaard 2003). Electrophysiology experiments testing the effects of additional 5-HT receptor subtypes on the properties of I_M in pMNs would reveal which receptor is responsible for the 5-HT-driven enhancement of I_M that we've observed. Identifying which 5-HT receptor subtype mediates the enhancement of I_M in pMNs will help further delineate mechanisms underlying I_M modulation.

5.5.3 Developmental changes to neuromodulatory influence on I_M in pMNs of developing zebrafish

In addition to having uncovered neuromodulators that differentially modulate the activity of I_M, we have revealed age-related differences in the effects of these neuromodulators during the 3 to 5 dpf time window. We show that muscarine enhances I_M at 4 and 5 dpf, but not at 3 dpf. This is particularly intriguing as this coincides with the reduction in the magnitude of I_M we have observed in pMNs from 3 dpf to 4 and 5 dpf (Chapter 4). It appears as though when I_M is already prominent in pMNs at 3 dpf, there is no mAChR-mediated enhancement of I_M. Furthermore, we show that 5-HT_{1A} receptor agonist 8-OH-DPAT inhibits I_M, but only at 3 dpf when the magnitude of I_M in pMNs is largest during the investigated time period. In this case, it appears that when basal levels of I_M are low, as they are at 4 and 5 dpf, there is no 5-HT_{1A} receptor mediated inhibition of I_M. These findings support the idea that different neuromodulator systems work together to fine-tune basal activity levels of I_M that change during development. At 3 dpf when larvae are largely inactive, I_M in pMNs is large. Inhibition of I_M by 5-HT_{1A} receptor signaling may help recruit pMNs for fast movements by alleviating the control I_M has on pMN excitability and repetitive firing. Muscarine may only come into play as an enhancer of I_M by 4-5 dpf because there may be no need for further enhancement of I_M at 3 dpf. By 4-5 dpf when larvae are more active, I_M is reduced in magnitude in pMNs compared to 3 dpf. At this point, pMNs may benefit from I_M enhancement by muscarine in contexts where pMN excitability and/or repetitive firing should be limited, for example during transitions from fast to slow swims when pMNs are no longer needed.

To conclude, we have revealed how different neuromodulators influence I_M in pMNs. We identify not only two neuromodulator systems that serve as a means to regulate the activity of I_M in pMNs

but also reveal how their influence on I_M in pMNs varies within a short developmental time window. This work highlights how distinct neuromodulatory systems can exert complimentary influences on the activity of ion currents. Whether this facilitates changes to spinal locomotor circuits during motor maturation remains to be determined.

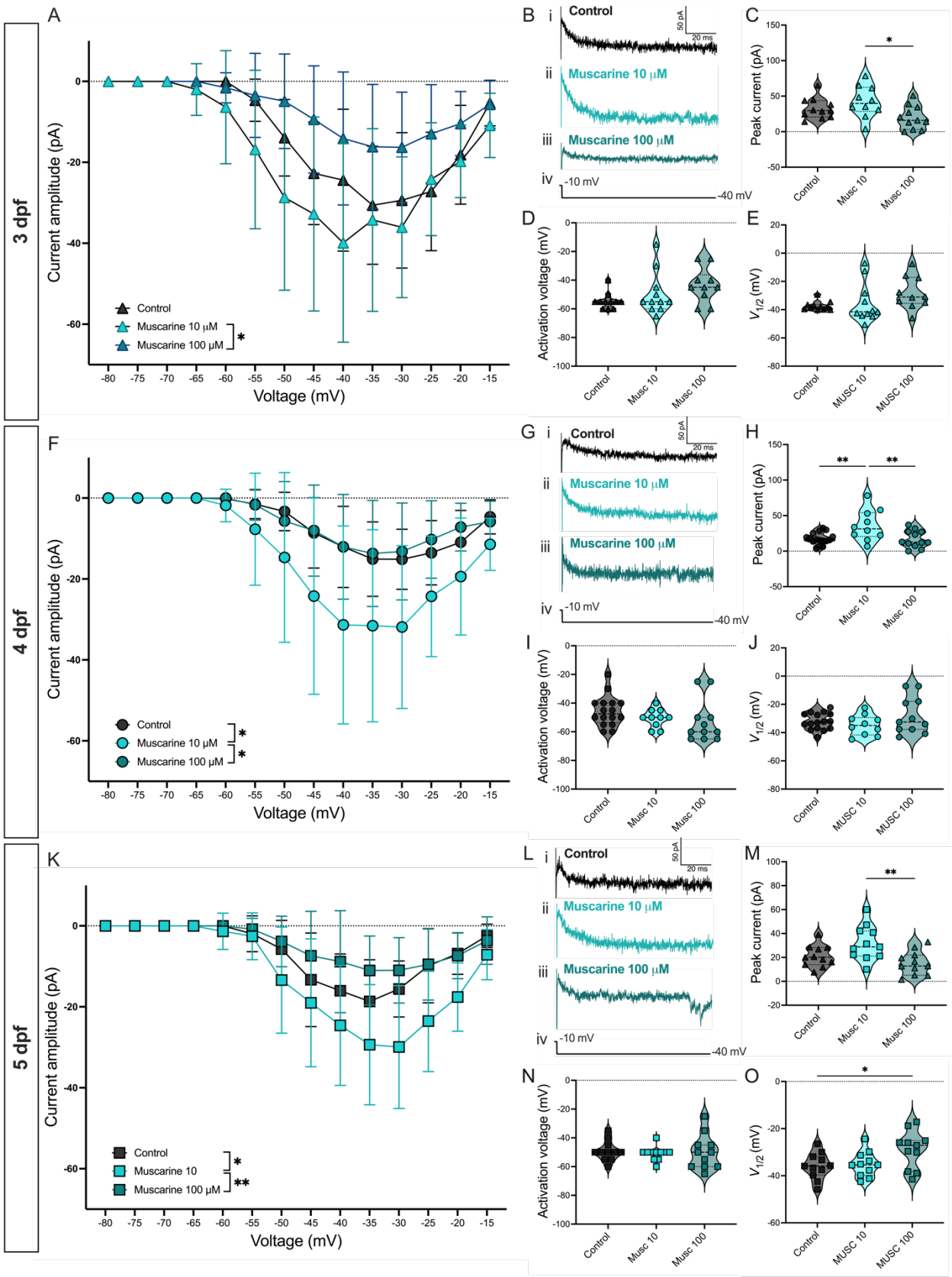
3 dpf
4 dpf
5 dpf
A
B
C
D
E
F
G
H
I
J
K
L
M
N
O
Current amplitude (pA)
Voltage (mV)
Control
Muscarine 10 μM
Muscarine 100 μM
Muscarine 10
Peak current (pA)
Activation voltage (mV)
$V_{1/2}$ (mV)
Control
Musc 10
Musc 100
MUSC 10
MUSC 100
50 pA
20 ms
-10 mV
-40 mV

Figure 5.1. Effects of muscarine on I_M in primary motoneurons of developing zebrafish. ***A***, Current-voltage relationship of I_M in three groups of 3 dpf pMNs: control (n = 11, N = 6), 10 μM muscarine (Musc) (n = 10, N = 4), 100 μM muscarine (n = 11, N = 4). ***B***, Examples of current responses from (*i*) control, (*ii*) 10 μM muscarine, and (*iii*) 100 μM muscarine pMNs in response to (*iv*) a -30 mV hyperpolarizing voltage step at 3 dpf. ***C***, Peak amplitude of I_M across treatment groups at 3 dpf. ***D***, Activation voltage of I_M across treatment groups at 3 dpf. ***E***, Voltage at which I_M reaches half its maximal amplitude ($V_{1/2}$) across treatment group at 3 dpf. ***F***, Current-voltage relationship of I_M in three groups of 4 dpf pMNs: control (n = 16, N = 6), 10 μM muscarine (n = 10, N = 3), 100 μM muscarine (n = 12, N = 5). ***G***, Examples of current responses from (*i*) control, (*ii*) 10 μM muscarine, and (*iii*) 100 μM muscarine pMNs in response to (*iv*) a -30 mV hyperpolarizing voltage step at 4 dpf. ***H***, Peak amplitude of I_M across the treatment groups at 4 dpf. ***I***, Activation voltage of I_M across treatment groups at 4 dpf. ***J***, Voltage at which I_M reaches half its maximal amplitude ($V_{1/2}$) across treatment group at 4 dpf. ***K***, Current-voltage relationship of I_M in three groups of 5 dpf pMNs: control (n = 11, N = 5), 10 μM muscarine (n = 10, N = 3), 100 μM muscarine (n = 11, N = 4). ***L***, Examples of current responses from (*i*) control, (*ii*) 10 μM muscarine, and (*iii*) 10 μM muscarine pMNs in response to (*iv*) a -30 mV hyperpolarizing voltage step at 5 dpf. ***M***, Peak amplitude of I_M across the treatment groups at 5 dpf. ***N***, Activation voltage of I_M across treatment groups at 5 dpf. ***O***, Voltage at which I_M reaches half its maximal amplitude ($V_{1/2}$) across treatment group at 5 dpf. *Statistical analysis,* (***A***, ***F***, ***K***) Mixed effects model analysis with Šídák's test for multiple comparisons, (***D-E***, ***I-J***, ***N***) Kruskal-Wallis test with Dunn's test for multiple comparisons, and (***C***, ***H***, ***M***, ***O***) ordinary one-way ANOVA with Tukey's test for multiple comparisons: * $P < 0.05$, ** $P < 0.01$; otherwise, not statistically significant.

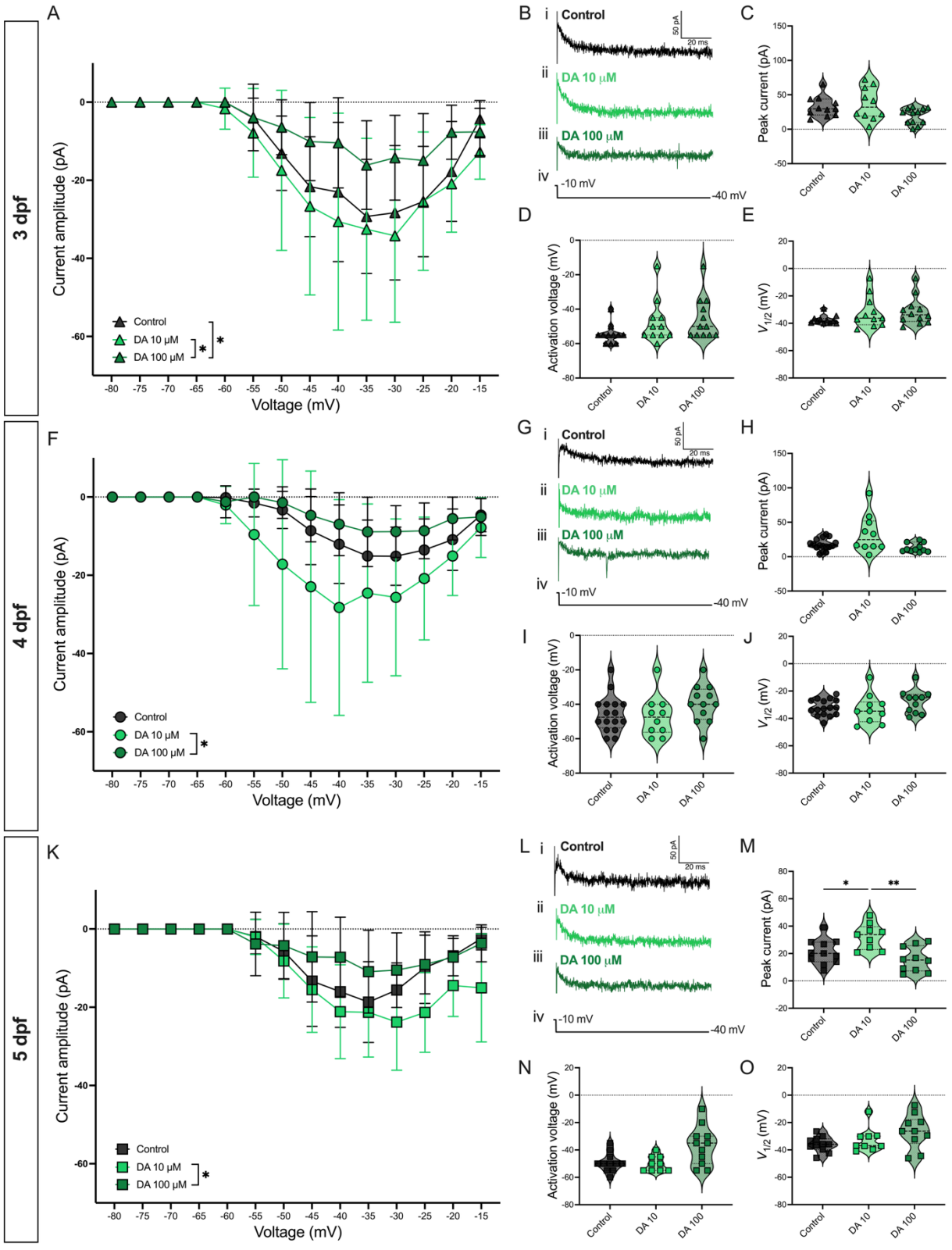
3 dpf
4 dpf
5 dpf
A
B
C
D
E
F
G
H
I
J
K
L
M
N
O
Current amplitude (pA)
Voltage (mV)
Control
DA 10 µM
DA 100 µM
Peak current (pA)
Activation voltage (mV)
$V_{1/2}$ (mV)
50 pA
20 ms
-10 mV
-40 mV

Figure 5.2. Effects of dopamine on I_M in primary motoneurons of developing zebrafish.

A, Current-voltage relationship of I_M in three groups of 3 dpf pMNs: control (n = 11, N = 6), 10 μM dopamine (DA) (n = 10, N = 3), 100 μM dopamine (n = 12, N = 5). ***B***, Examples of current responses from (*i*) control, (*ii*) 10 μM dopamine, and (*iii*) 10 μM dopamine pMNs in response to (*iv*) a -30 mV hyperpolarizing voltage step at 3 dpf. ***C***, Peak amplitude of I_M across treatment groups at 3 dpf. ***D***, Activation voltage of I_M across treatment groups at 3 dpf. ***E***, Voltage at which I_M reaches half its maximal amplitude ($V_{1/2}$) across treatment group at 3 dpf. ***F***, Current-voltage relationship of I_M in three groups of 4 dpf pMNs: control (n = 16, N = 6), 10 μM dopamine (n = 10, N = 4), 100 μM dopamine (n = 11, N = 3). ***G***, Examples of current responses from (*i*) control, (*ii*) 10 μM dopamine, and (*iii*) 100 μM dopamine pMNs in response to (*iv*) a -30 mV hyperpolarizing voltage step at 4 dpf. ***H***, Peak amplitude of I_M across the treatment groups at 4 dpf. ***I***, Activation voltage of I_M across treatment groups at 4 dpf. ***J***, Voltage at which I_M reaches half its maximal amplitude ($V_{1/2}$) across treatment group at 4 dpf. ***K***, Current-voltage relationship of I_M in three groups of 5 dpf pMNs: control (n = 11, N = 5), 10 μM dopamine (n = 9, N = 5), 100 μM dopamine (n = 10, N = 5). ***L***, Examples of current responses from (*i*) control, (*ii*) 10 μM dopamine, and (*iii*) 100 μM dopamine pMNs in response to (*iv*) a -30 mV hyperpolarizing voltage step at 5 dpf. ***M***, Peak amplitude of I_M across the treatment groups at 5 dpf. ***N***, Activation voltage of I_M across treatment groups at 5 dpf. ***O***, Voltage at which I_M reaches half its maximal amplitude ($V_{1/2}$) across treatment group at 5 dpf. *Statistical analysis,* (***A***, ***F***, ***K***) Mixed effects model analysis with Šídák's test for multiple comparisons, (***C-E, H, N-O***) Kruskal-Wallis test with Dunn's test for multiple comparisons, and (***I-J, M***) ordinary one-way ANOVA with Tukey's test for multiple comparisons: * $P < 0.05$, ** $P < 0.01$; otherwise, not statistically significant.

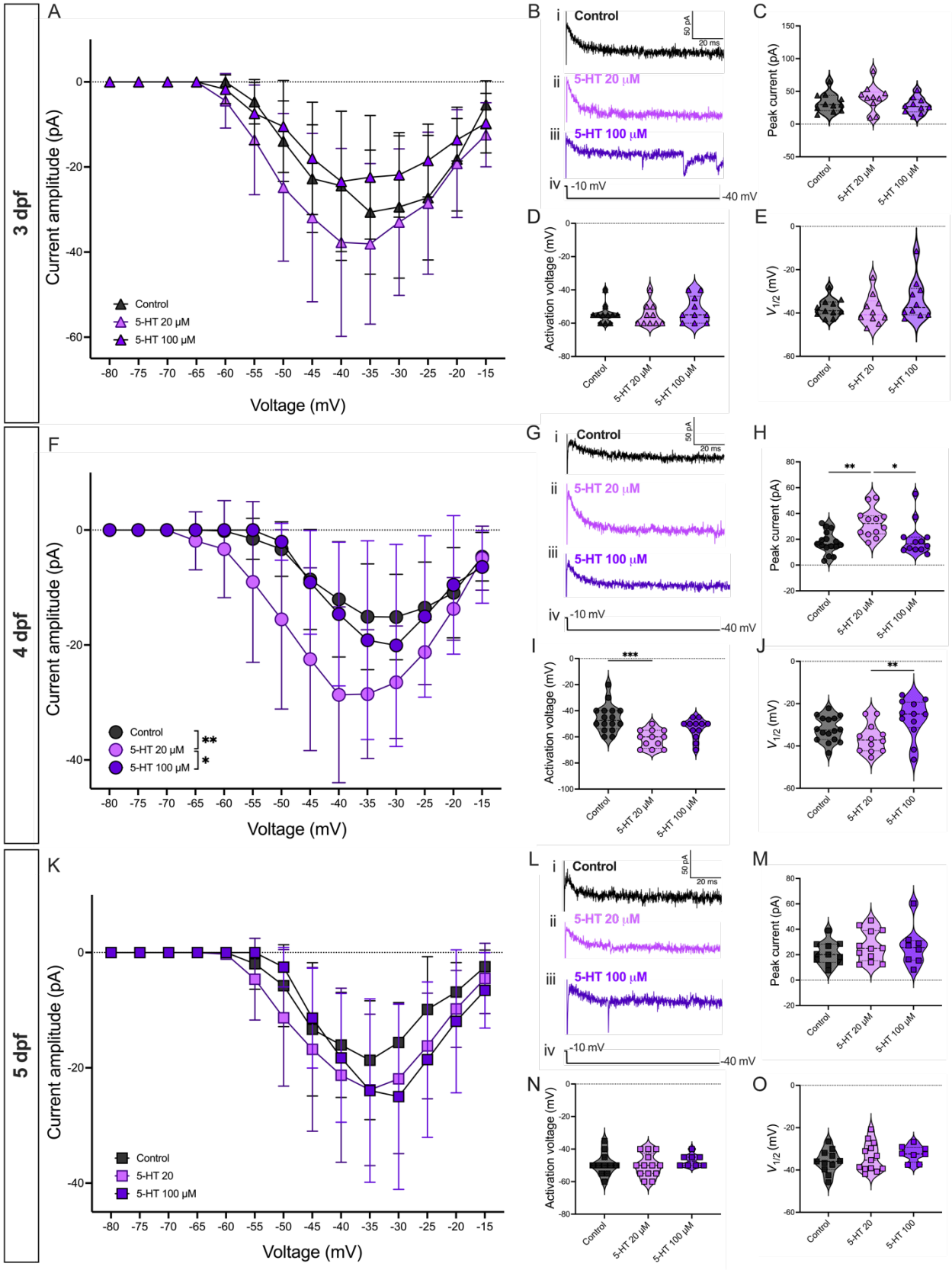
3 dpf
4 dpf
5 dpf
A
B
C
D
E
F
G
H
I
J
K
L
M
N
O
Current amplitude (pA)
Voltage (mV)
Control
5-HT 20 µM
5-HT 100 µM
5-HT 20
i
ii
iii
iv
-10 mV
-40 mV
50 pA
20 ms
Peak current (pA)
Activation voltage (mV)
$V_{1/2}$ (mV)
**
*
***

Figure 5.3. Effects of serotonin on I_M in primary motoneurons of developing zebrafish. ***A***, Current-voltage relationship of I_M in three groups of 3 dpf pMNs: control (n = 11, N = 6), 20 μM serotonin (5-HT) (n = 10, N = 5), 100 μM 5-HT (n = 10, N = 4). ***B***, Examples of current responses from (*i*) control, (*ii*) 20 μM 5-HT, and (*iii*) 100 μM 5-HT pMNs in response to (*iv*) a -30 mV hyperpolarizing voltage step at 3 dpf. ***C***, Peak amplitude of I_M across treatment groups at 3 dpf. ***D***, Activation voltage of I_M across treatment groups at 3 dpf. ***E***, Voltage at which I_M reaches half its maximal amplitude ($V_{1/2}$) across treatment group at 3 dpf. ***F***, Current-voltage relationship of I_M in three groups of 4 dpf pMNs: control (n = 16, N = 6), 20 μM 5-HT (n = 12, N = 4), 100 μM 5-HT (n = 12, N = 6). ***G***, Examples of current responses from (*i*) control, (*ii*) 20 μM 5-HT and (*iii*) 100 μM 5-HT pMNs in response to (*iv*) a -30 mV hyperpolarizing voltage step at 4 dpf. ***H***, Peak amplitude of I_M across the treatment groups at 4 dpf. ***I***, Activation voltage of I_M across treatment groups at 4 dpf. ***J***, Voltage at which I_M reaches half its maximal amplitude ($V_{1/2}$) across treatment group at 4 dpf. ***K***, Current-voltage relationship of I_M in three groups of 5 dpf pMNs: control (n = 11, N = 5), 20 μM 5-HT (n = 13, N = 5), 100 μM 5-HT (n = 8, N = 4). ***L***, Examples of current responses from (*i*) control, (*ii*) 20 μM 5-HT, and (*iii*) 100 μM 5-HT pMNs in response to (*iv*) a -30 mV hyperpolarizing voltage step at 5 dpf. ***M***, Peak amplitude of I_M across the treatment groups at 5 dpf. ***N***, Activation voltage of I_M across treatment groups at 5 dpf. ***O***, Voltage at which I_M reaches half its maximal amplitude ($V_{1/2}$) across treatment group at 5 dpf. *Statistical analysis,* (***A***, ***F***, ***K***) Mixed effects model analysis with Šídák's test for multiple comparisons, (***D-E***, ***H-I***, ***M-N***) Kruskal-Wallis test with Dunn's test for multiple comparisons, and (***C***, ***J, O***) ordinary one-way ANOVA with Tukey's test for multiple comparisons: * $P < 0.05$, ** $P < 0.01$, *** $P < 0.001$; otherwise, not statistically significant.

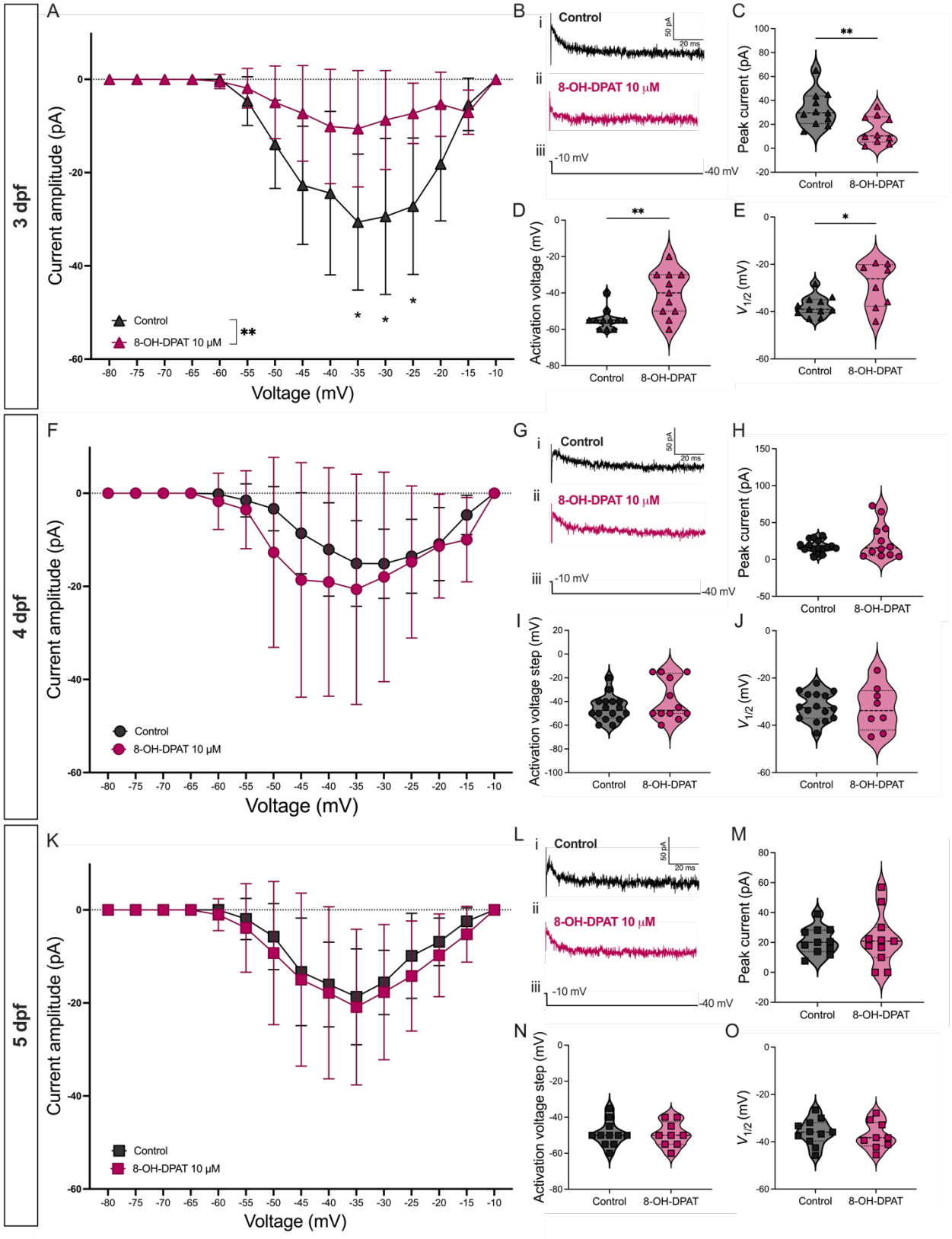
3 dpf
A
Current amplitude (pA)
Voltage (mV)
Control
8-OH-DPAT 10 µM
**
*
B
i
Control
50 pA
20 ms
ii
8-OH-DPAT 10 µM
iii
-10 mV
-40 mV
C
Peak current (pA)
**
Control
8-OH-DPAT
D
Activation voltage (mV)
**
Control
8-OH-DPAT
E
$V_{1/2}$ (mV)
*
Control
8-OH-DPAT
4 dpf
F
Current amplitude (pA)
Voltage (mV)
Control
8-OH-DPAT 10 µM
G
i
Control
50 pA
20 ms
ii
8-OH-DPAT 10 µM
iii
-10 mV
-40 mV
H
Peak current (pA)
Control
8-OH-DPAT
I
Activation voltage step (mV)
Control
8-OH-DPAT
J
$V_{1/2}$ (mV)
Control
8-OH-DPAT
5 dpf
K
Current amplitude (pA)
Voltage (mV)
Control
8-OH-DPAT 10 µM
L
i
Control
50 pA
20 ms
ii
8-OH-DPAT 10 µM
iii
-10 mV
-40 mV
M
Peak current (pA)
Control
8-OH-DPAT
N
Activation voltage step (mV)
Control
8-OH-DPAT
O
$V_{1/2}$ (mV)
Control
8-OH-DPAT

Figure 5.4. Effects of $5HT_{1A}$ receptor agonist on I_M in primary motoneurons of developing zebrafish.

A, Current-voltage relationship of I_M in two groups of 3 dpf pMNs: control (n = 11, N = 6) and 10 μM 8-OH-DPAT (n = 10, N = 4). ***B***, Examples of current responses from (*i*) control and (*ii*) 10 μM 8-OH-DPAT pMNs in response to (*iii*) a -30 mV hyperpolarizing voltage step at 3 dpf. ***C***, Peak amplitude of I_M across treatment groups at 3 dpf. ***D***, Activation voltage of I_M across treatment groups at 3 dpf. ***E***, Voltage at which I_M reaches half its maximal amplitude ($V_{1/2}$) across treatment group at 3 dpf. ***F***, Current-voltage relationship of I_M in two groups of 4 dpf pMNs: control (n = 16, N = 6), and 10 μM 8-OH-DPAT (n = 12, N = 5). ***G***, Examples of current responses from (*i*) control and (*ii*) 10 μM 8-OH-DPAT pMNs in response to (*iii*) a -30 mV hyperpolarizing voltage step at 4 dpf. ***H***, Peak amplitude of I_M across the treatment groups at 4 dpf. ***I***, Activation voltage of I_M across treatment groups at 4 dpf. ***J***, Voltage at which I_M reaches half its maximal amplitude ($V_{1/2}$) across treatment group at 4 dpf. ***K***, Current-voltage relationship of I_M in two groups of 5 dpf pMNs: control (n = 11, N = 5) and 10 μM 8-OH-DPAT (n = 9, N = 4). ***L***, Examples of current responses from (*i*) control and (*ii*) 10 μM 8-OH-DPAT pMNs in response to (*iii*) a -30 mV hyperpolarizing voltage step at 5 dpf. ***M***, Peak amplitude of I_M across the treatment groups at 5 dpf. ***N***, Activation voltage of I_M across treatment groups at 5 dpf. ***O***, Voltage at which I_M reaches half its maximal amplitude ($V_{1/2}$) across treatment group at 5 dpf. *Statistical analysis,* (***A***, ***F***, ***K***) Mixed effects model analysis with Šídák's multiple comparisons test, (***C***, ***E***, ***J***, ***M***, ***O***) unpaired t-tests, and (***D***, ***H-I***, ***N***) Mann-Whitney tests: * $P < 0.05$, ** $P < 0.01$; otherwise, not statistically significant.

Chapter 6

General Discussion

6.1 Overview

Since the discovery that an outward non-inactivating potassium current was susceptible to inhibition by muscarine in 1980 (Brown and Adams 1980), the M-current (I_M) has revealed itself as an ion current involved in a multitude of physiological processes. Pharmacological advances have permitted selective control over the activity of Kv7.2/7.3 channels that mediate I_M. Thanks to the development of these drugs, I_M has been revealed to play several roles within the nervous system of various species. A number of recent studies have determined that I_M makes important contributions to the control of motoneuron excitability, which can have consequences for motoneuron recruitment patterns (Sharples et al. 2023), timing and precision of motoneuron firing (Bothe et al. 2024) and locomotor speed in spinal circuits for locomotion in rodents (Verneuil et al. 2020b). Until now, the presence of I_M, let alone its putative functions, remained unknown in zebrafish spinal circuits.

The work presented in this thesis is the first to identify I_M within spinal locomotor circuits of larval zebrafish. Using electrophysiology techniques, we demonstrate that pharmacological modulation of I_M alters the amount of swimming generated in both the context of the escape response as well as when larval zebrafish are free-swimming. We demonstrate that this is due at least in part to modulation of I_M within spinal locomotor circuit neurons themselves and that I_M acts to limit circuit output. We next dove deeper within locomotor circuits and identified a role for I_M in regulating the excitability and repetitive firing of primary motoneurons (pMNs). This could be consistent

with our nerve recordings conducted in the presence of elevated K^+, if we assume that primary motoneurons are indeed active in this context, which show a decrease in the duration of locomotor bursts within each swimming episode when I_M is enhanced by ICA-069673. By limiting how long pMNs fire, it is possible that I_M shortens the duration of motor bursts. This data from larval zebrafish is in line with the role of I_M in rodents (Verneuil et al. 2020b). The role we find for I_M in limiting excitability of pMNs could underlie, at least in part, both the reduction in frequency of swimming and duration of swimming episodes caused by ICA-069673. The expression of I_M within pMNs could make it harder for the nervous system to recruit pMNs, which may contribute to limiting how often swimming episodes with larger body oscillations are produced. Furthermore, during many types of spontaneous swimming activity, pMNs are active for a very limited amount of time giving way to sMN activity and I_M could play a central role in limiting the duration of pMN activity to produce the desired ratio of fast versus slow muscle fiber activation; however, this remains to be tested.

My experiments have provided insights into 1) the network-wide role of I_M and 2) the pMN-specific role of I_M in spinal circuits for locomotion in developing zebrafish. Because we currently have no information on the presence of I_M in other neurons of the networks for motor control in zebrafish, we must remain cautious when relating findings from an individual neuron population to network-wide findings. While the role I_M plays in pMNs may contribute in part to network-wide effects observed during pharmacological manipulation of I_M, it remains to be seen what role I_M plays, if any, in other spinal locomotor circuit neurons of the developing zebrafish.

6.2 I_M in spinal locomotor circuits across species

Verneuil et al. demonstrate a control over burst firing by I_M that is ubiquitous across rodent lumbar spinal locomotor circuit neurons and that ultimately results in speeding up locomotion by limiting the amount of time muscles spend contracting (Verneuil et al. 2020b). In contrast, we found no differences to the frequency of motor bursts produced within individual episodes. While we observe that I_M in pMNs of developing zebrafish may play a similar role to control excitability and repetitive firing of motoneurons as has been observed in mice, the overall role I_M plays in the function of locomotor circuits of these species may differ. The role an ion current plays in the context of network-wide behaviours depends on where and how prominently it is expressed within the network. Naturally, differences in the patterns of locomotion across species are set up by differing spinal locomotor circuit architectures. Even if I_M were expressed in the same neurons across species, the way in which these neurons interact with one another across species will be inherently different thereby influencing final motor output differently. The role I_M plays in locomotion may therefore differ between species with key differences in the pattern of their locomotor activity such as the requirements of limb coordination in quadrupedal locomotion versus the prominence of axial tail bending during swimming.

6.3 I_{CaL} in motoneurons of developing zebrafish

In addition to $I_{M,}$ we identified the presence of an inward current likely mediated by L-type calcium channels in pMNs from 2 to 5 dpf. The magnitude of this current from 2 to 5 dpf does not change, unlike our observations relating to I_M, I_{NaP}, and $I_{CaP/Q}$. While I_M and I_{NaP} appear to work together to regulate and facilitate repetitive firing, respectively, it is still unclear what role I_{CaL} might play

in pMNs of zebrafish. The inward calcium current mediated by L-type channels has been implicated in generating plateau potentials observed in motoneurons across several species (Carlin et al. 2009; Perrier and Hounsgaard 2003; Zhang et al. 2006). Plateau potentials allow motoneurons to maintain depolarized membrane potentials conducive to sustaining firing without repetitive incoming synaptic drive (Kiehn and Eken 1998). Buss et al. demonstrate the presence of plateau potentials in motoneurons of zebrafish aged 2 to 4 dpf that is absent in the presence of cobalt, a known blocker of voltage-gated calcium channels (Buss et al. 2003). Furthermore, Tong and McDearmid reveal that blocking the L-type calcium current with nifedipine diminished the ability of spinal neurons to generate bursts of action potentials and frequency of depolarizations observed at 1 dpf (Tong and Jonathan Robert McDearmid 2012). These findings suggest a role for the L-type current in contributing to the generation of sustained firing by contributing to the maintenance of motoneuron plateau potentials in zebrafish. Electrophysiology experiments examining the effects of nifedipine on repetitive firing in pMNs will help elucidate whether its contribution to plateau potentials shapes pMN firing differently throughout early development.

6.4 Challenges with pharmacological and electrophysiological approaches to study ion currents and their contributions to neural function

We have attempted to elucidate the role of I_M in primary motoneurons of larval zebrafish by combining electrophysiology techniques and pharmacological manipulations. This approach allowed us to measure and observe changes to intrinsic and firing properties of pMNs as well as alterations to escape and swimming movements while modulating the activity of I_M. Together, this information can be used to speculate on the roles that I_M may play in spinal locomotor circuits through the modulation of neuron activity. The use of pharmacological agents to observe effects

brought on by increasing or decreasing ion channel activity is widespread. The legitimacy of the interpretation of resulting effects to activity, particularly at the level of the individual neuron, is tied to the selectivity of chosen pharmacological compounds to targeted ion channels and their mechanism of action. Lack of specificity can lead to off-target effects making it difficult to isolate its effect to the intended channel. We have done our best at preventing this by choosing the most selective pharmacological modulators of I_M available to us (XE-991 to inhibit and ICA-069673 to enhance Kv7.2/7.3-mediated I_M). Moreover, designed modulators for ion channel function manipulation can be state-dependent (Greene et al. 2017), as is the case for XE-991 which is more effective when I_M is activated at depolarized membrane potentials, making its efficacy entirely dependent on the state of the Kv7.2/7.3 channels at the time of experimentation. Furthermore, even the most specific pharmacological compounds come with caveats. Typical procedure for drug administration in larval zebrafish is by bath application of the pharmacological compound. In our patch-clamp electrophysiology experiments, we target one individual neuron within an entire network wherein all other neurons are also exposed to the bath-applied pharmacological agent. Without knowing whether the targeted ion current is expressed within other neurons of the network, one must consider that bath-application of the compound could have widespread effects to firing across neurons of the network, possibly altering synaptic inputs received by the recorded neuron and consequently its membrane dynamics. We have monitored input resistance and levels of synaptic inputs and did not notice any changes in the latter during XE-991 or ICA-069673 but effects on the activity of presynaptic neurons releasing neuromodulators are harder to assess and could certainly modulate passive and active properties of neurons.

While patch-clamping provides the powerful ability to monitor neuron firing activity and ion channel function, there are technical considerations that must be taken into account when interpreting this type of electrophysiology data. Space-clamp issues can alter the amplitude and voltage response of clamped currents and these issues become more severe in larger neurons and those with extensive dendritic arborization. During early zebrafish development, pMN soma size increases and so does the length and number of their dendrites (Kishore and Fetcho 2013; P. Myers et al. 1986). We must therefore consider the possibility that space-clamping issues may become more prominent in pMNs at 4 and 5 dpf compared to pMNs at 2 and 3 dpf that have a smaller soma and less extensive dendritic arborization. While we cannot rule out the influence of less effective voltage clamping to the apparent reduction in the magnitude of I_M in the 4-5 dpf pMNs, our current-clamp data demonstrating a greater effect of inhibiting I_M at 3 dpf compared to 4 and 5 dpf supports that this observed reduction may not exclusively be a result of space-clamp issues. Nonetheless, our findings that riluzole significantly reduced repetitive firing in pMNs at 5 dpf in current-clamp without reducing the amplitude of the PICs measured in 5 dpf pMNs in voltage-clamp highlight the utility of complementary biochemical or molecular approaches such as immunohistochemistry, in-situ hybridization or RNA-sequencing to observe other changes in ion currents that may be missed by electrophysiology and pharmacology.

Furthermore, with long-lasting whole-cell patch clamping experiments comes the confounding influence of cell dialysis where the intracellular components of the neurons become increasingly diluted with time. This can lead to changes in protein function that can alter membrane dynamics. It is for this reason that we focused our patch-clamping data on across-cell comparisons rather than within-cell comparisons. However, this type of comparison introduces more variability to the data

set and may be a large contribution to the rather large variability we observe across groups when investigating the influence of neuromodulators on the activity of I_M in pMNs. It is also important to consider that cell dialysis could still exert an influence on cell function, even in these shorter across cell experiments, which can alter the machinery required for neuromodulation of the activity of I_M and increase the variability of observed effects to I_M activity. In lieu of whole-cell patch-clamp, similar experiments performed using perforated patch-clamp would permit reliable within-cell comparisons by circumventing the potential confounding effects of cell dialysis in the neuron of interest. It would nonetheless be important to determine how the increase in access resistance during perforated patch-clamp experiments affects measured ion current amplitudes and whether subtle changes in amplitude can be resolved.

6.5 The "ideal" approach to identifying the definitive role of I_M in pMNs

How then can the role of an ion current in a neuron truly be revealed? Here I describe the "ideal" approach to obtain a definitive answer on the role an ion current plays using I_M in pMNs as an example. The role of an ion current is revealed by how increasing or decreasing its conductance affects function. If we're concerned with network function, modulation of conductance should be restricted to a targeted neuron population.

Functional assessment of ion channels via genetic manipulations is common. Knocking out KCNQ2 and KCNQ3 genes that encode the Kv7.2 and Kv7.3 channel subunits, respectively, would reveal how loss of function of I_M mediated by these channels alters both neuronal and network behaviours. A conditional knockout (cKO) strategy targeting KCNQ2/KCNQ3 gene disruption could be restricted to pMNs. The transcription factors isl1 and mnx1 are typically used

to restrict transgene expression in motoneurons of zebrafish. However, the former is specific to a subset of secondary motoneurons while the latter encompasses all motoneurons and is not restricted to only pMNs. Recent work by Pallucchi et al., have revealed potential novel markers for individual motoneuron subpopulations (Pallucchi et al. 2024). It remains to be seen whether any of these markers are limited in pMNs, and marker validation in transgenic lines targeting pMNs that have yet to be generated remains necessary. Assuming such a marker exists, it would be wise to consider only temporally controlled cKO of these channels as permanent knockout may either be lethal or result in compensatory mechanisms for the loss of Kv7.2/7.3 channels during development. Temporally controlled cKOs making use of the tamoxifen-induced Cre-Lox system have been successfully introduced to the zebrafish model (Hans et al. 2009). We could picture an experimental setup wherein Kv7.2/7.3 channels are conditionally knocked out in pMNs upon bath application of tamoxifen prior to extracellular nerve and patch-clamp recordings to monitor network behaviour and pMN behaviour, respectively. One caveat to this approach however that that it takes several hours for tamoxifen to activate the Cre-Lox system (Hans et al. 2009). While this approach would allow us to avoid the off-target effects associated with pharmacological manipulation of ion channel activity, limitations to the interpretations of our findings may lie within our reduced electrophysiology preparations as discussed above.

Furthermore, ion currents can play different roles depending on the location of their conductance densities. For example, P/Q-type calcium channels expressed in axon terminals are involved in synaptic release while those expressed at the neuron soma may be involved in other processes, such as spike frequency adaptation. Dissecting the role of conductances distributed in different

regions of the same neuron requires further molecular or technical advances that are not currently available.

There may be no ideal way to definitively identify the role of an ion current. Assessing the likely many roles of a singular ion current in the context of both neuronal and network behaviour is a challenging task. Ionic conductance densities vary within the neuron, are in constant interplay with other ion currents, and are under the influence of many endogenous compounds. Some approaches offer advantages over others, yet they all come with their own limitations. Taken together, we can use these context-specific findings from a variety of experimental approaches to piece together how ion currents shape both neuronal and network-wide behaviour.

6.6 Future projects

6.6.1 Delineating developmental changes to putative P/Q-type calcium currents in pMNs

We serendipitously found that pMNs expressed a second inward current in response to a slow depolarizing voltage ramp at membrane potentials more depolarized to PICs only at 4 and 5 dpf. Bath application of ω-agatoxin reveals that this current may be mediated, at least in part, by P/Q-type calcium channels. Assessing the contributions of P/Q-type calcium channels to signal transmission at the neuromuscular junction from 2 to 5 dpf would reveal whether there exist developmental differences in P/Q-mediated neurotransmitter release. This could be accomplished by patch-clamping fast muscle fibers and recording end-plate responses during either electrical or optogenetic activation of pMNs while P/Q-type calcium currents are inhibited. This would be further complemented by electrophysiology recordings in pMNs during inhibition of P/Q-type

calcium currents to assess potential effects to pMN firing should the developmental changes in the appearance of P/Q-type calcium currents reflect those of a somatic rather than axonal nature. Ultimately, these experiments have the potential to reveal the functional relevance of the putative P/Q-type calcium channel mediated inward current that appears only in pMNs at 4 dpf.

6.6.2 Elucidating the role I_M plays in primary motoneuron recruitment during development

A striking feature of larval zebrafish spinal locomotor circuits is the spatial organization of motoneurons within the motor column that is related not only to birth order but their speed-dependent recruitment. As zebrafish develop, they rid themselves of their earliest locomotor movements (i.e. coiling, double coiling, burst swimming) to make room for mature swimming made up of rhythmic low amplitude left-right alternating tail beats. How then is the recruitment of pMNs controlled during this transition from a pMN-dominant locomotor repertoire to one that is sMN-dominant? Studies in zebrafish have emerged suggesting that the size principle alone does not underlie orderly recruitment of pMNs but rather that this is mediated by the integration of multiple intrinsic properties as well as extrinsic influence (Gabriel et al. 2011; Kishore et al. 2014). We have identified how I_M, in addition to I_{NaP}, I_{CaL}, and $I_{CaP/Q}$, in pMNs changes from 2 dpf to 5 dpf yet the functional implications of these changes to locomotion at each of these ages remains to be elucidated.

Sharples et al. have recently uncovered a role for I_M in the recruitment of motoneurons (Sharples et al. 2023). They show that I_M is larger in fast motoneurons compared to slow motoneurons and that pharmacological modulation of I_M alters the recruitment of fast motoneurons only (Sharples et al. 2023). Could I_M be similarly involved in pMN recruitment in the developing zebrafish? If

so, is a larger I_M in pMNs at 3 dpf, compared to 4 and 5 dpf, necessary to restrict the recruitment of pMNs to fast locomotion? Do other mechanisms emerge by 4 dpf such that a large I_M is no longer necessary for control of pMN recruitment? Paired electrophysiology recordings between a pMN and a motor nerve in intact larval zebrafish during pharmacological manipulation of I_M would reveal if and how this ion current shapes the recruitment of pMNs during swimming activity of different locomotor frequency. Performing these experiments at 2, 3, 4, and 5 dpf would further elucidate how mechanisms of pMN recruitment change during development with motor maturation.

6.6.3 I_M in pMNs along the length of the spinal cord

The development of the vertebrate nervous system progresses in a rostrocaudal fashion with rostral regions getting formed prior to caudal ones. Consequently, the development of motoneurons is likely to proceed in a rostrocaudal manner. Indeed, rostrally located cervical motoneurons are born prior to more caudally located lumber motoneurons in the chick (Hollyday and Hamburger 1977). Smith and Brownstone have recently revealed the maturation of intrinsic properties guiding motoneuron firing in the mouse occurs in a rostral to causal fashion (Smith and Brownstone 2020). In zebrafish, do the ion currents pMNs express and their influence on pMN properties vary along the length of the spinal cord during development? Evidence supports that the incorporation of new-born pMNs to spinal circuits and their subsequent maturation proceeds rostrocaudally in the developing zebrafish (Myers, Eisen, and Westerfield 1986). Perhaps then the intrinsic properties of rostral pMNs differ from those located most caudally as zebrafish develop. Investigating how properties of I_M in pMNs might change along the length of the spinal cord could further reveal

shared principles underlying motor maturation across vertebrates. Furthermore, whether neuromodulation similarly influences I_M in pMNs located along the rostrocaudal axis will elucidate mechanisms by which intrinsic neuronal properties can be guided extrinsically by sources of neuromodulation found either within the spinal cord or originating from descending input from supraspinal regions.

6.7 Conclusion

The work presented in this thesis provides novel insights into the contributions of neuromodulation-susceptible ion currents to the intrinsic properties of motoneurons in the context of motor maturation during development. Identifying specific changes to the role and neuromodulation of ion currents in neurons of spinal locomotor circuits during development is important to understand how membrane dynamics set up neuronal behaviours and how they may change during development to facilitate the maturation of movements. Uncovering precise mechanisms underlying motor maturation is crucial to our understanding of how the nervous system produces movement.

References

Abicht, Angela, Juliane S. Müller, and Hanns Lochmüller. 1993. “Congenital Myasthenic Syndromes Overview.” in *GeneReviews®*, edited by M. P. Adam, J. Feldman, G. M. Mirzaa, R. A. Pagon, S. E. Wallace, and A. Amemiya. Seattle (WA): University of Washington, Seattle.

Adams, P. R., D. A. Brown, and A. Constanti. 1982. “M-currents and Other Potassium Currents in Bullfrog Sympathetic Neurones.” *The Journal of Physiology* 330(1):537–72. doi:10.1113/jphysiol.1982.sp014357.

Adams, Paul R., Halliwell, James V. 1982. “Voltage-Clamp Analysis of Muscarinic Excitation in Hippocampal Neurons.” 250:71–92.

Alaburda, Aidas, Perrier, Jean-François, and Hounsgaard, Jørn. 2002. “An M-like Outward Current Regulates the Excitability of Spinal Motoneurones in the Adult Turtle.” 540(3):875–81.

Albadri, Shahad, Filippo Del Bene, and Céline Revenu. 2017. “Genome Editing Using CRISPR/Cas9-Based Knock-in Approaches in Zebrafish.” *Methods (San Diego, Calif.)* 121–122:77–85. doi:10.1016/j.ymeth.2017.03.005.

Ampatzis, Konstantinos, Jianren Song, Jessica Ausborn, and Abdeljabbar El Manira. 2014. “Separate Microcircuit Modules of Distinct V2a Interneurons and Motoneurons Control the Speed of Locomotion.” *Neuron* 83(4):934–43. doi:10.1016/j.neuron.2014.07.018.

Ampatzis, Konstantinos, Jianren Song, Jessica Ausborn, and Abdeljabbar El Manira. 2013. “Pattern of Innervation and Recruitment of Different Classes of Motoneurons in Adult Zebrafish.” *Journal of Neuroscience* 33(26):10875–86. doi:10.1523/JNEUROSCI.0896-13.2013.

Antinucci, Paride, Adna Dumitrescu, Charlotte Deleuze, Holly J. Morley, Kristie Leung, Tom Hagley, Fumi Kubo, Herwig Baier, Isaac H. Bianco, and Claire Wyart. 2020. “A Calibrated Optogenetic Toolbox of Stable Zebrafish Opsin Lines.” *eLife* 9:e54937. doi:10.7554/eLife.54937.

Araneda, R., and R. Andrade. 1991. “5-Hydroxytryptamine2 and 5-hydroxytryptamine1A Receptors Mediate Opposing Responses on Membrane Excitability in Rat Association Cortex.” *Neuroscience* 40(2):399–412. doi:10.1016/0306-4522(91)90128-B.

Asakawa, Kazuhide, Maximiliano L. Suster, Kanta Mizusawa, Saori Nagayoshi, Tomoya Kotani, Akihiro Urasaki, Yasuyuki Kishimoto, Masahiko Hibi, and Koichi Kawakami. 2008. “Genetic Dissection of Neural Circuits by Tol2 Transposon-Mediated Gal4 Gene and Enhancer Trapping in Zebrafish.” *Proceedings of the National Academy of Sciences* 105(4):1255–60. doi:10.1073/pnas.0704963105.

Azevedo, Anthony W., Evyn S. Dickinson, Pralaksha Gurung, Lalanti Venkatasubramanian, Richard S. Mann, and John C. Tuthill. 2020. “A Size Principle for Recruitment of

Drosophila Leg Motor Neurons" edited by R. L. Calabrese and C. Q. Doe. *eLife* 9:e56754. doi:10.7554/eLife.56754.

Bar-Yehuda, Dan, and Alon Korngreen. 2008. "Space-Clamp Problems When Voltage Clamping Neurons Expressing Voltage-Gated Conductances." *Journal of Neurophysiology* 99(3):1127–36. doi:10.1152/jn.01232.2007.

Bello-Rojas, Saul, Ana E. Istrate, Sandeep Kishore, and David L. McLean. 2019. "Central and Peripheral Innervation Patterns of Defined Axial Motor Units in Larval Zebrafish." *The Journal of Comparative Neurology* 527(15):2557–72. doi:10.1002/cne.24689.

Benda, Jan, and Andreas V. M. Herz. 2003. "A Universal Model for Spike-Frequency Adaptation." *Neural Computation* 15(11):2523–64. doi:10.1162/089976603322385063.

Benda, Jan, André Longtin, and Len Maler. 2005. "Spike-Frequency Adaptation Separates Transient Communication Signals from Background Oscillations." *Journal of Neuroscience* 25(9):2312–21. doi:10.1523/JNEUROSCI.4795-04.2005.

Benedetti, Lorena, Anna Ghilardi, Elsa Rottoli, Marcella De Maglie, Laura Prosperi, Carla Perego, Mirko Baruscotti, Annalisa Bucchi, Luca Del Giacco, and Maura Francolini. 2016. "INaP Selective Inhibition Reverts Precocious Inter- and Motorneurons Hyperexcitability in the Sod1-G93R Zebrafish ALS Model." *Scientific Reports* 6(1):24515. doi:10.1038/srep24515.

Berg, Eva M., Leander Mrowka, Maria Bertuzzi, David Madrid, Laurence D. Picton, and Abdeljabbar El Manira. 2023. "Brainstem Circuits Encoding Start, Speed, and Duration of Swimming in Adult Zebrafish." *Neuron* 111(3):372-386.e4. doi:10.1016/j.neuron.2022.10.034.

Berger, A. J., and T. Takahashi. 1990. "Serotonin Enhances a Low-Voltage-Activated Calcium Current in Rat Spinal Motoneurons." *Journal of Neuroscience* 10(6):1922–28. doi:10.1523/JNEUROSCI.10-06-01922.1990.

Berger, Joachim, and Peter D. Currie. 2012. "Zebrafish Models Flex Their Muscles to Shed Light on Muscular Dystrophies." *Disease Models & Mechanisms* 5(6):726–32. doi:10.1242/dmm.010082.

Bernhardt, Robert R., Ajay B. Chitnis, Laurie Lindamer, and John Y. Kuwada. 1990. "Identification of Spinal Neurons in the Embryonic and Larval Zebrafish." *Journal of Comparative Neurology* 302(3):603–16. doi:10.1002/cne.903020315.

Bernhardt, Robert R, May B. Chltnis, Laurie Lind-Ft, and John Y. Kuwada. 1990. *Identification of Spinal Neurons in the Embryonic and Larval Zebrafish*. Vol. 302.

Bordas, Csilla, Adrienn Kovacs, and Balazs Pal. 2015. "The M-Current Contributes to High Threshold Membrane Potential Oscillations in a Cell Type-Specific Way in the

Pedunculopontine Nucleus of Mice." *Frontiers in Cellular Neuroscience* 9. doi:10.3389/fncel.2015.00121.

Bothe, Maximilian S., Tobias Kohl, Felix Felmy, Jason Gallant, and Boris P. Chagnaud. 2024. "Timing and Precision of Rattlesnake Spinal Motoneurons Are Determined by the KV72/3 Potassium Channel." *Current Biology* 34(2):286-297.e5. doi:10.1016/j.cub.2023.11.062.

Bothe, Maximilian S., Kohl, Tobias, Felmy, Felix, Gallant, Jason, and Chagnaud, Boris P. 2024. "Timing and Precision of Rattlesnake Spinal Motoneurons Are Determined by the KV72/3 Potassium Channel." 34(2):286–97.

Boyden, Edward S., Feng Zhang, Ernst Bamberg, Georg Nagel, and Karl Deisseroth. 2005. "Millisecond-Timescale, Genetically Targeted Optical Control of Neural Activity." *Nature Neuroscience* 8(9):1263–68. doi:10.1038/nn1525.

Brocard, Frédéric, Dorly Verdier, Isabel Arsenault, James P. Lund, and Arlette Kolta. 2006. "Emergence of Intrinsic Bursting in Trigeminal Sensory Neurons Parallels the Acquisition of Mastication in Weanling Rats." *Journal of Neurophysiology* 96(5):2410–24. doi:10.1152/jn.00352.2006.

Brown, A. M., P. C. Schwindt, and W. E. Crill. 1994. "Different Voltage Dependence of Transient and Persistent Na+ Currents Is Compatible with Modal-Gating Hypothesis for Sodium Channels." *Journal of Neurophysiology* 71(6):2562–65. doi:10.1152/jn.1994.71.6.2562.

Brown, D. A., and P. R. Adams. 1980. "Muscarinic Suppression of a Novel Voltage-Sensitive K+ Current in a Vertebrate Neurone." *Nature* 283(5748):673–76. doi:10.1038/283673a0.

Brown, David A., and Gayle M. Passmore. 2009. "Neural KCNQ (Kv7) Channels." *British Journal of Pharmacology* 156(8):1185–95. doi:10.1111/j.1476-5381.2009.00111.x.

Brown, T. Graham. 1914. "On the Nature of the Fundamental Activity of the Nervous Centres; Together with an Analysis of the Conditioning of Rhythmic Activity in Progression, and a Theory of the Evolution of Function in the Nervous System." *The Journal of Physiology* 48(1):18–46.

Brownstone, R. M., L. M. Jordan, D. J. Kriellaars, B. R. Noga, and S. J. Shefchyk. 1992. "On the Regulation of Repetitive Firing in Lumbar Motoneurones during Fictive Locomotion in the Cat." *Experimental Brain Research* 90(3). doi:10.1007/BF00230927.

Brustein, Edna, Mabel Chong, Bo Holmqvist, and Pierre Drapeau. 2003. "Serotonin Patterns Locomotor Network Activity in the Developing Zebrafish by Modulating Quiescent Periods." *Journal of Neurobiology* 57(3):303–22. doi:10.1002/neu.10292.

Budick, Seth A., and Donald M. O'Malley. 2000. "Locomotor Repertoire of The Larval Zebrafish: Swimming, Turning and Prey Capture." *Journal of Experimental Biology* 203(17):2565–79. doi:10.1242/jeb.203.17.2565.

Buskila, Yossi, Orsolya Kékesi, Alba Bellot-Saez, Winston Seah, Tracey Berg, Michael Trpceski, Justin J. Yerbury, and Lezanne Ooi. 2019. “Dynamic Interplay between H-Current and M-Current Controls Motoneuron Hyperexcitability in Amyotrophic Lateral Sclerosis.” *Cell Death & Disease* 10(4):1–13. doi:10.1038/s41419-019-1538-9.

Buss, Robert R., Charles W. Bourque, and Pierre Drapeau. 2003. “Membrane Properties Related to the Firing Behavior of Zebrafish Motoneurons.” *Journal of Neurophysiology* 89(2):657–64. doi:10.1152/jn.00324.2002.

Buss, Robert R. and Drapeau, Pierre. 2000. “Physiological Properties of Zebrafish Embryonic Red and White Muscle Fibers During Early Development.” 84(3):1545–57. doi:10.1152/jn.2000.84.3.1545.

Buss, Robert R., and Pierre Drapeau. 2001. “Synaptic Drive to Motoneurons During Fictive Swimming in the Developing Zebrafish.” *Journal of Neurophysiology* 86(1):197–210. doi:10.1152/jn.2001.86.1.197.

Carlin, K. P., K. E. Jones, Z. Jiang, L. M. Jordan, and R. M. Brownstone. 2000. “Dendritic L-Type Calcium Currents in Mouse Spinal Motoneurons: Implications for Bistability.” *European Journal of Neuroscience* 12(5):1635–46. doi:10.1046/j.1460-9568.2000.00055.x.

Carlin, Kevin P., Tuan V. Bui, Yue Dai, and Robert M. Brownstone. 2009. “Staircase Currents in Motoneurons: Insight into the Spatial Arrangement of Calcium Channels in the Dendritic Tree.” *The Journal of Neuroscience: The Official Journal of the Society for Neuroscience* 29(16):5343–53. doi:10.1523/JNEUROSCI.5458-08.2009.

Carver, Chase M., and Mark S. Shapiro. 2019. “Gq-Coupled Muscarinic Receptor Enhancement of KCNQ2/3 Channels and Activation of TRPC Channels in Multimodal Control of Excitability in Dentate Gyrus Granule Cells.” *Journal of Neuroscience* 39(9):1566–87. doi:10.1523/JNEUROSCI.1781-18.2018.

del Castillo, J., and B. Katz. 1954. “Quantal Components of the End-Plate Potential.” *The Journal of Physiology* 124(3):560–73.

Catterall, William A. 2000. “Structure and Regulation of Voltage-Gated Ca^{2+} Channels.” *Annual Review of Cell and Developmental Biology* 16(1):521–55. doi:10.1146/annurev.cellbio.16.1.521.

Chang, Nannan, Changhong Sun, Lu Gao, Dan Zhu, Xiufei Xu, Xiaojun Zhu, Jing-Wei Xiong, and Jianzhong Jeff Xi. 2013. “Genome Editing with RNA-Guided Cas9 Nuclease in Zebrafish Embryos.” *Cell Research* 23(4):465–72. doi:10.1038/cr.2013.45.

Cheng, Yi, Qiang Zhang, and Yue Dai. 2020. “Sequential Activation of Multiple Persistent Inward Currents Induces Staircase Currents in Serotonergic Neurons of Medulla in ePet-EYFP Mice.” *Journal of Neurophysiology* 123(1):277–88. doi:10.1152/jn.00623.2019.

Chia, Kelda, Anna Klingseisen, Dirk Sieger, and Josef Priller. 2022. “Zebrafish as a Model Organism for Neurodegenerative Disease.” *Frontiers in Molecular Neuroscience* 15. doi:10.3389/fnmol.2022.940484.

Colwill, Ruth M., and Robbert Creton. 2011. “Imaging Escape and Avoidance Behavior in Zebrafish Larvae.” *Reviews in the Neurosciences* 22(1):63–73. doi:10.1515/RNS.2011.008.

Cowley, Kristine C., Eugene Zaporozhets, Jason N. Maclean, and Brian J. Schmidt. 2005. “Is NMDA Receptor Activation Essential for the Production of Locomotor-like Activity in the Neonatal Rat Spinal Cord?” *Journal of Neurophysiology* 94(6):3805–14. doi:10.1152/jn.00016.2005.

Davis, Harvey, Neil Herring, and David J. Paterson. 2020. “Downregulation of M Current Is Coupled to Membrane Excitability in Sympathetic Neurons Before the Onset of Hypertension.” *Hypertension (Dallas, Tex. : 1979)* 76(6):1915. doi:10.1161/HYPERTENSIONAHA.120.15922.

Davis, S. F., and C. L. Linn. 2003. “Activation of NMDA Receptors Linked to Modulation of Voltage-Gated Ion Channels and Functional Implications.” *American Journal of Physiology-Cell Physiology* 284(3):C757–68. doi:10.1152/ajpcell.00252.2002.

Davis, Scott F., and Cindy L. Linn. 2003. “Mechanism Linking NMDA Receptor Activation to Modulation of Voltage-Gated Sodium Current in Distal Retina.” *American Journal of Physiology-Cell Physiology* 284(5):C1193–1204. doi:10.1152/ajpcell.00256.2002.

Deemyad, Tara, Leonard Maler, and Maurice J. Chacron. 2011. “Inhibition of SK and M Channel-Mediated Currents by 5-HT Enables Parallel Processing by Bursts and Isolated Spikes.” *Journal of Neurophysiology* 105(3):1276–94. doi:10.1152/jn.00792.2010.

Dewell, Richard B., and Fabrizio Gabbiani. 2018. “M Current Regulates Firing Mode and Spike Reliability in a Collision-Detecting Neuron.” *Journal of Neurophysiology* 120(4):1753–64. doi:10.1152/jn.00363.2018.

Dolphin, Annette C. 2020. “Functions of Presynaptic Voltage-Gated Calcium Channels.” *Function* 2(1):zqaa027. doi:10.1093/function/zqaa027.

Dominici, Nadia, Yuri P. Ivanenko, Germana Cappellini, Andrea d’Avella, Vito Mondì, Marika Cicchese, Adele Fabiano, Tiziana Silei, Ambrogio Di Paolo, Carlo Giannini, Richard E. Poppele, and Francesco Lacquaniti. 2011. “Locomotor Primitives in Newborn Babies and Their Development.” *Science* 334(6058):997–99. doi:10.1126/science.1210617.

Drapeau, Pierre, Louis Saint-Amant, Robert R. Buss, Mabel Chong, Jonathan R. McDearmid, and Edna Brustein. 2002a. “Development of the Locomotor Network in Zebrafish.” *Progress in Neurobiology* 68(2):85–111.

Drapeau, Pierre, Louis Saint-Amant, Robert R. Buss, Mabel Chong, Jonathan R. McDearmid, and Edna Brustein. 2002b. “Development of the Locomotor Network in Zebrafish.” *Progress in Neurobiology* 68(2):85–111. doi:10.1016/S0301-0082(02)00075-8.

Drion, Guillaume, Maxime Bonjean, Olivier Waroux, Jacqueline Scuvée-Moreau, Jean-François Liégeois, Terrence J. Sejnowski, Rodolphe Sepulchre, and Vincent Seutin. 2010. “M-Type Channels Selectively Control Bursting in Rat Dopaminergic Neurons.” *The European Journal of Neuroscience* 31(5):827. doi:10.1111/j.1460-9568.2010.07107.x.

Drouillas, Benoît, Cécile Brocard, Sébastien Zanella, Rémi Bos, and Frédéric Brocard. 2023. “Persistent Nav1.1 and Nav1.6 Currents Drive Spinal Locomotor Functions through Nonlinear Dynamics.” *Cell Reports* 42(9):113085. doi:10.1016/j.celrep.2023.113085.

Eccles, John C, Bernhard Katz, and Stephen W Kuffler. 1941. “NATURE OF THE ‘ENDPLATE POTENTIAL’ IN CURARIZED MUSCLE.” 4(5):331–426. doi:10.1152/jn.1941.4.5.362.

Eccles, John C., Bernhard Katz, and Stephen W. Kuffler. 1942. “EFFECT OF ESERINE ON NEUROMUSCULAR TRANSMISSION.” *Journal of Neurophysiology* 5(3):211–30. doi:10.1152/jn.1942.5.3.211.

Elliott, P., and D. I. Wallis. 1992. “Serotonin and L-Norepinephrine as Mediators of Altered Excitability in Neonatal Rat Motoneurons Studied in Vitro.” *Neuroscience* 47(3):533–44. doi:10.1016/0306-4522(92)90163-v.

Emran, Farida, Jason Rihel, and John E. Dowling. 2008. “A Behavioral Assay to Measure Responsiveness of Zebrafish to Changes in Light Intensities.” *Journal of Visualized Experiments : JoVE* (20):923. doi:10.3791/923.

Engel, Andrew G., Xin-Ming Shen, Duygu Selcen, and Steven M. Sine. 2015. “Congenital Myasthenic Syndromes: Pathogenesis, Diagnosis, and Treatment.” *The Lancet. Neurology* 14(4):420–34. doi:10.1016/S1474-4422(14)70201-7.

Fatt, P., and B. Katz. 1952. “Spontaneous Subthreshold Activity at Motor Nerve Endings.” *The Journal of Physiology* 117(1):109–28.

Fetcho, J. R., and D. M. O’Malley. 1995. “Visualization of Active Neural Circuitry in the Spinal Cord of Intact Zebrafish.” *Journal of Neurophysiology* 73(1):399–406. doi:10.1152/jn.1995.73.1.399.

Fetcho, Joseph R., and David L. McLean. 2010. “Some Principles of Organization of Spinal Neurons Underlying Locomotion in Zebrafish and Their Implications.” *Annals of the New York Academy of Sciences* 1198:94–104. doi:10.1111/j.1749-6632.2010.05539.x.

Fetcho, Jr, and Ds Faber. 1988. “Identification of Motoneurons and Interneurons in the Spinal Network for Escapes Initiated by the Mauthner Cell in Goldfish.” *The Journal of Neuroscience* 8(11):4192–4213. doi:10.1523/JNEUROSCI.08-11-04192.1988.

Friesen, W. Otto, and Gunther S. Stent. 1978. “NEURAL CIRCUITS FOR GENERATING RHYTHMIC MOVEMENTS.” *Annual Review of Biophysics* 7(Volume 7, 1978):37–61. doi:10.1146/annurev.bb.07.060178.000345.

Gabriel, Jens Peter, Jessica Ausborn, Konstantinos Ampatzis, Riyadh Mahmood, Emma Eklöf-Ljunggren, and Abdeljabbar El Manira. 2011. “Principles Governing Recruitment of Motoneurons during Swimming in Zebrafish.” *Nature Neuroscience* 14(1):93–99. doi:10.1038/nn.2704.

Gahtan, Ethan, and Donald M. O’Malley. 2003. “Visually Guided Injection of Identified Reticulospinal Neurons in Zebrafish: A Survey of Spinal Arborization Patterns.” *Journal of Comparative Neurology* 459(2):186–200. doi:10.1002/cne.10621.

Gao, Bao-Xi, and Lea Ziskind-Conhaim. 1998. “Development of Ionic Currents Underlying Changes in Action Potential Waveforms in Rat Spinal Motoneurons.” *Journal of Neurophysiology* 80(6):3047–61. doi:10.1152/jn.1998.80.6.3047.

Gasparini, Sonia, Alexander M. Kasyanov, Daniela Pietrobon, Leon L. Voronin, and Enrico Cherubini. 2001. “Presynaptic R-Type Calcium Channels Contribute to Fast Excitatory Synaptic Transmission in the Rat Hippocampus.” *The Journal of Neuroscience* 21(22):8715–21. doi:10.1523/JNEUROSCI.21-22-08715.2001.

Goulding, Martyn. 2009. “Circuits Controlling Vertebrate Locomotion: Moving in a New Direction.” *Nature Reviews. Neuroscience* 10(7):507–18. doi:10.1038/nrn2608.

Granit, R., D. Kernell, and G. K. Shortess. 1963. “Quantitative Aspects of Repetitive Firing of Mammalian Motoneurones, Caused by Injected Currents.” *The Journal of Physiology* 168(4):911–31. doi:10.1113/jphysiol.1963.sp007230.

Greene, Derek L., Seungwoo Kang, and Naoto Hoshi. 2017. “XE991 and Linopirdine Are State-Dependent Inhibitors for Kv7/KCNQ Channels That Favor Activated Single Subunits.” *The Journal of Pharmacology and Experimental Therapeutics* 362(1):177–85. doi:10.1124/jpet.117.241679.

Guertin, Pierre A., and Jorn Hounsgaard. 1998. “Chemical and Electrical Stimulation Induce Rhythmic Motor Activity in an in Vitro Preparation of the Spinal Cord from Adult Turtles.” *Neuroscience Letters* 245(1):5–8. doi:10.1016/S0304-3940(98)00164-5.

Hans, Stefan, Jan Kaslin, Dorian Freudenreich, and Michael Brand. 2009. “Temporally-Controlled Site-Specific Recombination in Zebrafish.” *PLoS ONE* 4(2):e4640. doi:10.1371/journal.pone.0004640.

Harding, Erika K., and Gerald W. Zamponi. 2022. “Central and Peripheral Contributions of T-Type Calcium Channels in Pain.” *Molecular Brain* 15(1):39. doi:10.1186/s13041-022-00923-w.

Harris-Warrick, Ronald M. 2010. “Chapter 14 - General Principles of Rhythmogenesis in Central Pattern Generator Networks.” Pp. 213–22 in *Progress in Brain Research*. Vol. 187, *Breathe, Walk and Chew: The Neural Challenge: Part I*, edited by J.-P. Gossard, R. Dubuc, and A. Kolta. Elsevier.

Harvey, P. J., X. Li, Y. Li, and D. J. Bennett. 2006. “5-HT2 Receptor Activation Facilitates a Persistent Sodium Current and Repetitive Firing in Spinal Motoneurons of Rats with and without Chronic Spinal Cord Injury.” *Journal of Neurophysiology* 96(3):1158–70. doi:10.1152/jn.01088.2005.

Henry, Clarissa A., Ian M. McNulty, Wendy A. Durst, Sarah E. Munchel, and Sharon L. Amacher. 2005. “Interactions between Muscle Fibers and Segment Boundaries in Zebrafish.” *Developmental Biology* 287(2):346–60. doi:10.1016/j.ydbio.2005.08.049.

Hille, Bertil. 2001. *Ion Channels of Excitable Membranes*. 3rd ed. Sinauer Associates, Inc.

Hollyday, Margaret, and Viktor Hamburger. 1977. “An Autoradiographic Study of the Formation of the Lateral Motor Column in the Chick Embryo.” *Brain Research* 132(2):197–208. doi:10.1016/0006-8993(77)90416-4.

Hounsgaard, J., and O. Kiehn. 1985. “Ca++ Dependent Bistability Induced by Serotonin in Spinal Motoneurons.” *Experimental Brain Research* 57(2). doi:10.1007/BF00236551.

Hounsgaard, J., and O. Kiehn. 1989. “Serotonin-Induced Bistability of Turtle Motoneurones Caused by a Nifedipine-Sensitive Calcium Plateau Potential.” *The Journal of Physiology* 414(1):265–82. doi:10.1113/jphysiol.1989.sp017687.

Howe, Kerstin, Matthew D. Clark, Carlos F. Torroja, James Torrance, Camille Berthelot, Matthieu Muffato, John E. Collins, Sean Humphray, Karen McLaren, Lucy Matthews, Stuart McLaren, Ian Sealy, Mario Caccamo, Carol Churcher, Carol Scott, Jeffrey C. Barrett, Romke Koch, Gerd-Jörg Rauch, Simon White, William Chow, Britt Kilian, Leonor T. Quintais, José A. Guerra-Assunção, Yi Zhou, Yong Gu, Jennifer Yen, Jan-Hinnerk Vogel, Tina Eyre, Seth Redmond, Ruby Banerjee, Jianxiang Chi, Beiyuan Fu, Elizabeth Langley, Sean F. Maguire, Gavin K. Laird, David Lloyd, Emma Kenyon, Sarah Donaldson, Harminder Sehra, Jeff Almeida-King, Jane Loveland, Stephen Trevanion, Matt Jones, Mike Quail, Dave Willey, Adrienne Hunt, John Burton, Sarah Sims, Kirsten McLay, Bob Plumb, Joy Davis, Chris Clee, Karen Oliver, Richard Clark, Clare Riddle, David Elliott, Glen Threadgold, Glenn Harden, Darren Ware, Sharmin Begum, Beverley Mortimore, Giselle Kerry, Paul Heath, Benjamin Phillimore, Alan Tracey, Nicole Corby, Matthew Dunn, Christopher Johnson, Jonathan Wood, Susan Clark, Sarah Pelan, Guy Griffiths, Michelle Smith, Rebecca Glithero, Philip Howden, Nicholas Barker, Christine Lloyd, Christopher Stevens, Joanna Harley, Karen Holt, Georgios Panagiotidis, Jamieson Lovell, Helen Beasley, Carl Henderson, Daria Gordon, Katherine Auger, Deborah Wright, Joanna Collins, Claire Raisen, Lauren Dyer, Kenric Leung, Lauren Robertson, Kirsty Ambridge, Daniel Leongamornlert, Sarah McGuire, Ruth Gilderthorp, Coline Griffiths, Deepa Manthravadi, Sarah Nichol, Gary Barker, Siobhan Whitehead, Michael Kay, Jacqueline Brown, Clare Murnane, Emma Gray, Matthew Humphries, Neil Sycamore,

Darren Barker, David Saunders, Justene Wallis, Anne Babbage, Sian Hammond, Maryam Mashreghi-Mohammadi, Lucy Barr, Sancha Martin, Paul Wray, Andrew Ellington, Nicholas Matthews, Matthew Ellwood, Rebecca Woodmansey, Graham Clark, James D. Cooper, Anthony Tromans, Darren Grafham, Carl Skuce, Richard Pandian, Robert Andrews, Elliot Harrison, Andrew Kimberley, Jane Garnett, Nigel Fosker, Rebekah Hall, Patrick Garner, Daniel Kelly, Christine Bird, Sophie Palmer, Ines Gehring, Andrea Berger, Christopher M. Dooley, Zübeyde Ersan-Ürün, Cigdem Eser, Horst Geiger, Maria Geisler, Lena Karotki, Anette Kirn, Judith Konantz, Martina Konantz, Martina Oberländer, Silke Rudolph-Geiger, Mathias Teucke, Christa Lanz, Günter Raddatz, Kazutoyo Osoegawa, Baoli Zhu, Amanda Rapp, Sara Widaa, Cordelia Langford, Fengtang Yang, Stephan C. Schuster, Nigel P. Carter, Jennifer Harrow, Zemin Ning, Javier Herrero, Steve M. J. Searle, Anton Enright, Robert Geisler, Ronald H. A. Plasterk, Charles Lee, Monte Westerfield, Pieter J. De Jong, Leonard I. Zon, John H. Postlethwait, Christiane Nüsslein-Volhard, Tim J. P. Hubbard, Hugues Roest Crollius, Jane Rogers, and Derek L. Stemple. 2013. “The Zebrafish Reference Genome Sequence and Its Relationship to the Human Genome.” *Nature* 496(7446):498–503. doi:10.1038/nature12111.

Huguenard, J. R. 1996. “Low-Threshold Calcium Currents in Central Nervous System Neurons.” *Annual Review of Physiology* 58(Volume 58, 1996):329–48. doi:10.1146/annurev.ph.58.030196.001553.

Hwang, Woong Y., Yanfang Fu, Deepak Reyon, Morgan L. Maeder, Shengdar Q. Tsai, Jeffry D. Sander, Randall T. Peterson, J. R. Joanna Yeh, and J. Keith Joung. 2013. “Efficient Genome Editing in Zebrafish Using a CRISPR-Cas System.” *Nature Biotechnology* 31(3):227–29. doi:10.1038/nbt.2501.

Jabre, J. F., and N. T. Spellman. 1996. “The Demonstration of the Size Principle in Humans Using Macro Electromyography and Precision Decomposition.” *Muscle & Nerve* 19(3):338–41. doi:10.1002/(SICI)1097-4598(199603)19:3<338::AID-MUS9>3.0.CO;2-E.

Jao, Li-En, Susan R. Wente, and Wenbiao Chen. 2013. “Efficient Multiplex Biallelic Zebrafish Genome Editing Using a CRISPR Nuclease System.” *Proceedings of the National Academy of Sciences* 110(34):13904–9. doi:10.1073/pnas.1308335110.

Jay, Michael, Francesca De Faveri, and Jonathan Robert McDearmid. 2015. “Firing Dynamics and Modulatory Actions of Supraspinal Dopaminergic Neurons during Zebrafish Locomotor Behavior.” *Current Biology* 25(4):435. doi:10.1016/j.cub.2014.12.033.

Jha, Urvashi, and Vatsala Thirumalai. 2020. “Neuromodulatory Selection of Motor Neuron Recruitment Patterns in a Visuomotor Behavior Increases Speed.” *Current Biology : CB* 30(5):788-801.e3. doi:10.1016/j.cub.2019.12.064.

Jia, Zhanfeng, Junjie Bei, Lise Rodat-Despoix, Boyi Liu, Qingzhong Jia, Patrick Delmas, and Hailin Zhang. 2008. “NGF Inhibits M/KCNQ Currents and Selectively Alters Neuronal Excitability in Subsets of Sympathetic Neurons Depending on Their M/KCNQ Current

Background." *Journal of General Physiology* 131(6):575–87. doi:10.1085/jgp.200709924.

Jiang, Ling, Anastasia Kosenko, Clinton Yu, Lan Huang, Xuejun Li, and Naoto Hoshi. 2015. "Activation of M1 Muscarinic Acetylcholine Receptor Induces Surface Transport of KCNQ Channels through a CRMP-2-Mediated Pathway." *Journal of Cell Science* 128(22):4235–45. doi:10.1242/jcs.175547.

Jiao, Yusheng, Brendan Colvert, Yi Man, Matthew J. McHenry, and Eva Kanso. 2023. "Evaluating Evasion Strategies in Zebrafish Larvae." *Proceedings of the National Academy of Sciences* 120(7):e2218909120. doi:10.1073/pnas.2218909120.

Kaeser, Pascal S., and Wade G. Regehr. 2014. "Molecular Mechanisms for Synchronous, Asynchronous, and Spontaneous Neurotransmitter Release." *Annual Review of Physiology* 76:333–63. doi:10.1146/annurev-physiol-021113-170338.

Kavalali, Ege T., Min Zhuo, Haruhiko Bito, and Richard W. Tsien. 1997. "Dendritic Ca2+ Channels Characterized by Recordings from Isolated Hippocampal Dendritic Segments." *Neuron* 18(4):651–63. doi:10.1016/S0896-6273(00)80305-0.

Keenan, Samuel R., and Peter D. Currie. 2019. "The Developmental Phases of Zebrafish Myogenesis." *Journal of Developmental Biology* 7(2):12. doi:10.3390/jdb7020012.

Kernell, D., and A. W. Monster. 1982. "Time Course and Properties of Late Adaptation in Spinal Motoneurones of the Cat." *Experimental Brain Research* 46(2):191–96. doi:10.1007/BF00237176.

Kiehn, Ole, and Torsten Eken. 1998. "Functional Role of Plateau Potentials in Vertebrate Motor Neurons." *Current Opinion in Neurobiology* 8(6):746–52. doi:10.1016/S0959-4388(98)80117-7.

Kimmel, Charles B., William W. Ballard, Seth R. Kimmel, Bonnie Ullmann, and Thomas F. Schilling. 1995. "Stages of Embryonic Development of the Zebrafish." *Developmental Dynamics* 203(3):253–310. doi:10.1002/aja.1002030302.

Kishore, Sandeep, Martha W. Bagnall, and David L. McLean. 2014. "Systematic Shifts in the Balance of Excitation and Inhibition Coordinate the Activity of Axial Motor Pools at Different Speeds of Locomotion." *Journal of Neuroscience* 34(42):14046–54. doi:10.1523/JNEUROSCI.0514-14.2014.

Kishore, Sandeep, and Joseph R. Fetcho. 2013. "Homeostatic Regulation of Dendritic Dynamics in a Motor Map in Vivo." *Nature Communications* 4(1):2086. doi:10.1038/ncomms3086.

Knogler, Laura D., Joel Ryan, Louis Saint-Amant, and Pierre Drapeau. 2014. "A Hybrid Electrical/Chemical Circuit in the Spinal Cord Generates a Transient Embryonic Motor Behavior." *Journal of Neuroscience* 34(29):9644–55. doi:10.1523/JNEUROSCI.1225-14.2014.

Kohashi, Tsunehiko and Oda, Yoichi. 2008. “Initiation of Mauthner- or Non-Mauthner-Mediated Fast Escape Evoked by Different Modes of Sensory Input.” 28(42):10641–53.

Kroll, François, Gareth T. Powell, Marcus Ghosh, Gaia Gestri, Paride Antinucci, Timothy J. Hearn, Hande Tunbak, Sumi Lim, Harvey W. Dennis, Joseph M. Fernandez, David Whitmore, Elena Dreosti, Stephen W. Wilson, Ellen J. Hoffman, and Jason Rihel. 2021. “A Simple and Effective F0 Knockout Method for Rapid Screening of Behaviour and Other Complex Phenotypes” edited by S. C. Ekker, D. Y. Stainier, and D. Balciunas. *eLife* 10:e59683. doi:10.7554/eLife.59683.

Kuo, J. J., R. H. Lee, L. Zhang, and C. J. Heckman. 2006. “Essential Role of the Persistent Sodium Current in Spike Initiation during Slowly Rising Inputs in Mouse Spinal Neurones.” *The Journal of Physiology* 574(Pt 3):819–34. doi:10.1113/jphysiol.2006.107094.

Kurennyi, D. E., H. Chen, and P. A. Smith. 1997. “Low Concentrations of Muscarine Potentiate M-Current in Bullfrog Sympathetic B-Neurones.” *Journal of the Autonomic Nervous System* 67(1–2):89–96. doi:10.1016/s0165-1838(97)00103-3.

Laliberte, Alex M., Carl Farah, Kyra R. Steiner, Omar Tariq, and Tuan V. Bui. 2022. “Changes in Sensorimotor Connectivity to dI3 Interneurons in Relation to the Postnatal Maturation of Grasping.” *Frontiers in Neural Circuits* 15:768235. doi:10.3389/fncir.2021.768235.

Lambert, Aaron M., Joshua L. Bonkowsky, and Mark A. Masino. 2012. “The Conserved Dopaminergic Diencephalospinal Tract Mediates Vertebrate Locomotor Development in Zebrafish Larvae.” *Journal of Neuroscience* 32(39):13488–500. doi:10.1523/JNEUROSCI.1638-12.2012.

Lauzadis, Justas, Huilin Liu, Yong Lu, Mario J. Rebecchi, Martin Kaczocha, and Michelino Puopolo. 2020. “Contribution of T-Type Calcium Channels to Spinal Cord Injury-Induced Hyperexcitability of Nociceptors.” *Journal of Neuroscience* 40(38):7229–40. doi:10.1523/JNEUROSCI.0517-20.2020.

Lee, Manon, David Beeson, and Jacqueline Palace. 2018. “Therapeutic Strategies for Congenital Myasthenic Syndromes.” *Annals of the New York Academy of Sciences* 1412(1):129–36. doi:10.1111/nyas.13538.

Lee, R. H., and C. J. Heckman. 1996. “Influence of Voltage-Sensitive Dendritic Conductances on Bistable Firing and Effective Synaptic Current in Cat Spinal Motoneurons in Vivo.” *Journal of Neurophysiology* 76(3):2107–10. doi:10.1152/jn.1996.76.3.2107.

Lee, R. H., and C. J. Heckman. 1999. “Paradoxical Effect of QX-314 on Persistent Inward Currents and Bistable Behavior in Spinal Motoneurons In Vivo.” *Journal of Neurophysiology* 82(5):2518–27. doi:10.1152/jn.1999.82.5.2518.

Lee, R. H., and C. J. Heckman. 2001. “Essential Role of a Fast Persistent Inward Current in Action Potential Initiation and Control of Rhythmic Firing.” *Journal of Neurophysiology* 85(1):472–75. doi:10.1152/jn.2001.85.1.472.

Lee, Robert H., and C. J. Heckman. 2000. “Adjustable Amplification of Synaptic Input in the Dendrites of Spinal Motoneurons In Vivo.” *Journal of Neuroscience* 20(17):6734–40. doi:10.1523/JNEUROSCI.20-17-06734.2000.

Lescouzères, Léa, Cédric Hassen-Khodja, Anaïs Baudot, Benoît Bordignon, and Pascale Bomont. 2023. “A Multilevel Screening Pipeline in Zebrafish Identifies Therapeutic Drugs for GAN.” *EMBO Molecular Medicine* 15(7):e16267. doi:10.15252/emmm.202216267.

Li, Shi-Bin, Valentina Martinez Damonte, Chong Chen, Gordon X. Wang, Justus M. Kebschull, Hiroshi Yamaguchi, Wen-Jie Bian, Carolin Purmann, Reenal Pattni, Alexander Eckehart Urban, Philippe Mourrain, Julie A. Kauer, Grégory Scherrer, and Luis de Lecea. 2022. “Hyperexcitable Arousal Circuits Drive Sleep Instability during Aging.” *Science* 375(6583):eabh3021. doi:10.1126/science.abh3021.

Li, X., K. Murray, P. J. Harvey, E. W. Ballou, and D. J. Bennett. 2007. “Serotonin Facilitates a Persistent Calcium Current in Motoneurons of Rats With and Without Chronic Spinal Cord Injury.” *Journal of Neurophysiology* 97(2):1236–46. doi:10.1152/jn.00995.2006.

Li, Yang, Nikita Gamper, Donald W. Hilgemann, and Mark S. Shapiro. 2005. “Regulation of Kv7 (KCNQ) K+ Channel Open Probability by Phosphatidylinositol 4,5-Bisphosphate.” *Journal of Neuroscience* 25(43):9825–35. doi:10.1523/JNEUROSCI.2597-05.2005.

Li, Yunru, and David J. Bennett. 2003. “Persistent Sodium and Calcium Currents Cause Plateau Potentials in Motoneurons of Chronic Spinal Rats.” *Journal of Neurophysiology* 90(2):857–69. doi:10.1152/jn.00236.2003.

Li, Yunru, Monica A. Gorassini, and David J. Bennett. 2004. “Role of Persistent Sodium and Calcium Currents in Motoneuron Firing and Spasticity in Chronic Spinal Rats.” *Journal of Neurophysiology* 91(2):767–83. doi:10.1152/jn.00788.2003.

Lin, John Y., Michael Z. Lin, Paul Steinbach, and Roger Y. Tsien. 2009. “Characterization of Engineered Channelrhodopsin Variants with Improved Properties and Kinetics.” *Biophysical Journal* 96(5):1803–14. doi:10.1016/j.bpj.2008.11.034.

Liu, D. W., and M. Westerfield. 1988. “Function of Identified Motoneurones and Co-ordination of Primary and Secondary Motor Systems during Zebra Fish Swimming.” *The Journal of Physiology* 403(1):73–89. doi:10.1113/jphysiol.1988.sp017239.

Liu, Katharine S., and Joseph R. Fetcho. 1999. “Laser Ablations Reveal Functional Relationships of Segmental Hindbrain Neurons in Zebrafish.” *Neuron* 23(2):325–35. doi:10.1016/S0896-6273(00)80783-7.

Liu, Yen-Chyi, and Melina E. Hale. 2017. “Local Spinal Cord Circuits and Bilateral Mauthner Cell Activity Function Together to Drive Alternative Startle Behaviors.” *Current Biology* 27(5):697–704. doi:10.1016/j.cub.2017.01.019.

Lombardo, Joseph and Harrington, Melissa A. 2016. “Nonreciprocal Mechanisms in Up- and Downregulation of Spinal Motoneuron Excitability by Modulators of KCNQ/Kv7 Channels.” 116(5):2114–24.

Lu, Daniel C., Tianyi Niu, and William A. Alaynick. 2015. “Molecular and Cellular Development of Spinal Cord Locomotor Circuitry.” *Frontiers in Molecular Neuroscience* 8(June):1–18. doi:10.3389/fnmol.2015.00025.

Luebke, J. I., K. Dunlap, and T. J. Turner. 1993. “Multiple Calcium Channel Types Control Glutamatergic Synaptic Transmission in the Hippocampus.” *Neuron* 11(5):895–902. doi:10.1016/0896-6273(93)90119-c.

Mackay-Lyons, Marilyn. 2002. *Number 1*. Vol. 82.

Madamba, S. G., P. Schweitzer, and G. R. Siggins. 1999a. “Dynorphin Selectively Augments the M-Current in Hippocampal CA1 Neurons by an Opiate Receptor Mechanism.” *Journal of Neurophysiology* 82(4):1768–75. doi:10.1152/jn.1999.82.4.1768.

Madamba, S. G., P. Schweitzer, and G. R. Siggins. 1999b. “Nociceptin Augments K(+) Currents in Hippocampal CA1 Neurons by Both ORL-1 and Opiate Receptor Mechanisms.” *Journal of Neurophysiology* 82(4):1776–85. doi:10.1152/jn.1999.82.4.1776.

Madison, D. V., and R. A. Nicoll. 1984. “Control of the Repetitive Discharge of Rat CA 1 Pyramidal Neurones in Vitro.” *The Journal of Physiology* 354(1):319–31. doi:10.1113/jphysiol.1984.sp015378.

el Manira, A., J. Tegnér, and S. Grillner. 1994. “Calcium-Dependent Potassium Channels Play a Critical Role for Burst Termination in the Locomotor Network in Lamprey.” *Journal of Neurophysiology* 72(4):1852–61. doi:10.1152/jn.1994.72.4.1852.

Marrion, Neil V. 1997. “CONTROL OF M-CURRENT.” *Annual Review of Physiology* 59(Volume 59, 1997):483–504. doi:10.1146/annurev.physiol.59.1.483.

McDearmid, Jonathan R., and Pierre Drapeau. 2006. “Rhythmic Motor Activity Evoked by NMDA in the Spinal Zebrafish Larva.” *Journal of Neurophysiology* 95(1):401–17. doi:10.1152/jn.00844.2005.

McEwen, Melanie L., Carol Van Hartesveldt, and Donald J. Stehouwer. 1997. “L-DOPA and Quipazine Elicit Air-Stepping in Neonatal Rats with Spinal Cord Transections.” *Behavioral Neuroscience* 111(4):825–33. doi:10.1037/0735-7044.111.4.825.

McKiernan, Erin C. 2013. “Effects of Manipulating Slowpoke Calcium-Dependent Potassium Channel Expression on Rhythmic Locomotor Activity in Drosophila Larvae.” *PeerJ* 1:e57. doi:10.7717/peerj.57.

McLean, David L., Jingyi Fan, Shin-ichi Higashijima, Melina E. Hale, and Joseph R. Fetcho. 2007. “A Topographic Map of Recruitment in Spinal Cord.” *Nature* 446(7131):71–75. doi:10.1038/nature05588.

McLean, David L., and Joseph R. Fetcho. 2009. “Spinal Interneurons Differentiate Sequentially from Those Driving the Fastest Swimming Movements in Larval Zebrafish to Those Driving the Slowest Ones.” *Journal of Neuroscience* 29(43):13566–77. doi:10.1523/JNEUROSCI.3277-09.2009.

McMacken, Grace, Angela Abicht, Teresinha Evangelista, Sally Spendiff, and Hanns Lochmüller. 2017. “The Increasing Genetic and Phenotypical Diversity of Congenital Myasthenic Syndromes.” *Neuropediatrics* 48(4):294–308. doi:10.1055/s-0037-1602832.

van Meer, Noraly M. M. E., Johan L. van Leeuwen, Henk Schipper, and Martin J. Lankheet. 2024. “Axial Muscle-Fibre Orientations in Larval Zebrafish.” *Journal of Anatomy* n/a(n/a). doi:10.1111/joa.14161.

Menelaou, Evdokia, and David L. McLean. 2012. “A Gradient in Endogenous Rhythmicity and Oscillatory Drive Matches Recruitment Order in an Axial Motor Pool.” *Journal of Neuroscience* 32(32):10925–39. doi:10.1523/JNEUROSCI.1809-12.2012.

Miles, G. B., Y. Dai, and R. M. Brownstone. 2005. “Mechanisms Underlying the Early Phase of Spike Frequency Adaptation in Mouse Spinal Motoneurones.” *The Journal of Physiology* 566(Pt 2):519. doi:10.1113/jphysiol.2005.086033.

Montgomery, Jacob E., Sarah Wahlstrom-Helgren, Timothy D. Wiggin, Brittany M. Corwin, Christina Lillesaar, and Mark A. Masino. 2018. “Intraspinal Serotonergic Signaling Suppresses Locomotor Activity in Larval Zebrafish.” *Developmental Neurobiology* 78(8):807–27. doi:10.1002/dneu.22606.

Moore, S. D., S. G. Madamba, P. Schweitzer, and G. R. Siggins. 1994. “Voltage-Dependent Effects of Opioid Peptides on Hippocampal CA3 Pyramidal Neurons in Vitro.” *The Journal of Neuroscience: The Official Journal of the Society for Neuroscience* 14(2):809–20. doi:10.1523/JNEUROSCI.14-02-00809.1994.

Moore, Scott D., Samuel G. Madamba, Marian Joëls, and George R. Siggins. 1988. “Somatostatin Augments the M-Current in Hippocampal Neurons.” *Science* 239(4837):278–80. doi:10.1126/science.2892268.

Moreno, Rosa L., and Angeles B. Ribera. 2009. “Zebrafish Motor Neuron Subtypes Differ Electrically Prior to Axonal Outgrowth.” *Journal of Neurophysiology* 102(4):2477. doi:10.1152/jn.00446.2009.

Müller, Peter, Andreas Draguhn, and Alexei V. Egorov. 2024. “Persistent Sodium Currents in Neurons: Potential Mechanisms and Pharmacological Blockers.” *Pflugers Archiv* 476(10):1445–73. doi:10.1007/s00424-024-02980-7.

Myers, Paul Z. 1985. “Spinal Motoneurons of the Larval Zebrafish.” *Journal of Comparative Neurology* 236(4):555–61. doi:10.1002/cne.902360411.

Myers, Paul Z., Judith S. Eisen, and Monte Westerfield. 1986. *Development and Axonal Outgrowth of Identified Motoneurons in the Zebrafish*. Vol. 6.

Myers, Pz, Js Eisen, and M. Westerfield. 1986. “Development and Axonal Outgrowth of Identified Motoneurons in the Zebrafish.” *The Journal of Neuroscience* 6(8):2278–89. doi:10.1523/JNEUROSCI.06-08-02278.1986.

Nair, Arjun, Christy Nguyen, and Matthew J. McHenry. 2017. “A Faster Escape Does Not Enhance Survival in Zebrafish Larvae.” *Proceedings of the Royal Society B: Biological Sciences* 284(1852):20170359. doi:10.1098/rspb.2017.0359.

Nakayama, Hisako, and Yoichi Oda. 2004. “Common Sensory Inputs and Differential Excitability of Segmentally Homologous Reticulospinal Neurons in the Hindbrain.” *The Journal of Neuroscience* 24(13):3199–3209. doi:10.1523/JNEUROSCI.4419-03.2004.

Nasevicius, Aidas, and Stephen C. Ekker. 2000. “Effective Targeted Gene ‘Knockdown’ in Zebrafish.” *Nature Genetics* 26(2):216–20. doi:10.1038/79951.

Del Negro, Christopher A., Naohiro Koshiya, Robert J. Butera, and Jeffrey C. Smith. 2002. “Persistent Sodium Current, Membrane Properties and Bursting Behavior of Pre-Bötzinger Complex Inspiratory Neurons in Vitro.” *Journal of Neurophysiology* 88(5):2242–50. doi:10.1152/jn.00081.2002.

O’Connor, Emily, Vietxuan Phan, Isabell Cordts, George Cairns, Stefan Hettwer, Daniel Cox, Hanns Lochmüller, and Andreas Roos. 2018. “MYO9A Deficiency in Motor Neurons Is Associated with Reduced Neuromuscular Agrin Secretion.” *Human Molecular Genetics* 27(8):1434–46. doi:10.1093/hmg/ddy054.

Ohno, Kinji, Bisei Ohkawara, Xin-Ming Shen, Duygu Selcen, and Andrew G. Engel. 2023. “Clinical and Pathologic Features of Congenital Myasthenic Syndromes Caused by 35 Genes—A Comprehensive Review.” *International Journal of Molecular Sciences* 24(4):3730. doi:10.3390/ijms24043730.

O’Malley, Donald M., Yen-Hong Kao, and Joseph R. Fetcho. 1996. “Imaging the Functional Organization of Zebrafish Hindbrain Segments during Escape Behaviors.” *Neuron* 17(6):1145–55. doi:10.1016/S0896-6273(00)80246-9.

Orlovsky, Grigori, Deliagina, T. G., and Grillner, Sten. 2012. *Neuronal Control of Locomotion: From Mollusc to Man*. Oxford Academic.

Pace, Ryland W., Devin D. Mackay, Jack L. Feldman, and Christopher A. Del Negro. 2007. “Role of Persistent Sodium Current in Mouse preBötzinger Complex Neurons and Respiratory Rhythm Generation.” *Journal of Physiology* 580(2):485–96. doi:10.1113/jphysiol.2006.124602.

Pallucchi, Irene, Maria Bertuzzi, David Madrid, Pierre Fontanel, Shin-Ichi Higashijima, and Abdeljabbar El Manira. 2024. “Molecular Blueprints for Spinal Circuit Modules Controlling Locomotor Speed in Zebrafish.” *Nature Neuroscience* 27(1):78–89. doi:10.1038/s41593-023-01479-1.

Pang, Zhiping P., Ernestina Melicoff, Daniel Padgett, Yun Liu, Andrew F. Teich, Burton F. Dickey, Weichun Lin, Roberto Adachi, and Thomas C. Südhof. 2006. “Synaptotagmin-2 Is Essential for Survival and Contributes to Ca2+ Triggering of Neurotransmitter Release in Central and Neuromuscular Synapses.” *The Journal of Neuroscience* 26(52):13493–504. doi:10.1523/JNEUROSCI.3519-06.2006.

Parichy, David M., Michael R. Elizondo, Margaret G. Mills, Tiffany N. Gordon, and Raymond E. Engeszer. 2009. “Normal Table of Post-Embryonic Zebrafish Development: Staging by Externally Visible Anatomy of the Living Fish.” *Developmental Dynamics : An Official Publication of the American Association of Anatomists* 238(12):2975–3015. doi:10.1002/dvdy.22113.

Park, Choongseok, Katie N. Clements, Fadi A. Issa, and Sungwoo Ahn. 2018. “Effects of Social Experience on the Habituation Rate of Zebrafish Startle Escape Response: Empirical and Computational Analyses.” *Frontiers in Neural Circuits* 12. doi:10.3389/fncir.2018.00007.

Park, Jee-Young, Meghan Mott, Tory Williams, Hiromi Ikeda, Hua Wen, Michael Linhoff, and Fumihito Ono. 2014. “A Single Mutation in the Acetylcholine Receptor δ-Subunit Causes Distinct Effects in Two Types of Neuromuscular Synapses.” *The Journal of Neuroscience* 34(31):10211–18. doi:10.1523/JNEUROSCI.0426-14.2014.

Perrier, Jean-François, Aidas Alaburda, and Jørn Hounsgaard. 2003. “5-HT1A Receptors Increase Excitability of Spinal Motoneurons by Inhibiting a TASK-1-like K+ Current in the Adult Turtle.” *The Journal of Physiology* 548(Pt 2):485. doi:10.1113/jphysiol.2002.037952.

Perrier, Jean-François, and Rodolfo Delgado-Lezama. 2005. “Synaptic Release of Serotonin Induced by Stimulation of the Raphe Nucleus Promotes Plateau Potentials in Spinal Motoneurons of the Adult Turtle.” *Journal of Neuroscience* 25(35):7993–99. doi:10.1523/JNEUROSCI.1957-05.2005.

Perrier, Jean-François, and Jørn Hounsgaard. 2003. “5-HT2 Receptors Promote Plateau Potentials in Turtle Spinal Motoneurons by Facilitating an L-Type Calcium Current.” *Journal of Neurophysiology* 89(2):954–59. doi:10.1152/jn.00753.2002.

Picton, Laurence D., and Keith T. Sillar. 2016. “Mechanisms Underlying the Endogenous Dopaminergic Inhibition of Spinal Locomotor Circuit Function in Xenopus Tadpoles.” *Scientific Reports* 6:35749. doi:10.1038/srep35749.

Pringos, Emilie, Michel Vignes, Jean Martinez, and Valerie Rolland. 2011. “Peptide Neurotoxins That Affect Voltage-Gated Calcium Channels: A Close-Up on ω-Agatoxins.” *Toxins* 3(1):17–42. doi:10.3390/toxins3010017.

Pujala, Avinash, and Minoru Koyama. 2019. “Chronology-Based Architecture of Descending Circuits That Underlie the Development of Locomotor Repertoire after Birth” edited by V. Thirumalai, R. L. Calabrese, and C. Wyart. *eLife* 8:e42135. doi:10.7554/eLife.42135.

Rall, Wilfrid. 1957. “Membrane Time Constant of Motoneurons.” *Science* 126(3271):454–454.

Rall, Wilfrid. 1960. “Membrane Potential Transients and Membrane Time Constant of Motoneurons.” *Experimental Neurology* 2(5):503–32. doi:10.1016/0014-4886(60)90029-7.

Ramdas, Sithara, David Beeson, and Yin Yao Dong. 2024. “Congenital Myasthenic Syndromes: Increasingly Complex.” *Current Opinion in Neurology* 37(5):493. doi:10.1097/WCO.0000000000001300.

Ramirez, Jan-Marino, Henner Koch, Alfredo J. Garcia, Atsushi Doi, and Sebastien Zanella. 2011. “The Role of Spiking and Bursting Pacemakers in the Neuronal Control of Breathing.” *Journal of Biological Physics* 37(3):241–61. doi:10.1007/s10867-011-9214-z.

Revill, Ann L., Alexis Katzell, Christopher A. Del Negro, William K. Milsom, and Gregory D. Funk. 2021. “KCNQ Current Contributes to Inspiratory Burst Termination in the Pre-Bötzinger Complex of Neonatal Rats in Vitro.” *Frontiers in Physiology* 12(April). doi:10.3389/fphys.2021.626470.

Roberts, Adam C., Kaycey C. Pearce, Ronny C. Choe, Joseph B. Alzagatiti, Anthony K. Yeung, Brent R. Bill, and David L. Glanzman. 2016. “Long-Term Habituation of the C-Start Escape Response in Zebrafish Larvae.” *Neurobiology of Learning and Memory* 134(Pt B):360–68. doi:10.1016/j.nlm.2016.08.014.

Roca-Lapirot, Olivier, Houda Radwani, Franck Aby, Frédéric Nagy, Marc Landry, and Pascal Fossat. 2018. “Calcium Signalling through L-type Calcium Channels: Role in Pathophysiology of Spinal Nociceptive Transmission.” *British Journal of Pharmacology* 175(12):2362–74. doi:10.1111/bph.13747.

Roepke, T. A., A. W. Smith, O. K. Rønnekleiv, and M. J. Kelly. 2012. “Serotonin 5-HT2C Receptor-Mediated Inhibition of the M-Current in Hypothalamic POMC Neurons.” *American Journal of Physiology. Endocrinology and Metabolism* 302(11):E1399-1406. doi:10.1152/ajpendo.00565.2011.

Roussel, Yann, Stephanie F. Gaudreau, Emily R. Kacer, Mohini Sengupta, and Tuan V. Bui. 2021. “Modeling Spinal Locomotor Circuits for Movements in Developing Zebrafish” edited by V. Thirumalai, R. L. Calabrese, and R. Narayanan. *eLife* 10:e67453. doi:10.7554/eLife.67453.

Roussel, Yann, Melissa Paradis, Stephanie F. Gaudreau, Ben W. Lindsey, and Tuan V. Bui. 2020. “Spatiotemporal Transition in the Role of Synaptic Inhibition to the Tail Beat Rhythm of Developing Larval Zebrafish.” *Eneuro* 7(1):ENEURO.0508-18.2020. doi:10.1523/ENEURO.0508-18.2020.

Rudolf, Rüdiger, Muzamil Majid Khan, and Veit Witzemann. 2019. “Motor Endplate—Anatomical, Functional, and Molecular Concepts in the Historical Perspective.” *Cells* 8(5):387. doi:10.3390/cells8050387.

Sabatini, Bernardo L., and Karel Svoboda. 2000. “Analysis of Calcium Channels in Single Spines Using Optical Fluctuation Analysis.” *Nature* 408(6812):589–93. doi:10.1038/35046076.

Saint-Amant, L, and P. Drapeau. 2000. “Motoneuron Activity Patterns Related to the Earliest Behavior of the Zebrafish Embryo.” *The Journal of Neuroscience : The Official Journal of the Society for Neuroscience* 20(11):3964–72. doi:10.1523/JNEUROSCI.20-11-03964.2000.

Saint-Amant, Louis. 2010. “Chapter 4 - Development of Motor Rhythms in Zebrafish Embryos.” Pp. 47–61 in *Progress in Brain Research*. Vol. 187, *Breathe, Walk and Chew: The Neural Challenge: Part I*, edited by J.-P. Gossard, R. Dubuc, and A. Kolta. Elsevier.

Saint-Amant, Louis, and Pierre Drapeau. 1998. “Time Course of the Development of Motor Behaviors in the Zebrafish Embryo.” *Journal of Neurobiology* 37(4):622–32. doi:10.1002/(SICI)1097-4695(199812)37:4<622::AID-NEU10>3.0.CO;2-S.

Saint-Amant, Louis, and Pierre Drapeau. 2000. “Motoneuron Activity Patterns Related to the Earliest Behavior of the Zebrafish Embryo.” *Journal of Neuroscience* 20(11):3964–72. doi:10.1523/JNEUROSCI.20-11-03964.2000.

Saint-Amant, Louis, and Pierre Drapeau. 2001. “Synchronization of an Embryonic Network of Identified Spinal Interneurons Solely by Electrical Coupling.” *Neuron* 31(6):1035–46. doi:10.1016/S0896-6273(01)00416-0.

Santini, Edwin, and James T. Porter. 2010. “M-Type Potassium Channels Modulate the Intrinsic Excitability of Infralimbic Neurons and Regulate Fear Expression and Extinction.” *The Journal of Neuroscience* 30(37):12379–86. doi:10.1523/JNEUROSCI.1295-10.2010.

Satou, Chie, Yukiko Kimura, and Shin-ichi Higashijima. 2012. “Generation of Multiple Classes of V0 Neurons in Zebrafish Spinal Cord: Progenitor Heterogeneity and Temporal Control of Neuronal Diversity.” *Journal of Neuroscience* 32(5):1771–83. doi:10.1523/JNEUROSCI.5500-11.2012.

Sawczuk, A., R. K. Powers, and M. D. Binder. 1995. “Spike Frequency Adaptation Studied in Hypoglossal Motoneurons of the Rat.” *Journal of Neurophysiology* 73(5):1799–1810. doi:10.1152/jn.1995.73.5.1799.

Scheer, Nico, and José A. Campos-Ortega. 1999. “Use of the Gal4-UAS Technique for Targeted Gene Expression in the Zebrafish.” *Mechanisms of Development* 80(2):153–58. doi:10.1016/S0925-4773(98)00209-3.

Schweitzer, Paul, Samuel Madamba, and George Robert Siggins. 1990. “Arachidonic Acid Metabolites as Mediators of Somatostatin-Induced Increase of Neuronal M-Current.” *Nature* 346(6283):464–67. doi:10.1038/346464a0.

Schwindt, P. C., and W. E. Crill. 1980. “Properties of a Persistent Inward Current in Normal and TEA-Injected Motoneurons.” *Journal of Neurophysiology* 43(6):1700–1724. doi:10.1152/jn.1980.43.6.1700.

Sharples, Simon A., Matthew J. Broadhead, James A. Gray, and Gareth B. Miles. 2023. “M-Type Potassium Currents Differentially Affect Activation of Motoneuron Subtypes and Tune Recruitment Gain.” *The Journal of Physiology* 601(24):5751–75. doi:10.1113/JP285348.

Sharples, Simon A., and Gareth B. Miles. 2021. “Maturation of Persistent and Hyperpolarization-Activated Inward Currents Shapes the Differential Activation of Motoneuron Subtypes during Postnatal Development.” *eLife* 10:e71385. doi:10.7554/eLife.71385.

Sherrington, C. S. 1904. “Correlation of Reflexes and the Principle of the Common Path.” (70):460–66.

Shimojo, Masafumi, Joseph Madara, Sandra Pankow, Xinran Liu, John Yates, Thomas C. Südhof, and Anton Maximov. 2019. “Synaptotagmin-11 Mediates a Vesicle Trafficking Pathway That Is Essential for Development and Synaptic Plasticity.” *Genes & Development* 33(5–6):365–76. doi:10.1101/gad.320077.118.

Sims, S. M., L. H. Clapp, J. V. Walsh, and J. J. Singer. 1990. “Dual Regulation of M Current in Gastric Smooth Muscle Cells: Beta-Adrenergic-Muscarinic Antagonism.” *Pflugers Archiv: European Journal of Physiology* 417(3):291–302. doi:10.1007/BF00370995.

Sims, Stephen M., Joshua J. Singer, and John V. Walsh. 1988. “Antagonistic Adrenergic-Muscarinic Regulation of M Current in Smooth Muscle Cells.” *Science* 239(4836):190–93. doi:10.1126/science.2827305.

Singh, Jaskaran, and Shunmoogum A. Patten. 2022. “Modeling Neuromuscular Diseases in Zebrafish.” *Frontiers in Molecular Neuroscience* 15:1054573. doi:10.3389/fnmol.2022.1054573.

Smith, Calvin C., and Robert M. Brownstone. 2020. “Spinal Motoneuron Firing Properties Mature from Rostral to Caudal during Postnatal Development of the Mouse.” *The Journal of Physiology* 598(23):5467–85. doi:10.1113/JP280274.

Song, Jianren, Irene Pallucchi, Jessica Ausborn, Konstantinos Ampatzis, Maria Bertuzzi, Pierre Fontanel, Laurence D. Picton, and Abdeljabbar El Manira. 2020a. “Multiple Rhythm-Generating Circuits Act in Tandem with Pacemaker Properties to Control the Start and Speed of Locomotion.” *Neuron* 105(6):1048-1061.e4. doi:10.1016/j.neuron.2019.12.030.

Song, Jianren, Irene Pallucchi, Jessica Ausborn, Konstantinos Ampatzis, Maria Bertuzzi, Pierre Fontanel, Laurence D. Picton, and Abdeljabbar El Manira. 2020b. “Multiple Rhythm-

Generating Circuits Act in Tandem with Pacemaker Properties to Control the Start and Speed of Locomotion." *Neuron* 105(6):1048-1061.e4. doi:10.1016/j.neuron.2019.12.030.

Srinivasan, Shriya S., Benjamin E. Maimon, Maurizio Diaz, Hyungeun Song, and Hugh M. Herr. 2018. "Closed-Loop Functional Optogenetic Stimulation." *Nature Communications* 9(1):5303. doi:10.1038/s41467-018-07721-w.

Suh, Byung-Chang, and Bertil Hille. 2007. "Regulation of KCNQ Channels by Manipulation of Phosphoinositides." *The Journal of Physiology* 582(Pt 3):911–16. doi:10.1113/jphysiol.2007.132647.

Sur Abhinav, Yiqun Wang, Paulina Capar, Gennady Margolin, Morgan Kathleen Prochaska, and Jeffrey A Farrell. 2023. "Single-Cell Analysis of Shared Signatures and Transcriptional Diversity during Zebrafish Development." 58(24):3028–47.

Suster, Maximiliano L., Hiroshi Kikuta, Akihiro Urasaki, Kazuhide Asakawa, and Koichi Kawakami. 2009. "Transgenesis in Zebrafish with the Tol2 Transposon System." *Methods in Molecular Biology (Clifton, N.J.)* 561:41–63. doi:10.1007/978-1-60327-019-9_3.

Takahashi, T., and A. J. Berger. 1990. "Direct Excitation of Rat Spinal Motoneurones by Serotonin." *The Journal of Physiology* 423(1):63–76. doi:10.1113/jphysiol.1990.sp018011.

Takahashi, Tomoyuki, and Akiko Momiyama. 1993. "Different Types of Calcium Channels Mediate Central Synaptic Transmission." *Nature* 366(6451):156–58. doi:10.1038/366156a0.

Tazerart, Sabrina, Laurent Vinay, and Frédéric Brocard. 2008a. "The Persistent Sodium Current Generates Pacemaker Activities in the Central Pattern Generator for Locomotion and Regulates the Locomotor Rhythm." *Journal of Neuroscience* 28(34):8577–89. doi:10.1523/JNEUROSCI.1437-08.2008.

Tazerart, Sabrina, Laurent Vinay, and Frédéric Brocard. 2008b. "The Persistent Sodium Current Generates Pacemaker Activities in the Central Pattern Generator for Locomotion and Regulates the Locomotor Rhythm." *Journal of Neuroscience* 28(34):8577–89. doi:10.1523/JNEUROSCI.1437-08.2008.

Temizer, Incinur, Joseph C. Donovan, Herwig Baier, and Julia L. Semmelhack. 2015. "A Visual Pathway for Looming-Evoked Escape in Larval Zebrafish." *Current Biology* 25(14):1823–34. doi:10.1016/j.cub.2015.06.002.

Thiele, Tod R., Joseph C. Donovan, and Herwig Baier. 2014. "Descending Control of Swim Posture by a Midbrain Nucleus in Zebrafish." *Neuron* 83(3):679–91. doi:10.1016/j.neuron.2014.04.018.

Thirumalai, Vatsala, and Hollis T. Cline. 2008. “Endogenous Dopamine Suppresses Initiation of Swimming in Prefeeding Zebrafish Larvae.” *Journal of Neurophysiology* 100(3):1635. doi:10.1152/jn.90568.2008.

Tong, Huaxia, and Jonathan Robert McDearmid. 2012. “Pacemaker and Plateau Potentials Shape Output of a Developing Locomotor Network.” *Current Biology* 22(24):2285–93. doi:10.1016/j.cub.2012.10.025.

Tong, Huaxia, and Jonathan Robert McDearmid. 2012. “Pacemaker and Plateau Potentials Shape Output of a Developing Locomotor Network.” *Current Biology* 22(24):2285–93. doi:10.1016/j.cub.2012.10.025.

Trimmer, B. A. 1994. “Characterization of a Muscarinic Current That Regulates Excitability of an Identified Insect Motoneuron.” *Journal of Neurophysiology* 72(4):1862–73. doi:10.1152/jn.1994.72.4.1862.

Trovò, Luca, Stylianos Kouvaros, Jochen Schwenk, Diego Fernandez-Fernandez, Thorsten Fritzius, Pascal Dominic Rem, Simon Früh, Martin Gassmann, Bernd Fakler, Josef Bischofberger, and Bernhard Bettler. 2024. “Synaptotagmin-11 Facilitates Assembly of a Presynaptic Signaling Complex in Post-Golgi Cargo Vesicles.” *EMBO Reports* 25(6):2610–34. doi:10.1038/s44319-024-00147-0.

Verneuil, Jérémy, Cécile Brocard, Virginie Trouplin, Laurent Villard, Julie Peyronnet-Roux, and Frédéric Brocard. 2020a. *The M-Current Works in Tandem with the Persistent Sodium Current to Set the Speed of Locomotion.* Vol. 18.

Verneuil, Jérémy, Cécile Brocard, Virginie Trouplin, Laurent Villard, Julie Peyronnet-Roux, and Frédéric Brocard. 2020b. “The M-Current Works in Tandem with the Persistent Sodium Current to Set the Speed of Locomotion.” *PLOS Biology* 18(11):e3000738. doi:10.1371/journal.pbio.3000738.

Vickstrom, Casey R., Xiaojie Liu, Yuqi Zhang, Lianwei Mu, Thomas J. Kelly, Xudong Yan, Meng-ming Hu, Shana T. Snarrenberg, and Qing-song Liu. 2020. “T-Type Calcium Channels Contribute to Burst Firing in a Subpopulation of Medial Habenula Neurons.” *eNeuro* 7(4):ENEURO.0201-20.2020. doi:10.1523/ENEURO.0201-20.2020.

W van Raamsdonk, L van’t Veer, K Veeken, C Heyting, and C W Pool. 1982. “Differentiation of Muscle Fiber Types in the Teleost Brachydanio Rerio, the Zebrafish. Posthatching Development - PubMed.” 164(1):51–62.

Walogorsky, Michael, Rebecca Mongeon, Hua Wen, Nathan R. Nelson, Jason M. Urban, Fumihito Ono, Gail Mandel, and Paul Brehm. 2012. “Zebrafish Model for Congenital Myasthenic Syndrome Reveals Mechanisms Causal to Developmental Recovery.” *Proceedings of the National Academy of Sciences* 109(43):17711–16. doi:10.1073/pnas.1215858109.

Wang, Hong-Sheng, Zongming Pan, Wenmei Shi, Barry S. Brown, Randy S. Wymore, Ira S. Cohen, Jane E. Dixon, and David McKinnon. 1998. “KCNQ2 and KCNQ3 Potassium Channel Subunits: Molecular Correlates of the M-Channel.” *Science* 282(5395):1890–93. doi:10.1126/science.282.5395.1890.

Wang, Meng, Hua Wen, and Paul Brehm. 2008. “Function of Neuromuscular Synapses in the Zebrafish Choline-Acetyltransferase Mutant Bajan.” *Journal of Neurophysiology* 100(4):1995–2004. doi:10.1152/jn.90517.2008.

Wen, Hua, and Paul Brehm. 2010a. “Paired Patch Clamp Recordings from Motor-Neuron and Target Skeletal Muscle in Zebrafish.” *Journal of Visualized Experiments* (45):8–10. doi:10.3791/2351.

Wen, Hua, and Paul Brehm. 2010b. “Paired Patch Clamp Recordings from Motor-Neuron and Target Skeletal Muscle in Zebrafish.” *Journal of Visualized Experiments : JoVE* (45):2351. doi:10.3791/2351.

Wen, Hua, Kazumi Eckenstein, Vivien Weihrauch, Christian Stigloher, and Paul Brehm. 2020. “Primary and Secondary Motoneurons Use Different Calcium Channel Types to Control Escape and Swimming Behaviors in Zebrafish.” *Proceedings of the National Academy of Sciences of the United States of America* 117(42):26429–37. doi:10.1073/pnas.2015866117.

Wen, Hua, Jeffrey M. Hubbard, Benjamin Rakela, Michael W. Linhoff, Gail Mandel, and Paul Brehm. 2013. “Synchronous and Asynchronous Modes of Synaptic Transmission Utilize Different Calcium Sources.” *eLife* 2:e01206. doi:10.7554/eLife.01206.

Wen, Hua, Jeffrey Michael Hubbard, Wei-Chun Wang, and Paul Brehm. 2016. “Fatigue in Rapsyn-Deficient Zebrafish Reflects Defective Transmitter Release.” *Journal of Neuroscience* 36(42):10870–82. doi:10.1523/JNEUROSCI.0505-16.2016.

Wen, Hua, Michael W. Linhoff, Jeffrey M. Hubbard, Nathan R. Nelson, Donald Stensland, Julia Dallman, Gail Mandel, and Paul Brehm. 2013. “Zebrafish Calls for Reinterpretation for the Roles of P/Q Calcium Channels in Neuromuscular Transmission.” *Journal of Neuroscience* 33(17):7384–92. doi:10.1523/JNEUROSCI.5839-12.2013.

Wen, Hua, Michael W. Linhoff, Matthew J. McGinley, Geng-Lin Li, Glen M. Corson, Gail Mandel, and Paul Brehm. 2010. “Distinct Roles for Two Synaptotagmin Isoforms in Synchronous and Asynchronous Transmitter Release at Zebrafish Neuromuscular Junction.” *Proceedings of the National Academy of Sciences* 107(31):13906–11. doi:10.1073/pnas.1008598107.

Wen, Hua, Matthew J. McGinley, Gail Mandel, and Paul Brehm. 2016. “Nonequivalent Release Sites Govern Synaptic Depression.” *Proceedings of the National Academy of Sciences of the United States of America* 113(3):E378–86. doi:10.1073/pnas.1523671113.

Westerfield, M., Jv McMurray, and Js Eisen. 1986. “Identified Motoneurons and Their Innervation of Axial Muscles in the Zebrafish.” *The Journal of Neuroscience* 6(8):2267–77. doi:10.1523/JNEUROSCI.06-08-02267.1986.

Wheeler, David B., Andrew Randall, and Richard W. Tsien. 1994. “Roles of N-Type and Q-Type Ca2+ Channels in Supporting Hippocampal Synaptic Transmission.” *Science* 264(5155):107–12.

Whittaker, Roger G., David N. Herrmann, Boglarka Bansagi, Bashar Awwad Shiekh Hasan, Robert Muni Lofra, Eric L. Logigian, Janet E. Sowden, Jorge L. Almodovar, J. Troy Littleton, Stephan Zuchner, Rita Horvath, and Hanns Lochmüller. 2015. “Electrophysiologic Features of SYT2 Mutations Causing a Treatable Neuromuscular Syndrome.” *Neurology* 85(22):1964–71. doi:10.1212/WNL.0000000000002185.

Wiggin, Timothy D, Tatiana M. Anderson, John Eian, Jack H. Peck, and Mark A. Masino. 2012. “Episodic Swimming in the Larval Zebrafish Is Generated by a Spatially Distributed Spinal Network with Modular Functional Organization.” *Journal of Neurophysiology* 108(3):925–34. doi:10.1152/jn.00233.2012.

Wiggin, Timothy D., Tatiana M. Anderson, John Eian, Jack H. Peck, and Mark A. Masino. 2012. “Episodic Swimming in the Larval Zebrafish Is Generated by a Spatially Distributed Spinal Network with Modular Functional Organization.” *Journal of Neurophysiology* 108(3):925–34. doi:10.1152/jn.00233.2012.

Wiggin, Timothy D., Jack H. Peck, and Mark A. Masino. 2014. “Coordination of Fictive Motor Activity in the Larval Zebrafish Is Generated by Non-Segmental Mechanisms” edited by F. Del Bene. *PLoS ONE* 9(10):e109117. doi:10.1371/journal.pone.0109117.

Wilson, Jennifer M., Jeremy Rempel, and Robert M. Brownstone. 2004. “Postnatal Development of Cholinergic Synapses on Mouse Spinal Motoneurons.” *Journal of Comparative Neurology* 474(1):13–23. doi:10.1002/cne.20089.

Wladyka, Cynthia L., and Diana L. Kunze. 2006. “KCNQ/M-Currents Contribute to the Resting Membrane Potential in Rat Visceral Sensory Neurons.” *The Journal of Physiology* 575(Pt 1):175. doi:10.1113/jphysiol.2006.113308.

Womack, Mary D., Carolyn Chevez, and Kamran Khodakhah. 2004. “Calcium-Activated Potassium Channels Are Selectively Coupled to P/Q-Type Calcium Channels in Cerebellar Purkinje Neurons.” *Journal of Neuroscience* 24(40):8818–22. doi:10.1523/JNEUROSCI.2915-04.2004.

Wu, L. G., J. G. Borst, and B. Sakmann. 1998. “R-Type Ca2+ Currents Evoke Transmitter Release at a Rat Central Synapse.” *Proceedings of the National Academy of Sciences of the United States of America* 95(8):4720–25. doi:10.1073/pnas.95.8.4720.

Wu, Ling-Gang, Ruth E. Westenbroek, J. Gerard G. Borst, William A. Catterall, and Bert Sakmann. 1999. “Calcium Channel Types with Distinct Presynaptic Localization Couple

Differentially to Transmitter Release in Single Calyx-Type Synapses." *Journal of Neuroscience* 19(2):726–36. doi:10.1523/JNEUROSCI.19-02-00726.1999.

Wyart, Claire, Filippo Del Bene, Erica Warp, Ethan K. Scott, Dirk Trauner, Herwig Baier, and Ehud Y. Isacoff. 2009. "Optogenetic Dissection of a Behavioural Module in the Vertebrate Spinal Cord." *Nature* 461(7262):407–10. doi:10.1038/nature08323.

Wyart, Claire, Filippo Del Bene, Erica Warp, Ethan K. Scott, Dirk Trauner, Herwig Baier, and Ehud Y. Isacoff. 2009. "Optogenetic Dissection of a Behavioural Module in the Vertebrate Spinal Cord." doi:10.1038/nature08323.

Xu, Lulu, Guan, Na N., Huang, Chun-Xiao, Hua, Yunfeng, and Song, Jianren. 2021. "A Neuronal Circuit That Generates the Temporal Motor Sequence for the Defensive Response in Zebrafish Larvae." (31):3343–57. doi:https://doi.org/10.1016/j.cub.2021.06.054.

Xu, Weifeng, and Diane Lipscombe. 2001. "Neuronal CaV1.3α1 L-Type Channels Activate at Relatively Hyperpolarized Membrane Potentials and Are Incompletely Inhibited by Dihydropyridines." *The Journal of Neuroscience* 21(16):5944–51. doi:10.1523/JNEUROSCI.21-16-05944.2001.

Ye, Huan, Zhen-Xu Liu, Ya-Jie He, and Xin Wang. 2022. "Effects of M Currents on the Persistent Activity of Pyramidal Neurons in Mouse Primary Auditory Cortex." *Journal of Neurophysiology* 127(5):1269–78. doi:10.1152/jn.00332.2021.

Yu, S. P. 1995. "Roles of Arachidonic Acid, Lipoxygenases and Phosphatases in Calcium-Dependent Modulation of M-Current in Bullfrog Sympathetic Neurons." *The Journal of Physiology* 487(3):797–811. doi:10.1113/jphysiol.1995.sp020919.

Yue, Cuiyong, and Yoel Yaari. 2004. "KCNQ/M Channels Control Spike Afterdepolarization and Burst Generation in Hippocampal Neurons." *Journal of Neuroscience* 24(19):4614–24. doi:10.1523/JNEUROSCI.0765-04.2004.

Yue, Cuiyong, and Yoel Yaari. 2006. "Axo-Somatic and Apical Dendritic Kv7/M Channels Differentially Regulate the Intrinsic Excitability of Adult Rat CA1 Pyramidal Cells." *Journal of Neurophysiology* 95(6):3480–95. doi:10.1152/jn.01333.2005.

Zaitsev, A. V., N. V. Povysheva, D. A. Lewis, and L. S. Krimer. 2007. "P/Q-Type, But Not N-Type, Calcium Channels Mediate GABA Release From Fast-Spiking Interneurons to Pyramidal Cells in Rat Prefrontal Cortex." *Journal of Neurophysiology* 97(5):3567–73. doi:10.1152/jn.01293.2006.

Zamani, Alemeh, Shigeo Sakuragi, Toru Ishizuka, and Hiromu Yawo. 2017. "Kinetic Characteristics of Chimeric Channelrhodopsins Implicate the Molecular Identity Involved in Desensitization." *Biophysics and Physicobiology* 14:13–22. doi:10.2142/biophysico.14.0_13.

Zavala-Tecuapetla, C., M. A. Aguileta, J. J. Lopez-Guerrero, M. C. González-Marín, and F. Peña. 2008. “Calcium-Activated Potassium Currents Differentially Modulate Respiratory Rhythm Generation.” *European Journal of Neuroscience* 27(11):2871–84. doi:10.1111/j.1460-9568.2008.06214.x.

Zhang, Hailin, Liviu C. Craciun, Tooraj Mirshahi, Tibor Rohács, Coeli M. B. Lopes, Taihao Jin, and Diomedes E. Logothetis. 2003. “PIP2 Activates KCNQ Channels, and Its Hydrolysis Underlies Receptor-Mediated Inhibition of M Currents.” *Neuron* 37(6):963–75. doi:10.1016/S0896-6273(03)00125-9.

Zhang, Hua, Zhao-Fu Sheng, Jingxiong Wang, PeiRu Zheng, XunLei Kang, Hui-Ming Chang, Edward T. H. Yeh, and De-Pei Li. 2022. “Signaling Pathways Involved in NMDA-Induced Suppression of M-Channels in Corticotropin-Releasing Hormone Neurons in Central Amygdala.” *Journal of Neurochemistry* 161(6):478–91. doi:10.1111/jnc.15647.

Zhang, Mengliang, Natalya Sukiasyan, Morten Møller, Ilya Bezprozvanny, Hua Zhang, Jacob Wienecke, and Hans Hultborn. 2006. “Localization of L-Type Calcium Channel Ca(V)1.3 in Cat Lumbar Spinal Cord--with Emphasis on Motoneurons.” *Neuroscience Letters* 407(1):42–47. doi:10.1016/j.neulet.2006.07.073.

Zhong, Guisheng, Mark A. Masino, and Ronald M. Harris-Warrick. 2007. “Persistent Sodium Currents Participate in Fictive Locomotion Generation in Neonatal Mouse Spinal Cord.” *Journal of Neuroscience* 27(17):4507–18. doi:10.1523/JNEUROSCI.0124-07.2007.